THE UNIVERSITY
of EDINBURGH

Rational Ligand Design to Support Reactive Main-Group Compounds

A Thesis Submitted for the Degree of Doctor of Philosophy

Stephanie Jane Urwin

School of Chemistry

Science and Engineering

January 2018

Author Declaration

I declare that this thesis is an original report of my research, has been written by me and has not been submitted for any previous degree. Except where otherwise stated, experimental work is my own; collaborative contributions are acknowledged. Due references have been provided to all supporting literature and resources.

Stephanie Jane Urwin

Lay Abstract

The world's chemical industry relies on the use of precious metals which are in short supply, such as platinum and palladium. Scientists would like to utilise metals which are cheaper and more abundant for the same processes, sparking a recent surge in interest in the most abundant metal in earth's crust, aluminium. However, it is widely accepted that aluminium is generally incapable of the fundamental chemical reactions that make the precious metals so popular.

The most difficult of these processes for aluminium is reductive elimination, of which there is only one documented example. The first half of this thesis examines how and why this reported reductive elimination proceeds, to help enable the future design of systems which can mimic precious metal behaviour. Further, other fundamental reactions of aluminium in its unusual +1 oxidation state are examined.

The second half of this work deals with phosphorus and nitrogen based compounds, named "phosphaamidines". It was found that the geometry of the five prepared examples is dependant on the steric bulk of the organic substituents. Metallic complexes of these phosphaamidines have also been made, with lithium, magnesium and aluminium as the central atom. Three of these novel magnesium complexes are found to catalyse the preparation of a biodegradable plastic, polylactic acid.

Abstract

The chemistry of the tetrameric low-valent aluminium compoud $(Cp^*Al)_4$ (Cp^* = 1,2,3,4,5-pentamethylcyclopentadienyl) is relatively undeveloped compared to its monomeric cousin ^{dipp}NacNacAl (^{dipp}NacNac = 2,6-diisopropylphenyl-β-diketiminate). Given that the former can be formed by the reductive elimination of Cp*H from Cp^*_2AlH, a process common to transition metals yet rare with light main-group elements, using the Cp* ligand could unlock an abundance of unexpected reactivity for aluminium. An overview of the literature regarding the synthesis and reactivity of low oxidation state aluminium compounds is provided in chapter 1, as well as an introduction to relevant magnesium chemistry for this work.

Chapter 2 studies the mechanism of C-H reductive elimination from Cp^*_2AlH to form $(Cp^*Al)_4$, and the properties which allow reductive elimination to take place are revealed. A transition state is identified where the Cp* group has a higher hapticity than in the starting material, a process which is thought to enable the reductive elimination. Using this insight, aluminium hydride and halide complexes featuring 9-methylfluorenyl ligands are synthesised and reduction of the aluminium centre is investigated.

The reactivity of $(Cp^*Al)_4$ is considered in chapter 3 of this thesis. The formal cycloaddition reaction between $(Cp^*Al)_4$ and diphenylacetylene produces a Lewis acidic 1,4-dialuminacylohexadiene derivative. The inner Al_2C_4 ring of this complex is stable, with onward reactions happening at the complex's periphery. Insertion reactions in the Al-C_{Cp^*} bonds are observed with unsaturated C-N species. With 2,6-dimethylphenylisonitrile the Al_2C_4 complex forms a zwitterionic aluminate, featuring a stable carbocation derived from the Cp* group. An amidinate complex with an unusual Cp* backbone is formed from the insertion of carbodiimides into the Al-C_{Cp^*} bond of the 1,4-dialuminacyclohexadiene. Extending this, the insertion of carbon dioxide into the same bond is explored.

The use of amidine ligands is common in main-group chemistry, however literature relating to the related phosphaamidinate ligands ($[RPC(R)NR]^-$) is only reported sporadically. They have not been applied in a general manner to main-group chemistry thus far. Chapter 4 describes the synthesis of five new phosphaamidinate pro-ligands where the steric bulk of both the phosphorus and nitrogen components is increased systematically. To evaluate

these new ligands, their coordination chemistry with magnesium was investigated. Three examples of heteroleptic LMg^{n}Bu (L = phosphaamidinate) complexes are synthesised, which all show high activity for the ring-opening polymerisation of racemic lactide. The resulting polylactide chains show good molecular weights and polydispersity indices. The synthesis of homoleptic L_2Mg complexes is also described.

Chapter 5 applies these new phosphaamidinate ligands to aluminium chemistry. An aluminium hydride species is isolated, which is shown to form via a probable lithium aluminate intermediate. The lifetime of this intermediate is found to be heavily dependent on the reaction solvent.

Published Work

The work contained in this thesis has been published in part in the following journals:

"Aluminium-mediated carbon-carbon coupling of an isonitrile"
S. J. Urwin, G. S. Nichol and M. J. Cowley, *Chem Commun.*, 2018, **54**, 378-380

"Ligand coordination modulates reductive elimination from aluminium(III)"
S. J. Urwin, D. M. Rogers, G. S. Nichol and M. J. Cowley, *Dalton Trans.*, 2016, **45**, 13695-13699

Conferences Attended

The work contained in this thesis has been presented at the following conferences:

RSC Main Group Interest Annual Meeting, September 2017, London (Poster)
"A Monomeric, Three-Coordinate Alkyl Magnesium Complex Featuring a Super Bulky Phosphaamidinate"

Anglo-German Inorganic Chemistry Conference, August 2017, Göttingen (Poster)
"Aluminium Mediated C=C Coupling of an Isonitrile"

Joesph Black Conference, June 2017, Edinburgh (Oral Presentation)
"Towards Rationalising the Diverse Reactivity of Low Valent Aluminium Compounds"

ISACS: Challenges in Inorganic Chemistry, April 2017, Manchester (Poster)
"Isolation of a Zwitterionic Aluminate via Carbon Coupling of an Isonitrile"

Universities Scotland Inorganic Chemistry Conference, Aug 2016, Glasgow (Poster)
"Mechanism Determined Ligand Design: Using the Concept of Variable Hapicity to Stabilise Al(I)"

Joesph Black Conference, June 2016, Edinburgh (Poster)
"From Curiosity to Commonplace? An insight into ligand design for low valent aluminium"

RSC Dalton Conference, March 2016, Coventry (Poster)
"Reductive Elimination from Al(III): Exploring the Mechanism and the Effect of Coordinated Base"

Acknowledgments

I would like to wholeheartedly thank Dr Michael Cowley for mentoring me through three (and a wee bit) years, and for helping me find my way as a well-rounded scientist.

I would also like to thank the rest of the Cowley Cowboys, Amy Price, Martin Stanford, Daniel de Rosa, Clément Millet, Abigail Levy, Dr Rosalyn Falconer and Dr Lena Albers, for making the small office we shared a fun place to work, and for ensuring that not everything was about chemistry. Alongside Euan Doidge, Dr Helen O'Connor, Dr Catherine Weetman, and countless others in chemistry at Edinburgh, you made life happy and colourful.

Especially I would like to thank Amy Price, we've been there since the start, and to Martin Stanford for laying the foundations for chapters 4 and 5. Thank you to Dr Lena Albers for introducing me to computational chemistry, and for getting me into shape in more ways than one. Finally, thank you to the newest Cowboy, Dr Rosalyn Falconer, for proofreading parts of this thesis.

Thank you to Dr David Rogers for lending his computational expertise to chapter 2. I would also like to thank Dr Gary Nichol for solving all the crystal structures in this work, and not complaining too much when I persistently brought him gels instead of crystals. I also would like to thank Dr Jennifer Garden for her extensive guidance on polymerisations, and for making me a pseudo-polymer chemist. I would like to thank Alan Taylor for all his assistance with mass spectroscopy.

Most of all I would like to thank Nicolai. You have kept me sane and grounded, and put everything in perspective. You could probably write this thesis in almost as much detail, and for that I apologise.

Thesis Contents

List of Abbreviations

Ar*	2,6-bis(diphenylmethyl)-4-methyl phenyl
Bbp	2,6-[C(SiMe$_3$)$_2$H]-C$_6$H$_3$
cAAC	Cyclic alkyl amino carbene
Cod	1,5-Cyclooctadiene
COSY	Homonuclear correlation spectroscopy
Cp*	1,2,3,4,5-pentamethylcyclopentadienyl
Cy	Cyclohexyl
DCC	Dicyclohexylcarbodiimide
DIC	Diisopropylcarbodiimide
DCM	Dichloromethane
Dep	2,6-diethylphenyl
Dipp	2,6-diisopropylphenyl
DFT	Density functional theory
DMAP	Dimethylaminopyridine
DME	Dimethoxyethane
EI MS	Electron ionisation mass spectroscopy
FT-IR	Fourier transform infrared spectroscopy
GPC	Gel permeation chromatography
HBpin	Pinacolborane
HOMO	Highest occupied molecular orbital
LUMO	Lowest unoccupied molecular orbital
MALDI	Matrix assisted laser desorption/ionization
^{Me}I^{i}Pr	Diisopropyldimethylimidazolylidene
^{Me}IMe	Tetramethylimidazolylidene
Mes	2,4,6-trimethylphenyl
Mes*	2,4,6-tritertbutylphenyl
M_n	Number average molecular weight

NacNac	β-diketiminate
NHC	*N*-heterocyclic carbene
NMR	Nuclear magnetic resonance
NPA	Natural population analysis
ROP	Ring-opening polymerisation
Ph	Phenyl
PLA	Polylactide
Tbb	2,4,6-[$C(SiMe_3)_2H$]-C_6H_2
Tf	Triflate
Tipp	2,4,6-triisopropylphenyl
Ter	Terphenyl, (C_6H_3-2,6-Dipp)
THF	Tetrahydrofuran
TMEDA	*N,N,N'N'*-Tetramethylethylenediamine
TOF	Time of flight
Tol	p-Methylphenyl
WBI	Wiberg bond index
Xyl	2,6-dimethyl phenyl
$\%V_{bur}$	Percentage buried volume
Đ	Polydispersity index

I was taught that the way of progress was neither swift nor easy.

Marie Skłodowska Curie

Chapter 1:

Introduction

1. Introduction

Group 13 of the periodic table comprises boron, aluminium, gallium, indium and thallium. Despite being part of the same group these elements each have their own individual character, and so studying each of these elements in detail provides different challenges. For example, the +1/+3 redox pair is easily accessed for indium and thallium, but for aluminium is relatively undeveloped due to the difficulty associated with accessing the seemingly unpredictable Al(I) oxidation state.

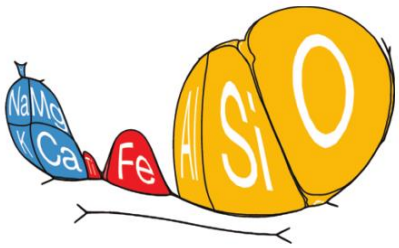

Figure 1 *Periodic table weighted according to relative abundance in the Earth's crust*[1]

Aluminium is the most abundant metal in the earth's crust. Whilst its compounds are being widely used in industrial processes, its reactivity in such applications are mostly limited in scope to Lewis acid behaviour. Organoaluminium reagents are very popular in organic synthesis, with $AlMe_3$ being the world's largest tonnage organometallic reagent.[2] There are numerous examples of its use;[2] a small selection includes polymerisation reactions, coupling reactions, conjugate addition reactions[3] and Lewis acid catalysed transformations such as the Friedel-Crafts reaction.[4] All major chemical applications of aluminium use compounds in the Al^{III} oxidation state, and indeed this is taught as the only oxidation state possible in undergraduate textbooks, however Al^{I} oxidation sate is accessible, though only under special circumstances.

1.1 Overcoming Disproportionation to Isolate Al(I)

1.1.1 Low Oxidation State Aluminium is Very Unstable

Where subvalent halides of indium and thallium are known to be solids at room temperature,[5] the corresponding E-X compounds of the lighter group 13 metalloids are primarily high temperature compounds. They are only isolable by complexation of a Lewis donor to form small clusters.[6] This inherent instability is demonstrated by the facile disproportionation of Al-Cl at ambient temperature to aluminium trichloride and elemental aluminium. This proceeds by the pathway described in Figure 2, through the formation of tetrameric metalloid clusters[6,7]

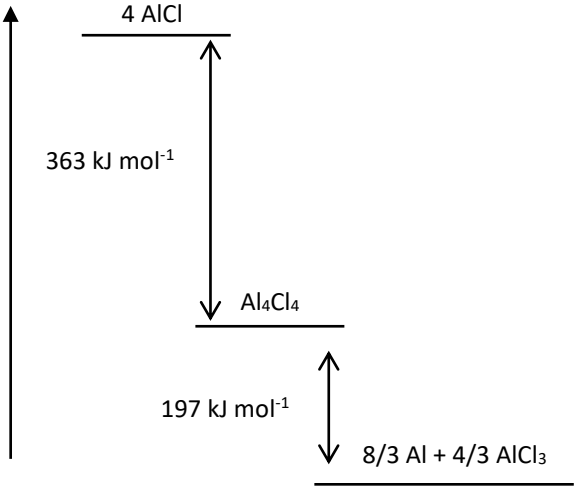

Figure 2 *Energy diagram showing the mechanism of disproportionation of AlCl*[5]

Studying monovalent AlX species isolated in argon matrices revealed reactivity uncharacteristic of traditional aluminium reagents (such as oxidative addition, section 1.2.2),[8–10] and the search for an isolable low valent aluminium complex began. Generation of AlCl on a preparative scale was first achieved by Schnöckel,[11] by heating Al metal and HX to 1000°C and condensing the resulting subvalent aluminium halide into an appropriate solvent at low temperature[5,12,13] producing a metastable Al-X (X = Cl, Br or I) solution for further transformations.[5]

$$2\,Al_{(s)} + 2\,HCl_{(g)} \xrightarrow{1000°C} 2\,AlCl_{(g)} + H_{2(g)}$$

Scheme 1 *Preparation of AlCl at high temperature*

1.1.2 It All Begins with the Isolation of a Tetramer

Whilst preparation of metastable monovalent AlCl was a significant discovery, its molecular transformation into a stable compound retaining a low oxidation state aluminium centre brought Al(I) into the spotlight. Transfer of pentamethylcyclopentadiene (Cp*) ligands from the homoleptic magnesium complex Cp^*_2Mg to monovalent AlCl results in the formation of $(Cp^*Al)_4$ **A**.[14] Unlike the metastable Al(I) starting materials, this prototypical isolable low valent aluminium species was found to be remarkably thermally stable, as the bulky Cp* ligands provide substantial kinetic stability. Thermal decomposition does not occur below 140 °C,[15] compared to decomposition above -30 °C for the unsubstituted $(CpAl)_4$ analogue.[5]

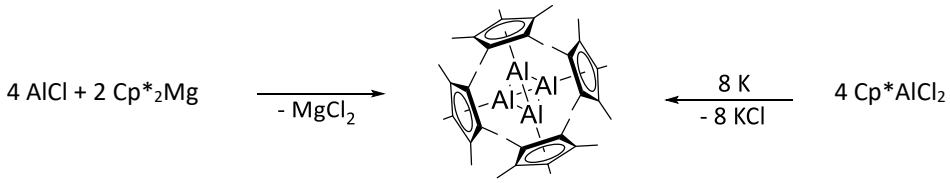

A

Scheme 2 *Methods of synthesis of tetrameric $(Cp^*Al)_4$*

The novelty of the aluminium cluster in **A** prompted investigations into the nature of the Al-Al endo- and Al-C exo-bonds. It was found that formal covalent Al-Al bonds do not exist along the edges of the tetrahedron, instead two electrons from each low valent centre are delocalised across each triangular face.[16] Expansion of the tetrameric core gives electron-rich Cp*Al based clusters,[17–20] leading to the application of **A** as a novel fuel and propellant being investigated.[20]

The challenging synthesis of AlX type compounds requires specialist equipment,[21] and so large-scale access to **A** was initially limited. A simpler synthetic route was later reported. The alkali metal reduction of Cp^*AlCl_2 produces **A** using standard laboratory techniques, albeit with a significant reduction in yield (20 % versus 44 % for the ligand transfer).[22] Reduction of the iodide analogue Cp^*AlI_2 allowed for the isolation of the symmetrical dialane Cp*(I)Al-Al(I)Cp*, indicating that this reduction is stepwise.[23] The reduction of other aluminium dihalide compounds has yielded tetrameric Al(I) compounds featuring bulky alkyl[24,25] and silyl groups.[26,27]

Many years later, Fischer reported the quantitative synthesis of **A** by the reductive elimination of Cp*H from Cp^*_2AlH,[28] a strategy which has recently been extended to include the reductive elimination of modified Cp* substituents, leading to the isolation of two new tetrameric Al(I) species **B** and **C**.[29]

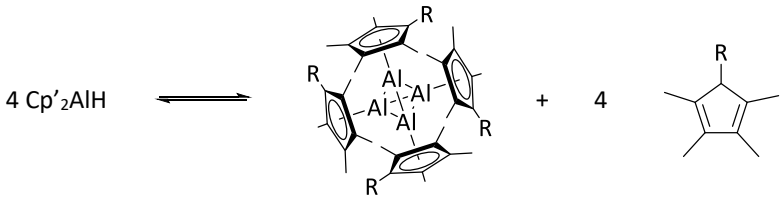

Scheme 3 *Reductive elimination of C-H bonds to form tetrameric low-valent aluminium species*

This reductive elimination of Cp*H from Cp^*_2AlH is reported to be reversible, with the exergonic equilibrium (ΔG_R^{298} = -3.7 kcal mol^{-1}) favouring formation of $(Cp^*Al)_4$ and Cp*H.[28]

Whilst isolated in its tetrameric form **A** at room temperature, $(Cp^*Al)_4$ can reversibly dissociate at elevated temperatures to form its constitutent Cp*Al monomer, $\mathbf{A^m}$.[14] This equilibrium was initially disputed as being an effect of atmospheric oxygen interacting with the cluster,[22] but the observable upfield shift of the ^{27}Al NMR signal at high temperature indicating **A** (^{27}Al δ = -79) had dissociated to form $\mathbf{A^m}$ (^{27}Al δ = -150) was later supported by detailed *ab initio* calculations.[30] The dissociation energy from **A** into $\mathbf{A^m}$ is calculated to be 150 ± 20 kJ mol^{-1}.[30] The interaction of **A** with O_2 was recently reported to produce a heterocubane cluster which gives a ^{27}Al NMR signal at δ = -13.5.[31]

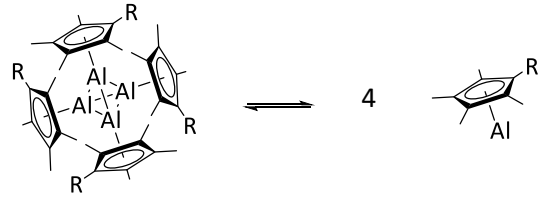

Scheme 4 *Dissociation of tetrameric aluminium(I) clusters into their monomeric components*

This dissociation has been shown to occur in another tetrameric Cp* derived cluster, **C**. Notably absent from this series is ^{n}Pr substituted Cp* derivative **B**, which can be prepared by the reductive elimination route described in Scheme 3, as **B** was found to not undergo the same facile dissociation. The ability of the tetrameric Al(I) species to dissociate is proposed to be dictated by ligand effects, and that non-covalent interactions between the Cp* derived ligands actually stabilises **B** relative to **A.**[29] Another prepared Al_4 cluster where R = H (according to Scheme 4), with a lesser steric bulk than **A**, also does not undergo dissociation.[32]

Gas-phase electron diffraction experiments on sublimed material at 139°C allowed for the structure of the monomer $\mathbf{A^m}$ to be investigated.[15] The Al-C bond lengths were found to elongate only slightly upon dissociation (**A**: 2.334 Å, $\mathbf{A^m}$: 2.388(7) Å), suggesting that the structure and bonding of monovalent Cp*Al is retained in the tetrameric cluster. Monomeric $\mathbf{A^m}$ cannot be isolated at room temperature, but it can be trapped as a Lewis basic terminal ligand for transition metal complexes.[33–39] Tetrameric **A** is fairly unreactive, with most reported reactivity requiring high temperatures, presumably to allow dissociation of **A** into $\mathbf{A^m}$**.**

1.1.3 Landmark Isolation of a Monomeric Al(I) Species

The preparation of stable Al(I) complexes can be achieved by the reduction of the corresponding aluminium dihalide, for example the reduction of Cp^*AlCl_2 to $(Cp^*Al)_4$.[22] Reduction of an aluminium diiodide supported by a β-diketiminate ligand resulted in the isolation of NacNacAl **D**.[40] Its remarkable monomeric structure was established by X-ray crystallography, with no interactions between metal centres in adjacent monomers noted.

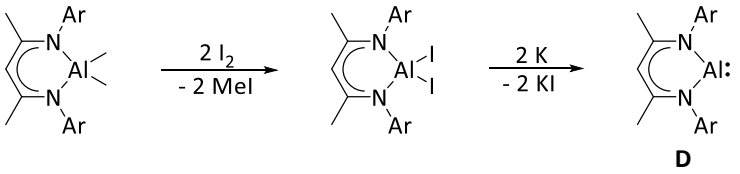

Scheme 5 *Synthesis of monomeric NacNacAl*

Using a Laplacian map of electron density it was shown that much electron density resides at the metal centre in **D**.[40] Density functional theory calculations demonstrated that the HOMO of **D** was an aluminium based s-orbital, which houses the localised lone pair,[41,42] and the empty p-orbital characteristic of group 13 elements is located perpendicular to the plane of the NacNac ligand in the LUMO+1. Hence **D** is truly isoelectronic with a carbene.

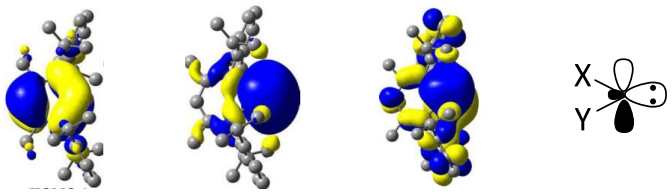

HOMO-1 HOMO LUMO+1 *(carbene)*

Figure 3 *Calculated molecular orbitals of NacNacAl, reproduced from the literature[42] and the frontier orbitals of an organic carbene for comparison[43]*

From the solid-state structure of **D**, it was also noted that the aluminium atom lies in plane with the anionic NacNac ligand.[40] The HOMO-1 revealed that the aluminium is part of a 6-electron π-system, where the lone pairs from the nitrogen atoms adjacent to the aluminium centre are donated to the metal centre.[41] This bonding situation results in onward reactivity of **D** where the supporting ligand is not innocent.[44–47] The diverse reactivity of **D** is understandably different than that of $(Cp^*Al)_4$, both of which will be discussed further in section 1.2.

1.1.4 A No Longer Elusive Double Bond

Neutral examples of homoatomic multiple bonds between the group 13 elements boron,[48] gallium,[49] indium[50] and thallium[51] have been reported for more than ten years. Boron, the lightest congener of this series, requires extra electronic stabilisation from *N*-heterocyclic carbenes, whilst the metallic derivatives are isolated base-free. At the beginning of this work, a corresponding aluminium example was noticeably missing from this series.

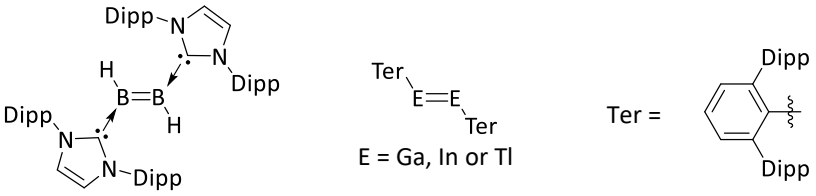

Figure 4 *Examples of neutral group 13 π-bonds*

Synthetic attempts at an Al=Al double bond began with the reduction of tetrakis-substituted dialanes, $R_2Al\text{-}AlR_2$. Addition of lithium to silyl-substituted dialane **E** in diethyl ether results in the formation of a thermally unstable radical salt, which can be made isolable by complexation of the lithium cation by tetramethylethylenediamine (tmeda).[52] Partial multiple bond character was confirmed by the observation of a shortened Al-Al bond distance in the solid-state structure of $\mathbf{E}^{\bullet-}$ when compared to its dialane starting material ($\mathbf{E}^{\bullet-}$: 2.53(1) Å, **E**: 2.660(1) Å).[52,53]

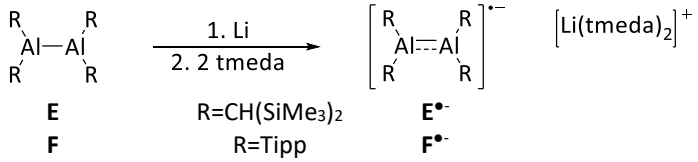

E R=CH(SiMe$_3$)$_2$ $\mathbf{E}^{\bullet-}$

F R=Tipp $\mathbf{F}^{\bullet-}$

Scheme 6 *Lithium reduction of substituted dialanes to form salts with Al-Al multiple bond character. Tipp = 2,4,6-triisopropylphenyl*

The same reactivity was also observed with the aryl substituted analogue $Tipp_4Al_2$.[54] As well as significant shortening of the Al-Al bond in $\mathbf{F}^{\bullet-}$ due to the formation of an one electron Al-Al π-bond, lengthening of the Al-C bonds was observed ($\mathbf{F}^{\bullet-}$: 2.021(1) Å, **F**: 1.996(3) Å).

The isolation of a dialumene edged closer with the reduction of bulky dihalo-aluminium complexes. The stepwise potassium graphite reduction of an aluminium diiodide with a

bulky terphenyl substituent is reported to produce the corresponding dialumene *in situ*,[55] however the sole isolated product of this reaction is the toluene adduct **G**. A formal [2+4] cycloaddition between the Al=Al π-system of the proposed dialumene and one equivalent of toluene has occurred, breaking the aromaticity of the solvent molecule.

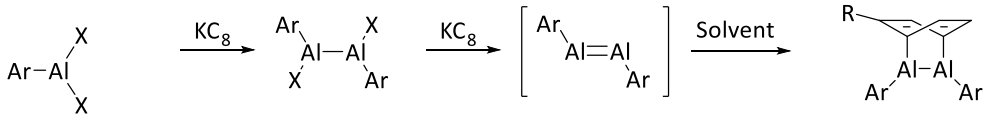

Ar = Ter; X = I
Ar = Bbp; X = Br

R = Me **G**
R = H **H**

Scheme 7 *Preparation of barrelene dialanes resulting from solvent activation by an unisolable dialumene. Ter = C_6H_3-2,6-$Dipp_2$, Dipp = C_6H_3-2,6-^{i}Pr. Bbp = 2,6-$(CH\text{-}(SiMe_3)_2)_2C_6H_3$*

It was ten years before another similar barellene dialane **H** (Scheme 7) was isolated using a bulky silylated aryl substituent Bbp.[56] Addition of aromatic polycyclic hydrocarbons (naphthalene or anthracene) to **H** were found to displace the C_6H_6 moiety at room temperature, demonstrating the lability of this solvent derived substituent. This intermolecular exchange behaviour suggests that **H** can be used as a dialumene source in solution, an idea which is supported by the observed reactivity of **H** (discussed further in section 1.3).

The stepwise reduction of the terphenyl aluminium dihalide from Scheme 7 with 6 equivalents of sodium in place of potassium results in the formation of disodium dialuminyne **I**.[57] The metal cations are coordinated by arene interactions with the terphenyl ligand. Whilst some multiple bond character exists between the aluminium centres in **I**, it is not a formal triple bond (Al-Al: 2.428(1) Å). DFT calculations showed non-bonding lone pair character at both aluminium centres in the HOMO-1 orbital of **I**.

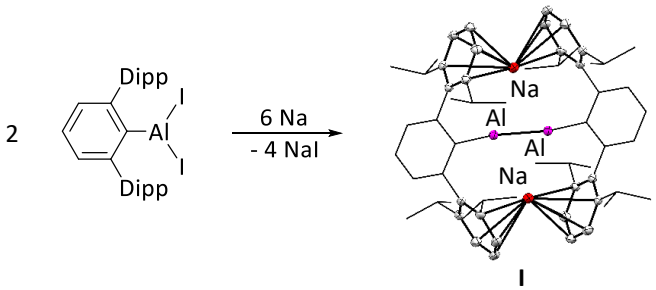

I

Scheme 8 *Preparation of a dialuminyne. Dipp = 2,6-diisopropylphenyl.*

The very recently reported neutral dialumene **J** by Inoue completes the journey to an isolable neutral Al=Al double bond.[58] It was achieved using a similar methodology to the preparation of **G** and **H**, by reduction of the corresponding dihalide species. The low-valent metal centres are flanked by bulky silyl groups, and further stabilised by an *N*-heterocyclic carbene. It is this combination of σ-donors that allows for the isolation of **J**.

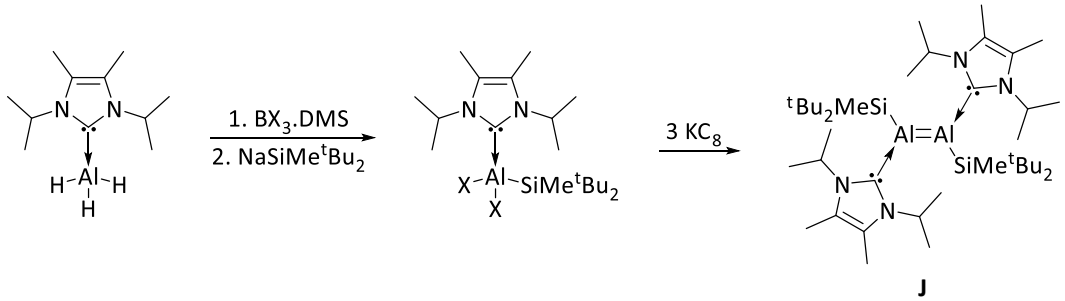

J

Scheme 9 *Preparation of a stable neutral dialumene. X=I or Br. DMS=dimethylsulfide.*

The solid-state structure of **J** shows a trans-bent geometry, directly comparable to similar NHC-stabilised diborene compounds[48,59] and unstabilised digallenes.[49] An inter-aluminium distance of 2.3943(16) Å is significantly shorter than the corresponding bond distances in lithium salts $\mathbf{E}^{\bullet-}$ (2.53(1) Å)[52] and $\mathbf{F}^{\bullet-}$ (2.470(2) Å),[54] which both feature partial Al=Al double bonds. Whilst it was calculated that a dialumene would have singlet diradical character,[60] the π-bonding HOMO of **J** confirms multiple bond character is present, as does the calculated Wiberg bond index of 1.70.

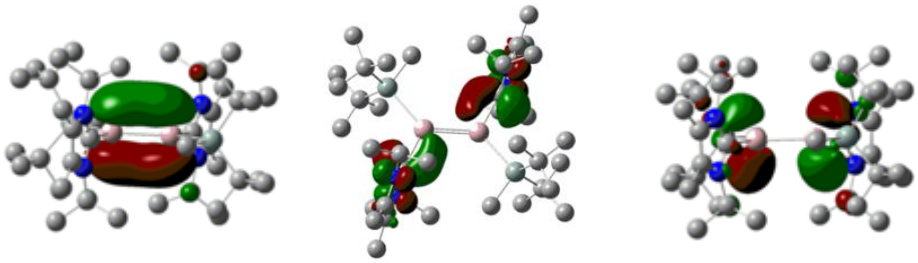

HOMO LUMO LUMO+1

Figure 5 *Calculated molecular orbitals of dialumene **J**, reproduced from literature[58]*

1.2 Reactivity of Isolable Low Oxidation State Aluminium Complexes

Marked differences in the reactivity of the two most common complexes of low oxidation state aluminium, $(Cp^*Al)_4$ **A** and NacNacAl **D**, are attributed to their very different structures at room temperature. Uses of tetrameric **A** have focused on the formation of larger clusters.[17,61] Metalloid clusters have been synthesised which feature mixed valency metal centres, containing both Al(I) and Al(0) centres.[18,19] As clusters do not feature in this work, this branch of low oxidation state aluminium chemistry will not be discussed. The reactivity of monomeric NacNacAl **D** is more focused on transformations involving a single metal centre, resulting in oxidised aluminium centres.

An illustrative example of these differences is the reaction of **A** and **D** with dioxygen. The resulting complexes **K** and **L** have the same general alumoxane formula $[LAlO]_n$ linked by bridging oxygens, but the nature of the bridges is different. In heterocubane **K** the tetrameric cluster has been expanded by two equivalents of O_2, and each oxygen is bridging three aluminium centres, held in the cube by non-covalent interactions.[31] Dimeric oxo-bridged **L** forms from an unstable $LAl(\eta^2\text{-}O_2)$ intermediate, which reacts with a further equivalent of **D**.[62] Each oxygen in **L** bridges two aluminium centres by Al-O σ-bonds.

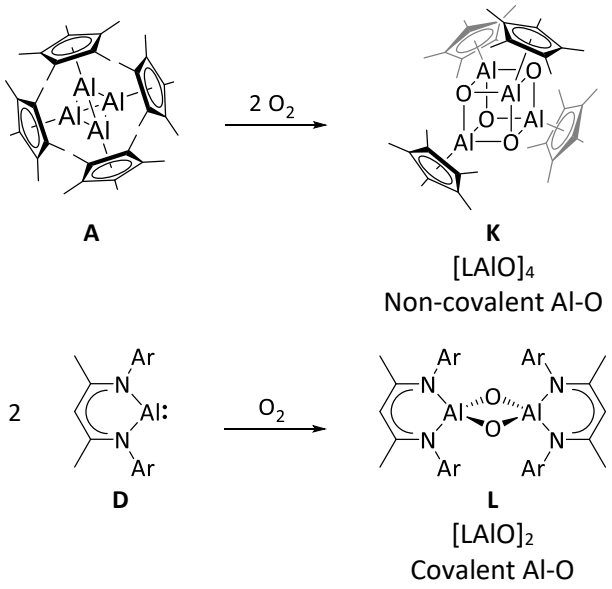

Scheme 10 *Reaction of **A** and **D** with dioxygen*

The supporting ligand can have consequences for the reactivity of the Al(I) compound. Whilst Cp* is typically a spectator, products formed from reactions with **D** sometimes feature a modified NacNac framework (typically C-H activation of the methyl backbone), indicating the ligand has participated in the reaction.[44–47] This is facilitated by the aluminium atom participating in the π-system of the NacNac ligand in **D**.[41]

1.2.1 A Source of Lewis Basic Aluminium

Even though monomeric Cp*Al **A^m** cannot be isolated, reactions conducted at elevated temperatures where **A^m** is generated *in situ* allow its chemistry can be investigated. Heating tetrameric **A** with a platinum(0) precursor traps the monomeric **A^m** formed at high temperature as a terminal Lewis base in novel complex **M** (Figure 6).[63] A calculated Al-Pt bond order of 0.52 indicates that this bond is dative, and further DFT studies confirmed π-back donation from the Pt to the aluminium centre. This demonstrates the weak π-accepting abilities of **A^m**, and draws further parallels between monomeric Al(I) and organic carbenes.

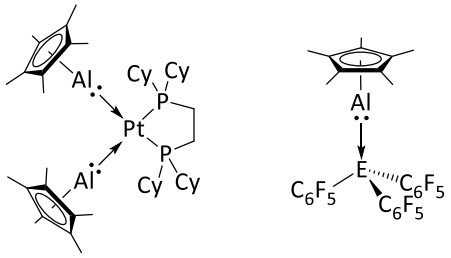

M E = B **N**
Al **O**

Figure 6 *Complexes featuring monomeric Cp*Al as a terminal ligand*

However, this back-bonding stabilisation is not a prerequisite for the formation of a dative bond from the lone pair of **A^m**. For example the complexation of **A^m** to the Lewis acidic group 13 centres in $E(C_6F_5)_3$ results in Lewis adducts **N** and **O**.[64,65] In **O** the inter-metallic distance at 2.591(3) Å is relatively short for a dialane, suggesting a dative interaction[65] (covalent Al-Al: $(Me_3Si)_2(H)C\}_4Al_2$ 2.660(1) Å; $^tBu_{12}Si_4Al_2$ 2.751(2) Å).[53,66]

The idea of Al(I) coordination to a transition metal centre has allowed for the trapping of a transient dialumene as a monomeric Al(I) fragment.[67] Isolated as barrelene-type dialane **H**, the dissociation of the benzene moiety is proposed to generate BbpAl=AlBbp *in situ*, which can then break apart to monomeric BbpAl: and coordinate a platinum(0) centre. The resulting complex **P** is stabilised by π-back donation from the electron rich metal centre to the empty p-orbital at the aluminium centre, analogous to the Al-Pt bond in **M**.

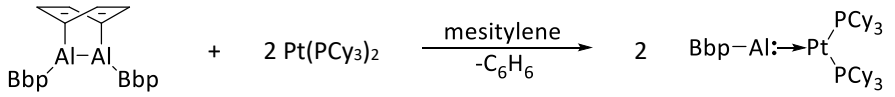

H **P**

Scheme 11 *In situ generation of BbpAl which is trapped by a Pt(0) complex. Bbp = 2,6-(CH-(SiMe$_3$)$_2$)$_2$C$_6$H$_3$*

Due to the increased steric bulk of the Bbp aryl group compared to Cp*, only one alumdiyl equivalent is coordinated to the platinum centre in **P**, compared with two Cp*Al units present in **M**. A slightly shorter Al-Pt bond distance in **P** (2.2857(18) Å) than in **M** (2.327(2)/2.335(2) Å) suggests a stronger inter-metallic interaction in **P**.

Even though the location of a discrete lone pair in NacNacAl **D** was demonstrated by DFT,[41] this low oxidation state aluminium compound has not been applied as broadly as **A^m** as a Lewis basic ligand. One reported instance is the palladium(0) complex in Figure 7.[68]

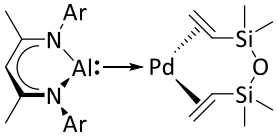

Figure 7 *Palladium(0) complex featuring a terminal NacNacAl ligand*

Other reactions where NacNacAl was expected to form Lewis adducts resulted in the insertion of the **D** into another bond. This is discussed further in section 1.2.2.

1.2.2 Oxidation of Low Valent Aluminium Centres

Aluminium in the +3 oxidation state is more favourable than the +1 oxidation state, therefore reactions with low valent aluminium centres will favour an increase in oxidation state to Al(III). In transition metal chemistry, a common way to increase the oxidation state by two increments is by the oxidative addition of σ-bonds. One major mechanism is the donation of electron density from the metal centre to the σ*-antibonding orbitals of the substrate, causing concerted breakage of the initial σ-bond and formation of two new metal-substrate bonds. As monovalent Al(I) bears a lone pair, species containing this centre should be able to undergo oxidative addition, forming Al(III).

The photo-induced oxidative addition of dihydrogen to monomeric Cp*Al (**A^m**) has been achieved in an Ar matrix at low temperature.[69] The resulting dihydride species was shown to be monomeric under these conditions, however its later independent synthesis *via* salt metathesis of Cp*K with $ClAlH_2$ lead to a "trimeric" isolated product $(Cp^*AlH_2)_3$ linked by bridging hydrides.[28]

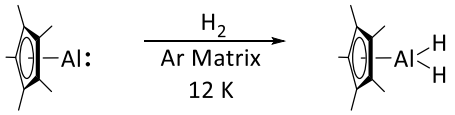

A^m

Scheme 12 *Oxidative addition of dihydrogen to monomeric Cp*Al in an argon matrix*

Oxidative addition of H_2 to **A** has not been achieved under standard preparative conditions. The only reported instance of preparative oxidative addition to **A** is the reversible oxidative addition of Cp*H to **A,** resulting in the formation of Cp^*_2AlH[28] (discussed in section 1.1.2). Conversely, the oxidative addition of a variety of bonds to monomeric **D** is well documented, ranging from E-H type bonds of lighter group 13, 14 and 15 elements,[70] to heavier E-E analogues.[71] Challenging C-F bonds have also been activated, resulting in a NacNacAl(F)R type product.[72,73]

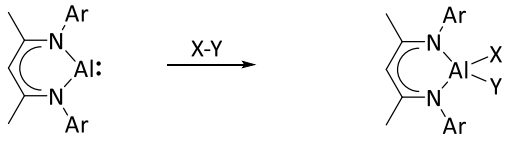

D

X=Y=H, Sb or Bi
X=SiHR$_2$, Bpin. Cp*, NHR,
PPh$_2$ or O^{i}Pr; Y=H
X=Aryl or alkyl; Y=F

Scheme 13 *Oxidative addition of a wide range of substrates to NacNacAl*

Slight differences in the mechanism of these σ-bond additions have been calculated using density functional theory. Concerted transition metal style oxidative addition is seen in the splitting of dihydrogen by **D**; the H-H σ-bond is activated by donation from **D**'s non-bonding electron pair into the σ* orbital.[42] As such, a transition state is identified as **D**[η^2-H$_2$], and from this heterolytic-cleavage of the H-H bond occurs forming the dihydride product **D**H$_2$. This is directly analogous to the mechanism of dihydrogen activation by cyclic alkyl amino carbenes.[74]

Transition Metal Style Oxidative Addition:

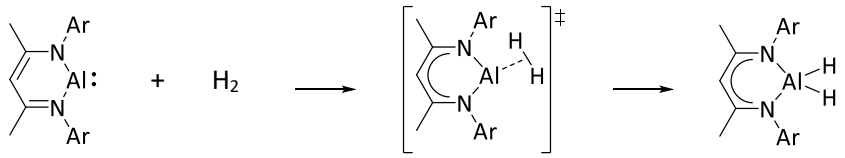

Stepwise Addition of Si-H:

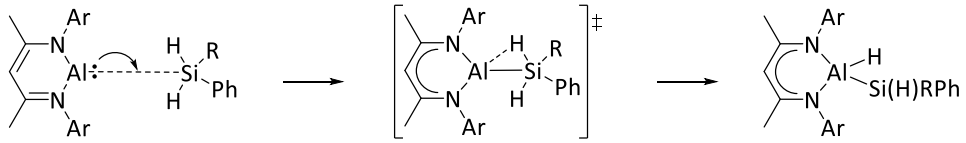

Initial Lewis Base Formation:

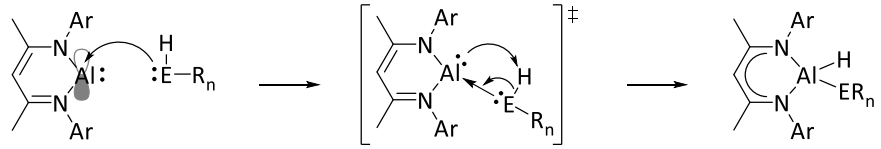

Scheme 14 *Calculated mechanisms of E-H oxidative addition to **D***

Other E-H oxidative additions proceed through slightly different mechanisms, dependant on the nature of the substrate.[42,75,76] For Si-H bonds, a stepwise mechanism is observed, where the aluminium based lone pair first enables the formation of the Al-Si bond in the transition state, and then hydride transfer completes the oxidative addition process[42]. Reaction of **D**

with Lewis basic substrates exploits the latent Lewis acidic properties of **D** (in the form of the vacant p-orbital identified in the LUMO+1 orbital[41]). Donation of electron density from the Lewis base into this empty orbital forms an Al-E bond in the transition state, and then subsequent hydrogen transfer furnishes the oxidative addition product.

The mechanism of addition of Cp*H to **D** is highlighted in Scheme 15, and proceeds via an initial protonation of the aluminium centre, identified through a $[NacNacAlH]^{+}[Cp^*]^{-}$ transition state.[42] This protonation makes the transferred hydrogen slighty hydridic, and once this hydrogen is fully associated, Al-C coupling occurs. A moderate calculated free energy barrier 87.4 kJ mol^{-1} (M062x/6−31G(d) level of theory) is complementary to a reaction which experimentally requires 3 days at 70 °C.[70]

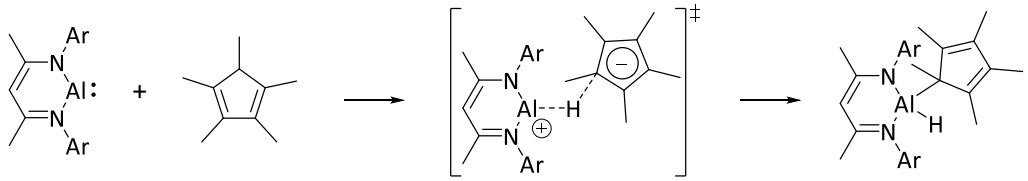

Scheme 15 *Calculated mechanism of the oxidative addition of Cp*H to NacNacAl*

For the addition of R-F bonds to **D**, compounds with aryl substituents were found to add in a concerted manner,[76] where compounds with alkyl substituents were shown to first add a fluoride to the metal centre, followed by the formation of the Al-C bond.[73,76] This latter mechanism is analogous to the mechanism of Cp*H addition to **D**.

NacNacAl **D** can also oxidatively add Al-H or Al-X bonds to form dialanes.[77,78] Both of these insertions are formal comproportionation reactions, each transforming Al(I)/Al(III) to Al(II)/Al(II). The first example of this was the oxidative addition of $NacNacAlH_2$ to **D**, which was shown to be in a thermal equilibrium with the corresponding reductive elimination process.[77] The mechanism of this Al-H oxidative addition is shown to proceed through a concerted, but non-synchronous, hydride transfer process, with a bimolecular transition state.[42]

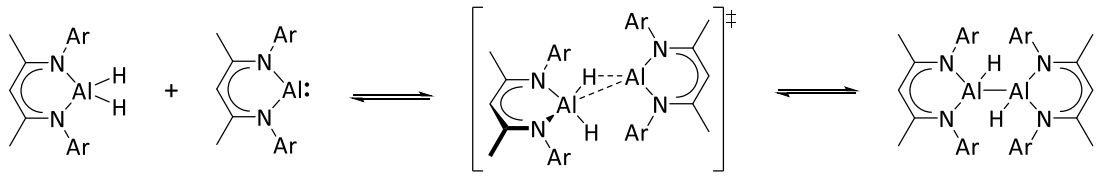

DH_2 **D** **D**$_2H_2$

Scheme 16 *Oxidative addition of an Al-H bond to* ***D***

Recently, the insertion of **D** into a cyclic alkyl aminio carbene (cAAC) supported Al-X bond was also reported.[78] Here an unsymmetrical dialane is formed, where both metal centres have a four-coordinate tetrahedral geometry.

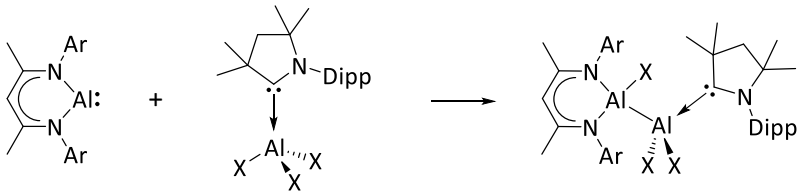

D

Scheme 17 *Insertion of* ***D*** *into a cAAC supported Al-X bond. X = Cl or I.*

Oxidative addition to Al(I) complexes made *in situ* is also possible. Exposing barrelene-type dialane **H** to a dihydrogen atmosphere results in formation of aluminium dihydride **Q** quantitatively at room temperature. Variable temperature ^{1}H NMR and crossover experiments featuring modified Bbp ligands suggested that this dimeric bridging species is in thermal equilibrium with its corresponding monomer **Q^m**.

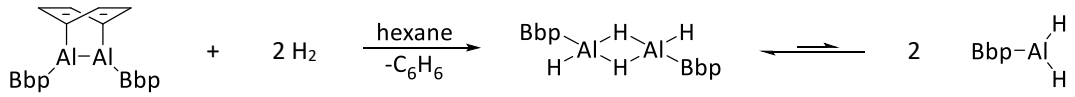

H **Q** **Q^m**

Scheme 18 *Dihyrdrogen activation by a dialumene made in situ. Bbp = 2,6-(CH-(SiMe$_3$)$_2$)$_2$C$_6$H$_3$*

The reverse process of oxidative addition, reductive elimination, is very rare in aluminium chemistry. Only two molecular examples are currently reported, which have already been mentioned in this text. Both of these are thermal equilibria, the elimination of Cp*H from Cp*$_2$AlH to form (Cp*Al)$_4$ **A** (Scheme 3, page 6) and the other the reversible addition of an Al-H bond to NacNacAl **D** (Scheme 16, page 19).

1.2.3 Formation of Al-Metallacycles

Activation of a σ-bond is not the only bond forming process available to Al(I). The high concentration of electron density at the metal centre produces cycloaddition-type activity with unsaturated C-C substrates such as alkenes or alkynes. This reactivity is seen across all examples of Al(I), with the structure of the products being dependant on the structure of the initial aluminium reagent.

Warming a solution of metastable AlCl to room temperature in the presence of dimethylacetylene forms 1,4-dialuminacyclohexadiene derivative **R** as the thermodynamic product.[79] A similar reaction is also possible using diethylacetylene.[80] X-ray crystallography of **R** revealed a stacked dimer solid-state structure, held together by Al-olefin interactions which are persistent even the gas phase.[81] Even though the Al…Al distance within one Al_2C_4 ring is relatively long (3.37 Å), a weak bonding interaction is calculated by density functional theory.

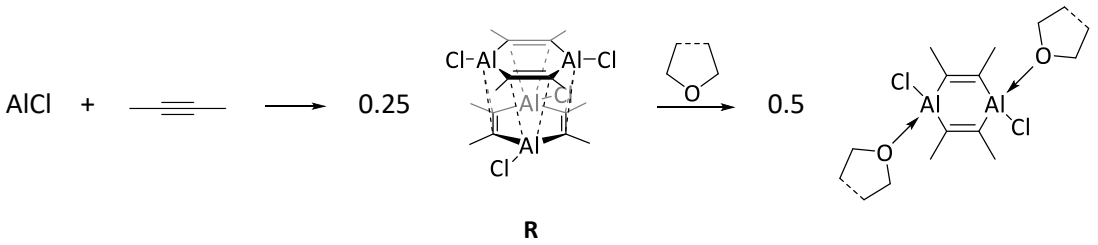

R

Scheme 19 *Activation of dimethylacetylene using metastable AlCl*

Delocalisation of the C=C π-system into the vacant 3p-orbital of the aluminium centre in the adjacent monomer creates a three-centre Al-C σ-bond. These Al-olefin contacts can be broken by the addition of an ethereal solvent (diethyl ether or tetrahydrofuran), causing the dissociation of **R** and the formation four-coordinate aluminium centres.[81]

The formal addition of Cp*Al $\mathbf{A^m}$ across the alkene bonds of tetramethyl-divinyl-disiloxane (dvds) gives $\mathbf{A^m}_2$(dvds).[82] Although no mechanistic insight is reported, it is the addition of $\mathbf{A^m}$ across each terminal C=C bond, followed by a cyclisation. This 1,4-dialuminacyclohexane containing product is the only reported instance of $\mathbf{A^m}$ activating an unsaturated C-C bond.

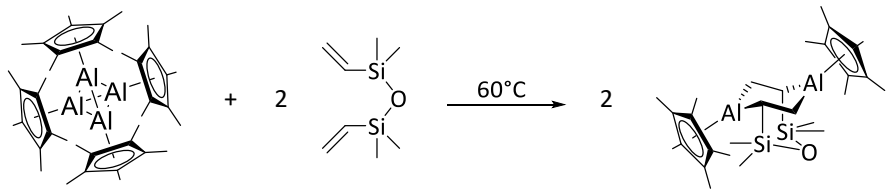

A **A^{m}$_2$(dvds)**

Scheme 20 *Addition of a dialkene to (Cp*Al)$_4$ gives a 1,4-dialuminacyclohexane derivative*

The lack of C=C bonds in **A^{m}$_2$(dvds)** leads to a chair conformation of the bimetallic Al_2C_4 heterocycle in the solid-state. This differs from the almost planar configuration of the dialumina-cyclohexadiene rings in **R**. The η^5 hapticity of the Cp* rings provides electronic stabilisation in **A^{m}$_2$(dvds)**.

Direct reaction of NacNacAl **D** with sterically unhindered acetylenes forms alumina-cyclopropene compounds of the type **S**.[83] These cycloaddition reactions occur spontaneously at temperatures as low as -100°C in toluene, demonstrating the highly reactive nature of **D**.

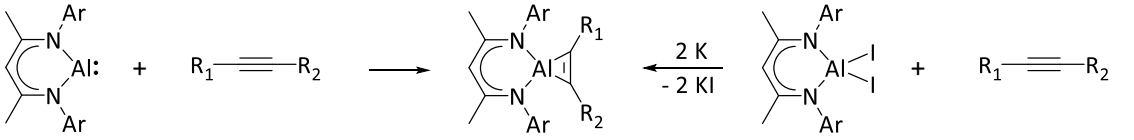

D R_1=R_2=H (**a**) R_1=R_2=Me (**b**) R_1=H R_2=Ph (**c**) **S** **D**I_2 R_1=R_2=$SiMe_3$ (**d**) R_1=R_2=Ph (**e**)

Scheme 21 *Preparation of alumina-cylopropene derivatives based on **D***

With bulky internal acetylenes, the corresponding alumina-cyclopropene products were not accessible from cycloaddition with **D**. However, the reaction of the corresponding diiodide **D**I_2 with potassium in the presence of the alkyne furnishes the desired **S** derivative in high yields.[84] The reaction of **D**I_2 with these internal alkynes is thought to proceed through aluminium based radicals from the partial reduction of **D**I_2, and hence is not a cycloaddition.

In the case of bis-trimethylsilylacetylene derivative **Sd**, it was found that the alkyne unit can be regenerated, displaced by two equivalents of tert-butylcyanide. The C-C coupling of these organic units generates a new bis(iminato) ligand at the aluminium centre.[84]

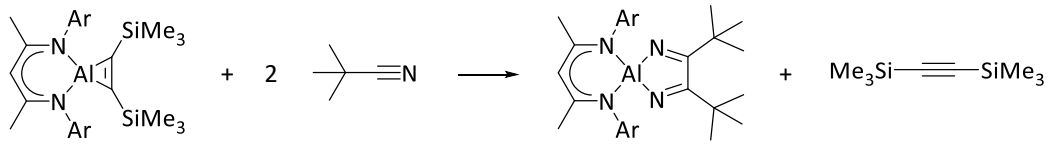

Sd

Scheme 22 *Bis-trimethylsilylacetylene cleavage and subsequent C-C coupling by a bulky cyanide*

Low oxidation state compounds where a dialumene is present are perfectly positioned for the activation of unsaturated C-C bonds. Barrelene dialane **H** is the product of a [2+4] cycloaddition of benzene and the corresponding dialumene, for which the reverse process is shown to happen at room temperature in solution.[56] Other cycloaddition reactions are possible from this Al=Al synthon, with the 1:1 reaction of **H** with diphenylacetylene giving two metallacyclic products **Ta** and **Tb** (Scheme 23).[85]

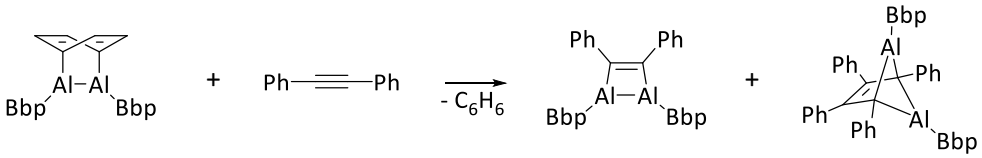

H **Ta** **Tb**

Major *Minor*

Scheme 23 *Reaction of barrellene **H** with diphenylacetylene*

The product distribution of **Ta** and **Tb** is dependent on the reaction conditions. As **Ta** cannot be transformed into **Tb**, these products are proposed to arise from two different reaction pathways.[85] Dialane **Ta** is formed in a [2+2] cycloaddition between **H** and diphenylacetylene. Formation of tricyclic **Tb** is more complex. Initially, the dialumene Bbp-Al=Al-Bbp is generated, which then dissociates to the Bbp-Al.[67] A [1+2] cycloaddition of Bbp-Al with the alkyne forms an alumina-cyclopropene product similar to **S**, which immediately dimerises to form **Tb.**

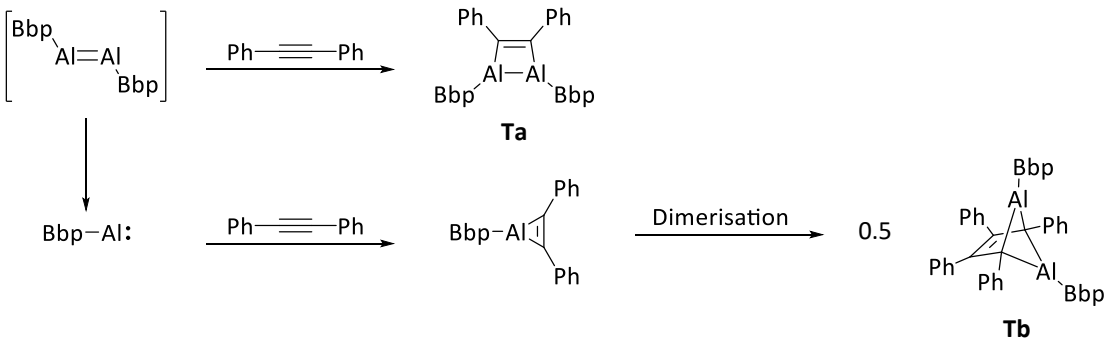

Figure 8 *Proposed mechanism of multiple product formation from a proposed dialumene and diphenylacetylene*

Whilst NacNac supported alumina-cyclopropene derivatives **S** were found to be thermally stable, the corresponding suggested BbpAl heterocycle dimerises immediately to form bi-metallic product **Tb**. Perhaps the four-coordinate aluminium centre enables the isolation of **S**. The crystallographically analysed examples of aluminacyclopropenes (**Sa**,**b**,**d**,**e**) shows the two bidentate ligands around the metal centre are at almost perfect right angles,[83,84] making onward reactivity sterically hindered.

The presence of an NHC in isolated dialumene **J** does not affect its cycloaddition capabilities. The 1,2-addition of both an alkene and a terminal alkyne was demonstrated in the initial report, with phenylacetylene producing two separate products.[58] The relationship between these products it not noted, however it seems likely that they are formed by two separate mechanisms.

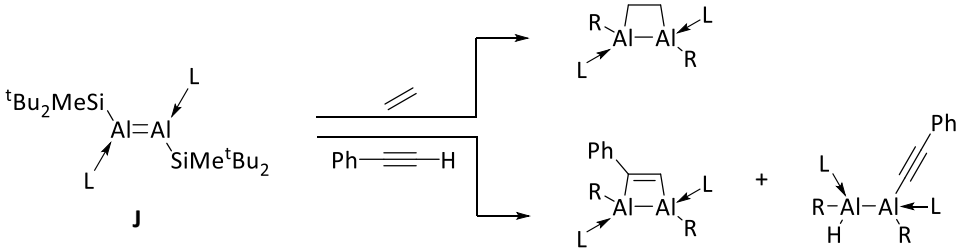

Scheme 24 *Reaction of isolated dialumene **J** with unsaturated C-C bonds. L = $^{Me}{}^{i}$Pr*

The mode of reactivity of low-oxidation state aluminium compounds with unsaturated C-C bonds is dependent on the structure of the aluminium starting material. Products typically feature multiple aluminium centres, and dimerisation can occur to produce a thermodynamically stable product.

1.3 Magnesium: A cheap, abundant and bio-compatible metal

Magnesium is the lightest alkaline earth metal with widespread synthetic application. In its metallic elemental state chemists use magnesium as a mild reducing agent, or to activate organo-halide bonds to form Grignard reagents. Complexes of the Mg^{2+} cation featuring mono- or polydentate ligands are plentiful, and have a wide range of uses.

There are some similarities between magnesium and aluminium, one of which is the lack of accessible d-orbitals. Further, they are both hard electropositive ions, and favour bonding to hard donor sites such as nitrogen and oxygen. The s-block elements are known for forming primarily ionic bonds; covalent bonds are rare. For this reason, polydentate anionic ligands are easily complexed to magnesium.

The lack of a suitable magnesium redox pair precludes any oxidative addition or reductive elimination chemistry utilising a single metal centre, and almost all reactivity retains the Mg^{2+} oxidation state (see section 1.3.2 for exceptions). This does not prevent magnesium from catalysing many molecular transformations.[86,87] Ring-opening polymerisations of cyclic esters such as lactide or ε-caprolactone initiated by magnesium complexes are well explored,[88–90] owing to the metal's inherent biocompatibility[91] and the products' biomedical uses.[92,93]

1.3.1 Heterocycles with a reactive Mg-X bond

Grignard reagents are ubiquitous across many synthetic chemistry disciplines, and their reactions with electrophiles is an important carbon-carbon bond forming transformation. Whilst Grignard reagents traditionally feature monodentate organic groups, many other reactive magnesium complexes can be synthesised featuring bidentate ligands which form magnesium containing heterocycles. The coordination of nitrogen based-ligands is abundant, and a diverse range of multidentate ligands of varying bite-angle are now reported. Reactivity is not limited to compounds with magnesium halide bonds, other common substituents include alkyl groups and hydrides.

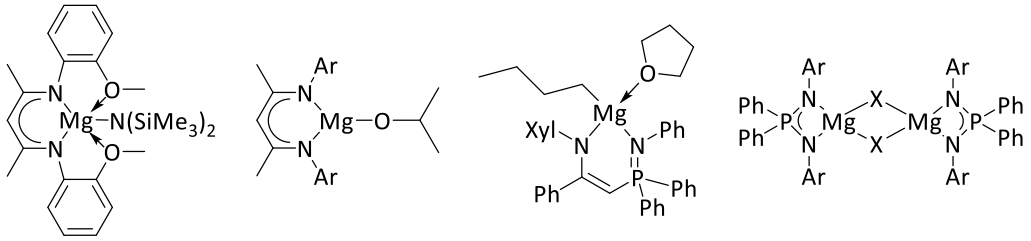

Figure 9 *A Snapshot of ligand diversity in reactive magnesium containing metallcycles*[94–97]

The synthesis of heteroleptic alkyl magnesium complexes of the type LMg^{n}Bu is commonly achieved by reaction of the protonated form of the ligand with the commercially available di-butylmagnesium, to eliminate butane.[96,98–101] It is possible that double substitution of the butyl groups can occur at the magnesium centre, resulting in a homoleptic complex L_2Mg.[100,102–104] This occurs when the ligand does not provide enough kinetic stabilisation in the heteroleptic LMgBu complex, and a second equivalent of ligand displaces the reactive alkyl group. Scheme 25 depicts an example of this, where the addition of steric bulk to ortho-position on the aryl nitrogen substituent enables the isolation of the LMg^{n}Bu complex.[104]

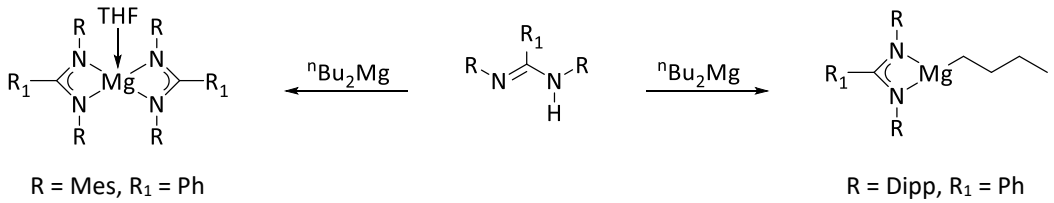

Scheme 25 *Addition of $^{n}Bu_2Mg$ to an amidine gives different products depending on the steric bulk of the ligand.*

In heteroleptic LMg^{n}Bu complexes, the Mg-C bond is typically reactive, leading to extensive further reactivity. The reaction of an alkyl magnesium species with phenylsilane transfers a hydride to the metal centre, enabling the isolation of bridging magnesium hydride species **U**.[99] One prolific example is the in-situ formation of a Dipp-substituted NacNacMg(μ-H) (Scheme 26, R = Me, Ar = Dipp) which can catalyse a diverse range of bond-forming transformations.[105–110]

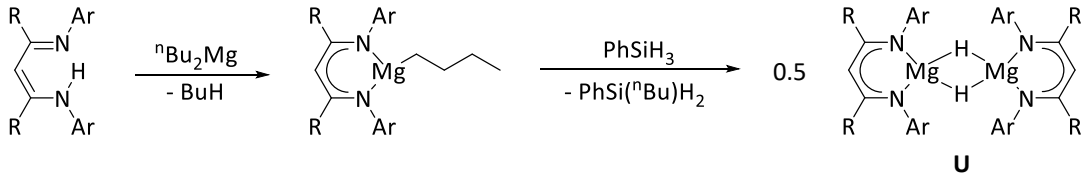

U

Scheme 26 *Preparation of a catalytically active NacNac supported Mg-H*

Kinetic stabilisation is again a major factor in determining molecularity of a magnesium hydride complex. Addition of dimethylaminopyridine to a moderately bulky derivative of **U** (R = ^{t}Bu, Ar = Dipp) can break apart the dimeric structure to form a four-coordinate terminal magnesium hydride.[99] Increasing the steric bulk of the aryl substituent on the supporting NacNac ligand (R=Me, Ar= $C_6H_2\{C(H)Ph_2\}_2{}^i$Pr-2,6,4) led to the isolation of a three-coordinate terminal magnesium hydride complex.[111]

A labile Mg-C bond in LMg^{n}Bu can also be used as an initiator in ring-opening polymerisation of cyclic esters such as lactide,[96,100] an example of which is shown in Scheme 27.[96] Magnesium-based initiators with N-based spectator ligands are typically very active in ring-opening polymerisation reactions.[88–90]

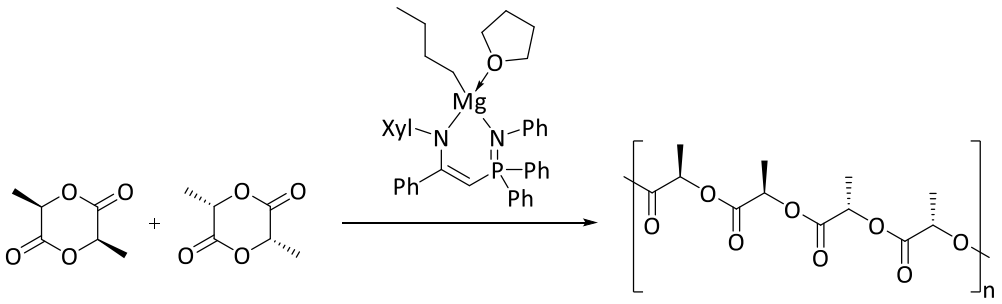

Lactide *Polylactide*

Scheme 27 *Preparation of heterotactic polylactide using an alkyl magnesium complex*

1.3.2 Accessing the Mg(I) Oxidation State

Magnesium in the +1 oxidation state was first reported in 2007, formed by the alkali metal reduction of a NacNac supported Mg-I precursor.[112] Many more examples have since been reported featuring various ligands bonded though a nitrogen atom, all of which have a dimeric structure with a Mg-Mg bond.[101, 113–115]

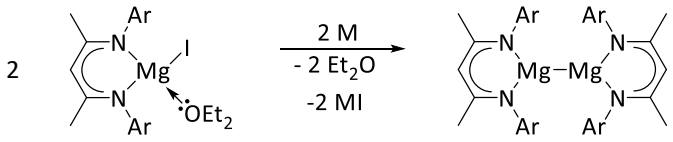

V

Scheme 28 *Preparation of a NacNac supported Mg-Mg bond. Ar = Dipp, Dep or Mes.*

As there is a high amount electron density held the centre of the Mg-Mg σ-bond,[116,117] three-coordinate magnesium(I) complexes supported by NacNac ligands (**V**) are powerful reducing agents.[118] Many diverse stoichiometric reductions across organic and inorganic chemistry have been reported.[118,119] One example of the reducing capability of **V** is in the isolation of diiminophosphinato Mg(I) species **W**, a compound not accessible by reduction of the corresponding LMgX species using traditional alkali metal reducing agents.[97] It was found to be facile when heated with ^{Mes}**V**, making the formation of **W** a formal Mg(I)/Mg(II) redox reaction.

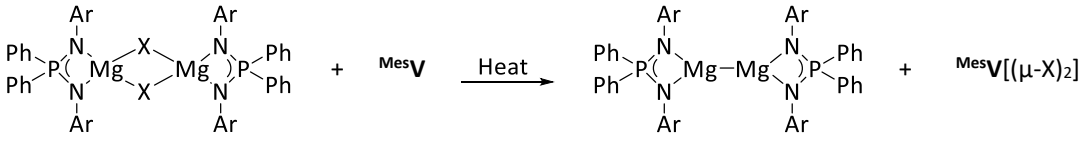

X = Br or I

W

Scheme 29 *Synthesis of diiminophosphinato magnesium(I) species via a Mg(I)/Mg(II) redox reaction.*

Of the structural diversity is seen in ligands capable of supporting a Mg-Mg bond, most are κ^2 monoanionic ligands which lead to three-coordinate Mg(I) centres. One notable exception is the bulky silyl amide derivative in Figure 10, which bears two-coordinate Mg(I) centres.[120]

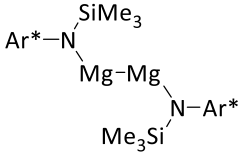

Figure 10 *A two-coordinate Mg-Mg has been reported. Ar* = $C_6H_2\{C(H)Ph_2\}_2{}^iPr$-2,6,4.*

1.4 Aims and Scope of this Work

The widespread implementation of transition metals in catalysis stems from their inherent redox flexibility allowing for reversible oxidative addition and reductive elimination reactivity. Whilst Al(I), in particular NacNacAl, has shown extensive oxidative addition reactivity, examples of reductive elimination remain limited. Understanding these latter scarce reports to allow the design of new aluminium systems specifically targeted at redox-type reactivity is one aim of this thesis. Alongside this, exploration of bond activation by $(Cp^*Al)_4$ will be investigated, both in the form of oxidative addition and reactions with unsaturated substrates.

Following this, the accompanying development of new ligand systems which can support reactive aluminium (and other main group) species will be explored. As amidine ligands are widely applied in organometallic chemistry, their phosphorus analogues will be specifically investigated.

The overall goal of this work is to expand the fledging field of low oxidation state aluminium chemistry by providing new reactivity of the prototypical example $(Cp^*Al)_4$, as well as building new frameworks which could support unusual, or perhaps even low valent, novel species.

1.5 References

1 M. J. Winter, *J. Chem. Educ.*, 2011, **88**, 1507–1510.

2 T. Bluemke, Y. H. Chen, S. Dagorne, M. Dieguez, V. A. D'yakonov, U. M. Dzhemilev, C. Fliedel, K. Groll, P. Knochel, A. Kolb, J. Lewinski, K. Maruoka, Y. Naganawa, O. Pamies, S. Schulz, P. von Zezschwitz, R. J. Wehmschulte and A. E. H. Wheatley, *Modern Organoaluminium Reagents: Preparation, Structure, Reactivity and Use*, Springer, Berlin, 2013.

3 S. C. Jha and N. N. Joshi, *Tetrahedron: Asymmetry*, 2001, **12**, 2463–2466.

4 C. C. Price, *Aromatic Compounds by the Friedel-Crafts Method*, 1946.

5 C. Dohmeier, D. Loos and H. Schnockel, *Angew. Chem. Int Ed. Engl.*, 1996, **35**, 129–149.

6 H. Schnoeckel and H. Kohnlein, *Polyhedron*, 2002, **21**, 489–501.

7 M. Huber, P. Henke and H. Schnöckel, *Chem. Eur. J.*, 2009, **15**, 12180–12183.

8 H. Schnöckel, *Z. Naturforsch. B31*, 1976, 1291–1292.

9 A. J. Downs, H. J. Himmel and L. Manceron, *Polyhedron*, 2002, **21**, 473–488.

10 H. J. Himmel and C. Klaus, *Zeitschrift fur Anorg. und Allg. Chemie*, 2003, **629**, 1477–1484.

11 M. Tacke and H. Schnoeckel, *Inorg. Chem.*, 1989, **28**, 2895–2896.

12 H. Schnockel, M. Leirnkuehler, R. Lotz and R. Mattes, *Angew. Chem. Int. Ed. Engl.*, 1986, **25**, 921–922.

13 C. Dohmeier, R. Mattes and H. Schnockelt, *J. Chem. Soc., Chem. Commun.*, 1990, 358–359.

14 C. Dohmeier, C. Robl, M. Tacke and H. Schnockel, *Angew. Chem. Int. Ed. Engl.*, 1991, **30**, 564–565.

15 A. Haaland, K.-G. Martinsen, S. A. Shlykov, H. V. Volden, C. Dohmeier and H. Schnockel, *Organometallics*, 1995, **14**, 3116–3119.

16 W. Uhl, *Naturwissenschaften*, 2004, **91**, 305–319.

17 A. Schnepf and H. Schnöckel, *Angew. Chem. Int. Ed.*, 2002, **41**, 3532–3552.

18 D. Bono, J. Hartig, M. Huber, H. Schnöckel and L. J. De Jongh, *J. Clust. Sci.*, 2007, **18**, 319–331.

19 J. Vollet, J. R. Hartig and H. Schnöckel, *Angew. Chem. Int. Ed.*, 2004, **43**, 3186–3189.

20 K. S. Williams and J. P. Hooper, 2011, 14100–14109.

21 H. Schnöckel and A. Schnepf, *Adv. Organomet. Chem.*, 2001, **47**, 235–281.

22 S. Schulz, H. W. Roesky, H. J. Koch, G. M. Sheldrick, D. Stalke and A. Kuhn, *Angew. Chem. Int. Ed. Engl.*, 1993, **32**, 1729–1731.

23 S. G. Minasian and J. Arnold, *Chem. Commun.*, 2008, 4043–4045.

24 E. P. Schram and N. Sudha, *Inorganica Chim. Acta*, 1991, **183**, 213–216.

25 C. Schnitter, H. W. Roesky, C. Röpken, R. Herbst-Irmer, H. G. Schmidt and M. Noltemeyer, *Angew. Chem. Int. Ed.*, 1998, **37**, 1952–1955.

26 A. Purath, C. Dohmeier, A. Ecker, H. Schnöckel, K. Amelunxen, T. Passler and N. Wiberg, *Organometallics*, 1998, **17**, 1894–1896.

27 A. Purath and H. Schnoeckel, *J. Org. Chem.*, 1999, **579**, 373–375.

28 C. Ganesamoorthy, S. Loerke, C. Gemel, P. Jerabek, M. Winter, G. Frenking and R. Fischer, *Chem. Commun.*, 2013, **49**, 2858–2860.

29 W. W. Tomlinson, D. H. Mayo, R. M. Wilson and J. P. Hooper, *J. Phys. Chem. A*, 2017, **121**, 4678–4687.

30 J. Gauss, U. Schneider, R. Ahlrichs, C. Dohmeier and H. Schnockel, *J. Am. Chem. Soc.*, 1993, **115**, 2402–2408.

31 A. C. Stelzer, P. Hrobárik, T. Braun, M. Kaupp and B. Braun-Cula, *Inorg. Chem.*, 2016, **55**, 4915–4923.

32 M. Huber and H. Schnöckel, *Inorganica Chim. Acta*, 2008, **361**, 457–461.

33 C. Dohmeier, H. Krautscheid and H. Schnöckel, *Angew. Chem. Int. Ed. Engl.*, 1994, **33**, 2482–2483.

34 J. Weiss, D. Stetzkamp, B. Nuber, R. A. Fischer, C. Boehme and G. Frenking, *Angew. Chemie Int. Ed. Engl.*, 1997, **36**, 70–72.

35 C. Üffing, A. Ecker, R. Köppe and H. Schnöckel, *Organometallics*, 1998, **17**, 2373–2375.

36 Q. Yu, A. Purath, A. Donchev and H. Schnoeckel, *J. Organomet. Chem.*, 1999, **584**, 94–97.

37 R. A. Fischer and J. Weiss, *Angew. Chem. Int. Ed.*, 1999, **98**, 2830–2850.

38 G. Linti and H. Schnöckel, *Coord. Chem. Rev.*, 2000, 285–319.
39 J. Weßing, C. Göbel, B. Weber, C. Gemel and R. A. Fischer, *Inorg. Chem.*, 2017, **56**, 3517–3525.
40 C. Cui, H. W. Roesky, H. Schmidt, M. Noltemeyer, H. Hao and F. Cimpoesu, *Angew. Chem. Int. Ed. Engl.*, 2000, **39**, 4274–4276.
41 W. W. Schoeller and G. D. Frey, *J. Organomet. Chem.*, 2013, **744**, 172–177.
42 X. Zhang and Z. Cao, *Dalton Trans.*, 2016, **45**, 10355–10365.
43 A. J. Arduengo, *Acc. Chem. Res.*, 1999, **32**, 913–921.
44 X. Li, X. Cheng, H. Song and C. Cui, *Organometallics*, 2007, **26**, 1039–1043.
45 J. Li, X. Li, W. Huang, H. Hu, J. Zhang and C. Cui, *Chem. Eur. J.*, 2012, **18**, 15263–15266.
46 T. Chu, S. F. Vyboishchikov, B. M. Gabidullin and G. I. Nikonov, *Inorg. Chem.*, 2017, **56**, 5993–5997.
47 T. Chu, S. F. Vyboishchikov, B. M. Gabidullin and G. I. Nikonov, *J. Am. Chem. Soc.*, 2017, **139**, 8804–8807.
48 Y. Wang, B. Quillian, P. Wei, C. S. Wannere, Y. Xie, R. B. King, H. F. Schaefer, P. R. Schleyer and G. H. Robinson, *J. Am. Chem. Soc.*, 2007, **129**, 12412–12413.
49 N. J. Hardman, R. J. Wright, A. D. Phillips and P. P. Power, *Angew. Chem. Int Ed.*, 2002, **41**, 2842–2844.
50 R. J. Wright, A. D. Phillips, N. J. Hardman and P. P. Power, *J. Am. Chem. Soc.*, 2002, **124**, 8538–8539.
51 R. J. Wright, A. D. Phillips, S. Hino and P. P. Power, *J. Am. Chem. Soc.*, 2005, **127**, 4794–4799.
52 C. Pluta, K. R. Poerschke, C. Krueger and K. Hildenbrand, *Angew. Chem. Int. Ed. Engl.*, 1993, **32**, 388–390.
53 W. Uhl, *Z. Naturforsch.*, 1988, **43b**, 1113–1118.
54 R. J. Wehmschulte, K. Ruhlandt-Senge, M. M. Olmstead, H. Hikon, B. E. Sturgeon and P. P. Power, *Inorg. Chem*, 1993, **32**, 2983–2984.
55 R. J. Wright, A. D. Phillips and P. P. Power, *J. Am. Chem. Soc*, 2003, **125**, 10784–10785.
56 T. Agou, K. Nagata and N. Tokitoh, *Angew. Chem. Int. Ed.*, 2013, **52**, 10818–10821.
57 R. J. Wright, M. Brynda and P. P. Power, *Angew. Chem. Int. Ed.*, 2006, **45**, 5953–5956.
58 P. Bag, A. Porzelt, P. J. Altmann and S. Inoue, *J. Am. Chem. Soc.*, 2017, **139**, 14384–14387.
59 Y. Wang, B. Quillian, P. Wei, Y. Xie, C. S. Wannere, R. B. King, H. F. Schaefer III, P. R. Schleyer and G. H. Robinson, *J. Am. Chem. Soc.*, 2008, **130**, 3298–3299.
60 J. Moilanen, P. P. Power and H. M. Tuononen, *Inorg. Chem.*, 2010, **49**, 10992–11000.
61 H. Schnöckel and H. Köhnlein, *Polyhedron*, 2002, **21**, 489–501.
62 H. Zhu, J. Chai, V. Jancik, H. W. Roesky, W. A. Merrill and P. P. Power, *J. Am. Chem. Soc.*, 2005, **127**, 10170–10171.
63 D. Weiss, T. Steinke, M. Winter, R. a. Fischer, N. Frohlich, J. Uddin and G. Frenking, *Organometallics*, 2000, **19**, 4583–4588.
64 J. D. Gorden, A. Voigt, C. L. B. Macdonald, J. S. Silverman and A. H. Cowley, *J. Am. Chem. Soc.*, 2000, 950–951.
65 J. D. Gorden, C. L. B. Macdonald and A. H. Cowley, *Chem. Commun.*, 2001, **997**, 75–76.
66 N. Wiberg, K. Amelunxen, T. Blank, H. No and D.- Mu, 1998, **751**, 5431–5433.
67 K. Nagata, T. Agou and N. Tokitoh, *Angew. Chem. Int. Ed.*, 2014, **53**, 3881–3884.
68 A. Kempter, C. Gemel and R. A. Fischer, *Chem. Eur. J.*, 2007, **13**, 2990–3000.
69 H. J. Himmel and J. Vollet, *Organometallics*, 2002, **21**, 5972–5977.
70 T. Chu, I. Korobkov and G. I. Nikonov, *J. Am. Chem. Soc.*, 2014, **136**, 9195–9202.
71 C. Ganesamoorthy, D. Bläser, C. Wölper and S. Schulz, *Angew. Chem. Int. Ed.*, 2014, **53**, 11587–11591.
72 M. R. Crimmin, M. J. Butler and A. J. P. White, *Chem. Commun.*, 2015, **51**, 15994–15996.
73 T. Chu, Y. Boyko, I. Korobkov and G. I. Nikonov, *Organometallics*, 2015, **34**, 5363–5365.
74 G. D. Frey, V. Lavallo, B. Donnadieu, W. W. Schoeller and G. Bertrand, *Science*, 2007, **316**, 439–442.
75 Y. García-Rodeja, F. M. Bickelhaupt and I. Fernández, *Chem. Eur. J.*, 2016, **22**, 13669–13676.

76 C. E. Pitsch and X. Wang, *Chem. Commun.*, 2017, **53**, 8196–8198.
77 T. Chu, I. Korobkov and G. I. Nikonov, *J. Am. Chem. Soc.*, 2014, **136**, 9195–9202
78 H. W. Roesky, B. Li, S. Kundu, H. Zhu, H. Keil, R. Herbst-Irmer, D. Stalke, G. Frenking and D. M. Andrada, *Chem. Commun.*, 2017, **53**, 2543-2546
79 B. H. Schnockel, M. Leirnkuehler, R. Lotz and R. Mattes, *Angew. Chem. Int. Ed. Engl.*, 1986, **25**, 921–922.
80 C. Üffing, A. Ecker, R. Köppe, K. Merzweiler and H. Schnöckel, *Chem. Eur. J.*, 1998, **4**, 2142–2147.
81 R. Ahlrichs, M. Häser, H. Schnöckel and M. Tacke, *Chem. Phys. Lett.*, 1989, **154**, 104–110.
82 B. Buchin, T. Steinke, C. Gemel, T. Cadenbach and R. A. Fischer, *Zeitschrift fur Anorg. und Allg. Chemie*, 2005, **631**, 2756–2762.
83 H. Zhu, R. B. Oswald, H. Fan, H. W. Roesky, Q. Ma, Z. Yang, H. Schmidt, M. Noltemeyer, K. Starke and N. S. Hosmane, *J. Am. Chem. Soc.*, 2006, **128**, 5100–5108.
84 C. Cui, S. Koepke, R. Herbst-Irmer, H. W. Roesky, M. Noltemeyer, H.-G. Schmidt and B. Wrackmeyer, *J. Am. Chem. Soc.*, 2001, **123**, 9091–9098.
85 T. Agou, K. Nagata, T. Sasamori and N. Tokitoh, *Chem. Asian J.*, 2014, **9**, 3099–4101.
86 M. S. Hill, D. J. Liptrot, C. Weetman and M. S. Hill, *Chem. Soc. Rev.*, 2016, **45**, 972–988.
87 R. Rochat, M. J. Lopez, H. Tsurugi and K. Mashima, *ChemCatChem*, 2016, **81**, 10–20.
88 G. W. Coates, *Dalton Trans.*, 2002, 467–475.
89 C. A. Wheaton, P. G. Hayes and B. J. Ireland, *Dalton Trans.*, 2009, 4832–4846.
90 M. J. Stanford and A. P. Dove, *Chem. Soc. Rev.*, 2010, 486–494.
91 *Magnesium (in Biological Systems)*, Van Nostrand's Scientific Encyclopedia, 2006.
92 K. Madhavan Nampoothiri, N. R. Nair and R. P. John, *Bioresour. Technol.*, 2010, **101**, 8493–8501.
93 S. Agarwal, J. Curtin, B. Duffy and S. Jaiswal, *Mater. Sci. Eng. C*, 2016, **68**, 948–963.
94 M. H. Chisholm, J. C. Gallucci and K. Phomphrai, *Inorg. Chem.*, 2005, **44**, 8004–8010.
95 B. M. Chamberlain, M. Cheng, D. R. Moore, T. M. Ovitt, E. B. Lobkovsky and G. W. Coates, *J. Am. Chem. Soc*, 2001, **123**, 3229–3238.
96 H. Xie, Z. Mou, B. Liu, P. Li, W. Rong, S. Li and D. Cui, *Organometallics*, 2014, **33**, 722–730.
97 A. Stasch, *Angew. Chem. Int. Ed.*, 2014, **53**, 10200–10203.
98 C. N. Ayala, M. H. Chisholm, J. C. Gallucci and C. Krempner, *Dalton Trans.*, 2009, 9237–9245.
99 S. J. Bonyhady, C. Jones, S. Nembenna, A. Stasch, A. J. Edwards and G. J. McIntyre, *Chem. Eur. J.*, 2010, **16**, 938–955.
100 M. H. Chisholm, K. Choojun, J. C. Gallucci and P. M. Wambua, *Chem. Sci.*, 2012, 3445–3457.
101 A. J. Boutland, D. Dange, A. Stasch, L. Maron and C. Jones, *Angew. Chem. Int.*, 2016, **55**, 9239–9243.
102 A. R. Sadique, M. J. Heeg and C. H. Winter, *Inorg. Chem.*, 2001, **40**, 6349–6355.
103 N. Nimitsiriwat, V. C. Gibson, E. L. Marshall, P. Takolpuckdee, A. K. Tomov, A. J. P. White, D. J. Williams, M. R. J. Elsegood, S. H. Dale and L. Le, *Inorg. Chem.*, 2007, **46**, 9988–9997.
104 G. J. Moxey, F. Ortu, L. G. Sidley, H. N. Strandberg, A. J. Blake, W. Lewis and D. L. Kays, *Dalton Trans.*, 2014, **43**, 4838–4846.
105 M. Arrowsmith, M. S. Hill, T. Hadlington, G. Kociok-Köhn and C. Weetman, *Organometallics*, 2011, **30**, 5556–5559.
106 M. Arrowsmith, M. S. Hill and G. Kociok-Köhn, *Chem. Eur. J.*, 2013, **19**, 2776–2783.
107 M. S. Hill, D. J. Macdougall and M. F. Mahon, *Dalton Trans.*, 2010, **39**, 11129–11131.
108 M. D. Anker, M. S. Hill, J. P. Lowe and M. F. Mahon, *Angew. Chem. Int Ed.*, 2015, **54**, 10009–10011.
109 M. D. Anker, C. E. Kefalidis, Y. Yang, J. Fang, M. S. Hill, M. F. Mahon and L. Maron, *J. Am. Chem. Soc.*, 2017, **139**, 10036–10054.
110 Y. Yang, M. D. Anker, J. Fang, M. F. Mahon, L. Maron, C. Weetman and M. S. Hill, *Chem. Sci.*, 2017, **8**, 3529–3537.
111 M. Arrowsmith, B. Maitland, G. Kociok-Köhn, A. Stasch, C. Jones and M. S. Hill, *Inorg. Chem.*, 2014, **53**, 10543–10552.

112 S. P. Green, C. Jones and A. Stasch, *Science*, 2007, **318**, 1754–1757.
113 R. Köppe, P. Henke and H. Schnöckel, *Angew. Chem. Int. Ed.*, 2008, **47**, 8740–8744.
114 Y. Liu, S. Li, X.-J. Yang, P. Yang and B. Wu, *J. Am. Chem. Soc.*, 2009, **131**, 4210–4211.
115 A. J. Boutland, I. Pernik, A. Stasch and C. Jones, *Chem. Eur. J.*, 2015, **21**, 15749–15758.
116 J. Overgaard, C. Jones, A. Stasch and B. B. Iversen, *J. Am. Chem. Soc.*, 2009, **131**, 4208–4209.
117 J. A. Platts, J. Overgaard, C. Jones, B. B. Iversen and A. Stasch, *J. Phys. Chem. A*, 2011, **115**, 194–200.
118 C. Jones, *Nat. Rev. Chem.*, 2017, 1-9.
119 A. Stasch and C. Jones, *Dalton Trans.*, 2011, **40**, 5659-5672
120 A. J. Boutland, D. Dange, A. Stasch, L. Maron and C. Jones, *Angew. Chem. Int. Ed.*, 2016, **55**, 9239-9243

Chapter 2:

Understanding Reductive Elimination from Al(III)

2. Understanding Reductive Elimination from Al(III)

2.1 Reductive Elimination of Cp*H from Cp^*_2AlH

The redox flexibility of transition metals is central to their widespread use in bond forming catalysis. Oxidative addition and reductive elimination reactions are common, and their application in redox-cycle catalysis is extensive. Applying this type of reactivity to main-group chemistry is more challenging - there is a strong preference for an element to remain in a single oxidation state. Low oxidation state compounds of the lighter main-group elements are highly reactive, frequently undergoing unwanted transformations such as disproportionation. Still, much effort has been expended into developing oxidative addition, and to a lesser extent reductive elimination reactivity with main-group complexes.[1]

Whilst a I/III redox pair exists for aluminium, accessing the lower oxidation state is hindered by its favourable disproportionation to Al(0) and Al(III) (section 1.1.1). Thus using reductive elimination to form the rare Al(I) oxidation state, whilst also performing a bond-forming process seems highly challenging from a thermodynamic viewpoint. The thermal degradation of the common laboratory reagent $LiAlH_4$ has been shown to be a formal reductive elimination with respect to aluminium.[2,3] Two instances of Cp*H (Cp* = 1,2,3,4,5-pentamethylcyclopentadienyl) reductive elimination from an aluminium centre were reported by Fischer in 2013.[4]

$$Cp^*AlH_2 \longrightarrow Al + Cp^*H + 0.5\ H_2$$

$$Cp^*_2AlH \rightleftharpoons 0.25\ (Cp^*Al)_4 + Cp^*H$$

Scheme 30 *Reductive elimination of a C-H bond from Al(III) complexes*

From Cp^*AlH_2, the isolated products of reductive elimination are Cp*H, H_2 and elemental aluminium, the latter products due to proposed decomposition of Al-H immediately after its formation.[5] Cp*H is eliminated from Cp^*_2AlH to form the low oxidation state species $(Cp^*Al)_4$, isolated in almost quantitative yield. Using this report as a starting point, this chapter investigates reductive elimination of C-H bonds from tri-valent aluminium complexes, as understanding this process will aid the future design of compounds capable of this unusual reactivity.

2.1.1 NMR Evidence for a True Equilibrium

Reductive elimination of Cp*H from Cp*$_2$AlH **1** forms the prototypical low valent aluminium species (Cp*Al)$_4$ **2**, isolated in yields as high as 93%.[4] The elimination process is reported to be an exergonic thermal equilibrium (calculated ΔG_{298} = -15.5 kJ mol^{-1}), overall favouring the formation of the **2**.

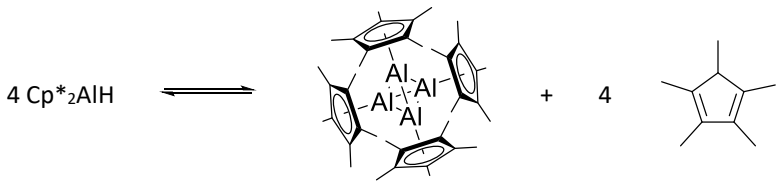

1 **2**

Scheme 31 *Fischer's equilibrium of Cp*$_2$AlH with Cp*H and Cp*Al*

To experimentally demonstrate this thermal equilibrium, variable temperature ^{1}H NMR spectroscopy was used to monitor a sample of **1** as it was heated to 100°C, and then cooled in a stepwise fashion (Figure 11). At the peak temperature, a single singlet is observed at δ = 1.89 corresponding to (Cp*Al)$_4$ **2**. Integration of the other signals confirms one equivalent of Cp*H in the remainder of the sample, indicating full conversion of Cp*$_2$AlH to Cp*Al and Cp*H.

When the sample is returned to 30 °C, Cp*$_2$AlH is not completely regenerated. Two sets of signals are present corresponding to **1** and **2** + Cp*H. It is reasonable that oxidative addition of Cp*H only occurs to monomeric Cp*Al, and cooling the reaction causing tetramerization, thus limiting formation of **1** at 30 °C.

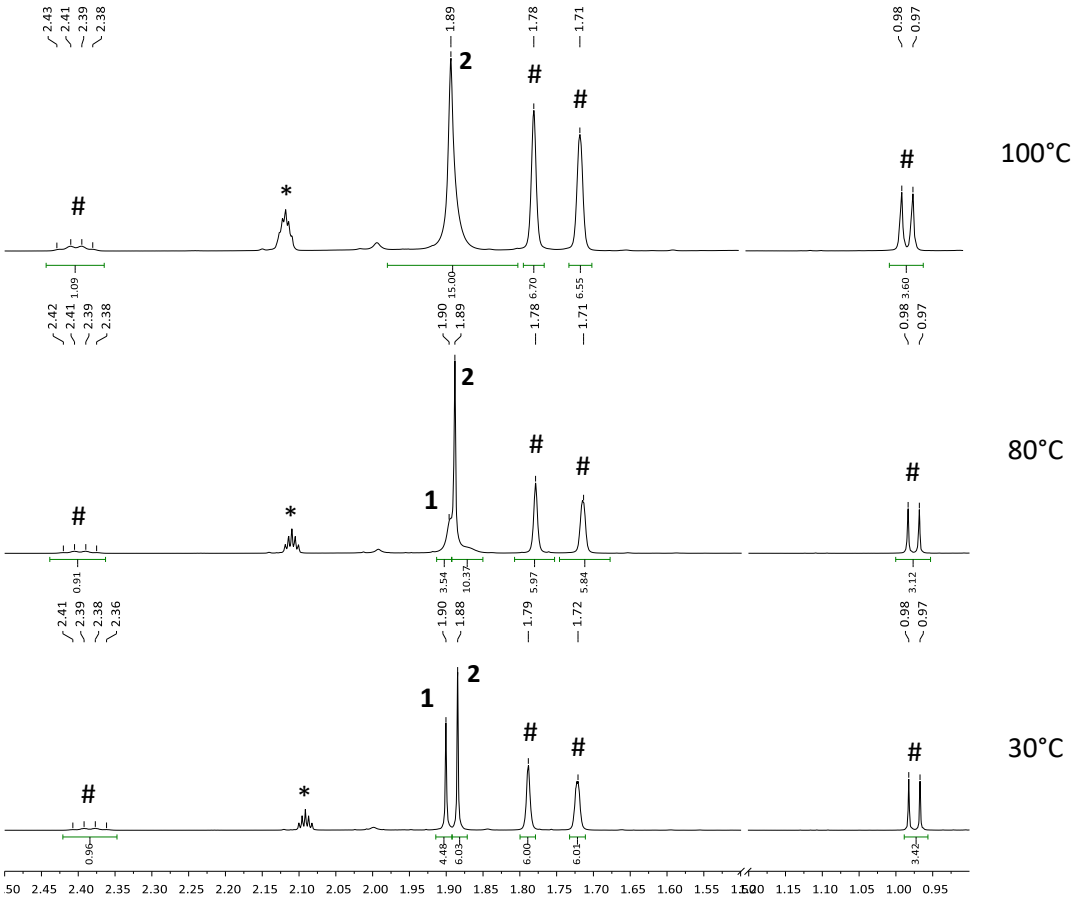

Figure 11 *^{1}H Variable temperature NMR (tol-d_8, 500 MHz) cooling Cp^*_2AlH from 100 °C to 30 °C. Chemical shift referenced to an internal standard of tritertbutylbenzene (δ = 1.34). Spectrum omitted between δ = 1.50-1.20. Residual tol-d_8 signal denoted *. Cp*H denoted #.*

Dissociation of $(Cp^*Al)_4$ at high temperature forms monomeric Cp*Al, which can be observed by acquiring ^{27}Al NMR spectra at high temperatures.[6–8] The appearance of a signal at ^{27}Al δ = - 149 at elevated temperature is indicative of monomer formation, considerably upfield of tetrameric **2** at ^{27}Al δ = - 79.[7]

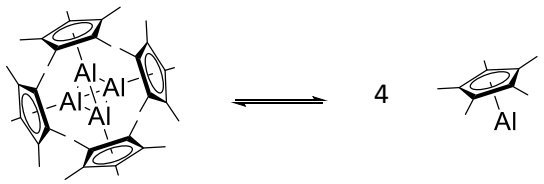

^{27}Al δ = -79 **2** ^{27}Al δ = -149 **2^m**

Scheme 32 *Thermal equilibrium of tetrameric and monomeric Cp*Al.*

This equilibrium has been disputed,[9] and so as part of this work, a sample of **2** was suspended in tol-d_8 and a ^{27}Al NMR spectrum was acquired at 353 K (Scheme 32). This spectrum shows formation of monomeric **2^m** as a signal at δ = - 149.

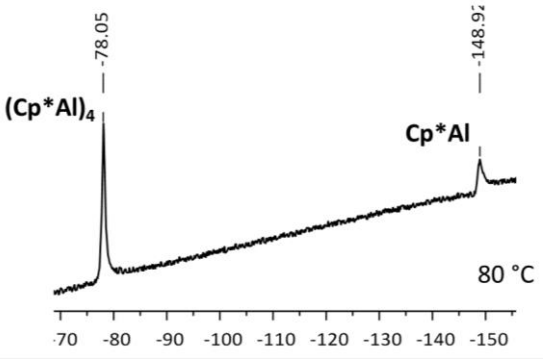

Figure 12 *^{27}Al NMR (tol-d_8, 130 MHz, 353 K) spectroscopy shows the formation of monomeric Cp*Al. Baseline shape is due to interference from aluminium in the NMR probe.*

2.1.2 Estimation of Kinetic Parameters of Reductive Elimination

In order to gain some insight into the mechanism of reductive elimination of Cp*H from Cp^*_2AlH, the kinetics of this reaction were investigated using ^1H NMR spectroscopy. The considered equilibrium is shown in Scheme 33. An important assumption made in these experiments is that the barrier to tetramerisation of Cp*Al **2^m** to form $(Cp^*Al)_4$ **2** is insignificant compared to the barrier to reductive elimination. It was shown in section 2.1.1 that under the same conditions as Cp*H reductive elimination, monomeric Cp*Al is in equilibrium with $(Cp^*Al)_4$. Thermodynamically, tetramerisation of Cp*Al to $(Cp^*Al)_4$ is favourable, with tetramerisation energy of -150 ± 20 kJ mol^{-1} estimated using variable temperature ^{27}Al NMR spectroscopy.[7]

1 **2^m**

Scheme 33 *Equilibrium to be examined*

To investigate the rate of the reaction depicted in Scheme 33, the reductive elimination was followed by ^1H NMR spectroscopy. Solutions with a known starting concentration of **1** were monitored over time using ^1H NMR spectroscopy at a range of temperatures. The concentration of Cp*H at each time point was calculated by integral comparison with a tritertbutyl benzene internal standard. This concentration can be compared with the initial concentration of **1** to give a value for conversion, an example of which is shown in Figure 13 (full reaction profiles in section 7.2.1).

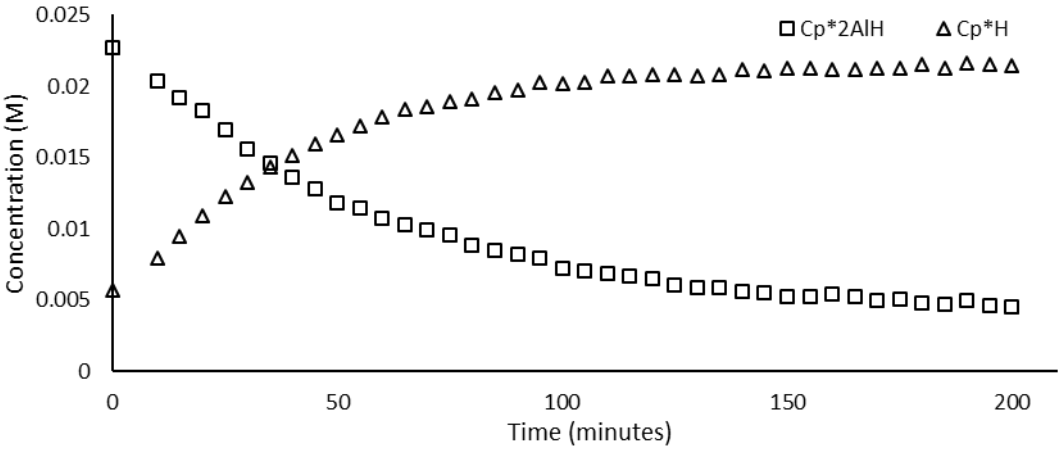

Figure 13 *An example of a reaction profile showing the progress of reductive elimination at 353 K*

Using this concentration data and the kinetics software DYNAFIT,[10] rate constants for reductive elimination (k_1) and oxidative addition (k_2) were estimated, which are listed in Table 1. A stable k_2 value for 313 K could not be reached using this method.

Temperature	k_1 (x 10^{-4})	k_2 (x 10^{-4})
313 K	1.9 ± 0.02	---
323 K	5.6± 0.1	120 ± 20
333 K	14.6 ± 0.4	350 ± 40
343 K	60.0 ± 3.0	1100 ± 100
353 K	176.0 ± 8	2300 ± 300

Table 1 *Calculated rate constants for the reductive elimination equilibrium*

Given that the k_2 values are two orders of magnitude higher than that of the values for k_1, oxidative addition occurs at a much faster rate than reductive elimination. This observation was anticipated; Al(I) is highly reactive as this oxidation state is inherently less stable than the Al(III) oxidation state for aluminium (section 1.1.1). The sluggish reductive elimination is suggestive of either an endothermic reaction, where the formation of **1** is lower in energy than formation of $\mathbf{2^m}$ and Cp*H, or a very high activation barrier for reductive elimination.

Using the obtained values for rate constants k_1 and k_2, plots fitting the linear Eyring equation (1) were constructed, allowing for several reaction parameters to be determined.

The Eyring equation is not influenced by collision theory, unlike the widely used Arrhenius equation.

$$\ln\frac{k}{T} = \frac{-\Delta H^{\neq}}{R}\frac{1}{T} + \ln\frac{k_B}{h} + \frac{\Delta S^{\neq}}{R} \qquad (1)$$

Eyring plots from the reductive elimination (k_1) and oxidative addition (k_2) reactions are shown in Figure 14 and Figure 15 respectively. A weighted least squares regression demonstrates good linear correlation in both cases, with R^2 values of 0.990 and 0.987. The regression gradient gives an estimated enthalpy of activation ($\Delta H^{\neq}$) for reductive elimination of 95.53 ± 4.74 kJ mol^{-1}.

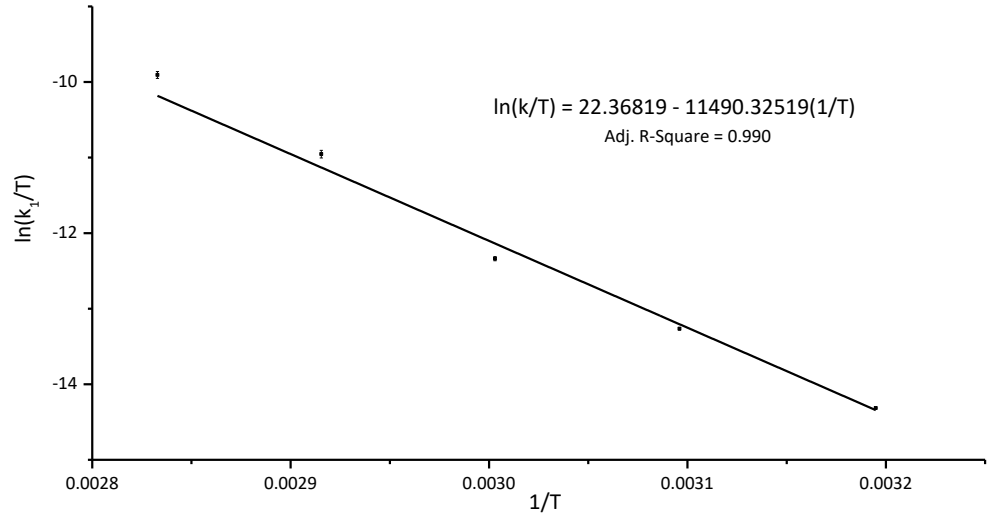

Figure 14 *Eyring plot for the reductive elimination of Cp*H from Cp*$_2$AlH in tol-d$_8$. Gradient standard error 570.51506, intercept standard error 1.7892*

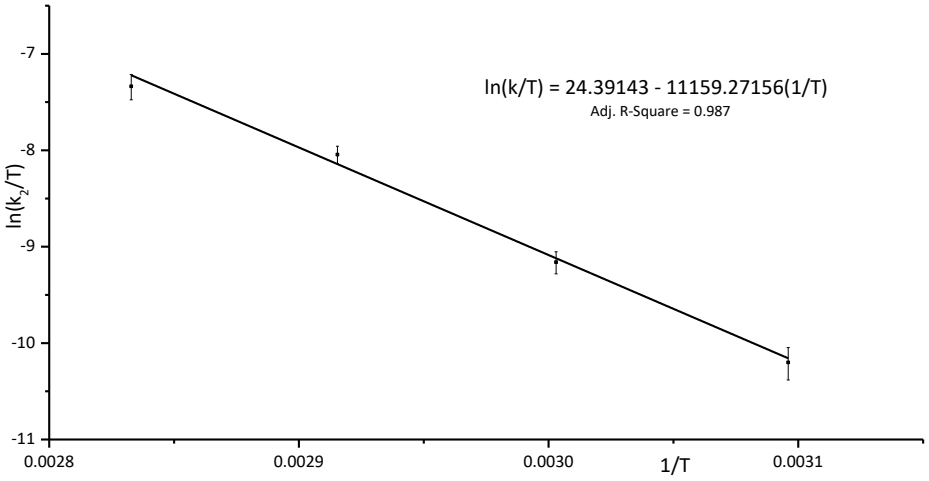

Figure 15 *Eyring plot for the oxidative addition of Cp*H to Cp*Al in tol-d_8. Gradient standard error 733.13411, intercept standard error 2.15979. As there are only four data points estimations based on this regression are less accurate.*

Examination of the y-intercept of the regression in Figure 14 gives a negligible estimated entropy of activation ($\Delta S^{\neq}$) for reductive elimination of -0.167 ± 2.64 kJ mol^{-1}. Given the comparatively large error on this value, no conclusions can be drawn from this value regarding the direction in which the entropy lies. A small value for this parameter is suggestive of a mechanism up to the rate determining step which is unimolecular.

An estimation of the enthalpy of activation ($\Delta H^{\neq}$) of the oxidative addition of Cp*H to Cp*Al of 92.78 ± 6.09 kJ mol^{-1} is found from the gradient of the regression in Figure 15. The magnitude of this value hints at an overall endothermic process, as it is smaller than $\Delta H^{\neq}$ for reductive elimination. The estimated $\Delta S^{\neq}$ is again negligible, at 0.0759 ± 2.59 J mol^{-1}. Table 2 summarises the values estimated by analysis of rate constants k_1 and k_2. The Gibbs energy of activation ($\Delta G^{\neq}_{300}$) describes the energy required of the starting material **1** to reach its transition state. A value of 95.48 ± 3.95 kJ mol^{-1} is consistent with a reaction which occurs at elevated temperatures.

Parameter	Reductive Elimination	Oxidative Addition
$\Delta H^{\neq}$	95.53 ± 4.74 kJ mol^{-1}	92.78 ± 6.09 kJ mol^{-1}
$\Delta S^{\neq}$	-0.167 ± 2.64 J mol^{-1}	0.0759 ± 2.59 J mol^{-1}
$\Delta G^{\neq}_{300}$	95.48 ± 3.95 kJ mol^{-1}	92.80 ± 5.32 kJ mol^{-1}

Table 2 *Summary of kinetic values calculated using Eyring plots*

2.1.3 Estimation of Thermodynamic Parameters of Reductive Elimination

The thermodynamic properties of the reaction at equilibrium can be estimated by using the same *in situ* ^{1}H NMR spectroscopic techniques, and would show whether the starting hydride or resulting low oxidation state aluminium complex is favoured. Solutions of Cp^*_2AlH **1** in tol-d_8 were heated to various temperatures inside an NMR spectrometer until they were observed to reach a stable equilibrium. An average of the ^{1}H NMR integrals of many spectra acquired at equilibrium allow the average final conversion to Cp*H to be determined. Hence the equilibrium constant K_{eq} can be calculated using equation (2).

$$K_{eq} = \frac{[Cp^*H][Cp^*Al]}{[Cp^*_2AlH]} \qquad (2)$$

The resulting K_{eq} values are listed Table 3. Reactions performed below 333 K were found to be very slow, and still had not reached equilibrium after 36 hours, hence their omission here. A value for K_{eq} is could not be calculated at 373 K as the equilibrium gives 100 % Cp*H and Cp*Al at this temperature (section 2.1.1, Figure 11).

Temperature	K_{eq} (x 10^{-3})	k_1/k_2 (x 10^{-3})
333 K	40.170 ± 1.912	41.7
343 K	75.649 ± 3.856	54.5
353 K	145.548 ± 7.137	76.5
363 K	216.573 ± 12.833	---

Table 3 *Calculated equilibrium constants for the reductive elimination equilibrium*

The values of K_{eq} were fitted to the van't Hoff equation (3). The natural log of K_{eq} shows a strong negative correlation with reciprocal temperature, with an R^2 value of 0.989 in Figure 16. The negative gradient of this regression line immediately indicates that the reductive elimination of Cp*H from Cp^*_2AlH is an endothermic, non-spontaneous process.

$$\ln K_{eq} = \frac{-\Delta H}{RT} + \frac{\Delta S}{R} \qquad (3)$$

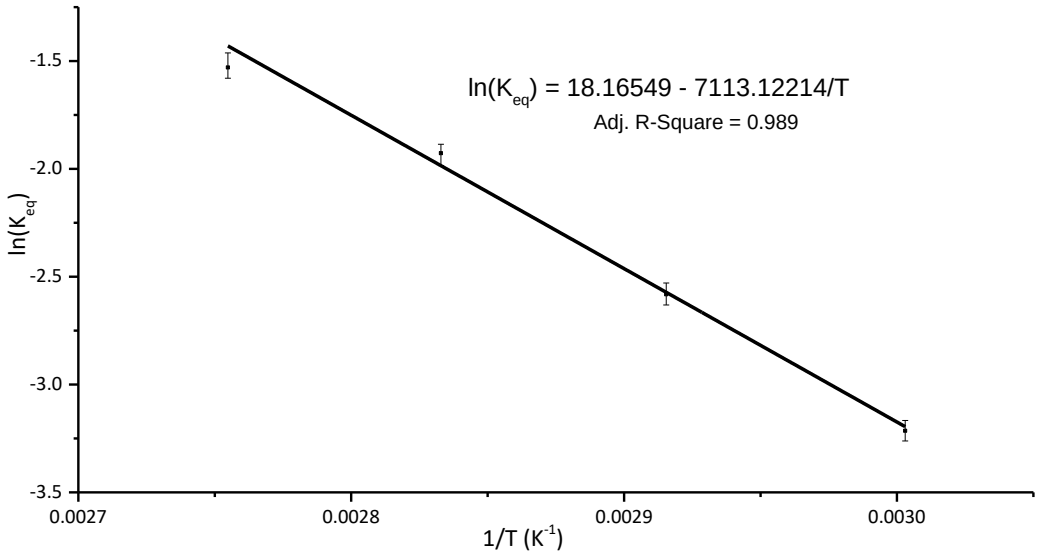

Figure 16 *Van't Hoff plot for the equilibrium of Cp*H and Cp*Al with Cp*$_2$AlH in tol-d$_8$ using the equilibrium constants K_{eq}. Line calculated using weighted least squares regression. Gradient standard error 430.32089, intercept standard error 1.24294.*

From the value of this negative gradient, the enthalpy of reductive elimination (ΔH) is estimated to be 59.14 ± 3.58 kJ mol^{-1} and an estimated reaction entropy (ΔS) of 151.04 ± 10.33 J mol^{-1}.

Using these values for ΔH and ΔS, the overall Gibbs free energy of reaction can be estimated using equation (4). The value at 300 K, ΔG_{300}, was estimated at 13.83 ± 0.48 kJ mol^{-1}. Therefore, the reductive elimination of Cp*H from Cp*$_2$AlH is an endothermic process.

$$\Delta G = \Delta H - T\Delta S \qquad (4)$$

Whilst an endothermic equilibrium was anticipated (the reduction from Al^{III} to Al^{I} is known to be unfavourable), it is in contrast with the same value calculated in Fischer's initial report. Using density functional theory (DFT) methods, it was reported that the equilibrium in Scheme 34 is exergonic, ΔG_{298} = -15.5 kJ mol^{-1} at the BP86/TZVPP level of theory.[4]

2.1.4 Calculation of a transition state and reaction parameters

All computations were carried out by Dr David Rogers in Edinburgh.

To probe the reductive elimination of Cp*H from Cp^*_2AlH (**1**) further, density functional theory (DFT) was employed to give insights into the mechanism. Initially, the geometries of the starting aluminium hydride **1**, and the reaction products Cp*H and Cp*Al were optimised using BP86/def2-SVP, shown in Scheme 34.

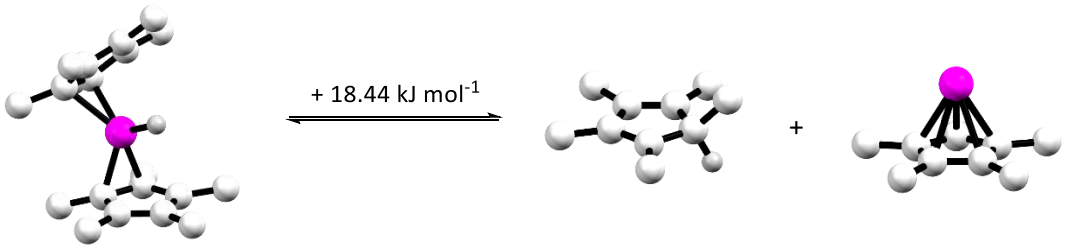

1# **2**#

Scheme 34 *Geometry optimised structures (BP86/def2-SVP) of Cp_2^*AlH (**1**), Cp*H and monomeric Cp*Al (**2.2**). Hydrogens (except the reacting hydrogen) are omitted for clarity*

Differences are noted between the reported solid-state structure of **1** and optimised structure **1**#. Most notably, in **1**# both Cp* rings have adopted an η^2 hapticity where in **1** they are coordinated in a η^2/η^3 fashion. This lower hapticity in **1**# was concluded based on the Al-C interatomic distances. Distances denoted with bonds for **1**# in Scheme 34 lie between 2.167 Å and 2.271 Å, where the next shortest Al-C distance is much longer, at 2.582 Å. In the solid-state structure of **1** all five Al-C bond lengths (2 from one ligand, and 3 from the other) are between 2.1504(16) Å and 2.3361(17) Å.

The Gibbs free energy of transforming reactant **1**# into products **2**# and Cp*H was found to be +18.44 kJ mol^{-1} (energies calculated BP86/TZVPP level using BP86/def2-SVP optimised geometries), indicating an endergonic process. This agrees well with the experimentally determined values for the Gibbs free energy in section 2.1.3, ΔG = 13.83 ± 0.48 kJ mol^{-1}, also indicating an overall endothermic process. As previous discussed, this differs with the reported value ΔG_{298} = -15.5 kJ mol^{-1}, calculated at the same level of theory used here (BP86/TZVPP).[4] The geometry optimised structure **1**# has a slightly different bonding situation between the aluminium and Cp* ligands to the reported solid-state structure. The

reported optimised structure is very comparable with **1**$^{\#}$, also featuring η^2 bonded Cp* ligands, with Al-C bond lengths ranging between 2.149 Å and 2.267 Å. The energy values in both cases were treated with a zero-point energy correction, perhaps providing a source of the disparity in the final values. As an endothermic equilibrium for reductive elimination was shown experimentally in section 2.1.3, it supports the positive value calculated.

Encouraged by the close agreement of the thermodynamic values determined, a transition state search at the BP86/def2-SVP level was undertaken. This identified **TS$_{1\text{-}2}$** as facilitating the transformation of **1**$^{\#}$ to **2**$^{\#}$ and Cp*H. The geometry optimised structure is shown in Figure 17, identified as a transition state by possession of one imaginary frequency at 724i.

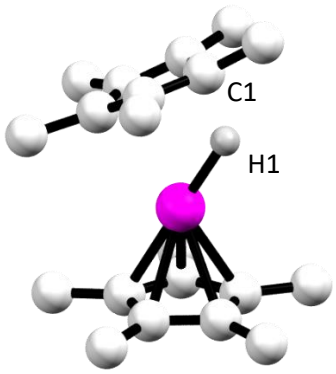

Figure 17 *Geometry optimised transition state* ***TS$_{1\text{-}2}$*** *(BP86/def2-SVP). Hydrogen atoms (apart from Al-H) omitted for clarity*

The most noticeable change is in the coordination modes of the Cp* rings. Where in the starting material **1**$^{\#}$ they both exhibit η^2 hapticity, in **TS$_{1\text{-}2}$** one Cp* ligand has begun to dissociate from the aluminium centre (Average Al-C: 2.879 Å) whilst the other has switched to η^5 hapticity. This latter haptotropic shift has aromatised the Cp* ligand,[11] possibly providing an energy offset for the unfavourable formation of a low oxidation state aluminium centre (Al^{III} to Al^{I}). **TS$_{1\text{-}2}$** could be considered as $[Cp^*AlH]^+[Cp^*]^-$.

Inspection of the Al-C bond lengths of the η^5 Cp* ligand in **TS$_{1\text{-}2}$** reveals that they are very similar to the Al-C bond lengths in **2**$^{\#}$ (Average Al-C **TS$_{1\text{-}2}$**: 2.358 Å; **2**$^{\#}$: 2.355 Å); the bonds for the low valent aluminium moiety are a constitute part of the transition state.

An increase in the Al-H bond length in **$TS_{1\text{-}2}$** (**$1^{\#}$**: 1.579 Å; **$TS_{1\text{-}2}$**: 1.837 Å) indicates weakening of the Al-H bond in **$TS_{1\text{-}2}$**. Comparison of the natural population analysis (NPA) charges show that this hydrogen also becomes less hydridic in the transition state, with the charge increasing from -0.373 in **$1^{\#}$** to -0.049 in **$TS_{1\text{-}2}$**. Looking closely at the dissociated Cp* ring a possible C-H interaction is identified, with an inter-atomic distance of C1-H1 1.461 Å as depicted in Figure 17. Coupling the observations of a less hydridic character with this C-H interaction, it is clear that the departing $[Cp^*]^-$ ring can deprotonate the $[Cp^*AlH]^+$ moiety, resulting in the formation Cp*H and Cp*Al.

Using **$TS_{1\text{-}2}$** the activation energy of reductive elimination (E_a^{RE}) from **$1^{\#}$** was calculated, and found to be 91.54 kJ mol^{-1} (BP86/TZVPP). This agrees well with the experimentally determined value from section 2.1.2 of 95.48 ± 4.74 kJ mol^{-1}, indicating the formation of **$TS_{1\text{-}2}$** is likely the reaction pathway taken by **1** to transform into **2** and Cp*H upon heating.

2.1.5 Summary of Mechanism and its Implications in Ligand Design

Combining the experimentally estimated parameters from section 2.1.2 and calculated transition state from section 2.1.4, a proposed mechanism for the reductive elimination of Cp*H from Cp^*_2AlH is shown in Scheme 35.

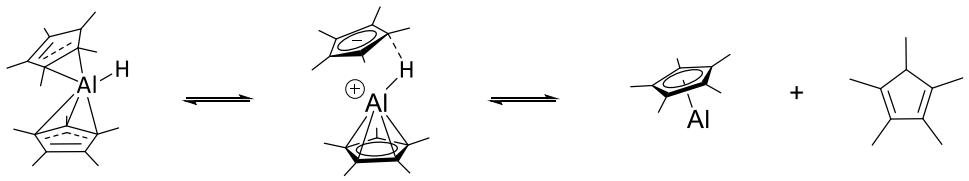

1 **$TS_{1\text{-}2}$** **2**

Scheme 35 *Mechanism of reductive elimination of Cp^*_2AlH*

This mechanism fits well with the calculated mechanism of oxidative addition of Cp*H to NacNacAl[12] (reported immediately prior to the submission of this work for publication), which is shown to proceed through a transition state similar to that of **$TS_{1\text{-}2}$**.

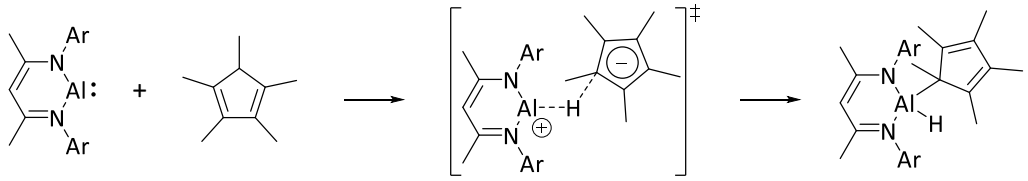

Scheme 36 *Calculated mechanism of the oxidative addition of Cp*H to NacNacAl[12]*

The ability of the Cp* ligand to undergo haptotropic shifts to higher coordination modes, which allows the formation of **$TS_{1\text{-}2}$**, is clearly important in the reductive elimination. Another important property of the Cp* ligand is that its anion is basic enough to deprotonate the Al^+ centre in **$TS_{1\text{-}2}$**, thus forming Cp*H and the low oxidation state aluminium centre. It is the combination of these two properties which enables this remarkable reaction to occur.

Evidently, the consideration of ligand properties will be vital to the future design of aluminium systems capable of reductive elimination to form low oxidation state centres. The idea of energy gain from haptotropic shift could be applied more generally to include other structural changes, such as a denticity shift to create a chelating coordination mode.

2.2 Tetrahedral Aluminium Centres Prevent Reductive Elimination

Tri-valent compounds of group 13 elements in the +3 oxidation are excellent Lewis acids, due to their characteristic empty p-orbital readily accepting non-bonding electron density. A large-scale use of aluminium chloride utilises this reactivity in Friedel-Crafts reaction of benzene and phosgene to form anthraquinone, where $AlCl_3$ uses its Lewis acidity to abstract a chloride from the phosgene.[13] The coordination of external Lewis bases to form Lewis adducts is facile in the case of group 13 compounds.

N-heterocyclic carbenes (NHCs) are Lewis bases which are strong σ-donors and weak π-acceptors, their use in group 13 chemistry is extensive.[14] Examples of NHC-coordinated alkyl,[15] halo[16–18] and hydro[18–20] aluminium(III) complexes are reported, where the metal centre is commonly tetrahedral. Beyond the formation of simple adducts, NHCs have been used to stabilise both Al(II)[20] and Al(I),[18,21] including the very recent report of the first isolable dialumene by Inoue.[21]

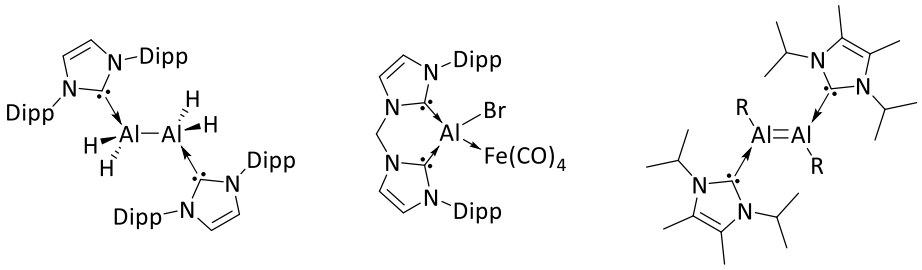

Figure 18 *Low oxidation state aluminium compounds stabilised by NHCs[18,21,22] R = Si(tBu)2Me. Dipp = 2,6-diisopropylphenyl*

The presence of an external base promotes reductive elimination from trihydrostannanes,[22,23] as it allows the metal centre to first be deprotonated. Given the demonstrated importance of deprotonation in the mechanism of Cp*H elimination from Cp^*_2AlH, the effect of NHCs on the reductive elimination was investigated.

2.2.1 Coordination of Lewis Bases to Cp$_2$AlH*

Addition of tetramethylimadzolylidene (^{Me}IMe) to a C_6D_6 solution of Cp*$_2$AlH **1** results in the formation of the simple Lewis base adduct **3**. Coordination of the NHC to the metal centre causes only marginal shift in the singlet signal associated with the Cp* groups, from δ = 1.91 for Cp*$_2$AlH[4] to δ = 1.98 in adduct **3**. The signals associated with the NHC in **1** are shifted significantly from their uncoordinated values.[24] All four methyl groups are now inequivalent, with the alkene methyl groups seen at δ = 3.27 and 2.64, and the nitrogen methyl groups at δ = 1.29 and 1.15 (uncoordinated NHC δ = 3.35 and 1.59).

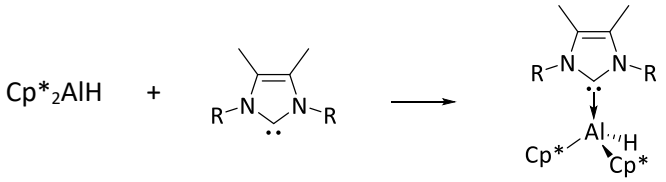

1

R = Me **3**

R = ^{i}Pr **4**

Scheme 37 *Synthesis of base coordinated adducts of Cp*$_2$AlH*

Further NMR studies revealed a broad ^{27}Al NMR signal for **3** at δ = 136.9 ($\nu_{1/2}$ ≈ 634 Hz), which is significantly shifted from the Cp*$_2$AlH doublet signal (δ = -22.4, $^1J_{Al\text{-}H}$ 591 Hz) suggesting a major structural change to the aluminium centre. A low-field signal usually associated with a carbene carbon is missing from the ^{13}C NMR spectrum of **3**. This is attributed to coupling to the aluminium nucleus (*I* = 5/2) broadening this signal into the baseline.

Repeating the reaction on a preparative scale allowed for the isolation of **3** as an orange powder in 65% yield. X-ray quality crystals were grown from a saturated hexane solution at -20°C, and the resulting solid-state structure is shown in Figure 19. It features a distorted tetrahedral aluminium centre, accounting for the low field ^{27}Al NMR chemical shift. The angle between the Cp* ligands, C8-Al1-C18 121.42(6)°, is much larger than the tetrahedral ideal of 109.5°, owing to the large steric bulk of these pentamethylcyclopentadienyl rings. A comparable value can be found in the corresponding angle in the gallium analogue of **3**, Cp*$_2$GaH.NHC, C-Ga-C 121.9(2)°.[25]

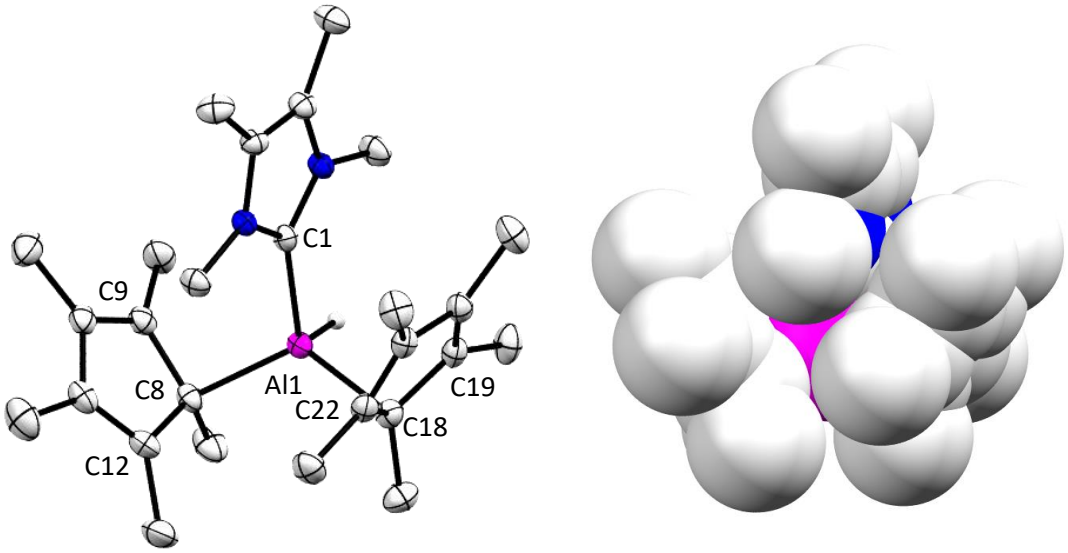

Figure 19 *X-Ray crystal structure of* ***3*** *and corresponding spacefill view. Hydrogen atoms (except Al-H) omitted for clarity. Selected bond distances (Å): Al1-C1 2.0517(15), Al1-C8 2.0901(15), Al1-C18 2.0857(16), Al1-C9 2.70808(8), Al1-C12 3.03754(10), Al1-C19 2.654437(8) and Al1-C22 2.79902(7). Selected bond angles (°): C1-Al1-C8 114.16(6), C1-Al1-C18 107.24(6) and C8-Al1-C18 121.42(6).*

The change to a tetrahedral geometry is accompanied by a lowering of the hapticity of the Cp* rings in **3** when compared to the solid-state structure of the Cp^*_2AlH **1** (η^2/η^3).[4] The presence of the strongly σ-donating NHC has decreased the metal's need for π-donation from the Cp* rings, causing this ring-slippage to form a σ-bond. Higher hapticity was ruled out based on long Al-C distances, for example Al1-C9 2.70808(8) Å and Al1-C12 3.03754(10) Å.

The Al-C bond lengths are unremarkable, falling into the normal range for such σ-bonds. The Al1-C1 bond, at 2.0517(15) Å, is comparable with other Al-NHC dative bonds.[26]

It was earlier noted that the four NHC methyl groups are inequivalent in the ^{1}H NMR spectrum of **3**, which can reasoned by inspection of the spacefill model shown in Figure 19. The position of Cp* groups is such that a "pocket" is created, which the small, planar NHC fits into. The rotation of the protons in the coordinated base is therefore hindered, giving rise to the four separate signals in the ^{1}H NMR spectrum.

Increasing the steric bulk of the nitrogen substituents from methyl to isopropyl, the reaction of Cp^*_2AlH with diisopropyldimethylimidazolylidene ($^{Me}I^iPr$) was investigated next.

Similar to the formation of NHC adduct **3**, $^{Me}I^{i}Pr$ was added to a C_6D_6 solution of Cp^*_2AlH to form Lewis base adduct **4** (Scheme 37). A slight downfield shift of the Cp* singlet signal to δ = 2.04 (Cp^*_2AlH: δ = 1.91) is the first hint of successful coordination. Where in ^{Me}IMe adduct **3** the NHC substituents were all inequivalent, in **4** the backbone methyl groups share a single signal at δ = 1.45, as do the ^{i}Pr methyl groups at δ 1.12 (d, $^{1}J_{H\text{-}H}$ = 6.9 Hz) (uncoordinated NHC: δ = 1.74 and 1.47).[24] The isopropyl CH protons are now inequivalent, with two broad signals observed at δ = 6.08 and 3.59, the former shifted significantly downfield of the non-coordinated signal δ = 3.59. A broad low-field signal in the ^{27}Al NMR spectrum of **4** at δ = 137.5 ($\nu_{1/2}$ ≈ 2029 Hz) further supports the formation of a tetrahedral Lewis base adduct analogous to **3**.

This slightly bulkier adduct **4** was found to be less soluble than its tetramethyl congener **3**, and as such single crystals precipitated upon formation from C_6D_6. The solid-state structure is shown in Figure 20. It features the same tetrahedral aluminium centre as ^{Me}IMe adduct **3** with some distortion in the angles. The angle between the two Cp* ligands in **4**, C12-Al1-C22 120.96(10)° is comparable to the analogous angle in **3** (121.42(6)°), as are the angles between the Cp* ligands and the NHC (**4**: C1-Al1-C12 115.99(9)° and C1-Al1-C22 107.27(9)°, **3**: C1-Al1-C8 114.16(6)°, C1-Al1-C18 107.24(6)°).

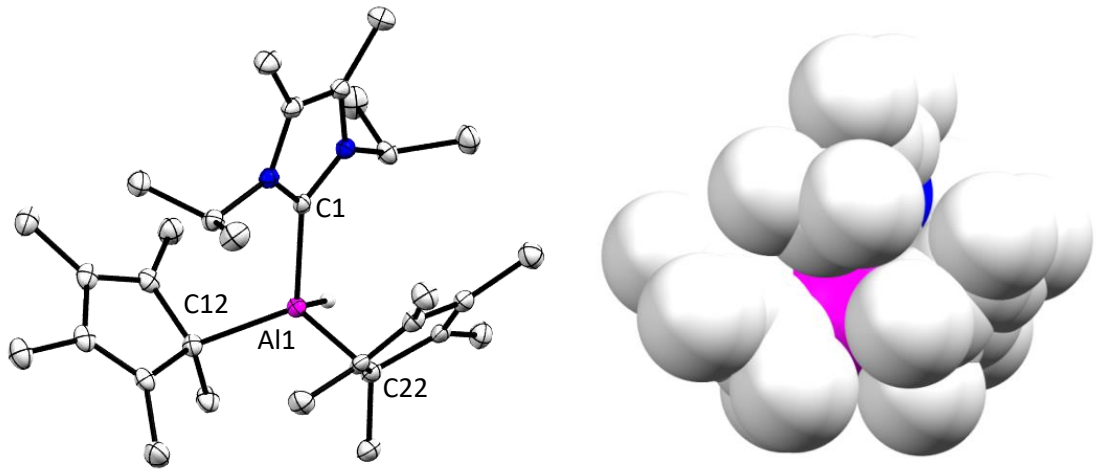

Figure 20 *X-Ray structure of **4** and corresponding spacefill view. Hydrogen atoms (except Al-H) omitted for clarity. Selected bond distances (Å): Al1-C1 2.069(2), Al1-C12 2.082(2) and Al1-C22 2.072(2). Selected bond angles (°): C1-Al1-C12 115.99(9), C1-Al1-C22 107.27(9) and C12-Al1-C22 120.96(10).*

The dative Al1-C1 bond length in **4** (2.069(2) Å) is comparable to the corresponding dative bond length in **3** (2.0517(15) Å), as are the Al1-C12 and Al1-C22 σ-bonds, 2.082(2) Å and 2.072(2) Å respectively (**3**: 2.0901(15) Å and 2.0857(16) Å).

To increase the steric bulk further, 1,3-bis(2,6-diisopropylphenyl)imidazol-2-ylidene (IPr) was added to a C_6D_6 solution of Cp^*_2AlH. No reaction was observed even after prolonged reaction times. Heating this reaction resulted in the reductive elimination of Cp*H and formation of $(Cp^*Al)_4$, while the IPr remained unreacted. It is proposed that IPr is too sterically encumbered to form a Lewis base adduct with Cp^*_2AlH.

Changing focus and moving to a coordinating amine base, the interaction between Cp^*_2AlH and dimethyl amino pyridine (DMAP) was investigated. In a similar fashion to NHC adducts **3** and **4**, the addition of DMAP to a C_6D_6 solution of Cp^*_2AlH resulted in Lewis base adduct **5**.

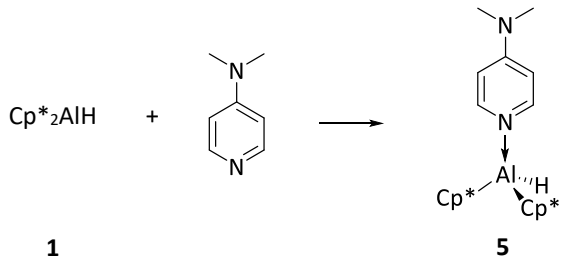

1 **5**

Scheme 38 *Preparation of DMAP adduct of Cp^*_2AlH*

A slight downfield field shift in the ^1H NMR signal associated with the Cp* groups is noted, to δ = 2.02 (Cp^*_2AlH: δ = 1.91, **3**: δ = 1.98, **4**: δ = 2.04). The signals associated with the coordinated DMAP fragment are found significantly upfield of the uncoordinated chemical shifts. The aromatic pyridine signals are found at δ = 7.52 (d, $^1J_{H\text{-}H}$ = 6.0 Hz) and δ = 5.60 (d, $^1J_{H\text{-}H}$ = 7.0 Hz), where corresponding protons in the uncoordinated form have resonances at δ = 8.44 (d, $^1J_{H\text{-}H}$ = 4.9 Hz) and δ = 6.10 (d, $^1J_{H\text{-}H}$ = 4.9 Hz). A singlet signal for the amino methyl groups is seen at δ = 1.93, compared to δ = 2.25 in uncoordinated DMAP. The ^{27}Al NMR spectrum of **5** displays a very broad signal at δ = 143.7 ($\nu_{1/2} \approx 3931$ Hz), similar to both NHC adducts **3** (^{27}Al δ = 136.9) and **4** (^{27}Al δ = 137.5)

Repeating the reaction in Scheme 38 on a preparative scale allowed for the isolation of DMAP adduct **5** in 68% isolated yield, which is comparable with ^{Me}IMe adduct **3** (65%). Single crystals were grown from a saturated benzene solution at room temperature, and the solid state structure is shown in Figure 21.

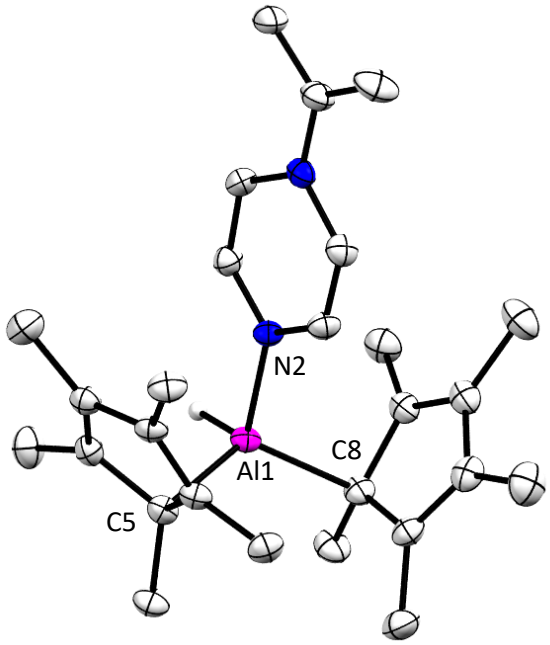

Figure 21 *X-Ray crystal structure of **5**. Hydrogen atoms (except Al-H) omitted for clarity. Selected bond distances (Å): Al1-N1 1.943(2), Al1-C8 2.081(3) and Al1-C5 2.067(3). Selected bond angles (°): C5-Al1-C8 122.45(11), C5-Al1-N2 104.04(10) and C8-Al1-N2 110.61(10).*

A tetrahedral aluminium centre is seen in DMAP adduct **5**, similar to that of NHC adducts **3** and **4**. The angle between the Cp* ligands C5-Al1-C8 122.45(11)° is the largest angle around the metal centre in **5**. The angles between the Cp* ligands and the coordinated base in **5** are closer to the ideal tetrahedral angle of 109.5°; C5-Al1-N2 104.04(10)° and C8-Al1-N2 110.61(10)°. The Al1-C5 and Al1-C8 bonds are unremarkable, and are in the normal range for σ-bonds, 2.067(3) Å and 2.081(3) Å respectively.

2.2.2 The Effect of Base on Reductive Elimination

With the NHC-coordinated adducts **3** and **4**, and DMAP adduct **5** in hand, their reductive elimination activity was investigated. Solutions of **3** or **4** in tol-d_8 were heated to 100°C for prolonged periods of time, and upon cooling ^{1}H and ^{27}Al NMR spectra were collected. Under these conditions there was no evidence of reductive elimination occurring, with only starting materials observed in the ^{1}H NMR spectrum after 6 days at 85°C.

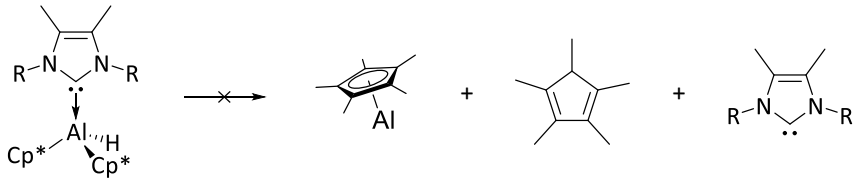

R = Me **3**
R = ^{i}Pr **4**

Scheme 39 *Attempted reductive elimination of Cp*H from NHC adducts **3** and **4***

Variable temperature ^{1}H NMR experiments were carried out in search of an equilibrium, however no change was observed when a tol-d_8 solution of **3** or **4** was heated in stepwise increments to 90°C. It can be concluded that NHC adducts **3** or **4** are unable to reductively eliminate Cp*H to form a low-valent aluminium species.

It is noted here that separate experiments were carried out where $(Cp^*Al)_4$ was heated with a range of carbenes (^{Me}IMe, ^{Me}I^{i}Pr, IPr and a cylic alkylamino carbene). No reaction was observed except in the case of the smallest example ^{Me}IMe, where an intractable mixture resulted.

This lack of reactivity supports the proposed mechanism in section 2.1.5. Reductive elimination of Cp*H from Cp^*_2AlH is enabled by the ability of the Cp* ligand to adopt a higher coordination mode (η^5) than is seen in the starting aluminium hydride (η^2/η^3), forming the low oxidation state Cp*Al moiety in the transition state. Because of the presence of the strongly σ-donating NHC in base adducts **3** and **4**, the Cp* ligands are bonded to the aluminium with pure σ-bonding, making this change to a higher hapticity unfavourable and high in energy.

Contrasting reactivity is observed for DMAP adduct **5**. When a tol-d_8 solution of **5** is heated some production of $(Cp^*Al)_4$ and Cp*H is observed by ^1H and ^{27}Al NMR spectroscopy, along with uncoordinated DMAP as a by-product. However, despite very long reaction times, full conversion of **5** to Cp*Al, Cp*H and DMAP was not achieved.

To investigate this intriguing observation, the reaction was monitored in a similar manner to the kinetics experiments described in section 2.1.2. DMAP adduct **5** was dissolved in a tol-d_8 with a known concentration of tritertbutylbenzene as an internal standard. This was then heated to 353 K, and ^1H NMR spectra were acquired every 20 minutes for 16 hours. The production of Cp*H was calculated by comparing the integrals of the Cp*H signals to tritertbutyl benzene signals.

Comparison of this conversion data with that of a similar reaction curve of Cp*H elimination from base-free Cp^*_2AlH (section 2.1.2) immediately indicates a much slower rate of reductive elimination from DMAP adduct **5** (Figure 22). In the case of Cp^*_2AlH after 100 minutes at 80 °C, 90.7 % of the starting aluminium hydride had been consumed, whereas only 31.3 % of DMAP adduct **5** had been converted in Cp*H and $(Cp^*Al)_4$. Equilibrium was not reached for adduct **5** until approximately 11 hours and 40 minutes, with only 35% conversion observed at equilibrium.

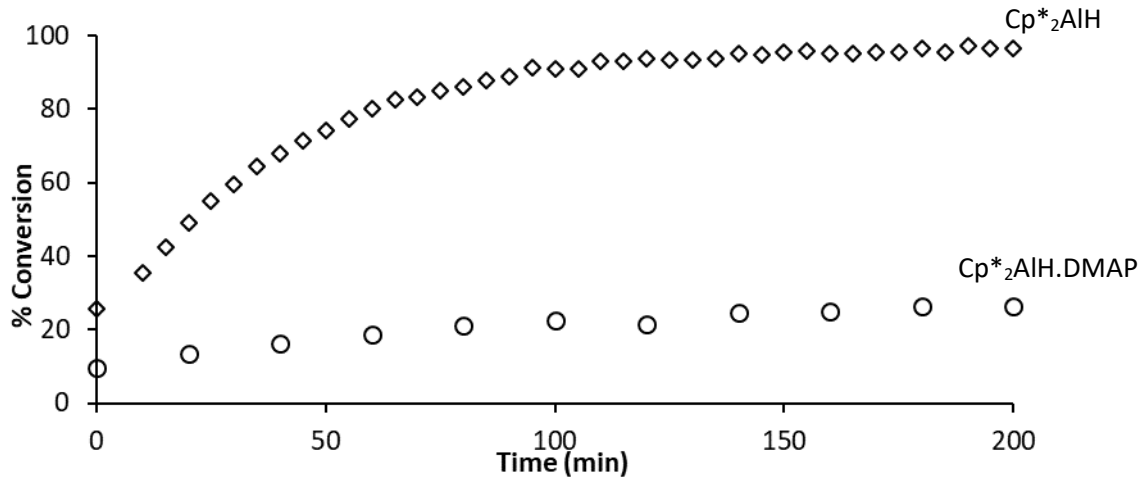

Figure 22 *Comparison of percentage conversion to Cp*Al and Cp*H over time from Cp^*_2AlH and DMAP adduct **5** at 353 K in tol-d_8. Conversions calculated by ^1H NMR against an internal standard of tritertbutylbenzene*

The presence of DMAP either significantly hinders the reductive elimination, or the reductive elimination proceeds *via* a different, less efficient mechanism than that described for Cp^*_2AlH. Closer inspection of the variable temperature ^1H NMR data revealed time-averaged chemical shift of the signals associated with **5** when uncoordinated DMAP is present, which is demonstrated in Figure 23.

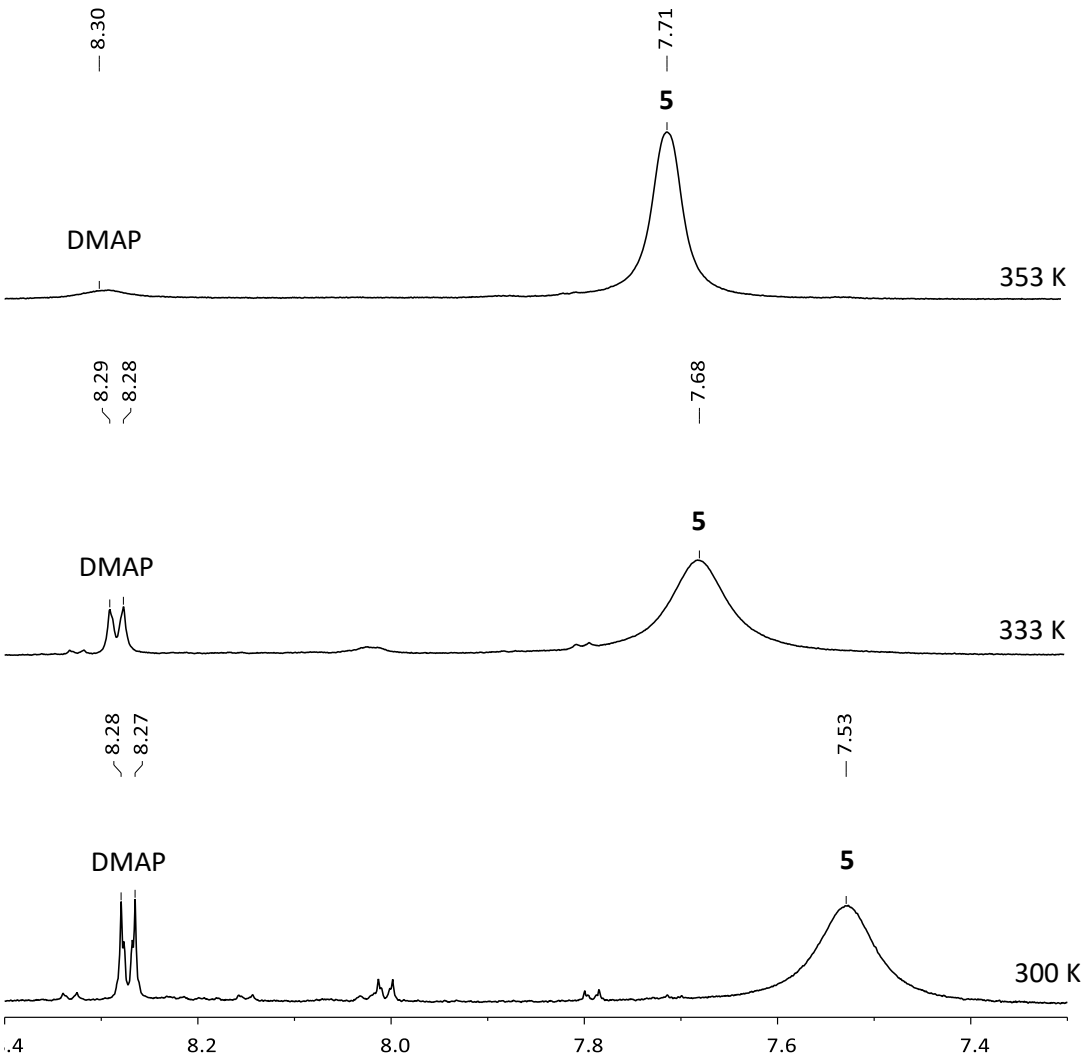

Figure 23 *Variable temperature ^1H NMR in tol-d_8 showing rapid exchange of free/coordinated DMAP from adduct **5** at elevated temperatures. Signals shown correspond to aromatic CH protons of the DMAP*

To collect the data in Figure 23, a tol-d_8 sample of **5** was heated to 353 K and after acquisition of a ^1H NMR spectrum immediately cooled to 333 K, and finally 300K. The broadness of the signal associated with **5**, as well as its change in chemical shift with temperature, suggest a rapid exchange of coordinated and uncoordinated DMAP to the

aluminium centre. This introduces a second equilibrium in the transformation of DMAP adduct **5** into Cp*Al **2**^{m} and Cp*H (Scheme 40). The dissociation of the base from the metal centre at high temperature produces Cp*$_2$AlH, which then undergoes reductive elimination under the reaction conditions. Evidently the rate of dissociation of DMAP is slow, and the presence of this second equilibrium limits the overall conversion to Cp*Al.

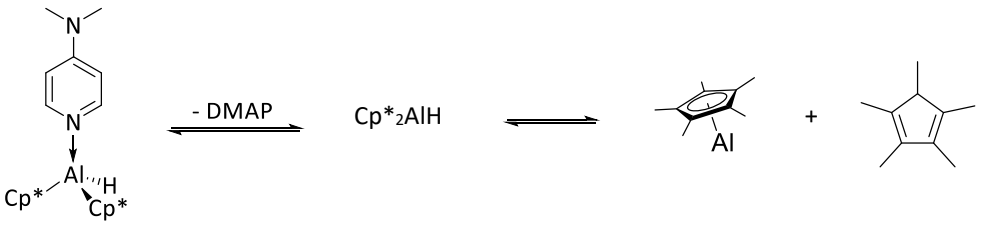

5 **1** **2**^{m}

Scheme 40 *Influence of DMAP on Fischer's equilibrium*

The weaker σ-donating ability of DMAP compared to that of NHC's allows the pyridine base to dissociate from the metal centre at high temperature. The Al-N dative bond in **5** is most likely significantly weaker than the corresponding Al-C dative bonds in NHC adducts **3** and **4**.

2.3 Aluminium Complexes Supported by 9-Methylfluorene

In order to investigate whether this mechanism of reductive elimination of C-H bonds could be applied generally to aluminium chemistry, the design of a new metal complex which would fit the criteria outlined in section 2.1.5 was undertaken. This would feature a basic ligand featuring a central ring with coordinative flexibility.

The tricylic organic compound fluorene was chosen as a good candidate to support a low valent aluminium centre. It has diverse reactivity; reactions can happen at the outer phenyl rings or at the bridging 9-poisition. Seven modes of coordination of fluorene-based ligands to metal centres are documented,[27] with hapticity ranging from η^1 to η^6 (Figure 24). Haptotropic rearrangements have been reported with transition metals,[28] demonstrating the desired coordinative flexibility sought to apply to aluminium chemistry here.

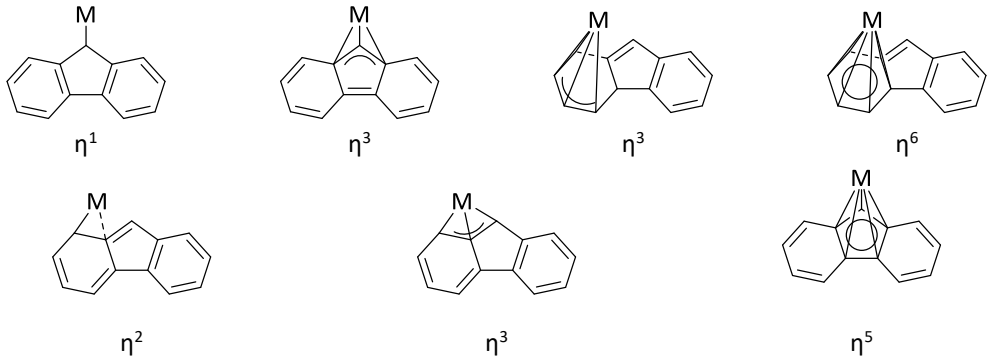

Figure 24 *Different coordination modes available to metallic fluorene complexes*

The chemistry of metal fluorenyl complexes is varied. Sandwich compounds featuring a zirconium centre are capable of efficient polymerisation of ethylene[29] and propylene.[30–32] Some interesting group 13 reactivity is reported, for example the isolation of a fluorenyl flanked B-B bond,[33] where the ligands are non-innocent, and participate in further reactivity.[34–36] Complexation of thallium to a fluorenyl-based ligand produces an unusual thallium-arene interaction.[37]

2.3.1 Preparation of bis-fluorenyl aluminium hydride and it's adducts

In order to avoid the presence of a labile C-H proton at the 9-position in any metallic complexes synthesised, a methyl group was first installed to the bridgehead carbon in the parent fluorenyl ligand.[38] Fischer's preparation of Cp^*_2AlH consists of reacting Cl_2AlH with Cp*K to eliminate two equivalents of KCl. A similar synthetic route was used to prepare an aluminium monohydride bearing 9-methyl fluorenyl ligands.

Low temperature addition of ^{n}BuLi to a diethyl ether solution of 9-methylfluorene gives the previously colourless solution a bright red hue. This fluorenyl lithium solution was added to bis-chloroaluminium hydride, which was made *in situ* by the addition of $LiAlH_4$ to $AlCl_3$.[4,39] Isolation of the aluminium hydride **6** was achieved by recrystallisation from hot hexane, affording **6** as a peach coloured solid, with a reproducibly low isolated yield of 33%.

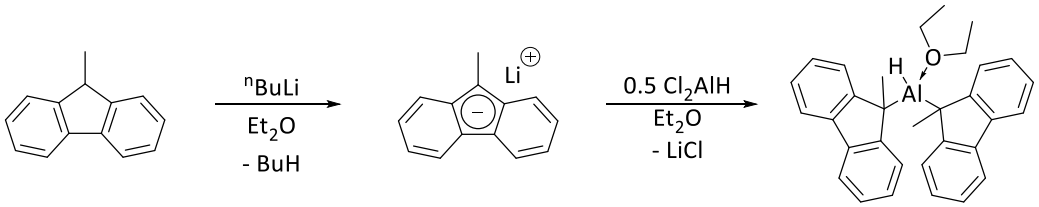

6

Scheme 41 *Preparation of **6** from 9-methylfluorene and bis-chloroaluminium hydride*

The formation of **6** was confirmed by ^{1}H NMR spectroscopy. A singlet signal corresponding to the 9-methyl group is observed at δ = 1.60, downfield of the corresponding group in the 9-methylfluorene starting material δ = 1.25 (d, $^1J_{H\text{-}H}$ = 7.4 Hz). Aromatic signals complete the identification of a new fluorenyl ligand environment, a doublet of doublets (δ = 7.83 $^1J_{H\text{-}H}$ = 6.8 Hz), a doublet of triplets (δ = 7.77 $^1J_{H\text{-}H}$ = 7.3 and 1.1 Hz) and two multiplets (δ = 7.50-7.46 and 7.29-7.18) are all observed. Upon close inspection, a broad singlet signal ($\nu_{1/2}$ ≈ 152 Hz) corresponding to the Al-H is identified at δ = 4.30 (Cp^*_2Al**H** δ = 3.44). Integration of this signal against the ligand signals confirms two fluorenyl ligands per hydride.

Observation of both a quartet signal at δ = 2.27 ($^1J_{H\text{-}H}$ = 7.1 Hz) and a triplet signal at δ = -0.04 ($^1J_{H\text{-}H}$ = 7.1 Hz) in the ^{1}H NMR spectrum confirm that one equivalent of diethyl ether is present in **6**. As these signals are significantly shifted upfield of the residual solvent

values,[40] the diethyl ether is coordinated to the aluminium centre. No signal for **6** is seen in the ^{27}Al NMR spectrum.

X-ray quality crystals were grown from a saturated hexane solution, and the resulting X-ray crystal structure confirms formation of **6**. The hydride was found in the difference map and allowed to refine freely.

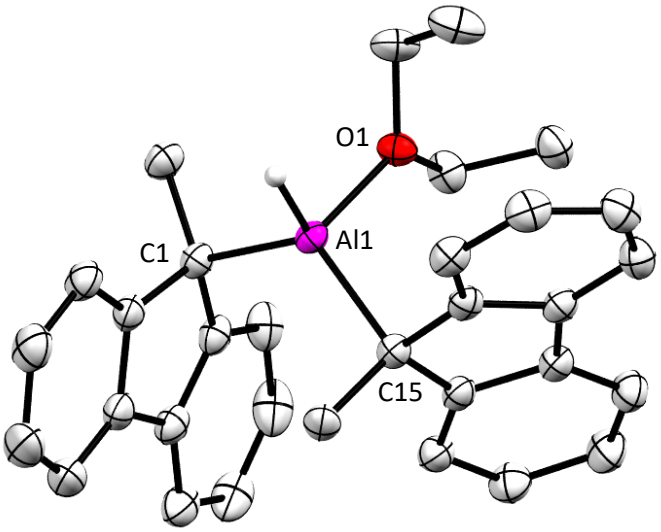

Figure 25 *X-Ray crystal structure of **6**. C-H protons omitted for clarity. Selected bond lengths (Å): Al1-O1 1.9045(16), Al1-C1 2.036(2) and Al1-C15 2.039(2). Selected bond angles (°): C1-Al1-C15 119.71(9), C1-Al1-O1 105.00(8) and C15-Al1-O1 108.16(8).*

Comparison of solid-state structure of **6** to that of tetrahedral Cp*$_2$AlH.NHC adducts **3** and **4** shows some sterically induced differences. The Al-$C_{fluorenyl}$ bond distances in **6** (Al1-C1 2.036(2) Å and Al1-C15 2.039(2) Å) are slightly shorter than the comparable Al-C_{Cp*} bond distances in **3** and **4** (**3**: 2.0901(15) Å and 2.0857(15) Å; **4**: 2.082(2) Å and 2.072(2) Å), perhaps indicating marginally stronger bonds. The bond angles around the aluminium centre in **6** between the fluorenyl ligand and the coordinated ether (C1-Al1-O1 105.00(8)° and C15-Al1-O1 108.16(8)°) show little deviation from the ideal tetrahedral angle of 109.5°. A very large angle between the fluorenyl ligands (C1-Al1-C15 119.71(9)°) is attributed to the steric bulk.

The central five-membered ring of the 9-methylfluroene ligand is coordinated in an η^1 fashion to the aluminium centre. The 9-methyl group is out of plane with the ring indicating the carbon at the 9- position is sp^3 hybridised.

The presence of a tetrahedral aluminium centre in **6** was expected based on the ^{1}H NMR spectrum, however it is still unsatisfactory. Lewis base coordination was shown to prevent reductive elimination of Cp*H in section 2.2.2, and so the likelihood that **6** would demonstrate such reactivity is small. Fischer's preparation of Cp^*_2AlH is also carried out in diethyl ether,[4] however the product is isolated solvent-free. In the case of **6**, 9-methylfluorene must not be electron donating enough to adopt a higher hapticity which would satisfy the Lewis acidity of a three-coordinate aluminium centre.

2.3.2 Attempted Reductive Elimination of 9-Methylfluorene

Despite the setback of a tetrahedral aluminium centre, reductive elimination was investigated from bis-fluorenyl aluminium hydride etherate **6**. It is proposed that the coordinated ether molecule could be labile, like the weakly coordinating base in dimethylaminopyridine derivative **5** (section 2.2.2), with the added advantage of diethylether being very volatile, and so easily removed once dissociated.

Variable temperature ^{1}H NMR experiments were used to initially probe diethylether dissociation from **6**. Heating a C_6D_6 solution of **6** gradually to 70 °C showed no change to the ^{1}H NMR signals, only starting material remained.

Further attempts to cleave the diethylether moiety involved heating neat samples of **6** under dynamic vacuum for various periods of time in order to remove the volatile solvent. Heating to 60 °C had no observable effect and so the temperature was gradually increased. It was concluded **6** is stable to sublimation up to 130 °C, with no observable bond cleavage occurring. Heating a neat sample of **6** to 130 °C under dynamic vacuum resulted in the sublimation of a white solid, and a colour change of the remaining residue from peach to light grey. ^{1}H NMR spectroscopy revealed that the sublimed white solid was 9-methylfluorene, implying reductive elimination of a C-H bond has occurred from **6**.

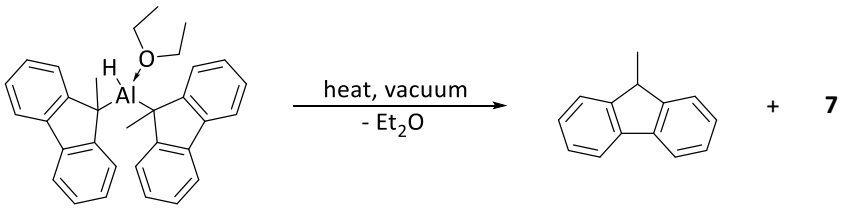

6

Scheme 42 *Sublimation of **6** results in cleavage of 9-methylfluorene*

The residual solid from this sublimation was found to be sparingly soluble in C_6D_6, and ^{1}H NMR spectroscopy showed this residue consisted of starting material **6** and one new fluorenyl containing product **7**. Identification of this new product was challenging as the ^{1}H NMR spectrum only displays signals associated with a new ligand environment. The lack of new diethyl ether signals confirms that it was indeed removed from the aluminium centre. Two new signals are observed in the alkyl region (δ = 0.82 and 0.44), and with a

reproducible relative ratio of 1:3 are attributed to activation of the 9-methyl group. No signal is observed is the ^{27}Al NMR spectrum. Attempts to isolate a pure sample of **7** were not successful, as were attempts at crystallisation for X-ray diffraction experiments.

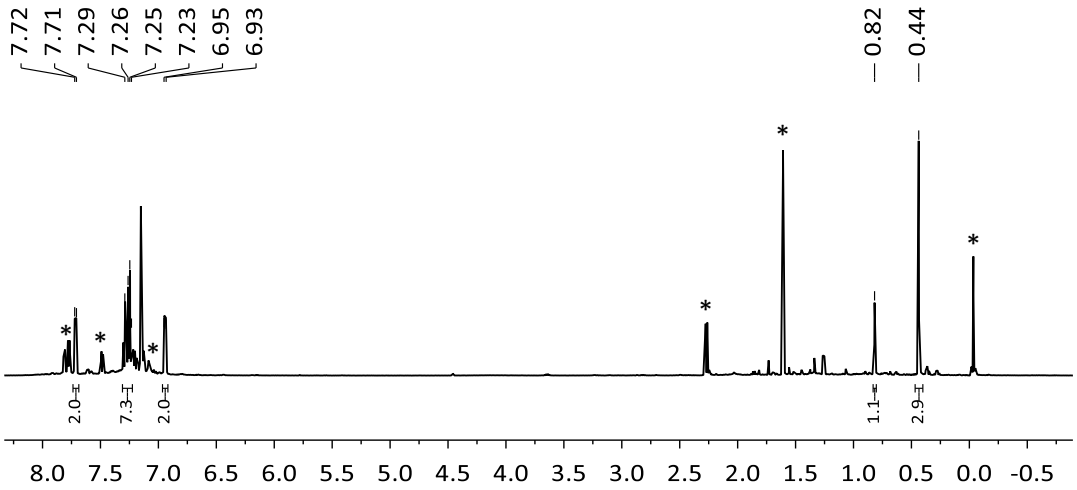

Figure 26 *^{1}H NMR spectrum of solid residue from sublimation of **6** (starting material denoted *)*

It is proposed that first diethylether dissociation occurs, and this then creates a very reactive aluminium centre which very quickly eliminates 9-methylfluorene at elevated temperatures, resulting in the formation of a low oxidation state aluminium centre. As increasing the steric bulk of the Cp* ligand stabilises tetramer formation in Cp*Al type compounds due to non-covalent interactions between the ligands,[8] it is therefore speculated that any resulting FluAl: could form a tetramer, where one of the fluorenyl ligands is orientated slightly differently. This would account for the extra methyl signal (and the ratio of 1:3) in the ^{1}H NMR spectrum of **7** and the tetrameric structure would account for the observed lack of solubility of the sublimation residue.

To react all of the starting material **6** and produce pure **7**, a neat sample of **6** was heated to 130°C under high vacuum for 18 hours. This resulted in a dark grey residual solid, which was completely insoluble in C_6D_6. This is thought to be metallic aluminium powder, from the disproportionation of an unstable Al(I) product.

To support the suggestion of 9-methylfluorene reductive elimination, a mixture of **6** and Cp*$_2$AlH in C_6D_6 was heated to 75°C for 24 hours. Since the dissociation of Cp*H from Cp*$_2$AlH has been shown to relatively facile under these conditions (section 2.1.1), should

the dissociation of 9-methylfluorene from **6** occur, it is reasonable to assume that ligand transfer should occur, producing Cp*Al(H)Flu **8** as a ligand cross-over product. Unfortunately heating for several days did not produce any reaction between **6** and Cp^*_2AlH, and only $(Cp^*Al)_4$ was formed.

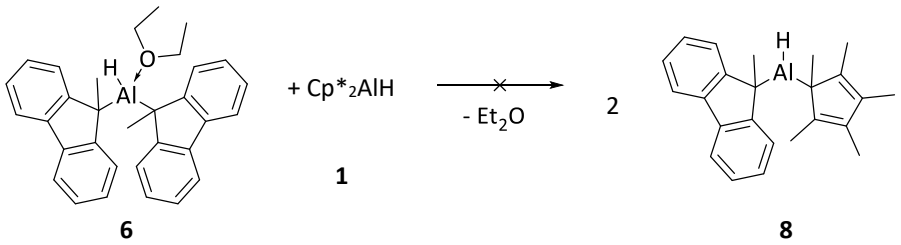

6 **1** **8**

Scheme 43 *Attempted preparation of Cp*Al(H)Flu by ligand crossover*

A follow up reaction where $(Cp^*Al)_4$ was heated with 9-methylfluorene in C_6D_6 also showed no new product by ^1H NMR spectroscopy. This implied that the oxidative addition of 9-methylfluorene to this low-valent aluminium species is not as straightforward as Cp*H. The oxidative addition of E-X bonds will be discussed further in section 3.1.1.

Many future experiments are required to confidently identify this new fluorenyl containing product **7**. For example, the addition of 9-methylfluorene to **7** should result in the formation of bis-fluorenyl aluminium hydride, similar to **6** but without the coordinated ether molecule. Another possible strategy is to trap a possible low oxidation state aluminium compound as a ligand on a transition metal complex. This method used by Schnöckel to conclusively prove monomeric Cp*Al,[41–43] and more recently Tokitoh to demonstrate the presence of his unisolable dialumene BbpAl=AlBbp.[44]

2.4 Summary

The previously reported reductive elimination of Cp*H from Cp*$_2$AlH has been shown in this work to be a unimolecular reaction, where the low oxidation state aluminium species Cp*Al is a constitute part of the transition state **TS$_{1\text{-}2}$**. It is the ligand properties which enable the reductive elimination to proceed, as Cp* is able to undergo the haptotropic shift to a higher hapticity, whilst being basic enough when dissociated to deprotonate the aluminium hydride, forming the observed products. The aromatisation of the η^5 coordinated Cp* in **TS$_{1\text{-}2}$** provides an energy offset for the formation of unfavourable low oxidation state aluminium.

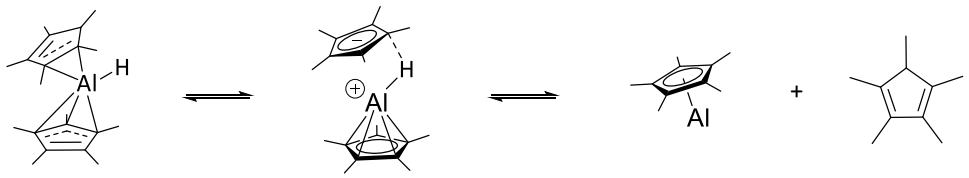

Scheme 44 *Mechanism of reductive elimination of Cp*H from Cp*$_2$AlH*

Combining experimentally collected data and computations (BP86/TZVPP), the reductive elimination process in Scheme 44 is shown to be an endothermic equilibrium, as ΔG_{300} = 13.83 ± 0.48 (18.44) kJ mol^{-1}. The energy required to access **TS$_{1\text{-}2}$** was found to be 95.53 ± 4.74 (91.54) kJ mol^{-1}, with both experimental and theoretical values in excellent agreement.

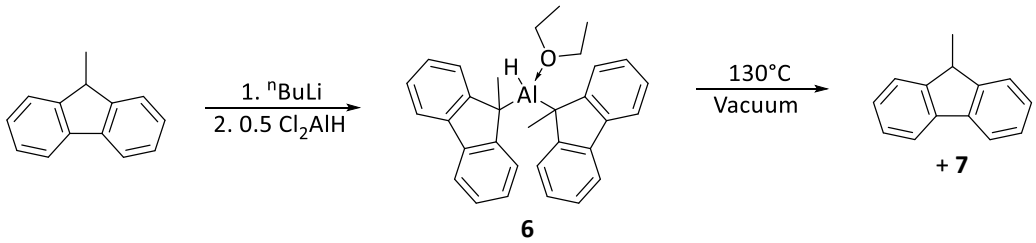

Scheme 45 *Synthesis of aluminium hydride **6** and further reductive elimination of 9-methylfluorene*

A rationally designed aluminium system which should be capable of reductive elimination of a C-H bond was synthesised. Bis-fluorenyl aluminium hydride **6** was found form a Lewis adduct with diethylether, from which the solvent molecule is difficult to remove under vacuum. Heating a neat sample of tetrahedral hydride **6** to 130°C under vacuum results in the sublimation of 9-methylfluorene, suggestive of ether dissociation and possible subsequent reductive elimination. The aluminium containing product of this reductive elimination was not conclusively identified.

2.5 References

1 P. P. Power, *Nature*, 2010, **463**, 171–177.
2 W. E. Garner and E. W. Haycock, *Proc. Ro. Soc. Ser. A*, 1952, **211**, 335–351.
3 J. Block and A. P. Gray, *Inorg. Chem.*, 1964, **4**, 304–305.
4 C. Ganesamoorthy, S. Loerke, C. Gemel, P. Jerabek, M. Winter, G. Frenking and R. Fischer, *Chem. Commun.*, 2013, **49**, 2858–2860.
5 W. L. Gladfelter, D. C. Boyd and K. F. Jensen, *Chem. Mater.*, 1989, **1**, 339–343.
6 C. Dohmeier, C. Robl, M. Tacke and H. Schnöckel, *Angew. Chem. Int. Ed. Engl.*, 1991, **30**, 564–565.
7 J. Gauss, U. Schneider, R. Ahlrichs, C. Dohmeier and H. Schnöckel, *J. Am. Chem. Soc.*, 1993, **115**, 2402–2408.
8 W. W. Tomlinson, D. H. Mayo, R. M. Wilson and J. P. Hooper, *J. Phys. Chem. A*, 2017, **121**, 4678–4687.
9 S. Schulz, H. W. Roesky, H. J. Koch, G. M. Sheldrick, D. Stalke and A. Kuhn, *Angew. Chem. Int. Ed. Engl.*, 1993, **32**, 1729–1731.
10 P. Kuzmic, *Anal. Biochem.*, 1996, **237**, 260–273.
11 P. Jutzi and N. Burford, *Chem. Rev.*, 1999, **99**, 969–990.
12 X. Zhang and Z. Cao, *Dalton Trans.*, 2016, **45**, 10355–10365.
13 N. N. Greenwood and A. Earnshaw, *Chemistry of the Elements*, Pergamon Press, 1984.
14 C. Fliedel, G. Schnee, T. Avilés and S. Dagorne, *Coord. Chem. Rev.*, 2014, **275**, 63–86.
15 A. Schmitt, G. Schnee, R. Welter and S. Dagorne, *Chem. Commun.*, 2010, **46**, 2480–2482.
16 A. Stasch, S. Singh, H. W. Roesky, M. Noltemeyer and H.-G. Schmidt, *Eur. J. Inorg. Chem.*, 2004, 4052–4055.
17 R. J. Baker, M. L. Cole, C. Jones and M. F. Mahon, *J. Chem. Soc., Dalton Trans.*, 2002, 1992–1996.
18 G. Tan, T. Szilvási, S. Inoue, B. Blom and M. Driess, *J. Am. Chem. Soc.*, 2014, **136**, 9732–9742.
19 A. J. Arduengo, H. V. Rasika Dias, J. C. Calabrese and F. Davidson, *J. Am. Chem. Soc.*, 1992, **114**, 9724–9725.
20 S. J. Bonyhady, D. Collis, G. Frenking, N. Holzmann, C. Jones and A. Stasch, *Nat. Chem.*, 2010, **2**, 865–869.
21 P. Bag, A. Porzelt, P. J. Altmann and S. Inoue, *J. Am. Chem. Soc.*, 2017, **139**, 14384–14387.
22 C. P. Sindlinger, A. Stasch, H. F. Bettinger and L. Wesemann, *Chem. Sci.*, 2015, **6**, 4737–4751.
23 A. V Protchenko, J. I. Bates, L. M. Saleh, M. P. Blake, A. D. Schwarz, E. L. Kolychev, A. L. Thompson, C. Jones, P. Mountford and S. Aldridge, *J. Am. Chem. Soc.*, 2016, **138**, 4555–4564.
24 N. Kuhn and T. Kratz, *Synthesis*, 1993, **6**, 561–562.
25 J. D. Gorden, C. L. B. Macdonald and A. H. Cowley, *J. Organomet. Chem.*, 2002, **643**–**644**, 487–489.
26 R. S. Ghadwal, H. W. Roesky, R. Herbst-Irmer and P. G. Jones, *Z. Anorg. Allg. Chem.*, 2009, **635**, 431–433.
27 E. Kirillov, J. Y. Saillard and J. F. Carpentier, *Coord. Chem. Rev.*, 2005, **249**, 1221–1248.
28 E. Kirillov, S. Kahlal, T. Roisnel, T. Georgelin, J. Y. Saillard and J. Carpentier, *Organometallics*, 2008, **27**, 387–393.
29 H. G. Alt and E. Samuel, *Chem. Soc. Rev.*, 1998, **27**, 323–329.
30 J. A. Ewen, R. L. Jones, A. Razavi and J. D. Ferrara, *J. Am. Chem. Soc.*, 1988, **110**, 6255–6256.
31 A. Razavi, V. Bellia, Y. De Brauwer, K. Hortmann, L. Peters, S. Sirole, S. Van Belle and U. Thewalt, *Macromol. Chem. Phys.*, 2004, **205**, 347–356.
32 S. A. Miller and J. E. Bercaw, *Organometallics*, 2004, **23**, 1777–1789.
33 H. Nöth and M. Wagner, *Chem. Ber.*, 1991, **124**, 1963–1972.
34 R. Littger, N. Metzler, H. Nöth and M. Wagner, *Chem. Ber.*, 1994, **127**, 1901–1908.
35 H. Braunschweig, M. Gross, K. Hammond, M. Friedrich, M. Kraft, A. Oechsner, K. Radacki and S. Stellwag, *Chem. Eur. J.*, 2008, **14**, 8972–8979.
36 H. Braunschweig, T. Kupfer, J. Mies and A. Oechsner, *Eur. J. Inorg. Chem.*, 2009, 2844–2850.
37 W. Frank, D. Kuhn, S. Müller-Becker and A. Razavi, *Angew. Chemie Int. Ed. Engl.*, 1993, **32**,

90–92.
38 C. A. Fleckenstein and H. Plenio, *Chem. Eur. J.*, 2007, **13**, 2701–2716.
39 J. L. Cabioch and J. M. Denis, *J. Organomet. Chem.*, 1989, **377**, 227–233.
40 G. R. Fulmer, A. J. M. Miller, N. H. Sherden, H. E. Gottlieb, A. Nudelman, B. M. Stoltz, J. E. Bercaw and K. I. Goldberg, *Organometallics*, 2010, **29**, 2176–2179.
41 C. Dohmeier, H. Krautscheid and H. Schnöckel, *Angew. Chem. Int. Ed. Engl.*, 1994, **33**, 2482–2483.
42 Q. Yu, A. Purath, A. Donchev and H. Schnöckel, *J. Organomet. Chem.*, 1999, **584**, 94–97.
43 C. Üffing, A. Ecker, R. Köppe and H. Schnöckel, *Organometallics*, 1998, **17**, 2373–2375.
44 K. Nagata, T. Agou and N. Tokitoh, *Angew. Chem. Int. Ed.*, 2014, **53**, 3881–3884.

Chapter 3:

Activation of Unsaturated Bonds by $(Cp^*Al)_4$

3. Activation of Unsaturated Bonds by $(Cp^*Al)_4$

3.1 Oxidative addition of E-H bonds

Having rationalised the reductive elimination from an aluminium centre, attention turned to its reverse process, oxidative addition. As the concerted addition of a σ-bond to a metal centre increases oxidation state, in the case of relatively unstable aluminium(I) this process ought to be very favourable. Indeed, the addition of a wide variety of E-H[1–3] and main-group E-E[4,5] bonds to NacNacAl has been reported (section 1.2.2), as well as the oxidative cleavage of C=S bonds.[6] The oxidative addition of a C-H bond to $(Cp^*Al)_4$ **2** was discussed in chapter 2, however this chemistry has yet to be broadly investigated and so was the natural progression of this project.

Considering the oxidative addition of the C-H bond to **2** is exergonic, ΔG^0_{300} = -13.83 ± 0.48 kJ mol^{-1} (section 2.2.3), it was thought that the oxidative addition of a Si-H bond should also be relatively facile. As it was used for the studies with NacNacAl, triphenylsilane was chosen as a suitable substrate, and was added to a suspension of **2** in C_6D_6. No reaction was observed by ^1H or ^{27}Al NMR spectroscopy, even after heating this mixture for several days.

As Al-N bonds are well known, the next bond chosen for investigation was N-H. The addition of 2,6-diisopropylaniline to a C_6D_6 suspension of **2** causes full consumption of the starting material almost immediately at room temperature when monitored by ^{27}Al NMR specroscopy. No new signals were observed in the spectrum, suggesting perhaps an unsymmetrical aluminium centre. The ^1H NMR spectrum was extremely complex, and attempts to isolate a single product were met with failure.

Undeterred, the activation of B-H bonds was examined next. The addition of the commercially important pinacol borane to a suspension of $(Cp^*Al)_4$ **2** did not initiate a reaction, however heating this mixture for 72 hours resulted in the formation of a new product by ^1H and ^{11}B NMR spectroscopy. In the complex ^1H NMR spectra, it was first noted that the distinctive 1:1:1:1 quartet signal at δ = 4.22 ($^1J_{H\text{-}B}$ = 175 Hz) of the B-H was no longer present and an intense new singlet signal at δ = 0.96 was identified as a possible new Bpin environment. In the proton-coupled ^{11}B NMR spectrum, the doublet signal for pinacol borane at δ = 28.5 ($^1J_{B\text{-}H}$ = 174 Hz) is replaced with one new signal at δ = 33.6. As this is a singlet signal it is evident that the B-H functionality has reacted. The chemical shift value is

significantly different to the reported ^{11}B signal for Cp*Al→B(C_6F_5)$_3$ which features a dative Al-B interaction (^{11}B δ = -32.9),[7] and is suggestive of a three-coordinate boron centre.

Hence, the suggested product of this reaction is the oxidative addition product **9**. Although no Al-H signal is observed in the ^1H NMR spectrum, this is not unusual for such hydrides; the signal is broadened into the baseline by the aluminium nucleus (*I* = 5/2).

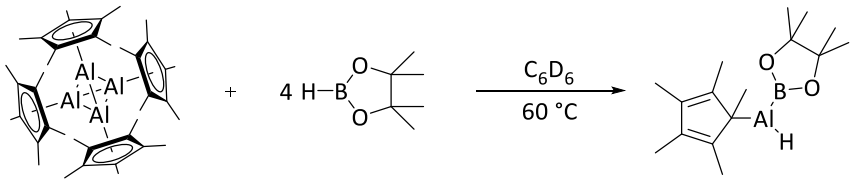

2 **9**

Scheme 46 *Reaction of (Cp*Al)$_4$ with pinacol borane.*

When repeated on a preparative scale, the reaction between (Cp*Al)$_4$ and pinacol borane proceeds as described for the NMR scale reaction, with *in situ* ^{11}B NMR spectrum of reaction aliquots showing the formation of **9**. Disappointingly, attempts to isolate this product resulted in degradation to many boron-containing products. It is thought that **9** is extremely air and moisture sensitive, and so any kind of manipulation causes the degradation, presumably through hydrolysis. Attempts to grow X-ray quality crystals were also unsuccessful.

In summary, unlike the C-H bond of Cp*H, the Si-H bond of triphenylsilane does not react with tetrameric (Cp*Al)$_4$ **2**. The reaction between the N-H bonds of diisopropylamine and **2** proceeds rapidly, however in an uncontrolled manner with no product confidently identified. *In situ* NMR experiments suggest that the reaction between **2** and pinacol borane results in the expected oxidative addition product **9**, but the product is too sensitive to isolate here.

3.2 Preparation of a 1,4-Dialuminacyclohexadiene Derivative

*3.2.1 Reaction of (Cp*Al)$_4$ with Internal Alkynes*

Soon after the preparation of metastable solutions of Al-Cl by Schöckel,[8] its reactivity with internal alkynes was investigated. Warming a solution of Al-Cl and dimethylacetylene from -196 °C to room temperature allows for the isolation of **10**, a dimeric 1,4-dialuminacyclohexadiene derivative featuring a central 6-membered Al_2C_4 moiety.[9] The solid state structure of **10** confirmed its dimeric structure, stabilised by donation from the new C=C π-bonds to the p-orbital of the Al atom of the adjacent monomer satisfying the Lewis acidity.

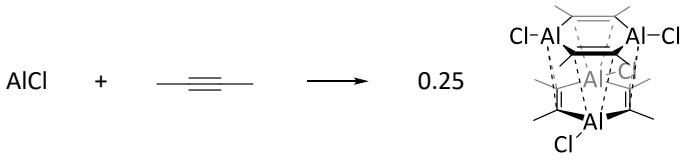

10

Scheme 47 *Reaction of AlCl with dimethylacetylene to form **10**, a compound with Al-olefin π bonding*

When monitored by ^{1}H and ^{27}Al NMR spectroscopy, heated solutions of (Cp*Al)$_4$ **2** with either dimethylacetylene or bis-trimethylsilylacetylene in C_6D_6 showed no evidence of reaction after several days. However, heating a solution of **2** with four equivalents of diphenylacetylene for 48 hours resulted in the clean formation of a single new product with full consumption of both starting materials. The characteristic ^{27}Al NMR signal for **2** at δ = -79 is now absent from the spectrum, and in the ^{1}H NMR spectrum new signals at δ = 1.71, 6.80 and 7.01 are present.

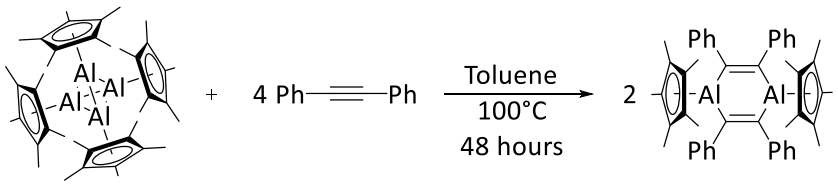

2 **11**

Scheme 48 *Reaction of Cp*Al with diphenylacetylene*

Repeating this reaction on a preparative scale allows product **11** to be isolated as an orange powder in yields up to 94 % (Scheme 48). The ^{1}H NMR is somewhat simple; a singlet signal for the Cp* methyl groups indicating all five groups are equivalent on the NMR timescale[10]

at δ = 1.71, and two multiplet aromatic signals around δ = 6.80 and 7.01 corresponding to the phenyl groups. A characteristic alkene carbon signal can be seen in the ^{13}C NMR spectrum at δ = 148.36. No signal is seen in the ^{27}Al NMR spectrum.

11 is stable in the solid state indefinitely, with samples stored under an argon atmosphere for over one year showing no degradation. Solutions of **11** in aromatic solvents are stable for several days, and solutions in coordinating solvents show adduct formation (see section 2.2.2).

High resolution electron ionisation mass spectroscopy (EI MS) of **11** confirms the molecular mass, with a signal of exact mass 680.355469 corresponding to $[C_{48}H_{50}Al_2]^+$ observed. The fragmentation pattern revealed a signal with an exact mass of 324.19729, corresponding to an ion with the molecular formula $[C_{20}H_{30}Al_2]^+$, which can be rationalised as [Cp*-Al=Al-Cp*]$^+$. This signal is not seen in EI MS spectra of starting material **2** under the same conditions. The corresponding neutral species Cp*-Al=Al-Cp* was shown to be present in small amounts in reactions conducted with $(Cp^*Al)_4$ in argon matrices at 12 K,[11] and given the recent report of the first neutral Al=Al species,[12] perhaps **11** could be used to access a corresponding Cp*-substituted dialumene.

X-Ray quality crystals of **11** were obtained from a saturated hexane solution after several weeks at room temperature, and the solid-state structure is shown in Figure 27. The central Al_2C_4 ring structure is in a boat conformation with the aluminium atoms out of plane with the C=C bonds. Because of this non-planar confirmation there is an absence of aluminium-olefin interactions which are seen in Schnöckel's compound, **10**. The average bond length for the alkene double bond in **11** at 1.363(2) Å, is comparable with 1.367 Å in **10**. Likewise the Al-C_{alkene} bonds are also similar to the corresponding bonds in **10**, ranging between 1.9870(17) Å and 1.9995(17) Å for **11** compared to an average distance of 1.990 Å for **10**.

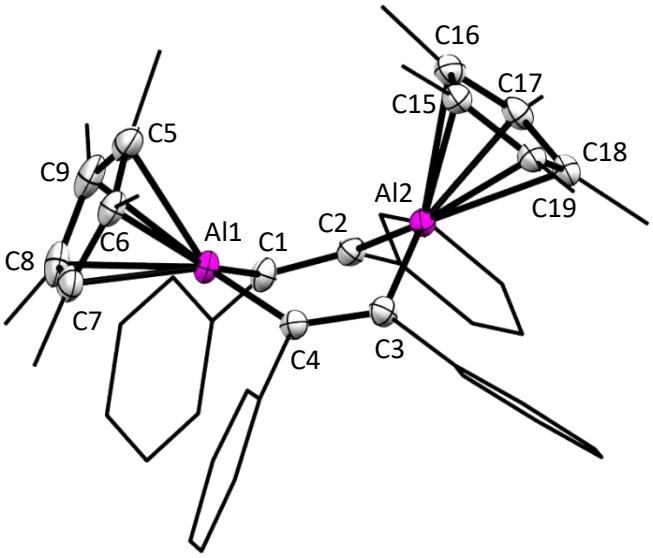

Figure 27 *X-Ray crystal structure of* ***11****. Hydrogen atoms are omitted for clarity, phenyl groups and terminal methyl groups are wireframe. Ellipsoids shown at 50 % probability. Selected bond lengths (Å) = C1-C2 1.362(2), C3-C4 1.363 (2), Al1-C1 1.9928(17), Al1-C4 1.9870(17), Al2-C2 1.9995(17). Al2-C3 1.9990(18), Al1-C5 2.3300(17), Al1-C6 2.3978(18), Al1-C7 2.2915(17), Al1-C8 2.2363(17), Al1-C9 2.2064(17), Al2-C15 2.2599(19), Al2-C16 2.3168(18), Al2-C17 2.2928(18), Al2-C18 2.2712(19), Al2-C19 2.2860(18). Selected bond angles (°) = A1-C1-C2 119.06(12), Al-C4-C3 118.89(12), A2-C3-C4 119.59(12), A2-C2-C1 119.26(12).*

The inter-aluminium distance in 1,4-dialuminacyclohexadiene derivative **11** is significantly elongated from that of the $(Cp^*Al)_4$ starting material (3.315 Å and 2.768 Å[13] respectively), and is too long for there to be any significant interaction. It is however slightly shorter than the comparable distance in dimethylacetylene product **10** (3.37 Å), for which a weak interaction has been calculated using density functional theory.[14]

Perhaps the most interesting feature of **11** that the Cp* rings retain their η^5 coordination mode from the $(Cp^*Al)_4$ starting material, and not the expected coordination modes η^1-η^3. This is consistent with the observation of a lone singlet signal in the ^{1}H NMR spectrum at δ = 1.71 corresponding to the Cp* group. Whilst this higher hapticity is seen in compounds with Al-M bonds (M = metal or metalloid)[15–18] where Cp*Al is a ligand, it is uncommon in compounds where aluminium is bonded only to carbon.[19] The electron-rich Cp* group donates electron density into the vacant p-orbital of the adajcent aluminium centre, providing intramolecular stabilisation analogous to the intermolecular Al-olefin bonding in **10**.

Following the successful isolation of **11**, reactions of $(Cp^*Al)_4$ **2** with other alkynes were carried out. Using 1-phenyl-2-trimethylsilylacetylene gave no observed reaction by ^1H and ^{27}Al NMR spectroscopy. Using terminal alkynes was also explored, however these reactions resulted in broad, complex ^1H NMR spectra.[20] It is known that reacting **2** with $LiN(SiMe_3)_2$ results in the production of Cp*Li and the formation of an Al-N bond,[21] so it may be possible that the terminal acetylene can cleave the Cp* group from $(Cp^*Al)_4$ by protonation, resulting in Cp*H and attaching the alkyne to the metal. The resulting products can form clusters or degrade, resulting in intractable mixtures of products.

3.2.2 Demonstrating the Lewis Acidity of 1,4-Dialumuminacyclohexadiene Derivative

A characteristic feature of compounds of the group 13 elements is an empty p-orbital at the main-group centre, which makes them excellent Lewis acids (section 2.2). The coordination of diethyl ether or tetrahydrofuran to Schnöckel's 1,4-dialuminacyclohexadiene derivative **10** disturbs the Al-olefin bond, breaking apart the dimeric structure to result in a four-coordinate tetrahedral aluminium centre (section 1.2.3).[22]

Even though electron density from the Cp* group is being donated into this p-orbital in the 1,2-dialuminacyclohexadiene derivative **11**, the complex can be thought of as bearing two 3-coordinate aluminium centres. Hence, **11** should demonstrate Lewis acidic behaviour. To experimentally validate this Lewis acidity, **11** was reacted stoichiometrically with coordinating solvents to form adducts. Small scale reactions were carried out by dissolving **11** in C_6D_6 and adding one equivalent of the solvent required, giving the ^{1}H NMR spectra shown in Figure 28. Three different solvents were used, diethylether (Et_2O), dimethoxyethane (DME) and tetrahydrofuran (THF).

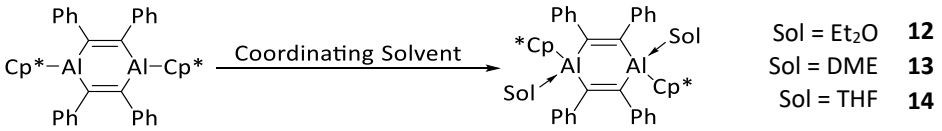

11

Scheme 49 *Synthesis of solvent adducts.*

Upon formation of diethyl ether adduct **12** there is little change to the signals in the ^{1}H NMR spectrum. The singlet signal for the Cp* methyl groups shifts slightly downfield from δ = 1.71 to δ = 1.74, and the aromatic signals remain unchanged. Evidence for coordination can be seen in the solvent's signals, which are shifted from the usual diethyl ether chemical shifts, from δ = 1.11 and 3.26[20] to δ = 1.05 and 3.23 in **12**.

A bigger change is observed when bidentate coordinating solvent DME is added to **11**. The Cp* signal is shifted further downfield, and is observed at δ = 1.90. The solvent signals are again changed from the uncoordinated values, at δ = 3.14 and 2.97 instead of δ = 3.12 and 3.33 ppm.[20] In the aromatic region there are three independent multiplet signals present for **13** at δ = 7.02-6.99, 6.96-6.95 and 6.84-6.81, indicating that the signals do not overlap as in **11** and **12**.

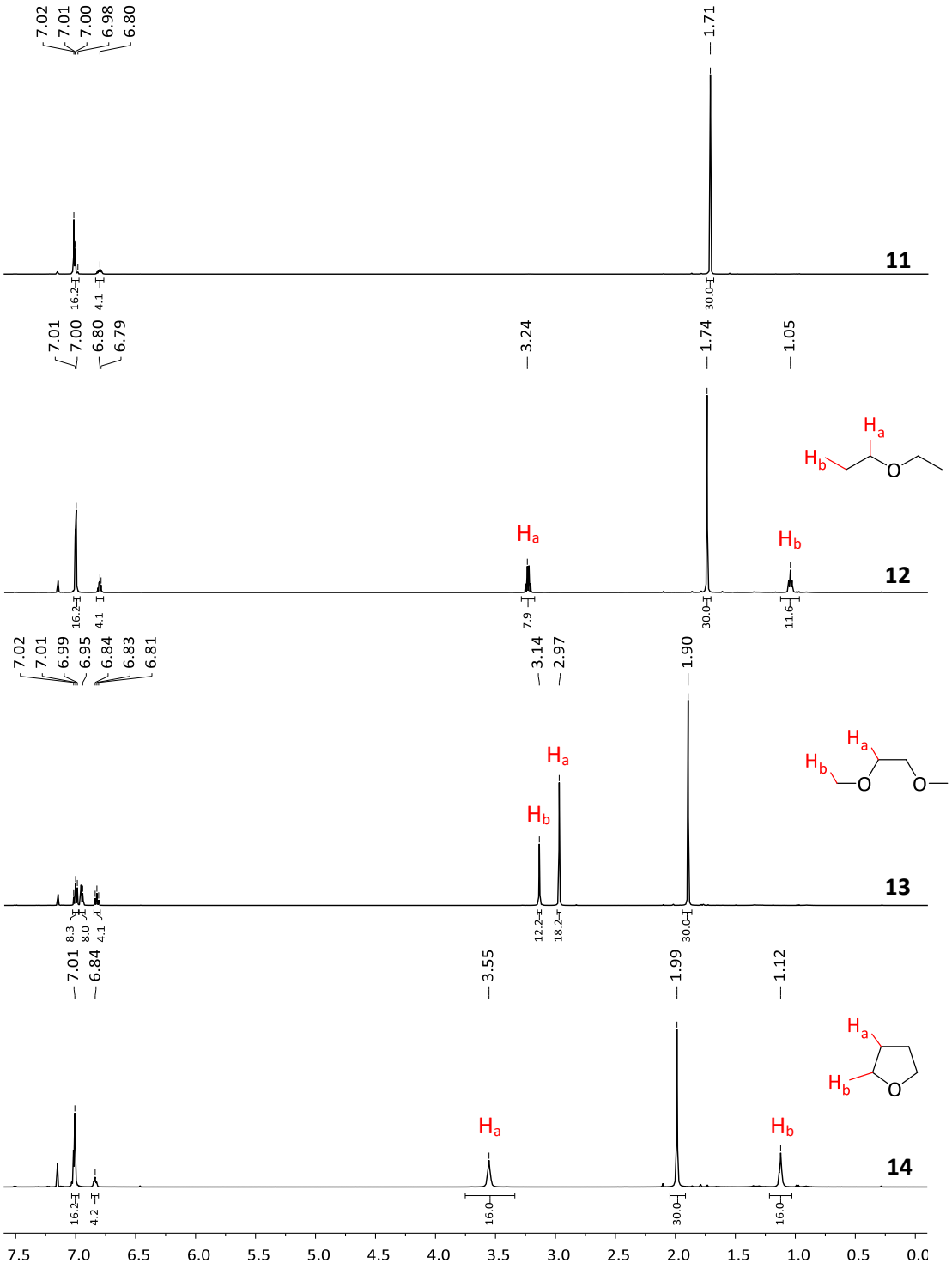

Figure 28 *^{1}H NMR (500 MHz, C_6D_6, 300 K) showing the coordination of solvents to* ***11***

The most strongly coordinating solvent of this trilogy causes the largest downfield movement of the singlet resonance. In the case of THF-adduct **14**, this signal is shifted to δ = 1.99, a downfield shift of δ = 0.28. The signals associated with the bound THF are broad

singlets, slightly shifted from their uncoordinated values.[20] Like in **12**, the aromatic resonances are virtually unchanged from that of **11**. Monitoring the C_6D_6 solution of **14** over time, there is some production of Cp*H and cis-stilbene.

None of these three solvent adducts have been isolated on a preparative scale, and so more about their structure is not known. It is assumed that as the metal centre is now four-coordinate, all three contain a tetrahedral aluminium centre. This would generate a planar central dialuminacyclohexadine ring. An analogous compound has been known since the 1970's,[21] with an ethyl group in place of the Cp* group (Scheme 50). The crystal structure of this complex shows a planar 6-membered ring, with an inter-aluminium distance of 3.4 Å.

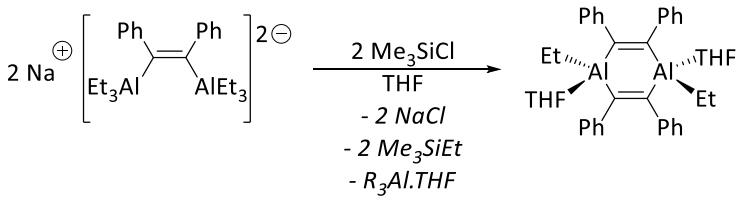

Scheme 50 *Reaction of an aluminium dianion to make a 1,4-dialuminacyclohexadiene derivative*

3.2.3 Attempted Preparation of Lewis Adducts with Stronger Lewis Bases

Following the Lewis acid character of **11** shown in section 2.2.2, the reactivity of bimetallic alane **11** with more strongly-coordinating bases to form Lewis base adducts was investigated. Addition of two equivalents of dimethylaminopyridine (DMAP) to a C_6D_6 solution of **11** triggered the precipitation of a white solid after a few minutes. ^{1}H NMR spectroscopy of the pale yellow solution showed full consumption of the starting material **11**, along with aromatic signals attributed to diphenylacetylene and alkyl signals associated to Cp*H. Signals indicating a minor product were noted; new doublet signals at δ = 9.10 ($^1J_{H\text{-}H}$ = 7.1 Hz) and 6.28 ($^1J_{H\text{-}H}$ = 7.2 Hz) and a new singlet at δ = 1.92 which combined display the correct ratio for a new DMAP environment (2:2:6). A new multiplet singlet in the aromatic region representing a new phenyl environment and three new singlets at δ = 2.26, 2.10 and 2.09 suggesting a new Cp* environment. This compound is proposed to be Lewis adduct **15**.

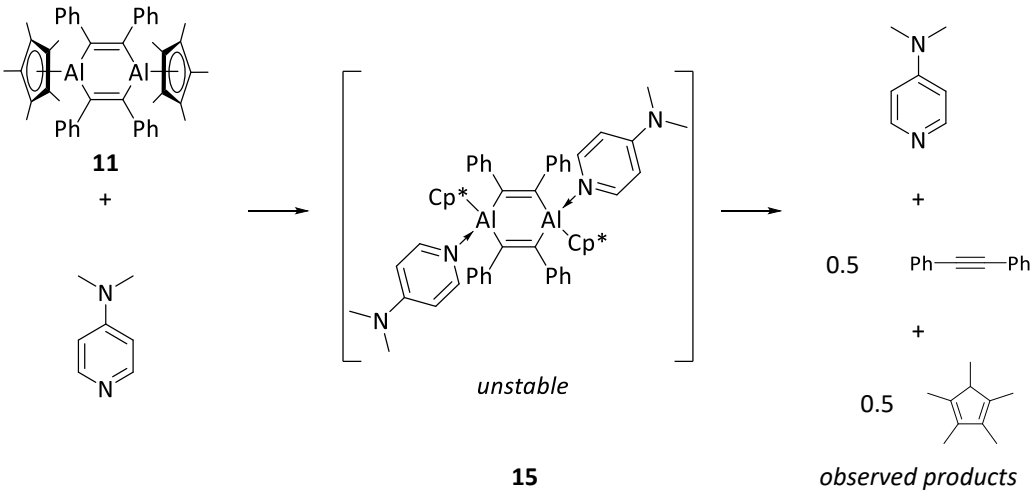

Scheme 51 *Coordination of DMAP to **11** and subsequent degradation*

Monitoring this solution for 18 hours by ^{1}H NMR spectroscopy resulted in the disappearance of **15** and the only compounds present were its organic counterparts: DMAP, diphenylacetylene and Cp*H. No aluminium containing product was identified, but it is assumed to be elemental aluminium given the other products present.

Repeating this reaction on a preparative scale allowed the reaction mixture to be kept at low temperature. DMAP was added to a toluene solution of **11** at -78°C, and the solution warmed to -30°C. The white solid that precipitated was collected and the solvent removed

at low temperature. The ^{1}H NMR spectrum of the solid indicated mostly degradation products with **15** as minor product. No pure sample of **15** could be isolated.

Moving to the more strongly σ-donating *N*-heterocyclic carbenes (NHC), **11** was reacted with tetramethylimdazolylidene (^{Me}IMe) in C_6D_6 resulting in a dark red-brown solution, the ^{1}H NMR spectrum of which was broad and undefined. Preparative scale reactions between **11** and ^{Me}IMe gave an inseparable complex mixture of products. Bulky carbenes 1,3-bis-(2,6-diisopropylphenyl)-imidazol-2-ylidene (IPr) and a cyclic (alkyl)(amino)carbene were also screened for reactivity, however no reaction was observed. This is possibly due to steric hinderance.

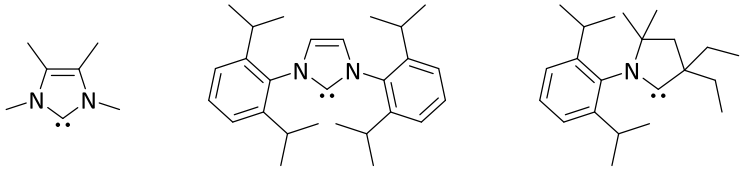

Figure 29 *N-heterocyclic carbenes reacted with diphenylacetylene product* ***11***

3.2.4 Attempted Reduction Of 1,4-Dialuminacyclohexadiene

It is possible to reduce aluminium containing heterocycles to make group 1 metal salts. For example, the reduction of an ethyl-substituted alumole with lithium metal to make a di-anionic aluminium containing ring sandwiched by two lithium cations in Scheme 52.[22]

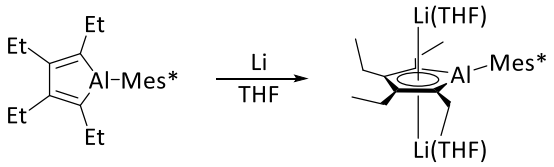

Scheme 52 *Reduction of an alumole with lithium to from an inverse sandwich complex*

Similar reactivity was investigated for **11**, with the aim of reducing the central Al_2C_4 ring to a 1,4-dialuminabenzene derivative. Following similar conditions to those seen in Scheme 52, a solution of **11** was added to a stoichiometric excess of lithium granules (7.7 eq) in THF. Initially there was some white precipitate formed which ^{1}H NMR spectroscopy identified as **14**, the THF adduct of **11**. After two hours, an aliquot of the reaction solution showed further formation of **14** and two other products, Cp*H and *cis*-stilbene. The alkene was identified by ^{1}H NMR spectroscopy as a characteristic singlet signal at δ = 6.49.[26] No aluminium-containing product can be identified.

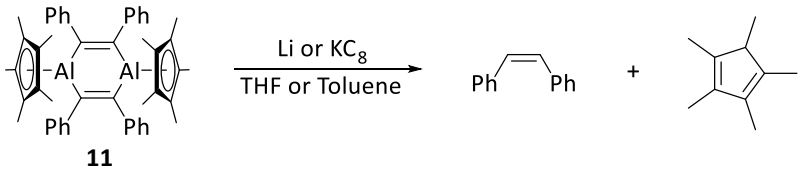

11

Scheme 53 *Reduction of **11** with Li granules or KC_8.*

Using two equivalents of potassium graphite in place of lithium under the same conditions gives the same products described in Scheme 53. It was thought that the formation of THF adduct **14** could be hindering the reduction of **3**, so the reaction was repeated using toluene as the solvent. ^{1}H NMR spectroscopy of the crude residue from this reaction confirmed the products as Cp*H and *cis*-stilbene. To gain some insight into any intermediates formed before degradation, the reaction was repeated in C_6D_6 and monitored by ^{1}H NMR spectroscopy, however no reaction had occurred after 4 days. It is concluded that **11** can be reduced by Li or KC_8, but the product of these reductions is unstable, reacting with the solvent to break apart into its organic constituents.

3.3 Insertion of Unsaturated Species Into Al-C Bonds

3.3.1 Aluminium-Mediated C=C Coupling via Insertion of an Isonitrile

It has now been shown that weak coordinating bases form stable Lewis adducts with 1,4-dialuminacyclohexadiene **11**, whilst the use of strong bases causes **11** to dissociate into its organic constituents. Looking for a base with intermediate coordinating properties, isonitriles were chosen as a possible candidate for coordination to the aluminium centre in **11**. Many examples of simple Lewis base adducts of alkyl aluminium compounds with isonitriles are reported.[27,28]

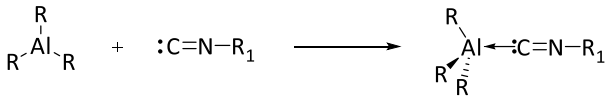

Figure 30 *Preparation of base adducts of alkyl aluminium complexes featuring an isonitrile. R=^{t}Bu, R_1=Me;[29] R=Me, Et, ^{i}Bu or ^{t}Bu, R_1=^{t}Bu or xylyl.[28]*

Insertion reactions are also possible. For the simple hydride and halide complexes $Me_3N.AlH_3$ and $AlCl_3$, their reactions with isonitriles result in insertion into the Al-Cl bond and the formation of metalloid clusters.[29,30] NacNacAl can react directly with isonitriles to form carbene-containing products,[31] but a NacNac-suuported aluminacyclopropene reacts *via* insertion of the isonitrile into the Al-C bond to expand the undoubtedly strained aluminacyclpropene ring.[32] The double insertion of two equivalents of an isonitrile into an Al-C bond of a cyclopentadienyl derivative forms two new C-C bonds and reduces the C-N bond to an imine (Scheme 55).[33]

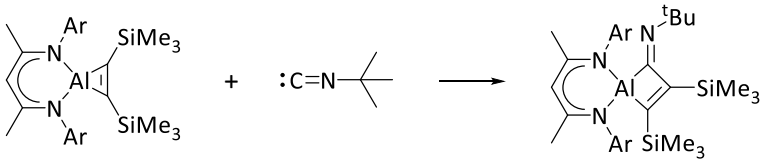

Scheme 54 *Reaction of aluminacyclopropene derivative with tert-butyl isonitrile*

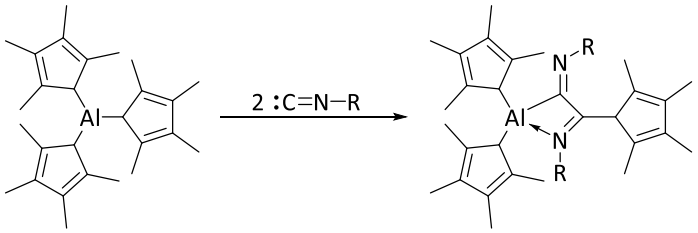

Scheme 55 *Double insertion of an isonitrile into a reactive Al-C bond.[34] R=^{t}Bu.*

Coupling of the terminal carbons of an isonitrile can result in C-C bonds with bond orders greater than 1. A barrelene dialane derived from a proposed dialumene[35] has been shown to react with four equivalents of tert-butyl isonitrile to cleave the Al-Al bond and create a diaminoalkyne (Scheme 56).[36]

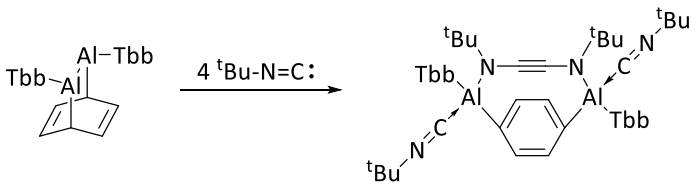

Scheme 56 *Isonitrile coupling to a triple bond by an Al(I) derived barrelene*

Evidently, diverse reactivity is possible when aluminium compounds are reacted with isonitriles, and the reactivity of $(Cp^*Al)_4$ and its diphenylacetylene adduct **11** with these organic substrates should prove fruitful. Aligned with the principal target of activating small molecules, 2,6-dimethylphenylisonitrile was employed here, as it is isoelectronic with carbon monoxide. A direct reaction between tetrameric $(Cp^*Al)_4$ **2** and 2,6-dimethylphenylisonitrile in C_6D_6 was carried out, however no reaction was observed, even with heating to 80 °C for several days.

Addition of four equivalents of 2,6-dimethylphenylisonitrile to a C_6D_6 solution of 1,4-dialuminacyclohexadiene derivative **11** resulted in an immediate colour change from pale orange to dark burgundy, and a crystalline solid began to precipitate (**16**). Where a singlet signal for the η^5 Cp* groups was present in the ^{1}H NMR spectrum of **11** (δ = 1.88), the same ligand in **16** gives three signals, shifted considerably upfield at δ = 1.41, 0.58 and 0.26, indicating the ring is no longer symmetrical and is less shielded. It is no longer in a high hapticity bonding mode, nor undergoing sigmatropic shifts on the NMR timescale. The ^{1}H NMR spectrum for **16** was in general very complex, with multiple signals observed in both the alkyl and the aromatic region. In the ^{13}C NMR spectrum of **16** a new very deshielded signal was observed in at δ = 152.3. Monitoring this solution over time, it was evident that initially two new species are formed, and over time one is transformed into the other. The intermediate species was not characterised.

Isolation of the crystals which had precipitated gave a pure sample of **16** in 32% yield, and the solid-state structure of zwitterionic was thus determined. The central Al_2C_4 functionality from **11** is retained, and the reaction with the isonitrile has occurred at the outer Al-Cp* bond. Two equivalents of the organic substrate have inserted into each of these Al-C bonds forming an unusual 2,3-diamidonorbornadienyl cationic ligand, where the cationic charge is localised at a bridgehead tertiary carbon from the former Cp* group. Overall, this complex reaction creates six new C-C bonds, two of which are double bonds from the coupling of isonitrile units.

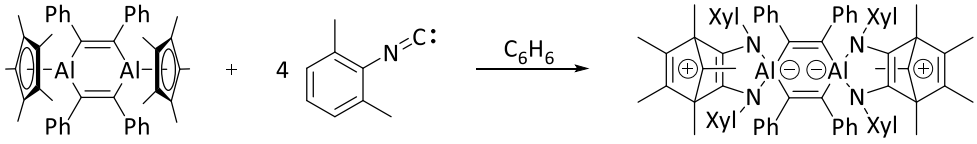

11 **16**

Scheme 57 *Reaction of **11** with 4 equivalents of isonitrile. Xyl=2,6-dimethylphenyl.*

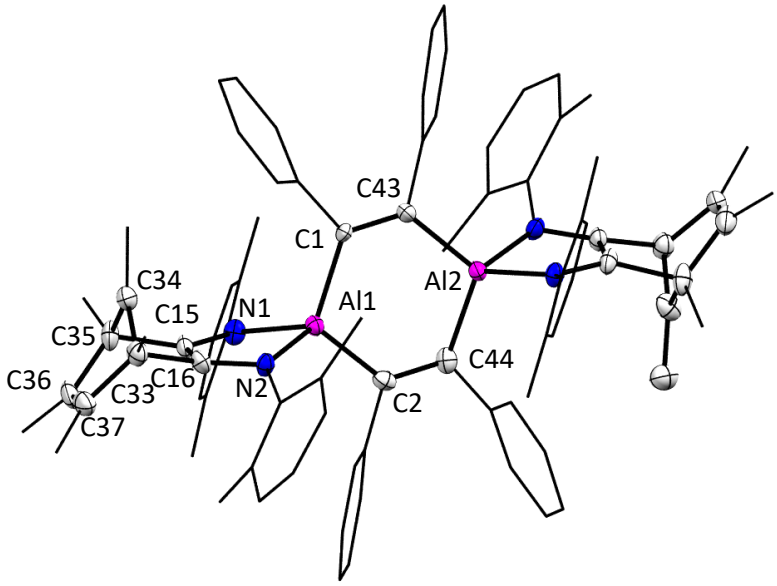

Figure 31 *X-Ray crystal structure of **16**. Hydrogen atoms and C_6D_6 of crystallisation are omitted for clarity. The xylyl and phenyl groups are wireframe for clarity. Ellipsoids shown at 50 % probability. Selected bond lengths (Å) = Al1-Al2 3.522, C2-C44 1.367(10), C1-C43 1.368(10), Al1-C2 1.977(7), Al1-C1 1.981(7), Al1-N1 1.946(6), Al1-N2 1.949(6), C15-C16 1.401(10), C36-C37 1.327(11), C15-C34 1.988(11), C16-C34 1.962(11). Selected bond angles(°) = C34-C33-C16 79.8(5), C34-C33-C15 81.6(5). Sum of angles around C34 359.9°.*

The solid-state structure of **16** is shown in Figure 31. A prominent feature is the planar central cyclohexadiene ring, markedly different from the boat confirmation seen in starting material **11**. This has increased the inter-aluminium distance from 3.315 Å in

diphenylacetylene product **11** to 3.522 Å in **16**. Aside from this conformational change, the bonding in this ring remains relatively unchanged. The alkene C=C and Al-C bond lengths are comparable; from 1.362(2) Å and 1.9870(17) Å in **11** to 1.367(10) Å and 1.977(7) Å in **16** respectively.

The presence of the bidentate diamido- ligand makes each aluminium centre in **16** four-coordinate, and therefore they now feature a distorted tetrahedral geometry. The small angle between N1-Al1-N2 of 86.3(2)° is compensated by the wider angles to the other substituents, for example C1-Al1-C2 113.4(3)°.

Close inspection of the bridgehead carbons in **16** leads to their cationic assignment. Both C34 and C76 are planar, with the sum of the angles around each of these atoms being 359.9(12)°. The angle between the bridging carbon and the isonitrile-derived C=C (e.g. C34-C33-C16) is acute at 79.8(5)°, significantly narrower than the corresponding angle to the Cp*-derived C=C (e.g. C34-C33-C37), at 102.5(6)°. This is suggestive of homoconjugation from the former alkene π-bond.

Product **16** co-crystallises with one molecule of C_6H_6, and when isolated crystals are re-dissolved into deuterated benzene, production of *cis*-stilbene is observed over time along with other unidentified products. This is attributed to the degradation of **16** in solution. It is thought that this rapid crystallisation from benzene upon formation enables the isolation of **16**, and in the solid state **16** is stable under an argon atmosphere for several months. The optimal solvent for recording NMR spectra of **16** was found to be CD_2Cl_2, solutions in which **16** was stable for several days. The fact that the carbocationic centre in **16** did not react with CD_2Cl_2 further attests to the intramolecular stabilisation provided by the π-bond and aluminate anions.

Using the solid-state structure, the complex ^{1}H NMR spectrum of **16** can be easily reasoned. The signals associated with the Cp*-derived unit were previously identified at δ = 1.41, 0.58 and 0.26, the most upfield signal of which can be assigned to the methyl-group attached to the bridging carbon. Singlet signals for the xylyl-methyl groups are found at δ = 2.71 and 1.50 and were differentiated from the Cp* signals by using a ^{1}H-^{1}H COSY experiment. The

same 2D-correlation allows the aromatic region to be assigned. The aromatic xylyl protons appear at δ = 7.19 (d, $^{1}J_{H\text{-}H}$ = 7.3 Hz), 7.03 (t, $^{1}J_{H\text{-}H}$ = 7.3 Hz) and 6.95 – 6.91, with a relative ratio of 1:1:1. The phenyl protons are found at δ = 7.19 (d, $^{1}J_{H\text{-}H}$ = 7.3 Hz), 7.03 (t, $^{1}J_{H\text{-}H}$ = 7.3 Hz), 6.95 – 6.91, 6.75 (d, $^{1}J_{H\text{-}H}$ = 8.2 Hz), 6.68 (d, $^{1}J_{H\text{-}H}$ = 8.2 Hz), 6.55 – 6.50, 6.46 (d, $^{1}J_{H\text{-}H}$ = 7.3 Hz) and 5.73 (d, $^{1}J_{H\text{-}H}$ = 7.3 Hz). The large number of signals is consistent with a lack of symmetry in the structure of **16**. No signal is seen in the ^{27}Al NMR spectrum.

Whilst the ^{13}C NMR chemical shift of a classical carbocation typically ranges between δ = 200-300,[37] intra-molecular stabilisation by homoconjugation results in significant lowering of this value. Some examples of isolated carbocations and their ^{13}C chemical shifts are shown for comparison in Figure 32. The earlier identification of a very de-shielded carbon at δ = 152.3 in the ^{13}C NMR spectrum can now be assigned to the bridging planar carbons in isonitrile product **16** (C34 and C76).

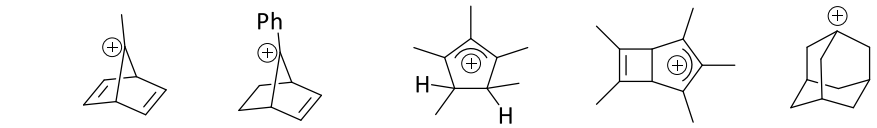

^{13}C δ = 66.7 108.6 153.6 155.8 300.0

Figure 32 *^{13}C NMR chemical shifts of stable carbocations[37–41]*

Few compounds can be found in the literature featuring a similar zwitterionic tricyclic system. The most similar example can be found in lanthanide chemistry, where the insertion of two carbon monoxide units into an M-C_{Cp^*} bond results in carbon coupling.[42–44] Analogous intra-molecular stabilisation of the carbocation is seen in the lanthanide examples.

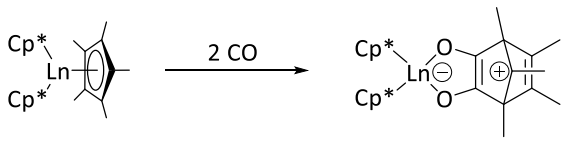

Scheme 58 *Reaction of lanthanide Cp* complexes with carbon monoxide. Ln = La, Ce, Pr, Nd or Sm*

Due to the isoelectronic relationship between carbon monoxide and isonitriles, a solution of **11** was exposed to a carbon monoxide atmosphere. A colour change from orange to dark brown was observed, however no reaction was detected using ^{1}H NMR spectroscopy.

3.3.2 Using Density Functional Theory to Confirm π-Homoconjugation

Density functional theory (DFT) has been used to confirm intra-molecular stabilisation in the well-studied adamantyl carbocation,[45] and so DFT was used here to further support the idea of the homoconjugation stabilising the cationic carbon in zwitterionic **16**. Using the solid-state structure of **16** as an initial geometry, the structure was optimised using B3LYP/6-31G(d,p) method and basis set.

Key bond lengths and angles in the solid-state structure **16** and optimised calculated structures **16$^{\#}$** are listed in Table 4. In all cases the bond lengths are slightly overestimated in the optimised structure **16$^{\#}$**, but with the largest discrepancy being 3.6% in the Al-N bond, they are still fairly comparable. The N-Al-N shows the largest difference in experimental/calculated angles values at 2.3% overestimation. Overall the geometry optimised structure provides an accurate representation of the experimental structure.

	16 - X-Ray (Å)	**16$^{\#}$ - B3LYP (Å)**		**16 - X-Ray (°)**	**16$^{\#}$ - B3LYP (°)**
$C{=}C_{ring}$	1.368(14)	1.375	C-Al-C	113.1(4)	113.3
$C{=}C_{iso}$	1.402(14)	1.419	N-Al-N	86.6(8)	85.8
Al-N	1.946(12)	1.996	C_{iso}-C-C^{+}	80.3(10)	80.8
Al-C	1.985(14)	2.021			

Table 4 *Comparison of selected bond lengths and in the experimental and calculated solid state structure of **16**. Averages were taken where more than one example of length or angle is present in molecule*

The HOMO-1 of **16$^{\#}$** is visualised in Figure 33. There is a significant bonding interaction between the cationic carbon and the newly formed alkene bond from the terminal isonitrile carbons. This indicates some electron donation from the π-bond system to this sp^2 hybridised carbon, providing electronic stabilisation. This interaction is simplified in Figure 34. The LUMO can also be viewed from these calculations (Figure 35) and shows the corresponding anti-bonding interaction.

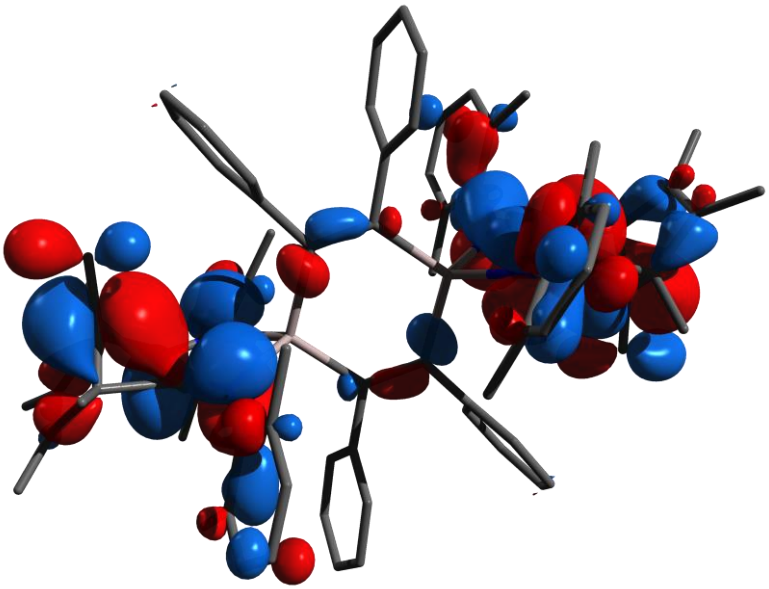

Figure 33 *Visualised HOMO-1 of* ***16#*** *(B3LYP/6-31G(d,p)). ISO=0.02*

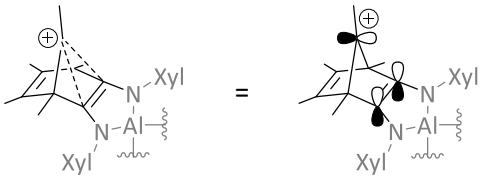

Figure 34 *Simplified orbital diagram depicted major interaction n the HOMO-1 of* ***16#***

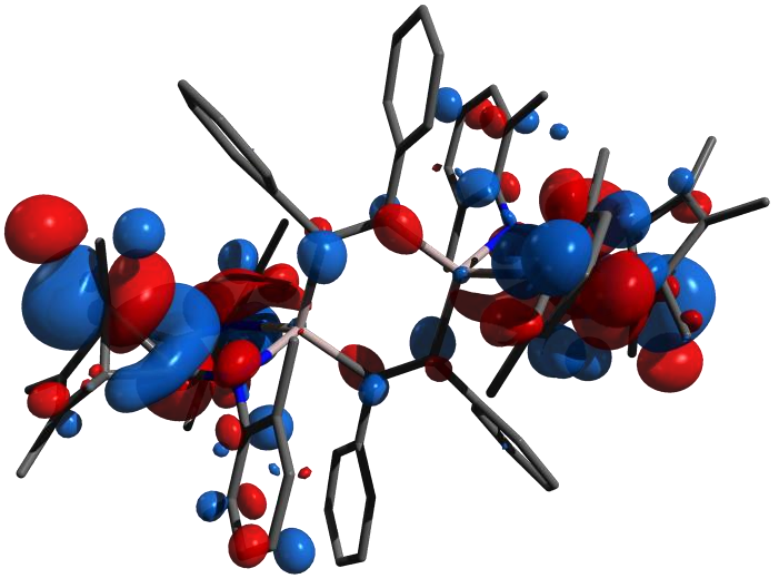

Figure 35 *Visualised LUMO of* ***16#*** *(B3LYP/6-31G(d,p)). ISO=0.02*

3.3.3 Unusual Amindate Ligands Formed from the Insertion of Carbodiimides

The insertion of carbodiimides into Al-C bonds is well documented, and is a typical synthetic route to amidinato aluminium complexes,[46,47] generalised in Scheme 59. The mechanism has been shown to proceed by the initial formation of a Lewis base adduct, followed by the insertion of the carbodiimide into the Al-C bond.[48] The resulting amidinate aluminium complexes are worthwhile targets as they have shown activity as catalysts for various polymerisations.[49]

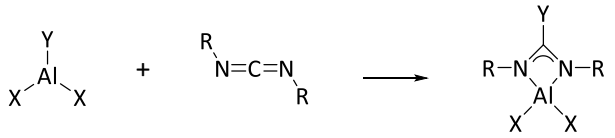

Scheme 59 *Preparation of amidinate aluminium complexes from carbodiimides*

As 1,4-dialuminacyclohexadiene **11** was shown to undergo insertion with isonitriles, it was questioned if this insertion chemistry could be extended to include carbodiimides. A solution of dicyclohexylcarbodiimide (DCC) in toluene was added slowly at low temperature to a dilute solution of **11**, and the resulting solution was allowed to reach room temperature over two hours. Removal of volatiles in vacuo and washing the resulting yellow oily residue with hexane allowed for the isolation of white solid **17**.

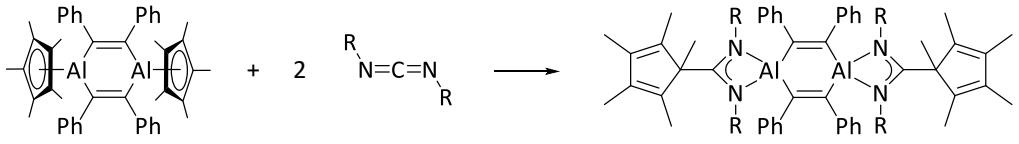

11

R = cyclohexyl **17**
or diisopropyl **18**

Scheme 60 *Insertion of carbodiimides into the Al-C bond of **11***

The aromatic region of the ^{1}H NMR spectrum of **17** indicates that only one compound is present. The phenyl groups give three multiplet signals at δ = 7.37-7.30, 7.12-7.07 and 6.92-6.86, with a relative ratio of 2:2:1 (ortho:meta:para). In starting material **11** the Cp* methyl groups appear as a singlet due to the high hapticity and fast rotation of the ligand, however as they are now inequivalent in **17** they give three singlet signals at δ = 1.55, 1.51 and 1.47 with a relative ratio of 2:1:2. Multiple overlapping resonances were identified for the four cyclohexyl groups in **17**, making the alkyl region of the ^{1}H NMR spectrum very complex.

A striking feature of the ^{1}H NMR spectrum of DCC product **17** was the signal associated with the ipso C-H proton of the cyclohexyl groups. Initally assigned as a "tented" doublet of triplets of triplets, upon closer inspection of the coupling constants it became apparent this is four separate signals. It is suggested that this is due to two isomers of **17** present due to the conformational flexibility of the cyclohexyl rings. Whilst variable temperature ^{1}H NMR experiments showed no change in the signals, this does not preclude conformational isomerism.

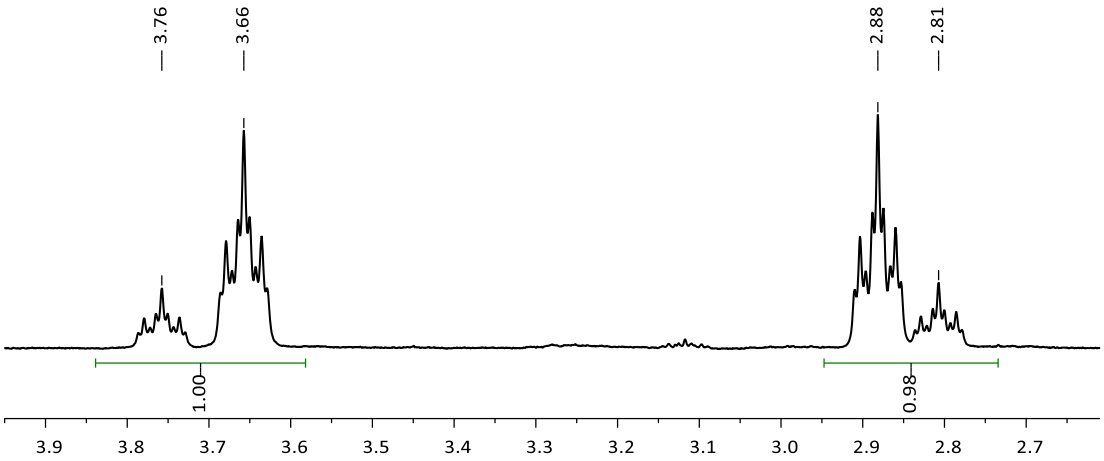

Figure 36 *A section of the ^{1}H NMR spectrum of **17** (500 MHz, 300K, C_6D_6) showing the ipso-CH signals*

The solid-state structure of **17** from crystals grown from a saturated hexane solution is shown in Figure 37. The central Al_2C_4 bimetallic ring from **11** is retained, although unlike the boat conformation seen in **11** the Al_2C_4 core in **17** is planar, and is comparable with isonitrile product **16**. The Al-C bond lengths are unperturbed from the starting material, in the range of 1.980(2) Å to 1.986(2) Å. The alkene bond lengths in **17** are slightly elongated at 1.366(8) Å and 1.367(3) Å, compared with 1.362(2) Å and 1.363(2) Å in starting material **11**. They are virtually identical to the analogous bond lengths in the zwitterionic compound **16** (1.367(10) Å and 1.368(10) Å).

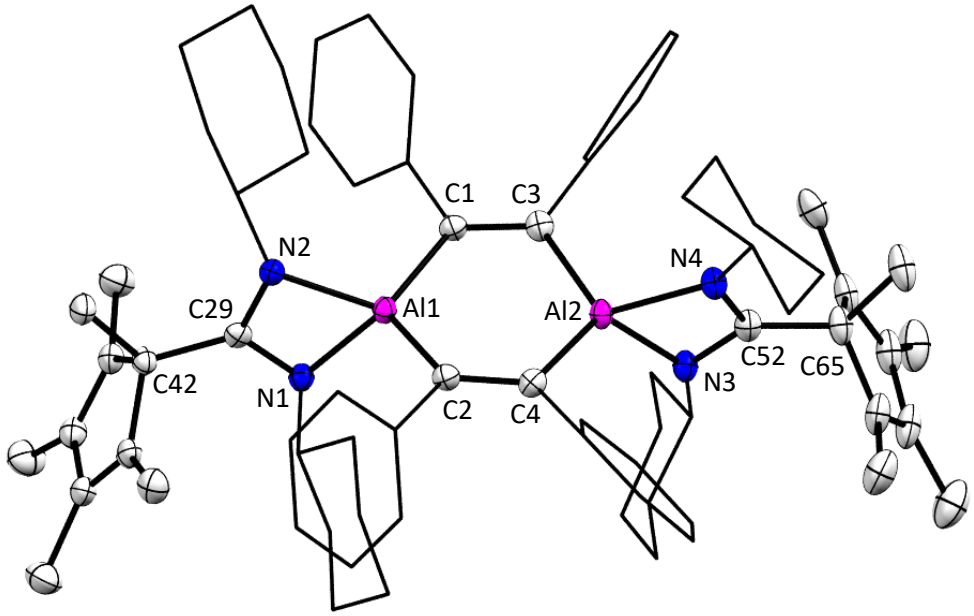

Figure 37 *X-Ray crystal structure of* ***17****. Hydrogen atoms and 2 molecules of co-crystallised hexane are omitted for clarity. Organic substituents are wireframe. Ellipsoids shown at 50 % probability. Selected bond lengths (Å) = Al1-Al2 3.424, C1-C3 1.367(3), C2-C4 1.366(3), Al1-C1 1.980(2), Al1-C2 1.986(2), Al1-N1 1.9213(17), Al1-N2 1.9162(17), C29-N1 1.336(3), C29-N2 1.351(3), C29-C42 1.540(3). Selected bond angles (°) = N1-C29-N2 107.97(16), C42-C29-N2 128.45(18), C42-C29-N1 123.47(16), C1-Al1-C2 116.12(9), N1-Al1-N2 68.98(7), N1-Al1-C2 118.95(8), N2-Al1-C1 114.56(8).*

Delocalisation across the amidine N-C-N unit is confirmed by an sp^2 hybridised central carbon, with the sum of angles around C29 and C52 being 359.9(30)°. The C-N bond lengths have a range of 1.336(3) Å to 1.351(3) Å, which is relatively short. The aluminium atoms are in a distorted tetrahedral geometry, with angles of C1-Al1-C2 116.12(9)° and N1-Al1-N2 68.98(7)° being far from the ideal 109.5°.

Even though the reaction between **11** and DCC to form **17** is quantitative when performed on an NMR scale, when synthesised on a preparative scale, pure samples were only isolated in very small quantities, and so **17** is not fully characterised.

In an effort to simplify the ^{1}H NMR spectrum of **17**, the reaction of diphenylacetylene product **11** with diisopropylcarbodiimide (DIC) was investigated. Using analogous conditions to the formation of **17**, DIC insertion product **18** was isolated. Indeed, the spectroscopic data was simplified, but still possess some noteworthy features. The isopropyl methyl groups are seen as four doublet signals at δ = 1.01 ($^1J_{H\text{-}H}$ = 6.3 Hz), 1.07 ($^1J_{H\text{-}H}$ = 6.1 Hz), 1.16 ($^1J_{H\text{-}H}$ = 6.4 Hz), 1.26 ($^1J_{H\text{-}H}$ = 6.1 Hz), which each couple to one of four

septet signals (δ = 3.21 ($^1J_{H\text{-}H}$ = 6.3 Hz), 3.28 ($^1J_{H\text{-}H}$ = 6.3 Hz), 3.99 ($^1J_{H\text{-}H}$ = 6.2 Hz), 4.09 ($^1J_{H\text{-}H}$ = 6.1 Hz)) in the ^{1}H-^{1}H COSY spectrum.

The signal for the Cp* methyl groups was assigned to the only remaining signal, a multiplet signal around δ = 1.51-1.47, which loosely resembles a triplet. However, this signal does not account for all thirty of the Cp*-based protons. Variable temperature ^{1}H NMR experiments revealed two other signals at 333 K, δ = 1.23 and 1.21, attributed to the missing methyl groups, which are concealed by one of the ^{i}Pr doublets at 300 K. Increasing the temperature further to 363 K allowed for six individual signals corresponding to inequivalent methyl groups to be observed. It is proposed that this behaviour is the result of thermally-induced chemical shift changes, rather than through dynamic behaviour.

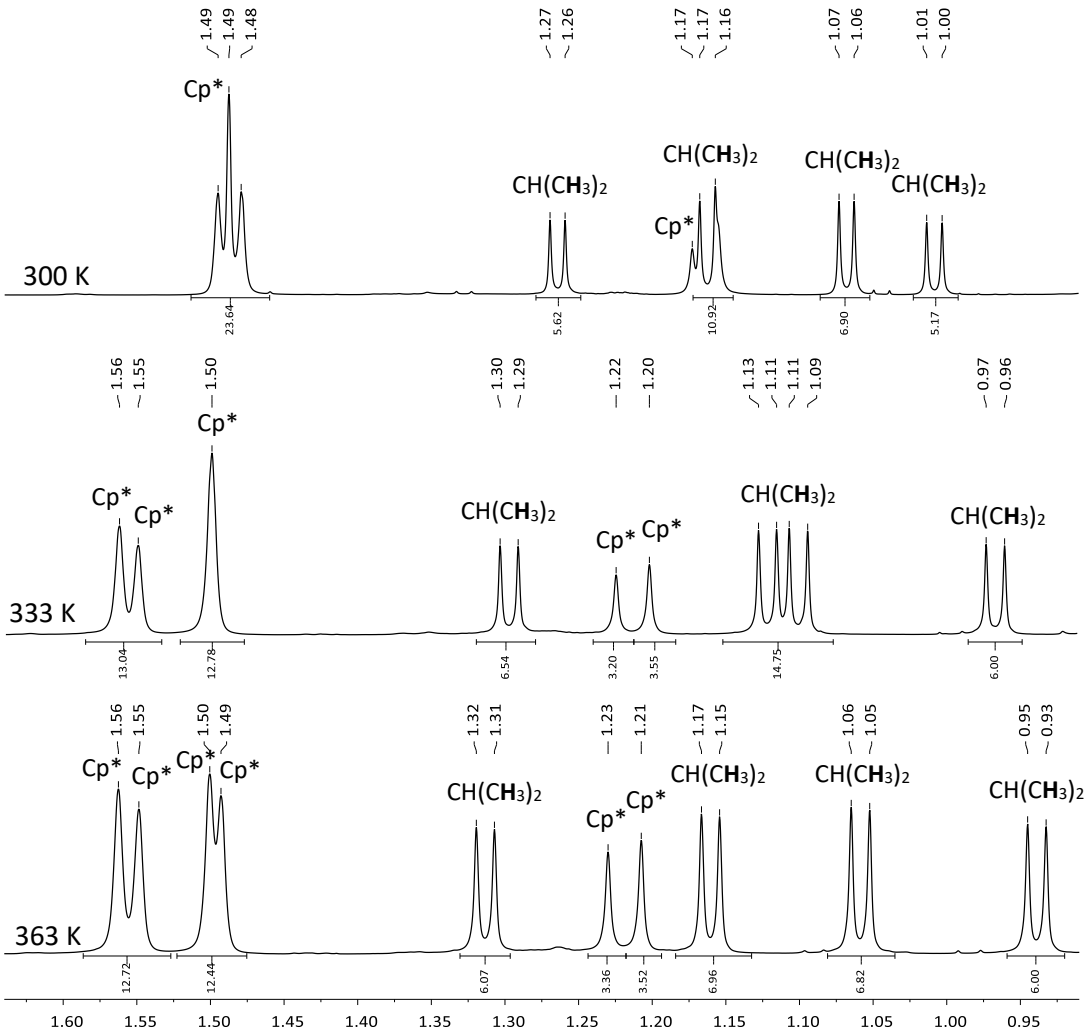

Figure 38 *Variable temperature ^{1}H NMR (500 MHz, tol-d_8) of DIC adduct*

3.3.4 A Proposed Bidentate Aluminium Carboxylate Species

Due to the significant strain associated with an AlO_2C ring, symmetrical aluminium mono-carboxylates **I** are difficult to isolate. Many attempts targeted at the isolation of this target have resulted in the isolation of either an unsymmetrical mono-chelate **II** or a bridging chelate **III**, with latter being calculated as the most stable bonding mode.[49]

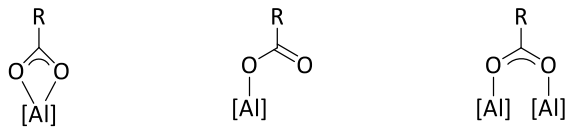

I **II** **III**

Figure 39 *Diverse chelating modes of a carboxylate ligand to aluminium complexes*

An example of an aluminium complex featuring a κ^2 carboxylate ligand is shown in Scheme 61. It is formed by the contraction of the corresponding eight-membered ring by coordination of a Lewis base.[50] When the reaction was repeated with Al-Me groups in place of the halide functionality results in a similar complex with an unsymmetrical carboxylate ligand (type **II**).[51]

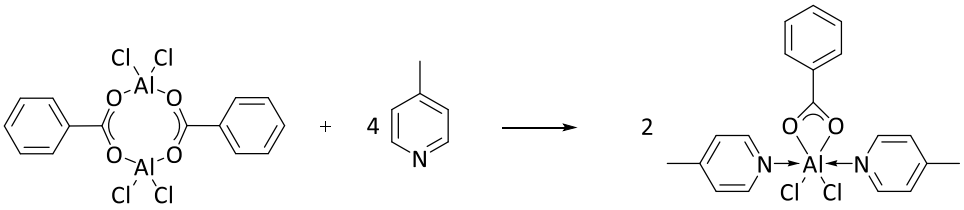

Scheme 61 *Formation of a mono-chelating aluminium carboxylate*

As carbodiimides are isoelectronic with carbon dioxide, it is expected that reactions of diphenylacetylene adduct **11** with CO_2 will proceed in a similar fashion to that of the formation of amidinate complexes **17** and **18**, to form an aluminium carboxylate. Since complex **11** features a bimetallic central ring, the isolation of an intramolecular bridging carboxylate is possible, however due to the amount of steric bulk present from the η^5 Cp* rings in **11** this is unlikely without cleavage of the Al_2C_4 alkene bonds. Equally, intermolecular bridging carboxylates are unlikely for the same reasons.

Exposing a degassed benzene solution of **11** to an atmosphere of CO_2 results in the almost immediate decolourisation of the orange solution and precipitation of a white solid, identified as insertion product **19**, with the favourable formation of Al-O bonds providing a driving force. The complexation of CO_2 was not reversible, as **19** was found to be stable under vacuum for prolonged periods.

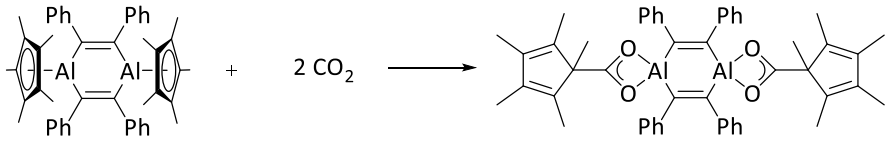

11 **19**

Scheme 62 *Reaction of phenylacetylene adduct **11** with CO_2*

Analysing the precipitated solid using NMR techniques was difficult due to its low solubility. It was found to be insoluble in benzene, toluene, hexane, pentane or dichloromethane. Dissolving the solid in THF-d_8 allowed for ^{1}H and ^{13}C NMR spectra to be immediately collected, however it was found that after around 30 minutes in solution the resulting spectra were broad and undefined, suggesting that **19** is unstable in solution, probably through reaction with THF.

The ^{1}H NMR spectrum (Scheme 60) of **19** shows few signals, but is strikingly different to starting material. In **11** the Cp* methyl groups appear as a single resonance at δ = 1.71, and in **19** three singlet signals for the now chemically equivalent protons at δ = 1.80, 1.76 and 1.73. Two signals **19** are seen in the aromatic region; a triplet signal at δ = 6.90 ($^{1}J_{H\text{-}H}$ = 7.5 Hz) and a multiplet signal around δ = 6.80 – 6.73.

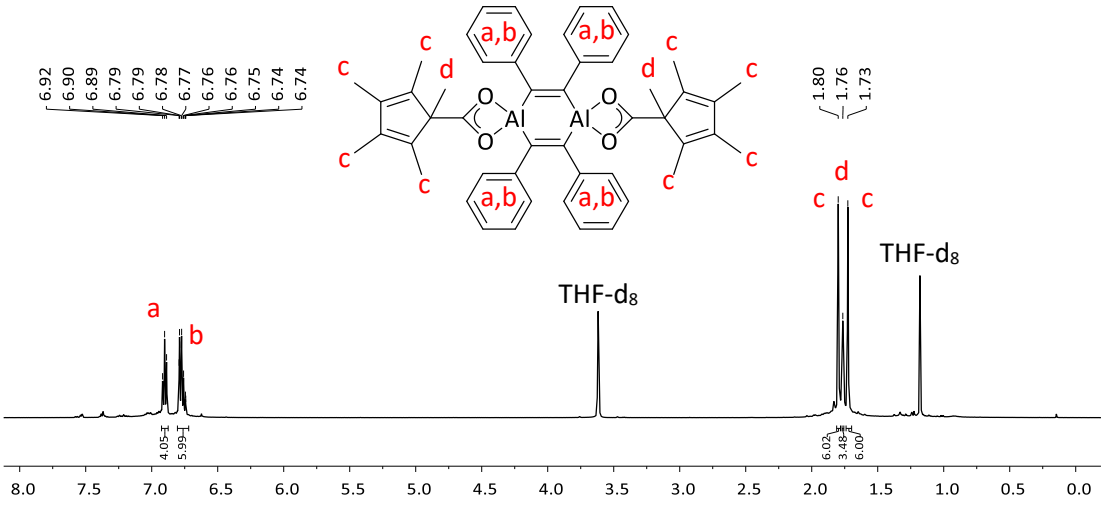

Figure 40 *^{1}H NMR spectrum of CO_2 insertion product **19** (500 MHz, 300 K, THF-d_8)*

A signal at δ = 180.5 in the ^{13}C NMR spectrum is attributed to the new carboxylate carbon in **19**. It is comparable with the analogous carbon signals in carbodiimide products **17** and **18**, at δ = 174.8 for both complexes. Other than this new signal, the ^{13}C NMR spectrum contains signals at similar chemical shifts to starting material **11**, with a greater number as the symmetry is now reduced. Due to the instability of **19** in solution, 2D NMR experiments were not possible. No signal was observed in the ^{27}Al NMR spectrum.

Due to its low solubility, it was difficult to obtain crystalline material of **19**, and attempts were made to crystallise the product upon formation. The reaction of **11** with carbon dioxide is rapid, and so very dilute solutions of **11** were employed, but with no success. Different solvents were trialled, as well as different pressures of CO_2, however no X-ray quality crystals were formed.

To confirm the molecularity of **19**, mass spectroscopy was carried out. High resolution EI MS shows a molecular ion signal at 769.34127, of which accurate mass experiments confirm the molecular formula as $[C_{50}H_{50}O_4Al_2]^+$, which is consistent with the incorporation of two equivalents of CO_2 into dialuminiacyclohexadiene **11**.

Without X-ray crystallography evidence the bonding mode of the carboxylate cannot be confirmed, however strong indications can be found using infrared spectroscopy. The solid-state FT-IR spectrum of **19** is shown in Figure 41. A strong, sharp stretch at 1425 cm^{-1} with

an adjacent weaker stretch at 1557 cm^{-1} indicates a symmetrical carbonyl with a low bond order.[50] This data fits well with the bidentate complex shown in Scheme 61, which has IR stretching frequencies at 1451 cm^{-1} and 1627 cm^{-1}.[50] If an unsymmetrical bonding mode was present, more stretching frequencies would be observed, most likely at higher wavenumber. Several stretches are seen in the alkyl region, at 2699 cm^{-1}, 2911 cm^{-1} and 2856 cm^{-1}, are caused by the methyl groups associated with the Cp* group.

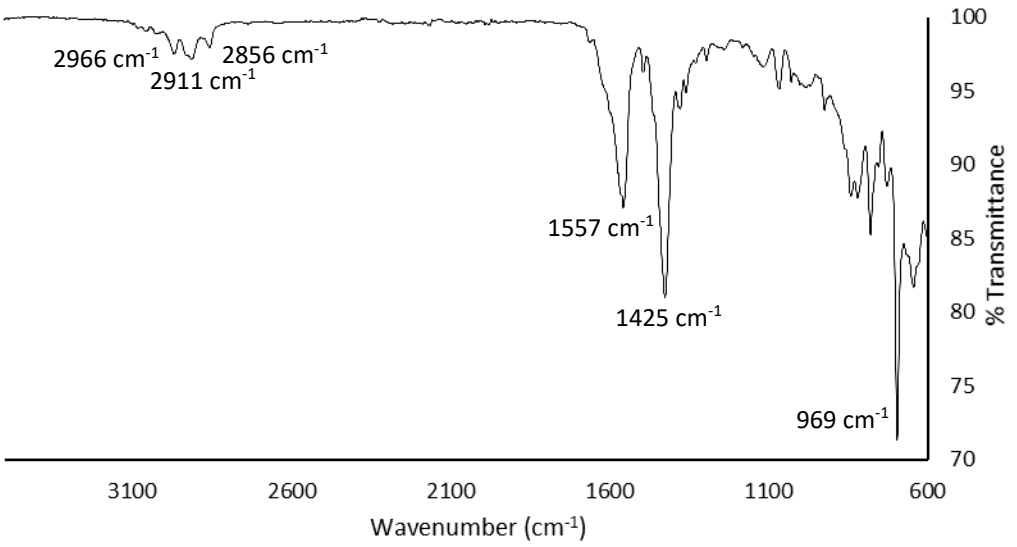

Figure 41 *IR Spectrum of CO_2 product* ***19***

3.4 Summary

Tetrameric $(Cp^*Al)_4$ can activate the E-H bonds of diisopropylaniline and pinacol borane, however the resulting products are difficult to separate and isolate. The low oxidation state metal centre can form a 1,4-dialuminacyclohexadiene derivative **11** from the activation of diphenylacetylene at high temperatures, the central C_4Al_2 bimetallic ring of which is stable and seemingly unreactive. In contrast, the outer Al-C_{Cp^*} bond readily undergoes insertion reactions by unsaturated N=C and C=O bonds to form 4- and 5-membered metallacycles.

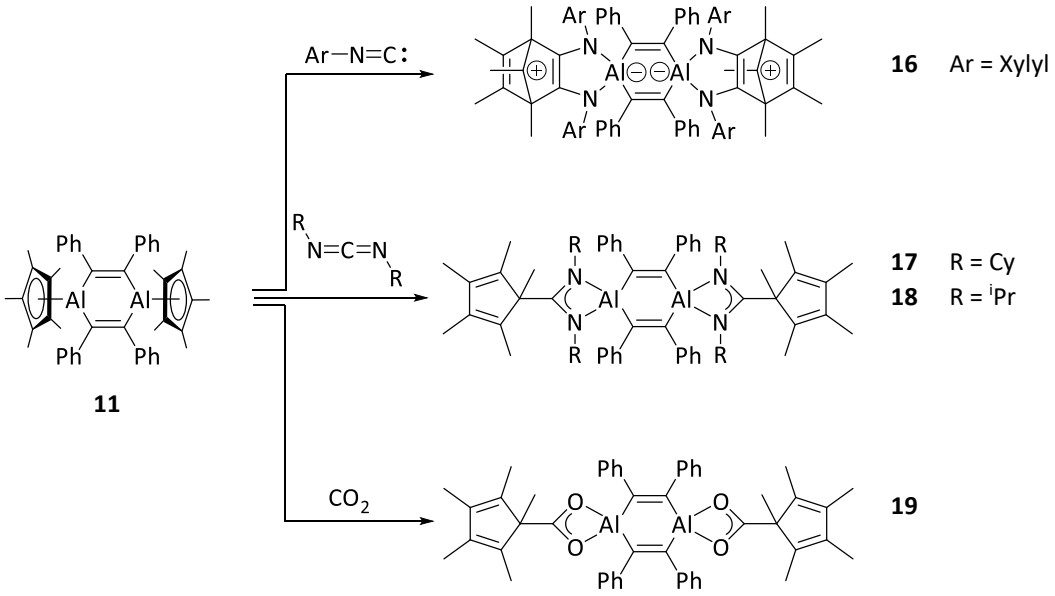

Scheme 63 *Summary of reactivity of 1,4-dialuminacyclohexadiene derivative* ***11***

The insertion of four equivalents of 2,6-dimethylphenyl isonitrile into the Al-C_{Cp^*} bonds of **11** results in the zwitterionic product **16**. The aluminium-mediated coupling of the terminal carbon atoms forms an alkene, which stabilises a bridging carbocation generated from the Cp* group. This homoconjugation can be visualised in the calculated molecular orbitals.

Amidine ligands with a Cp* backbone can be created by the insertion of two equivalents of a carbodiimide into the Al-C_{Cp^*} bonds of **11** . Two examples are shown here (**17** and **18**), of which the ^{1}H NMR spectrum shows little symmetry resulting in complicated spectra. A probable aluminium carboxylate is formed when exposing **11** to a carbon dioxide atmosphere, of which IR spectroscopy suggests an uncommon symmetricabidentate chelate structure, **19**.

3.5 References

1 T. Chu, I. Korobkov and G. I. Nikonov, *J. Am. Chem. Soc.*, 2014, **136**, 9195–9202.
2 M. R. Crimmin, M. J. Butler and A. J. P. White, *Chem. Commun.*, 2015, **51**, 15994–15996.
3 T. Chu, Y. Boyko, I. Korobkov and G. I. Nikonov, *Organometallics*, 2015, **34**, 5363–5365.
4 T. Chu, Y. Boyko, I. Korobkov, L. G. Kuzmina, J. A. K. Howard and G. I. Nikonov, *Inorg. Chem.*, 2016, **55**, 9099–9104.
5 C. Ganesamoorthy, D. Bläser, C. Wölper and S. Schulz, *Angew. Chem. Int. Ed.*, 2014, **53**, 11587–11591.
6 T. Chu, S. F. Vyboishchikov, B. Gabidullin and G. I. Nikonov, *Angew. Chem. Int. Ed.*, 2016, **55**, 13306–13311.
7 J. D. Gorden, A. Voigt, C. L. B. Macdonald, J. S. Silverman and A. H. Cowley, *J. Am. Chem. Soc.*, 2000, 950–951.
8 M. Tacke and H. Schnoeckel, *Inorg. Chem.*, 1989, **28**, 2895–2896.
9 H. Schnockel, M. Leirnkuehler, R. Lotz and R. Mattes, *Angew. Chem. Int. Ed. Engl.*, 1986, **25**, 921–922.
10 P. Jutzi, *Chem. Rev.*, 1986, **86**, 983–996.
11 H.-J. Himmel and J. Vollet, *Organometallics*, 2002, **21**, 5972–5977.
12 P. Bag, A. Porzelt, P. J. Altmann and S. Inoue, *J. Am. Chem. Soc.*, 2017, **139**, 14384–14387.
13 C. Dohmeier, C. Robl, M. Tacke and H. Schnockel, *Angew. Chem. Int. Ed. Engl.*, 1991, **30**, 564–565.
14 R. Ahlrichs, M. Häser, H. Schnöckel and M. Tacke, *Chem. Phys. Lett.*, 1989, **154**, 104–110.
15 G. Linti and H. Schnöckel, *Coord. Chem. Rev.*, 2000, 285–319.
16 Q. Yu, A. Purath, A. Donchev and H. Schnoeckel, *J. Organomet. Chem.*, 1999, **584**, 94–97.
17 P. E. Romero, W. E. Piers, S. A. Decker, D. Chau, T. K. Woo and M. Parvez, *Organometallics*, 2003, 1266–1274.
18 S. G. Minasian and J. Arnold, *Chem. Commun.*, 2008, 4043–4045.
19 J. M. Pietryga, J. D. Gorden, C. L. B. Macdonald, A. Voigt, R. J. Wiacek and A. H. Cowley, *J. Am. Chem. Soc*, 2001, **123**, 7713–7714.
20 The broadness of the ^{1}H NMR spectrum could suggest a paramagnetic compound, which are very unusual in aluminium chemistry. A metallic-like burgandy solid was isolated however was not subjected to any EPR measurments.
21 H. Sitzmann, M. F. Lappert, C. Dohmeier, C. Ueffing and H. Schnoeckel, *J. Organomet. Chem.*, 1998, **561**, 203–208.
22 C. Üffing, A. Ecker, R. Köppe, K. Merzweiler and H. Schnöckel, *Chem. Eur. J.*, 1998, **4**, 2142–2147.
23 G. R. Fulmer, A. J. M. Miller, N. H. Sherden, H. E. Gottlieb, A. Nudelman, B. M. Stoltz, J. E. Bercaw and K. I. Goldberg, *Organometallics*, 2010, **29**, 2176–2179.
24 H. Hoberg, V. Gotor, A. Milchereit, C. Krüger and J. C. Sekutowski, *Angew. Chem. Int. Ed. Engl.*, 1977, **16**, 539.
25 T. Agou, T. Wasano, P. Jin, S. Nagase and N. Tokitoh, *Angew. Chem. Int. Ed.*, 2013, **52**, 10031–10034.
26 K.-N. T. Tseng, J. W. Kampf and N. K. Szymczak, *J. Am. Chem. Soc.*, 2016, **33**, 10378–10381.
27 A. Meller and H. Batka, *Monatsh. Chem.*, 1970, **628**, 627–628.
28 N. B. Kingsley, K. Kirschbaum, J. A. Teprovich, R. A. Flowers and M. R. Mason, *Inorg. Chem.*, 2012, **51**, 2494–2502.
29 A. Meller and H. Batka, *Monatsh. Chem.*, 1970, **628**, 627–628.
30 W. Zheng, A. Stasch, J. Prust, H. W. Roesky, F. Cimpoesu, M. Noltemeyer and H.-G. Schmidt, *Angew. Chem. Int. Ed.*, 2001, **40**, 3461–3464.
31 X. Li, X. Cheng, H. Song and C. Cui, *Organometallics*, 2007, **26**, 1039–1043.
32 X. Li, C. Ni, H. Song and C. Cui, *Chem. Commun.*, 2006, 1763–1765.
33 P. J. Shapiro, A. Vij, G. P. A. Yap and A. L. Rheingold, *Polyhedron*, 1995, **14**, 203–209.
34 T. Agou, K. Nagata and N. Tokitoh, *Angew. Chem. Int. Ed.*, 2013, **52**, 10818–10821.
35 N. Koichi, T. Agou, T. Sasamori and N. Tokitoh, *Chem. Lett.*, 2005, **44**, 1610–1612.

36 V. Vrcek, O. Kronja and H. Siehl, *J. Chem. Soc., Perkin Trans. 2*, 1999, 1317–1321.
37 L. A. Paquette, M. Oku, W. B. Farnham, G. A. Olah and G. Liang, *J. Org. Chem.*, 1975, **40**, 700–703.
38 P. Von, R. ! Schleyer and C. Maerker, *Pure Appl. Chem*, 1995, **67**, 755–760.
39 M. Otto, D. Scheschkewitz, T. Kato, M. M. Midland, J. B. Lambert and G. Bertrand, *Angew. Chem. Int. Ed.*, 2002, **41**, 2275–2276.
40 H. Hogeveen and E. M. G. A. Van Kruchten, *J. Org. Chem.*, 1977, **42**, 1472–1474.
41 W. J. Evans, K. J. Forrestal and J. W. Ziller, *J. Am. Chem. Soc.*, 1995, **117**, 12635–12636.
42 W. J. Evans, S. A. Kozimor, G. W. Nyce and J. W. Ziller, *J. Am. Chem. Soc.*, 2003, **125**, 13831–13835.
43 W. J. Evans, J. M. Perotti, S. A. Kozimor, T. M. Champagne, B. L. Davis, G. W. Nyce, C. H. Fujimoto, R. D. Clark, M. A. Johnston and J. W. Ziller, *Organometallics*, 2005, **24**, 3916–3931.
44 G. A. Olah, G. Rasul and G. K. S. Prakash, *J. Org. Chem.*, 2000, 5956–5959.
45 M. P. Coles, D. C. Swenson, R. F. Jordan and V. G. Young, *Organometallics*, 1998, **7333**, 4042–4048.
46 C. Chang, C. Hsiung, H. Su, B. Srinivas, M. Y. Chiang, G. Lee and Y. Wang, *Organometallics*, 1998, **7333**, 1595–1601.
47 C. N. Rowley, G. A. DiLabio and S. T. Barry, *Inorg. Chem.*, 2005, **44**, 1983–1991.
48 F. Qian, K. Liu and H. Ma, *Dalton Trans.*, 2010, **39**, 8071–83.
49 C. E. Bethley, C. L. Aitken, C. J. Harlan, Y. Koide, S. G. Bott and a R. Barron, *Organometallics*, 1997, **16**, 329–341.
50 Z. Florjańczyk, W. Bury, E. Zygadło-Monikowska, I. Justyniak, R. Balawender and J. Lewińskl, *Inorg. Chem.*, 2009, **48**, 10892–10894.
51 I. Justyniak, D. Prochowicz, A. Tulewicz, W. Bury, P. Goś and J. Lewiński, *Dalton Trans.*, 2017, **46**, 669–677.

Chapter 4:

Development of Phosphaamidine Ligands and their Reactivity with Dibutyl-Magnesium

4. Development of Phosphaamidine ligands and their Reactivity with Dibutyl-Magnesium

4.1 New Members of the Ligand Family

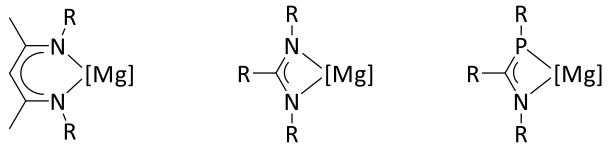

β-Diketiminate *Amidinate* *Phosphaamidinate*

Figure 42 *Structure of β-diketiminate, amidinate and phosphaamidinate ligands on magnesium*

The term "phosphaamidine" was coined in 1978 by Schmidt,[1] and is the name for an amidine ligand in which one of the nitrogen atoms is replaced by a phosphorus atom. Whilst these ligands have been known for some time, their use was stunted owing to their challenging synthesis and handling. Summarised in Scheme 64, the many methods of preparation are usually specific to just one example. In 2014, a general preparation of phosphaamidines was reported by Slootweg and Lammerstma showing a tolerance for a range of substituents (Scheme 64D).[2] It consists of the coupling a primary phosphine and a carbonitrilium triflate salt in the presence of triethylamine.

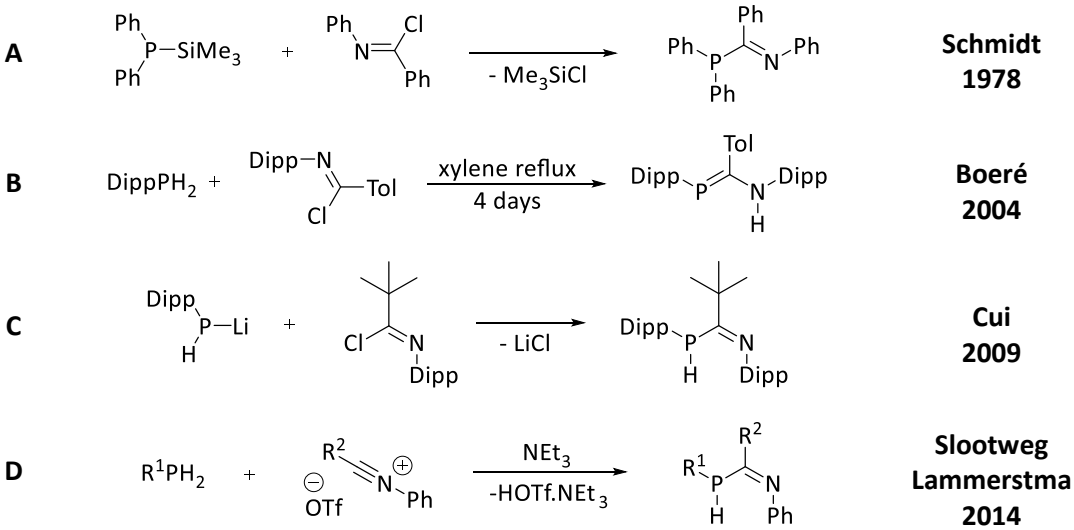

Scheme 64 *Varying methods of phosphaamidine synthesis[1–4] R^1=Phenyl, cyclohexyl or 1,3,5-tritertbutylphenyl, R^2 = ^{t}Bu or phenyl.*

Recently there has been a marked increase in the usage of deprotonatoned phosphaamidinates as anionic ligands; group 1[2,3,5] and transition metal complexes[1,2,6] are

now known. The only reported instance of group 2 complexes are formed *via* silyl-migration,[7] and thus are limited in scope. An example of a thallium complex represents the sole implementation of these ligands in p-block chemistry.[4]

The parent phosphaamidine $H_2PC(H)NH$ has four possible isomers, however the introduction of organic functionalities produces the eight possible configurations of substituted phosphaamidines shown in Figure 43. The relationship between these isomers varies, some are the result of a simple bond rotation, and others through a [1,3]-hydrogen shift. The organic substituents must play a major role in determining which isomer is formed, and in some cases multiple isomers are observed in solution by ^{31}P and ^{1}H NMR spectroscopy.[2,3] Density functional theory has been used to aid the identification of these isomeric mixtures by comparison of their relative energies.[2,8,9]

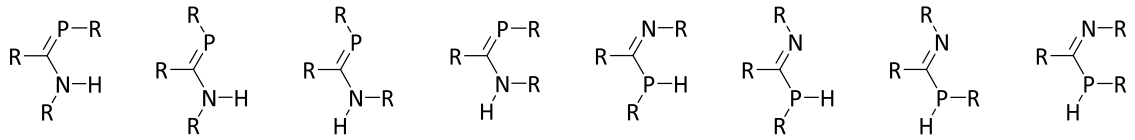

Z-anti (P=C)	*E-anti* (P=C)	*E-syn* (P=C)	*Z-syn* (P=C)	*Z-anti* (N=C)	*E-anti* (N=C)	*E-syn* (N=C)	*Z-syn* (N=C)

Figure 43 *Possible isomers of substituted phosphaamidines*

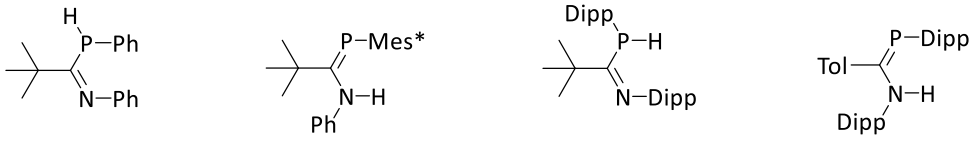

E	**F**	**G**	**H**
Z-syn N=C	Z-anti P=C	Z-anti N=C	Z-anti P=C

Figure 44 *Examples of the configurations found in structurally characterised phosphaamidines.*[2,3,9] *Mes* = 2,4,6-tritertbutylphenyl. Dipp = 2,6-diisopropylphenyl*

The P-C-N geometry has been unequivocally verified by X-ray crystallography in some cases, which are shown in Figure 44. The planar phenyl substituents of **E** can stack their π-systems, allowing the Z-syn N=C geometry to be favourable. Increasing the steric bulk of the phosphorus substituent to Mes* (**F**, Mes* = 2,4,6-tritertbutylphenyl) results in the isolation of the Z-anti P=C isomer. It was noted that upon formation of **F**, the initial product mixture consists of two phosphine isomers, observed by ^{31}P NMR spectroscopy (δ = -55.3 $^{1}J_{P\text{-}H}$ 243 Hz and -56.7 $^{1}J_{P\text{-}H}$ 252 Hz, corresponding to E-syn N=C and Z-syn N=C). Tautomerisation

through a [1,3] H-shift then forms the thermodynamic Z-anti P=C product shown (δ = 102.0), which is ultimately isolated.

Examples **G** and **H** demonstrate the effect of the backbone substituent on the overall geometry. The greater steric bulk of the ^{t}Bu group gives a phosphinoimine, where the planar tolyl group allows for an aminophosphaalkene to be isolated.

Evidently, the steric bulk of the phosphaamidine substituents is a key factor in determining the final geometry of the isolated species, which could have implications for further reactivity and complexation. This chapter aims to prepare novel phosphaamidines featuring a wide range of substituents to investigate this effect of steric bulk on ligand geometry further. The complexation of phosphaamidines with main-group metals to prepare functionalised complexes will also be examined.

*4.1.1 Preparation of MesP(H)C(tBu)NMes (**20**)*

Initial preparation of **20** was carried out by Martin W. Stanford at the University of Edinburgh.

Precursors for novel phosphaamidines were synthesised using literature procedures.[2] The addition of pivaloyl chloride to solution of mesitylaniline in the presence of triethylamine forms an amide with elimination of $[Et_3NH]^+Cl^-$. Heating this amide in neat thionyl chloride results in the evolution of sulphur dioxide and HCl gas, and formation of an imine chloride, which reacts with trimethylsilyltriflate to form the desired carbonitrilium triflate salt.

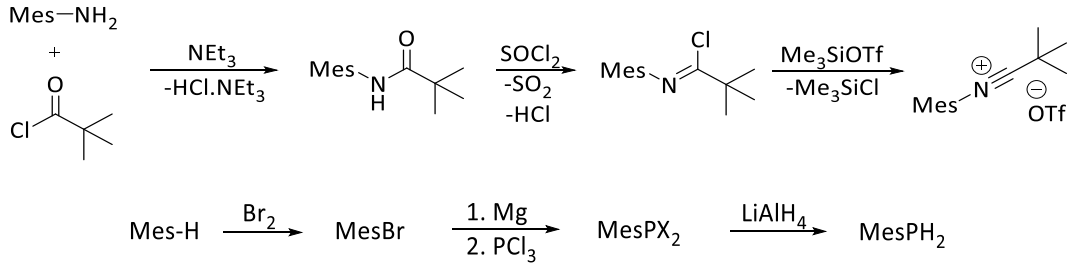

Scheme 65 *Preparation of phosphaamidine precursors, mesityl carbonitrilium salt and mesityl phosphine. X = Br or Cl. Mes = 2,4,6-trimethylphenyl.*

The aryl primary phosphine $MesPH_2$ was also synthesised via the corresponding halophosphine.[10] Addition of $MesPH_2$ to the carbonitrilium salt in the presence of triethylamine leads to the formation of novel phosphaamidine **20.** This reaction proceeds first with the formation of phosphonium triflate which is then deprotonated by the amine base.[4] An isolated yield of **20** of 64% is comparable with literature known phosphaamidines synthesised using this method.[2,11]

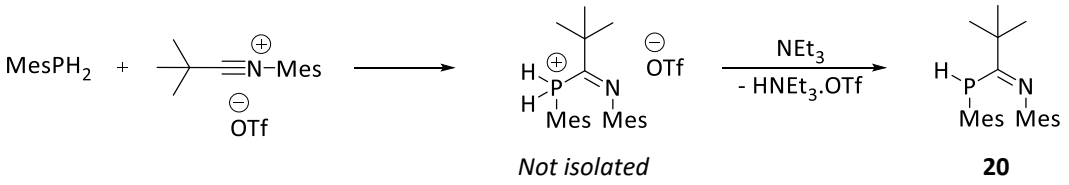

Scheme 66 *Preparation of mesityl-subsituted phosphaamidine **20**. Mes = 2,4,6-trimethylphenyl*

The ^1H NMR spectrum of **20** contains a doublet at δ = 4.97 ($^1J_{H\text{-}P}$ = 245 Hz), which corresponds to a doublet signal in the ^{31}P NMR spectrum at δ = -80.6 ($^1J_{P\text{-}H}$ = 244 Hz).

Therefore, **20** can be confidently assigned as a phosphino-imine, with an explicit P-H bond. A very lowfield signal was observed in the ^{13}C NMR spectrum at δ = 182.5 ppm, which has doublet multiplicity indicating coupling to an adjacent phosphorus atom ($^{1}J_{C\text{-}P}$ = 59 Hz). This was confirmed as a quaternary carbon signal by a ^{13}C DEPT135 NMR experiment, and is assigned to the central carbon atom of the P-C=N unit.

Crystals of **20** suitable for single crystal X-Ray crystallography were grown from a cold hexane solution (-20°C) and the resulting structure is shown in Figure 45. The phosphine hydrogen atom was found in the difference map and allowed to refine freely. Phosphino-imine **20** features a C=N double bond and a C-P single bond, with bond lengths at 1.279(4) and 1.872(3) Å respectively.

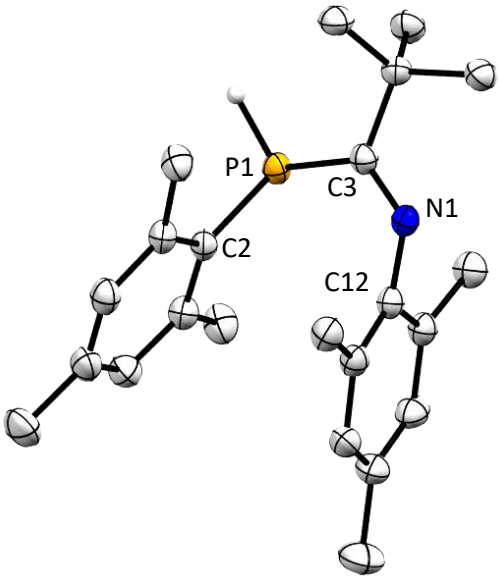

Figure 45 *X-Ray crystal structure of* ***20****. Hydrogen atoms (except P-H) omitted for clarity. Selected bond lengths (Å): P1-C3 1.872(3), C3-N1 1.279(4). Selected bond angles (°): P1-C3-N1 124.1(2), C3-N1-C12 122.5(2), C2-P1-C3 107.43(12).*

Due to the bulky tert-butyl group on the central carbon **20** adopts a Z-syn N=C arrangement of its aromatic substituents. This is consistent with the solid-state structures of previously reported phosphaamidines with a tert-butyl backbone.[5] The P1-C3=N1 internal angle of **20** at 124.1(2)° is comparable with those reported for phosphaamidines PhP(H)C(^{t}Bu)NPh and CyP(H)C(^{t}Bu)NPh (123.16(10)° and 125.22(10)°).[5]

4.1.2 Phosphaamidines with Bulky Phosphorus Substituents

Initial preparation of **21** and **22**, and the X-ray structure of **22** were performed by Martin W. Stanford in the University of Edinburgh.

As **20** is comparable with known phosphaamidines, the steric bulk around the phosphorus and nitrogen centres was increased in a systematic manner. The overall aim of this work is to utilise these ligands for supporting highly reactive main-group species, which require the sort of kinetic stabilisation large steric bulk can provide.

To investigate the effect of increasing the steric bulk on the phosphorus substituent, bulkier primary phosphines were synthesised in a similar method to mesitylphosphine; preparation and reduction of the RPX_2 type compound using lithium aluminium hydride. Substituents chosen here are Tipp (2,4,6-triisopropylphenyl)[12] and Mes* (2,4,6-tritertbutylphenyl).[13] These were then reacted with mesityl carbonitrilium triflate in the presence of triethylamine as in section 4.1.1, to form phosphaamidines **21** and **22**.

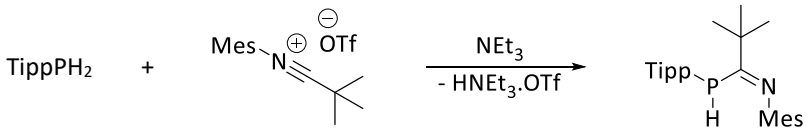

21

Scheme 67 *Preparation of a Tipp-substituted phosphaamidine. Tipp = 2,4,6-triisopropylphenyl*

Tipp derivative **21** was isolated and characterised without difficulty, and an isolated yield of 57 % is comparable with **20**. The ^{31}P NMR spectrum displays a doublet signal at δ = -88.9 ($^1J_{P\text{-}H}$ = 252 Hz) indicating a P-H bond is present. In the ^1H NMR spectrum of **21**, the signal associated with the *ortho*-isopropyl CH appears as a broad singlet signal at δ = 3.48, rather than the expected septet signal, indicating bond rotation on the NMR timescale. The methyl groups adjacent to this proton are now inequivalent showing two doublets at δ = 1.26 and 1.15 ($^1J_{H\text{-}H}$ = 6.8 Hz). The mesityl methyl groups are also inequivalent, with three singlet signals seen at δ = 2.28, 2.23 and 2.17. A lowfield ^{13}C NMR doublet signal is observed indicative of one-bond phosphorus coupling at δ = 182.7 ($^1J_{C\text{-}P}$ = 61 Hz) for the central P-C-N carbon.

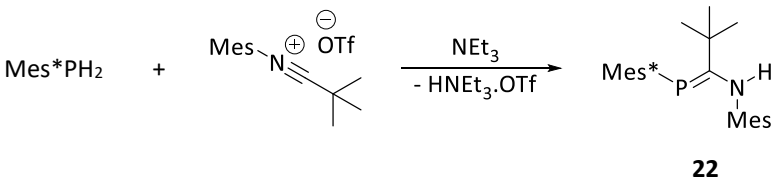

22

Figure 46 *Preparation of a Mes*-substituted phosphaamidine. Mes* = 2,4,6-tritertbutylphenyl*

The preparation of larger Mes* derivative **22** was also straightforward, with slight work-up modifications leading to an isolated yield comparable with previous phosphaamidines **20** and **21**. White crystals were isolated from cold hexane (-20°C) and the subsequent solid-state structure (Figure 47) confirms the formation of a phosphaamidine. In contrast to the solid-state structure of mesityl-substituted **20**, the central P=C-N unit in **22** has phosphaalkene functionality and the proton bonded to the nitrogen atom. When compared to the P-C bond in **20**, the P=C bond in **22** is significantly shorter at 1.7385(17) Å (**20**: P-C 1.872(3) Å), whilst the C-N bond is elongated at 1.375(6) Å (**20**: N=C 1.279(4) Å).

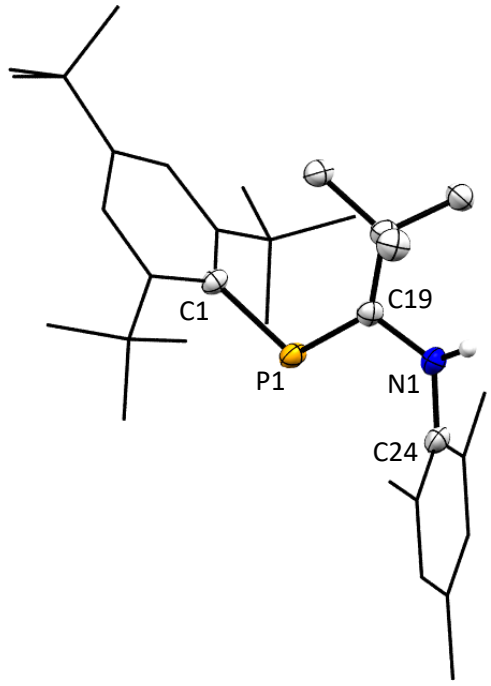

Figure 47 *X-Ray crystal structure of **22**. Hydrogen atoms (except N-H) omitted for clarity. Selected bond lengths (Å): P1-C1 1.8583(15), P1-C19 1.7385(17), C19-N1 1.375(6) C24-N1 1.428(2). Selected bond angles (°): P1-C19-N1 114.32(12).*

The internal angle of the P=C-N unit of **22** at 114.32(12)°, is considerably smaller than that of Mes derivative **20**, at 124.1(2)° respectively. The aminophosphaalkene **22** adopts an E-

syn P=C geometry, in contrast to the Z-syn N=C geometry of **20**. This is the expected result of the increased steric bulk of the Mes* phosphorus substituent, as the unfavourable interactions between the aromatic rings have increased. This E-syn P=C phosphaamidine geometry is seen also in a bulky derivative reported by Boeré DippP=C(Tol)N(H)Dipp[3] (Dipp = diisopropyl phenyl, Tol = *p*-tolyl).

The pure crystals were re-dissolved in C_6D_6 to obtain NMR spectra. The ^{31}P NMR spectrum of these crystals showed three distinct signals, as seen Figure 48; a doublet at δ = 98.3 ($^3J_{P-H}$ = 18 Hz), a singlet at δ = 80.1 and a doublet at δ = -53.6 ($^1J_{P-H}$ = 253 Hz). Variable temperature ^{31}P NMR spectroscopy showed no change in the distribution of these signals with increased temperature. It is therefore proposed that these signals are due to isomers which interconvert slower than the NMR timescale.

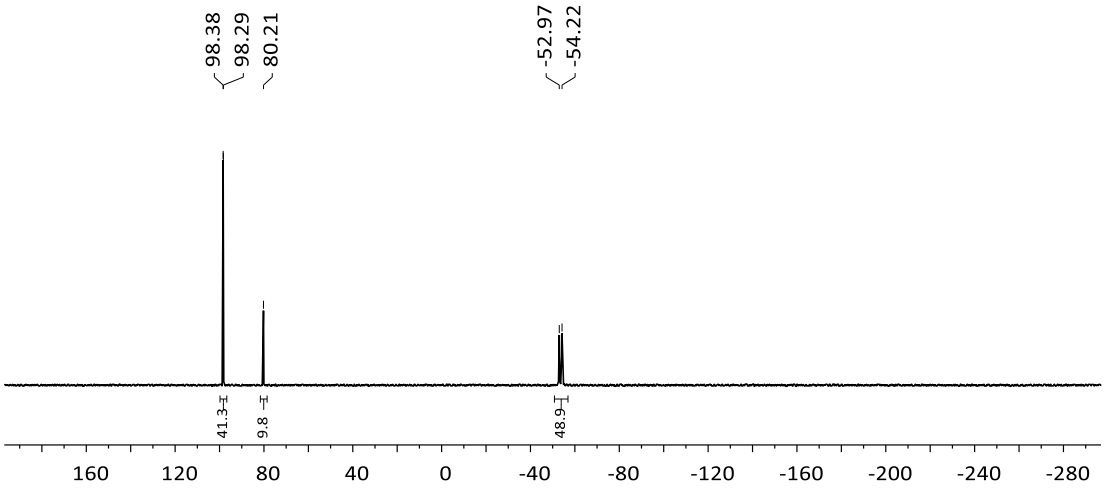

Figure 48 *^{31}P NMR spectrum (202.5 MHz, C_6D_6, 300K) of **22** isolated from toluene*

Presumably one of the isomers in solution is the E-syn P=C configuration observed in the solid-state structure. Judging by the chemical shift values and multiplicity, there is a second phosphaalkene (δ = 98.3 and 80.1) and a phosphine isomer (δ = -53.6) present. Without fractional recrystallization to explicitly confirm these unknown structures, computational methods were explored to aid their identification. Density functional theory (DFT) has been used to help identify the isomers present in other phosphaamidine mixtures.[2,8,9] By comparing the relative energies of the possible isomers, the configuration of the experimentally isolated compounds can be predicted.

First, the geometry of each of the possible eight isomers (Figure 43, page 106) was optimised using M062X/def2svp methods, until a thermodynamic minimum without imaginary frequencies was found. This process was successful in seven of the eight cases, with the E-anti N=C optimised structure consistently possessing an imaginary frequency despite several attempts. This is most likely a very high energy isomer or transistion state, as there is significant interaction between both aryl groups and the ^{t}Bu backbone, and this isomer will be omitted from this comparison. The Hartree-Fock energy of the remaining seven isomers was extracted, and the value scaled relative to the optimised crystal structure (E-syn P=C) is shown in Figure 49. The overall distribution has an energy range of 30.0 kJ mol^{-1}, which is comparable with that seen in Masuda's similar comprehensive isomer calculations (B3LYP/6-31G(d)) of phosphaamidine DippP=C(p-tolyl)N(H)Dipp (41.4 kJ mol^{-1}).[8]

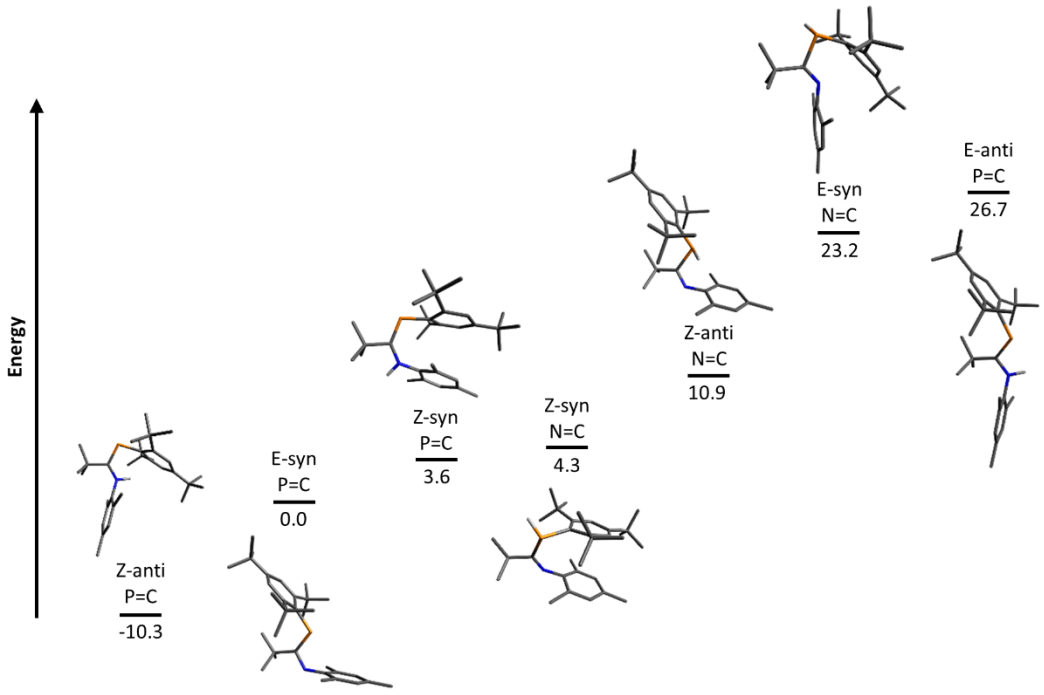

Figure 49 *Calculated relative energies (kJ mol^{-1}) of all eight isomers of phosphaamidine* ***22*** *(M062X/def2svp), relative to the optimised crystal structure E-syn P=C.*

The structural parameters of both **22** and optimised geometry of the E-syn P=C isomer **22$^{\#}$** are in good agreement. The experimental phosphaalkene bond length 1.7385(17) Å is predicted at 1.722 Å, representing a 1.0% difference. A smaller discrepancy (0.2%) is seen in

the amine bond length, at 1.375(6) Å versus 1.387 Å. It follows that the internal P-C-N angle of **22#** is consistent with the solid-state structure **22**, 114.7° and 114.32(12)° respectively.

The remaining six isomers give diverse structural parameters. The phosphaalkene bond lengths cover a range of 1.780 Å – 1.716 Å, (E-anti P=C and Z-syn P=C respectively), significantly shorter than the shortest phosphine bond length at 1.884 Å (Z-syn N=C). A narrower distribution of bond lengths is observed in the amine/imine bond lengths, with N=C double bonds lying between 1.271 Å – 1.264 Å (Z-anti N=C and E-syn N=C respectively) and N-C single bonds between 1.400 Å – 1.370 Å (E-anti P=C and Z-syn P=C). Both the largest and smallest internal P-C-N angles belong to phosphaalkene isomers, ranging from 135.3° (Z-syn P=C) to 109.7° (E-anti P=C). The key bond lengths and bond angles of the final optimised geometries are listed in Table 5.

	X-Ray	**Z-anti (P=C)**	**E-anti (P=C)**	**E-syn (P=C)**	**Z-syn (P=C)**	**Z-anti (N=C)**	**E-syn (N=C)**	**Z-syn (N=C)**
P-C (Å)	**1.7385(17)**	1.727	1.780	**1.722**	1.716	1.903	1.905	1.884
C-N(Å)	**1.375(6)**	1.373	1.400	**1.387**	1.370	1.271	1.264	1.267
P-C_{aryl} (Å)	**1.8583(15)**	1.875	1.863	**1.869**	1.866	1.863	1.843	1.859
N-C_{aryl} (Å)	**1.428(2)**	1.434	1.431	**1.424**	1.421	1.407	1.397	1.401
P-C-N (°)	**114.32(12)**	123.2	109.7	**114.7**	135.3	115.0	116.1	125.9
C_{tBu}-C-P (°)	**134.83(11)**	117.0	133.8	**135.1**	114.8	129.2	116.6	117.4
C_{tBu}-C-N (°)	**110.84(14)**	119.8	116.4	**110.3**	109.9	115.6	127.0	115.6

Table 5 *Comparison of the experimentally determined parameters of **22** with the structural parameters of the optimised structures of **22#***

The E-syn P=C solid-state structure of **22** has already been identified as one of the isomers present in the mixture. As it features a C-N single bond, it is reasonable that one of the other isomers present in the ^{31}P NMR spectrum would result from the rotation around the C-N bond, forming its E-anti P=C rotomer. The relative energy of these isomers suggests this is not the case here, as this rotation is accompanied with a significant energy gain perhaps through interaction of the substituents with the tert-butyl backbone.

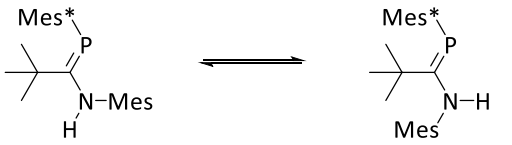

E-syn P=C | E-anti P=C

0.0 kJ mol^{-1} | + 26.7 kJ mol^{-1}

Figure 50 *Unfavourable rotation about the C-N bond of the solid-state configuration*

Unexpectedly, an isomer with an energy lower than that of the solid-state structure was identified. This Z-anti P=C configuration is therefore likely the other phosphaalkene isomer present in the ^{31}P NMR spectrum of **22**. Assigning the two P=C isomers to one of the ^{31}P NMR signals (δ = 98.3 $^{3}J_{P\text{-}H}$ = 18 Hz and δ = 80.2) requires consideration of the $^{3}J_{P\text{-}H}$ coupling constant of the former resonance. Further investigation of the geometry optimised structures should provide rationalisation for this observation.

Traditionally, Karplus curves[14–16] for specific molecular classes correlate the dihedral angle (θ; PCNH the case of **22**) with the observed $^{3}J_{P\text{-}H}$ coupling constants. A second parameter with an influence greater than θ in the case of P^{III} compounds has since been identified. This so-called non-Karplus angle, denoted by ω, is the dihedral angle between the phosphorus lone pair and the ^{3}J proton.[17] A larger $^{3}J_{P\text{-}H}$ coupling constant is associated with a small ω. The lone pair of the two isomers in question here (E-syn P=C and Z-anti P=C) was located in the visualised HOMO-2 molecular orbitals, and thus ω was estimated. A striking difference was observed, with ω for the E-syn P=C solid-state structure being negligible (7.8°) compared to the corresponding value for the lower energy isomer Z-anti P=C (165.9°). It is therefore suggested that the doublet signal at δ = 98.3 ($^{3}J_{P\text{-}H}$ = 18 Hz) corresponds to the E-syn P=C geometry (**22a**), and the singlet signal at δ = 80.2 the Z-anti P=C isomer (**22b**).

With two of the three experimentally observed isomers identified, reasoning for the third should be straightforward. According to the energy diagram Figure 49, the most likely candidate is the isomer closest in energy to the solid-state structure, Z-syn P=C, just 3.6 kJ mol^{-1} higher in energy. However, the ^{31}P NMR signal of the unidentified isomer, δ = -53.6 ($^{1}J_{P\text{-}H}$ = 253 Hz) precludes this isomer from consideration, as it possesses a P=C bond. It is the rotational isomer of the lowest energy configuration Z-anti P=C, which has already been proposed as one of the mixtures components.

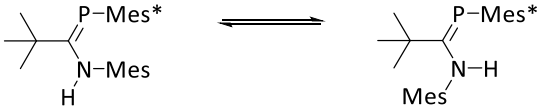

Z-syn P=C
3.6 kJ mol^{-1}
Not observed

Z-anti P=C
- 10.3 kJ mol
22b

Figure 51 *Favourable rotation around the N-H bond of Z-syn P=C results in **22b**, the calculated lowest energy isomer of **22***

At 4.3 kJ mol^{-1} higher in energy than the solid-state isomer, the Z-syn N=C is most likely the third component of **22**'s isomeric mixture. It fits the ^{31}P NMR spectroscopy data, bearing a P-H bond responsible for the large $^{1}J_{P\text{-}H}$ coupling constant (253 Hz). It is also a similar configuration to the solid-state of Mes-substituted **20** (section 4.1.1), which is prepared under analogous conditions. Correlating the results of these computations with the experimental ^{31}P NMR spectra allows each of the three signals to be assigned to an isomer, summarised in Figure 52.

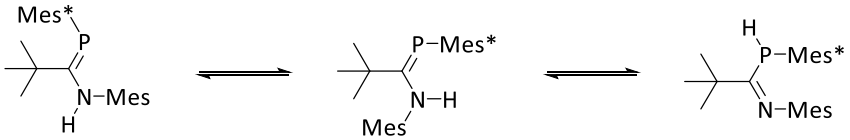

E-syn P=C
22a
^{31}P δ 98.3
$^{3}J_{P\text{-}H}$ = 18 Hz

Z-anti P=C
22b
^{31}P δ 80.2

Z-syn N=C
22c
^{31}P δ -53.6
$^{1}J_{P\text{-}H}$ = 253 Hz

Figure 52 *Possible resonance forms of **22** correlated to the ^{31}P NMR chemical shifts*

As discussed earlier, the comparison of the non-Karplus dihedral angle ω allows for the differentiation of phosphaalkene isomers **22a** and **22b**. Whilst **22b** is calculated as the lowest energy isomer, it represents the smallest percentage of the mixture. This suggests a high activation barrier to its formation, as this is not accounted for in these relative energy computations. Finally, the phosphine tautomer with the lowest calculated relative energy (**22c**) is assigned to the signal at ^{31}P δ = -53.6 ($^{1}J_{P\text{-}H}$ = 253 Hz), and is most likely stabilised by non-covalent interactions between the aryl rings.

It is perhaps counter-intuitive given the presence of three bulky ^{t}Bu groups in the phosphorus substituent in **22c** that these aryl groups can be so close together in space. However, visualising the molecular orbitals of the Z-syn N=C isomer reveals the reason for this seemingly odd arrangement. The HOMO-4 orbital shown in Figure 53 shows a significant bonding interaction between the aromatic systems of the organic substituents, hinting at π-stacking interactions. The close inter-atomic separation of the rings (3.549 - 3.944 Å) is in the reported range for similar parallel displaced aryl interactions.[18,19] To confirm these π interactions, further calculations of the potential energy surface are required, which is beyond the scope of this work.[19–21]

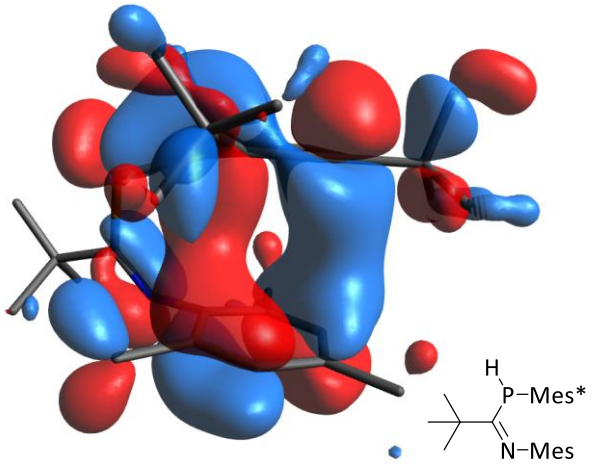

Z-syn N=C
HOMO-4

Figure 53 *Molecular orbital (M062x/def2svp) of Z-syn N=C isomer* ***22c*** *showing π-stacking interactions between the aryl substituents*

4.1.3 Phosphaamidines with Bulky Nitrogen Substituents

Two examples of phosphaamidines with more sterically demanding nitrogen were also synthesised. The first target features a diisopropylphenyl (Dipp) group, the carbonitrilium salt of which is reported.[11] The preparation of the corresponding phosphaamidine **23** was completed in an analogous manner to **20**, **21** and **22** in a similar high yield (69%).

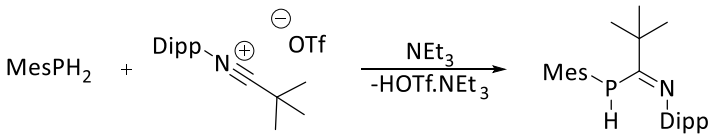

23

Scheme 68 *Preparation of phosphaamidine featuring a Dipp group. Dipp = 2,6-diisopropylphenyl*

The ^{31}P NMR spectrum of **23** shows a solitary doublet signal at δ = -78.5 ($^{1}J_{P\text{-}H}$ = 249 Hz), indicating only phosphine functionality, like the mesityl-substituted **20** and Tipp-substituted **21**. This is corroborated by a doublet signal in the ^{1}H NMR spectrum with the same $^{1}J_{P\text{-}H}$ coupling constant at δ = 4.89 ($^{1}J_{H\text{-}P}$ = 249 Hz). Also evident in the ^{1}H NMR spectrum is that the isopropyl groups of the Dipp-substituent are now inequivalent, with independent septet signals for the C-H protons at δ = 3.19 ($J_{H\text{-}H}$ = 6.9 Hz) and 2.87 ($J_{H\text{-}H}$ = 6.9 Hz), and four separate doublet signals for the methyl groups at δ = 1.35 ($J_{H\text{-}H}$ = 7.0 Hz), 1.26 ($J_{H\text{-}H}$ = 6.6 Hz), 1.23 ($J_{H\text{-}H}$ = 6.7 Hz) and 1.18 ($J_{H\text{-}H}$ = 6.8 Hz). As with all three examples of phosphaamidines already discussed, the quaternary P-C=N carbon gives a doublet signal in the ^{13}C NMR spectrum at δ = 182.3 ($^{1}J_{C\text{-}P}$ = 58.7 Hz).

To increase the steric bulk further, a 2,6-bis(diphenylmethyl)-4-methyl aniline **24** (Ar*NH_2) was synthesised by the condensation of *para*-toluidine and diphenylmethanol in the presence of catalytic acidic zinc(II) chloride.[22] This amine has been used to prepare a β-diketiminate ligand capable of supporting a probable terminal magnesium hydride,[23] and an example of a rare Mg-Mg bond.[24] The corresponding amidine has also been synthesised, however isolating main-group compounds featuring this ligand was found to be challenging.[25]

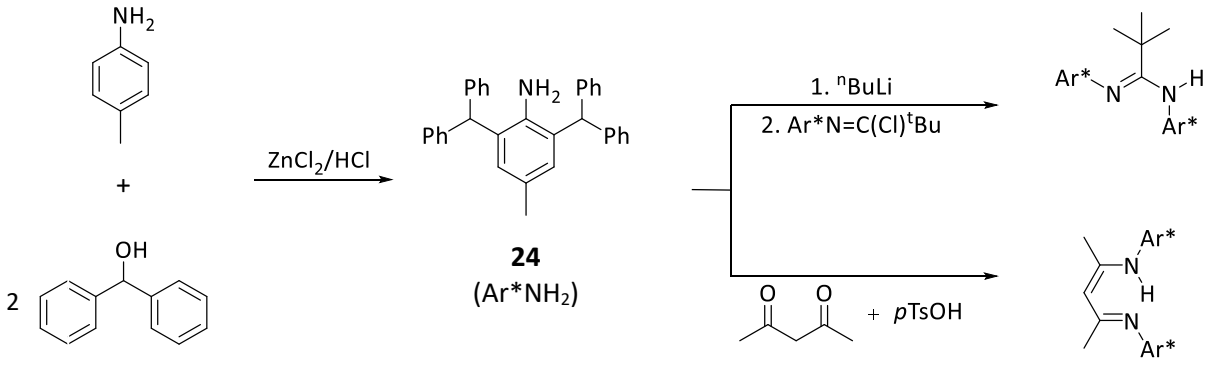

Scheme 69 *Preparation of **24**[22] and its use in the synthesis of amidine[25] and β-diketiminate[23] ligands. Ar* = 2,6-bis(diphenylmethyl)-4-methylphenyl.*

The corresponding amide **25** is reported,[25] and was synthesised using a slightly modified procedure (section 7.3.16). Refluxing **25** with excess PCl_5 (1.5 eq) in toluene for 48 hours gave the corresponding imodyl chloride **26** with the elimination of $POCl_3$ and HCl gas.[25] Reaction of **25** with thionyl chloride, the pathway used for the synthesis of the other carbonitrilium triflate salts discussed in this work, was not successful with this bulky amide.

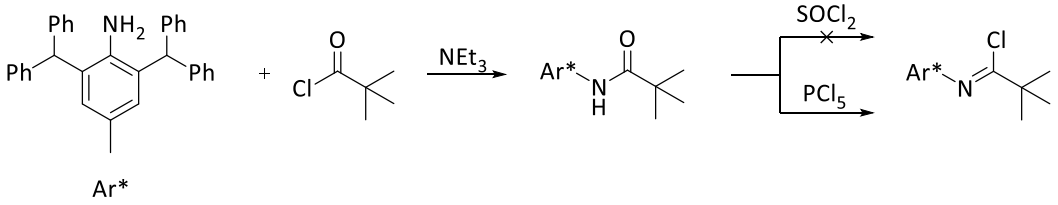

24 **25** **26**

Scheme 70 *Preparation of imodyl chloride **26***

With **26** in hand, attempts were made to synthesise the corresponding novel carbonitrilium salt **27** by the addition of trimethylsilyl triflate. A new product was formed as indicated by a slight downfield shift of the ^{1}H NMR signals, suggesting **27** had indeed formed. The ^{t}Bu signal can be found at δ = 1.07, compared with δ = 0.96 in imodyl chloride **26**. Similarly, the *para*-Me group of Ar* is observed at δ = 2.22 (**26**: δ = 2.13) and the "trityl" proton C(H)Ph_2 at δ = 6.11 (**26**: δ = 5.55). However even with inert atmosphere work-up **27** was found to undergo hydrolysis resulting in the isolation of amide **25** and no pure sample of **27** was obtained.

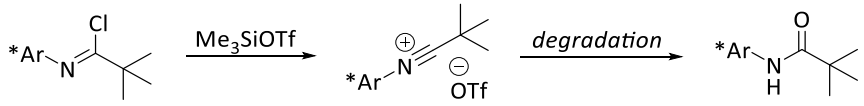

26 **27** **25**

Scheme 71 *Preparation of carbonitrilium triflate salt **27** and subsequent hydrolysis*

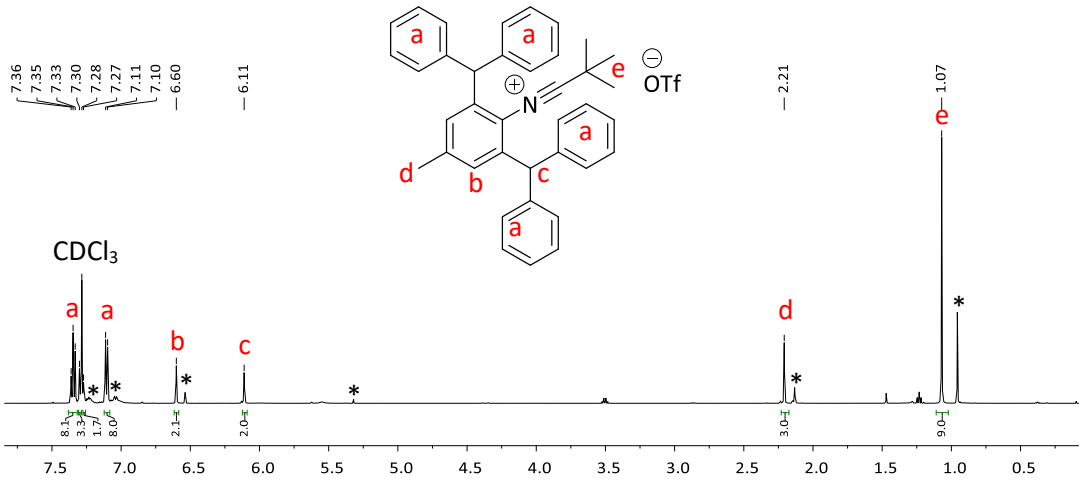

Figure 54 *^{1}H (500 MHz, $CDCl_3$, 300 K) NMR spectrum of crude sample carbonitrilium triflate **27**. Imodyl chloride **26** denoted **

As the imine is very bulky, chloride elimination from **26** should be favourable, and it was thought that the reaction with mesityl phosphine in the presence of NEt_3 would form the corresponding phosphaamidine without the need for the nitrilium triflate. However, no reaction was observed by ^{31}P NMR spectroscopy after 24 hours at room temperature.

4.1.4 A Super Bulky Phosphaamidine via a Different Mechanism

As the isolation of bulky carbonitrilium triflate **27** was challenging, the synthesis of the targeted super bulky phosphaamidine cannot be persued using the same method as **20**-**22.** Still with the target of a super bulky phosphaamidine in mind, a "one-pot" reaction was trialled, where the triflate salt **27** is formed and reacted *in situ*, avoiding its troublesome isolation.

A dichloromethane solution of imodyl chloride **26** was cooled to -78°C, after which trimethylsilyl triflate was added, followed immediately by mesitylphosphine and triethylamine. Warming this solution to room temperature and following the same work-up conditions as the previous phosphaamidines lead to the isolation of a white solid identified as the desired phosphaamidine **28**. The yield of this reaction was reproducibly very low, consistently around 32% (compare with **20** = 64%, **21** = 57%, **22** = 74%, **23** = 69%).

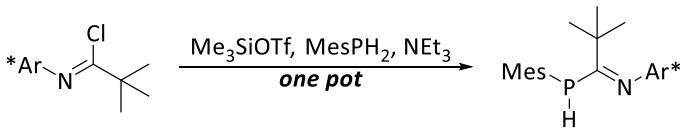

26 **28**

Scheme 72 *Preparation of super-bulky phosphaamidinate* ***28***

The ^{31}P NMR spectrum of **28** displays a doublet signal at δ = -74.9 ($^{1}J_{P\text{-}H}$ = 249 Hz), indicating **28** contains a P-H bond. The corresponding doublet signal in the ^{1}H NMR spectrum is seen at δ = 5.19 ($^{1}J_{H\text{-}P}$ = 250 Hz). Looking to the aromatic region of the ^{1}H NMR spectrum, multiple signals are present due to the presence of six inequivalent phenyl rings in **28**. The characteristic doublet signal for the central phosphaamidine carbon can be seen in the ^{13}C NMR spectrum at δ = 180.9 ($J_{C\text{-}P}$ = 59 Hz).

In order to improve the low yield of the reaction depicted in Scheme 72, alternative conditions were sought. Small scale reactions were carried out in deuterated solvents to follow any product formation by *in situ* ^{1}H and ^{31}P NMR experiments. Repeating the preparative scale conditions in CD_2Cl_2 revealed that after 12 hours at room temperature more than half the phosphine starting material unreacted, and overall conversion to **28**

stood at 46% by integration of the ^{31}P NMR spectrum. This indicated that the origin of the low yield was perhaps the reaction conditions, not the work-up procedure.

Changing the reaction solvent to C_6D_6 revealed something somewhat unexpected. Immediately after the addition of reagents, the ^{31}P NMR spectrum showed almost full consumption of the primary phosphine and a new high field doublet signal is now the major species in the spectrum at δ = -159 ($^1J_{P\text{-}H}$ = 207 Hz). After 2 hours at 75 °C a substantial amount of the desired phosphaamidine **28** had formed, and heating the solution to 75 °C for a further 12 hours increased the conversion to 82%. Heating this solution further did not produce any more product.

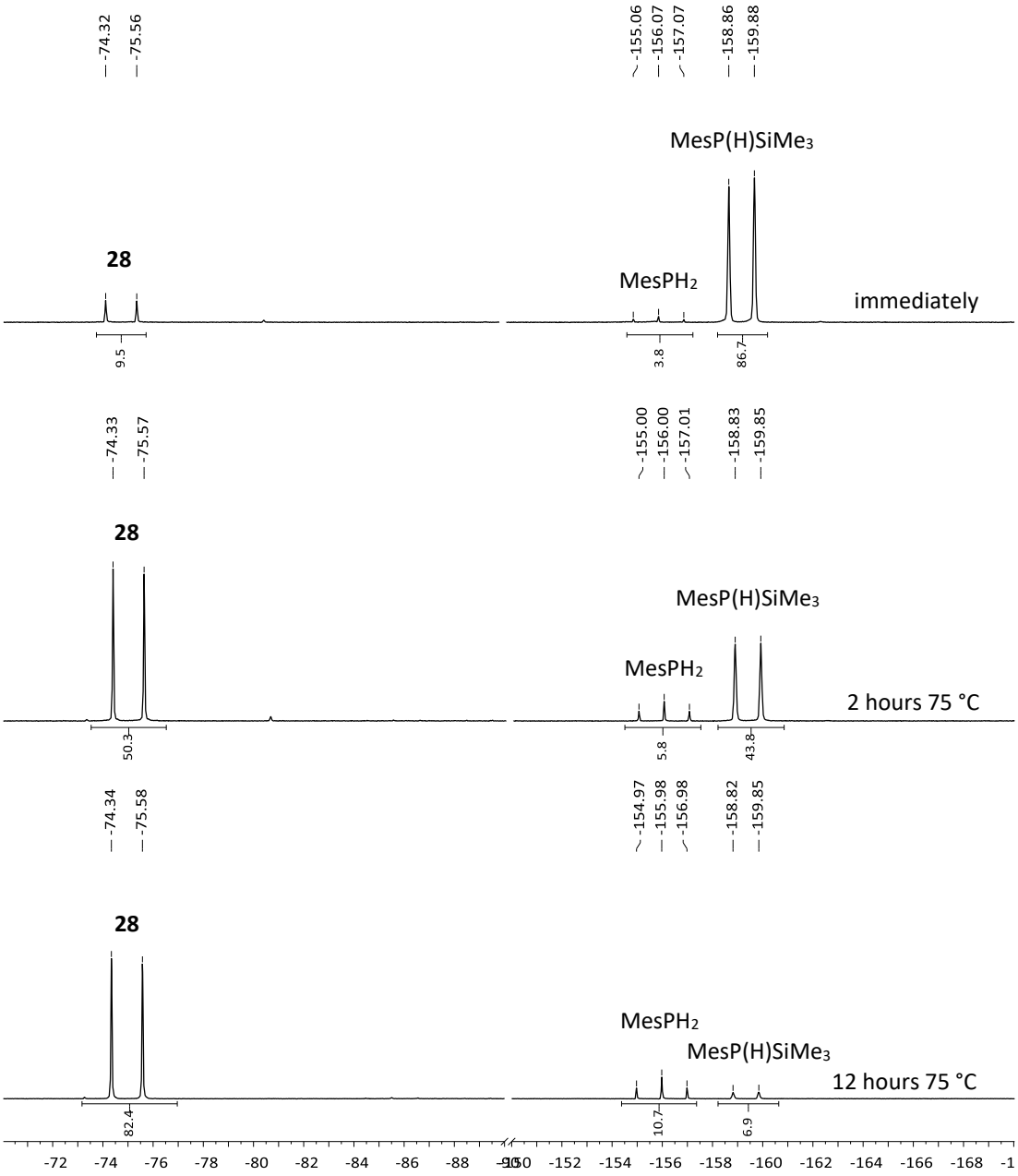

Figure 55 *^{31}P NMR spectra of reaction depicted in Scheme 72 in C_6D_6*

Due its multiplicity, the new high field signal at δ = -159 (J = 207 Hz) in the ^{31}P NMR spectrum of this reaction (Figure 55) is an intermediate of the type R_2PH. It was considered that the primary phosphine could react with Me_3SiOTf in the presence of NEt_3 to form $MesP(SiMe_3)H$ and $HNEt_3.OTf$, and that this would compete with the intended reaction to form the unisolable carbonitrilium triflate **27** *in situ*. When heated, this silyl phosphine can react with the imine chloride to favourably eliminate trimethylsilyl chloride and form the desired phosphaamidine. This process has precedence; the proto-typical phosphaamidine

$Ph_2PC(Ph)=NPh$ was synthesised by the reaction of a silyl phosphine and an imodyl chloride.[1]

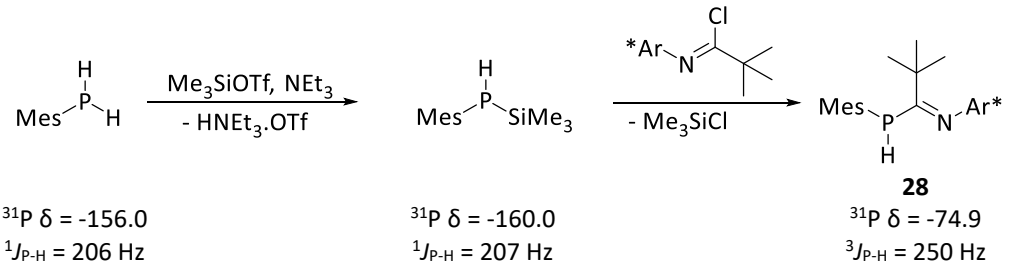

28

^{31}P δ = -156.0
$^{1}J_{P-H}$ = 206 Hz

^{31}P δ = -160.0
$^{1}J_{P-H}$ = 207 Hz

^{31}P δ = -74.9
$^{3}J_{P-H}$ = 250 Hz

Scheme 73 *Suggested mechanism of formation of phosphaamidinate* ***28*** *formation in aromatic solvents*

To investigate this observation further, a reaction was carried out where one equivalent of trimethylsilyl triflate was added to a C_6D_6 solution of mesityl phosphine. This addition caused the signals in the ^{1}H and ^{31}P NMR spectra to broaden, but the chemical shift did not change significantly. Addition of triethylamine to this mixture caused the formation of the same doublet signal that was seen in Figure 55, at δ -160 ($^{1}J_{P-H}$ = 207 Hz), and two phases were observed in the NMR tube.

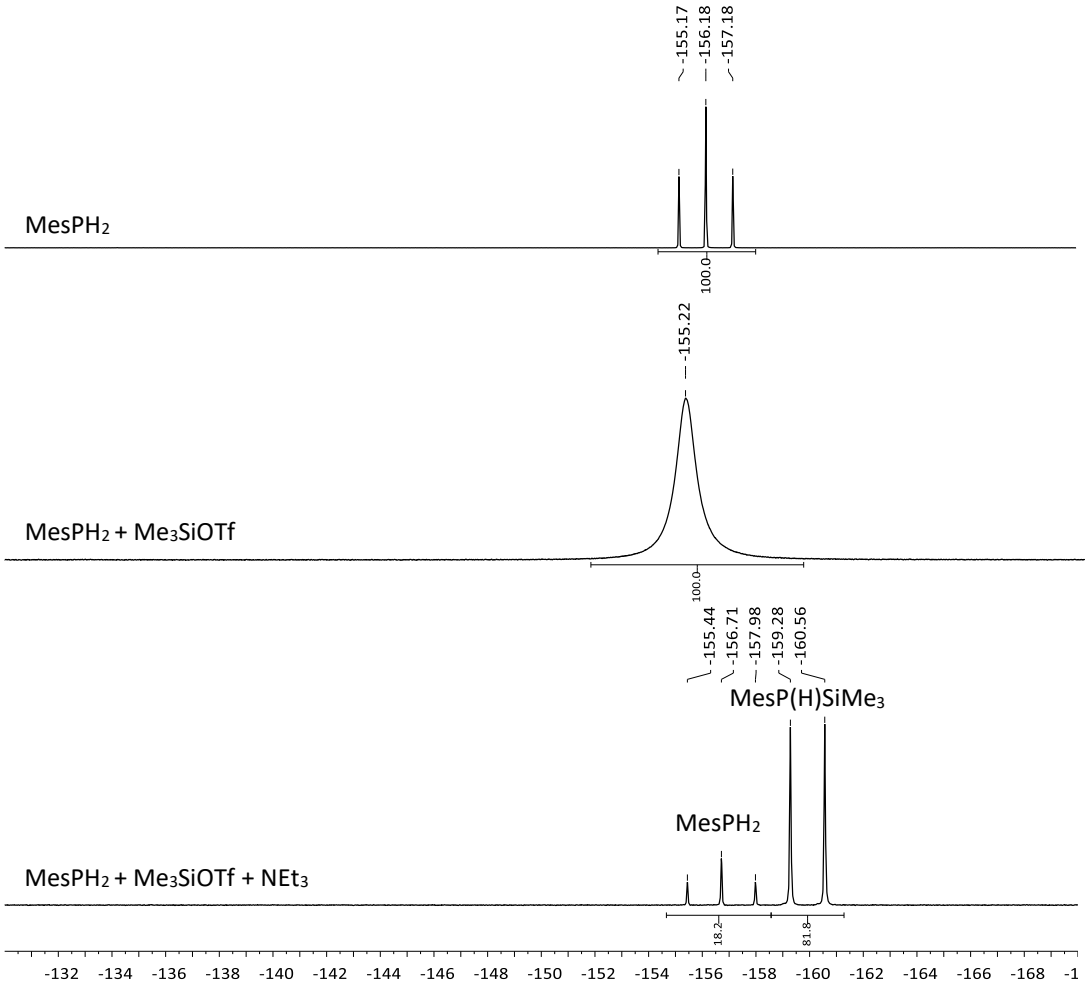

Figure 56 *^{31}P NMR (202 MHz, C_6D_6) spectra following the addition of trimethylsilyl triflate and triethylamine to mesityl phosphine.*

The preparation of silyl phosphines by the reaction of primary phosphines with trimethylsilyl triflate has been reported for smaller organic groups (Ph and ^{t}Bu),[26] however larger substituents (Mes, Dipp, Mes*) are synthesised by initial lithiation of the primary phosphine and addition of trimethylsilyl chloride, eliminating lithium chloride in a salt metathesis reaction.[27–29]

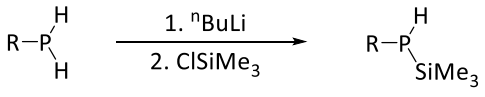

Scheme 74 *Preparation of aryl silyl phosphines. R = Mes, Dipp or Mes**

MesP(SiMe$_3$)H was synthesised for comparison by using the lithiation method in Scheme 74,[27] and the NMR data were consistent with the unknown doublet at δ = -159 ($^{1}J_{P\text{-}H}$ = 207

Hz). This procedure produced a high percentage (around 30%) of the *bis*-silylated product $MesP(SiMe_3)_2$ (δ = -162.5), something which is not seen during the reactions in Figure 56. Using the alternative method discussed here could provide a more efficient preparation of bulky silyl phosphines, and offer a different route to phosphaamidines where the isolation of a carbonitrilium triflate is not possible.

With this mechanistic insight in hand, the conditions to prepare the super bulky phosphaamidine **28** were modified. The reaction solvent was changed from dichloromethane to toluene, and the reaction components ($MesPH_2$, trimethylsiyl triflate, triethylamine and imidoyl chloride **26**) were added at room temperature, and the solution was then heated to 80 °C for 18 hours. This gave an isolated yield after work-up of 69%, a significant increase from using the previous method (32%).

X-ray quality crystals of **28** were grown from a saturated hexane solution at room temperature, and the resulting solid-state structure is shown Figure 57. The Z-anti N=C geometry of the phosphaamidine unit is different to both structurally characterised discussed previously (Mes-substituted **20** Z-syn N=C and Mes*-substituted **22** E-syn P=C). Due to the volume of the Ar* group, the opposite orientation at nitrogen (i.e. E-anti N=C or E-syn N=C) would not be possible as the substituent would move into space already occupied by the ^{t}Bu backbone. For similar reasons, the mesityl group is in an orientation as to avoid steric interaction with the Ar* group. This results in the observed Z-anti N=C isomer.

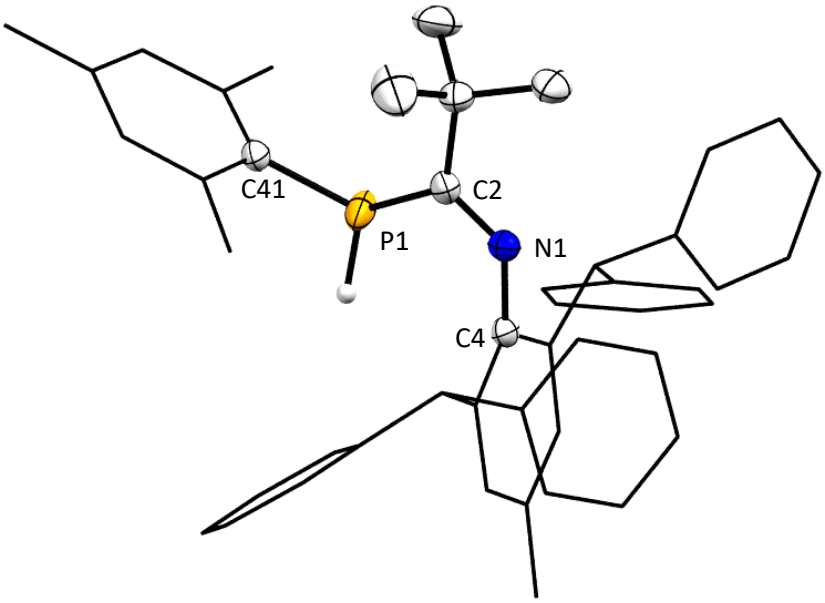

Figure 57 *X-Ray crystal structure of* ***28****. Hydrogen atoms (except P-H) omitted for clarity. Organic substituents are wireframe and disorder in mesityl group is omitted for clarity. Selected bond lengths (Å): P1-C2 1.8801(18), C2-N1 1.265(2). Selected bond angles (°): C2-P1-C41 109.58(16), C2-N1-C4 124.52(15), P1-C2-N1 118.50(13).*

The bond lengths of the central P-C=N unit in **28** are comparable with that of smaller mesityl-derivative **20**. The P1-C2 bond length in **28** is slightly elongated at 1.8801(18) Å and the C2=N1 length slightly shortened at 1.265(2) Å (compared with 1.872(3) Å and 1.279(4) Å respectively in **20**).

The internal angle (P-C=N) is significantly smaller than the analogous angle in **20**, however it is larger than in the Mes* derivative (**20** = 124.1(2)°; **22** = 114.32(12)°; **28** = 118.50(13)°) suggesting that the steric bulk of **22** is greater than that of **28**. This comparison is discussed further in section 4.3.3.

It is noted that each of the phosphaamidines characterised by X-ray crystallography in this work **20**, **22** and **28** display different core P-C-N structures, demonstrating that the geometry of a phosphaamidine, and perhaps further reactivity, is significantly dependent on the steric bulk of the aryl constituents.

4.2 Preparation of Magnesium Complexes

4.2.1 Preparation of Dimeric, Solvent-free Magnesium Complexes

Alkyl magnesium complexes are used as precursors for complexes featuring a functional Mg-R bond, such as magnesium hydrides.[30] A widely studied system is the β-diketiminate supported complex in Figure 58, which is used as a source of Mg-H for various catalytic transformations[31] (Mg-H discussed further in Section 4.2.5). A common procedure for the formation of butyl magnesium complexes is the addition of $^{n}Bu_2Mg$ to the corresponding protonated ligand. Solvated adducts typically result from preparation in coordinating solvents.

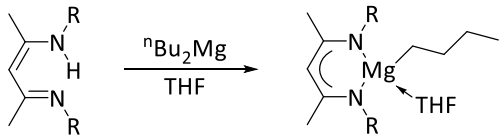

Figure 58 *Formation of an n-butyl magnesium complex supported by a β-diketiminate[32] which has many catalytic applications. R = 2,6-diisopropylphenyl.*

Treatment of the smallest phosphaamidine ligand in this series, mesityl-substituted **20**, with one equivalent of $^{n}Bu_2Mg$ in toluene at low temperature (-78 °C) causes the solution to change from colourless to bright yellow. The first indication of complexation can be seen in the ^{31}P NMR spectrum, where the characteristic doublet signal of **20** is replaced with a sharp signal, lacking phosphorus-hydrogen coupling, at δ = -41.9, corresponding to **29**. No analogous heteroleptic phosphaamidinate magnesium complexes have been reported.

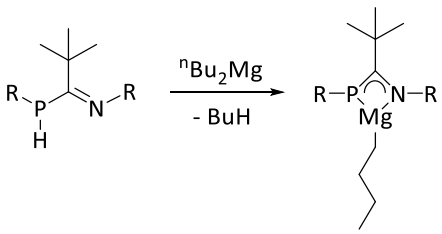

20	R_1=R_2=Mes	**29**
21	R_1=Tipp, R_2=Mes	**30**

Scheme 75 *Reaction of phosphaamidines **20** and **21** with $^{n}Bu_2Mg$*

The ^{1}H NMR spectrum of **29** shows signals which are similar to **20**, but shifted slightly, indicating a new ligand environment. For example, the singlet resonance associated with the ^{t}Bu backbone is shifted from δ = 1.33 in **20** to δ = 0.94 in **29**. All six methyl groups

associated with the mesityl groups are now inequivalent, with sharp six singlet resonances ranging from δ = 2.91 to 1.85. Crucially, the signal associated with the phosphine P-H proton of **20** (δ = 4.96, d, $^{1}J_{H\text{-}P}$ = 245 Hz) is not present in the ^{1}H NMR spectrum of **29**. Instead, signals associated with the ^{n}Bu group can also be identified and confidently assigned based on their multiplicity and a ^{1}H-^{1}H COSY experiment. The -CH_2 adjacent to the Mg is found at δ = 0.49, and the distinctive multiplicity is similar to that seen for such *n*-butyl groups in Chisholm's detailed ^{1}H NMR spectroscopic study of heteroleptic alkyl magnesium complexes supported by bidentate nitrogen donors.[33] The multiplicity arises from a AA'XX' spin system, where the α-protons are magnetically inequivalent and independently couple to the adjacent β-protons.

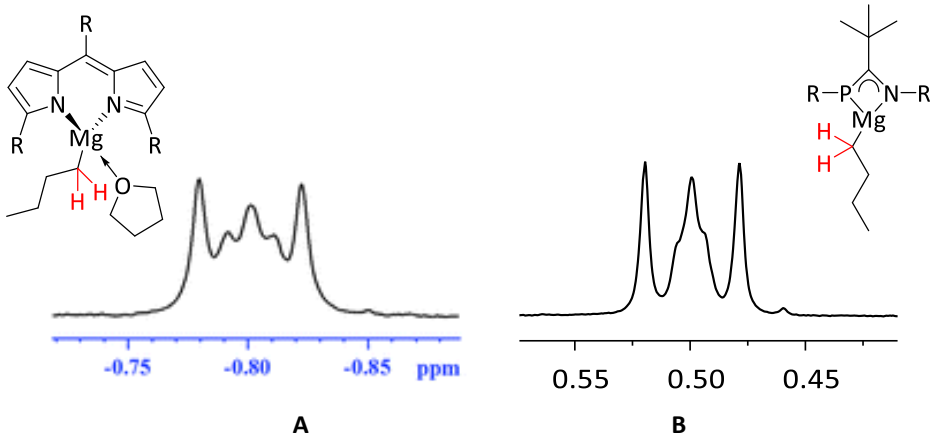

Figure 59 *^{1}H NMR spectra of α-protons to in LMg^{n}Bu complexes (R=Mes),* ***A*** *reproduced from literature*[33]

A key feature of the ^{13}C NMR spectrum of **29** is the retention of a downfield doublet at δ = 211.2 ($^{1}J_{C\text{-}P}$ = 14 Hz), corresponding to the central P-C=N carbon, shifted from δ = 182.5 ($J_{C\text{-}P}$ = 59 Hz) for the same carbon in protonated ligand **20**. The significant reduction in ^{1}J C-P coupling constant is indicative of a substantial change in the P-C bond or coordination of the lone pair.[5]

When prepared in benzene, **29** precipitates as a bright yellow crystalline solid, the single crystal X-ray diffraction analysis of which gives the solid-state structure shown in Figure 60. It reveals a dimeric structure in the unit cell, with the asymmetric unit corresponding to the Lewis structure shown in Scheme 75. The lone pair of the phosphorus in the asymmetric

unit is donated to the magnesium centre of the adjacent monomer, thereby providing electronic stabilisation usually associated with a coordinated solvent molecule.

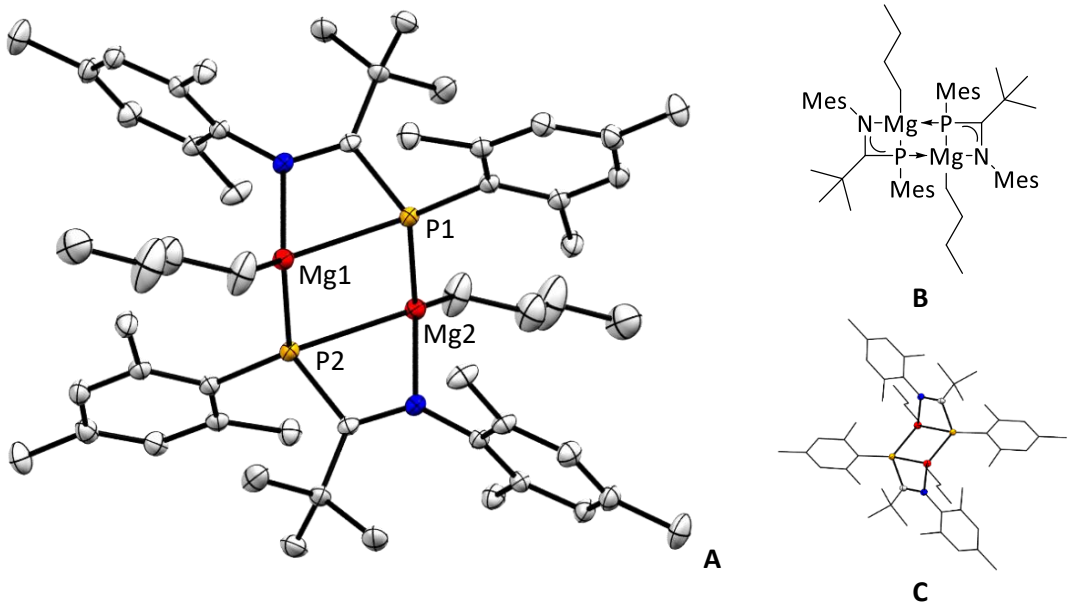

Figure 60 A *shows X-Ray crystal structure of* ***29****. Hydrogen atoms are omitted for clarity.* ***B*** *shows the Lewis structure and* ***C*** *shows the structure slightly rotated to show the conformation of the central tri-cyclic system. Selected bond lengths (Å): P2-Mg1 2.6185(8), P1-Mg2 2.6186(8).*

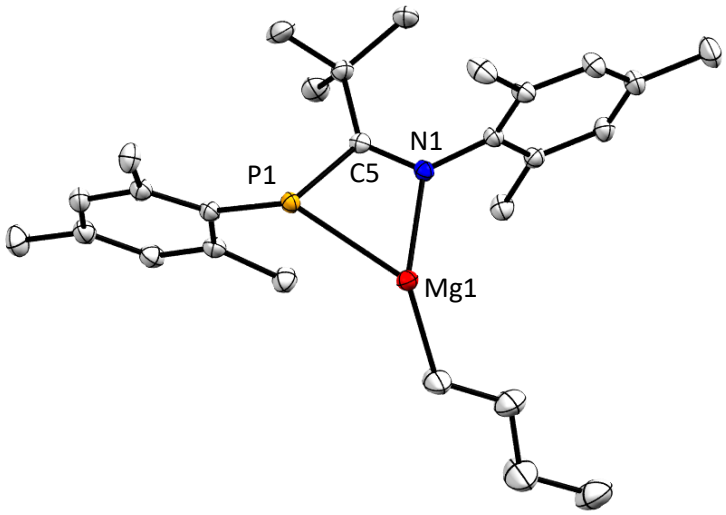

Figure 61 *Asymmetric unit of* ***29*** *Hydrogen atoms are omitted for clarity. Selected bond lengths (Å): Mg1-P1 2.5937(8), P1-C5 1.8527(19), C5-N1 1.303(3), N1-Mg1 2.1717(17). Selected bond angles (°): P1-C5-N1 108.03(13), C5-N1-C19 127.66(16), C5-P1-C10 111.93(9), P1-Mg1-N1 64.65(3).*

The P-C bond distance in **29** is slightly shorter compared to the same bond in the corresponding protonated ligand **20** (**20**: 1.872(3) Å, **29**: 1.8527(19) Å), indicating more double bond character in **29**. Conversely, the C-N bond distance has slightly elongated (**20**: 1.279(4) Å, **29**: 1.303(3) Å). This suggests some amount of delocalisation across the central P-C-N unit.

The bond lengths between the ligand and the magnesium atom in the asymmetric unit are long (P1-Mg1 2.5937(8) Å and N1-Mg1 2.1717(17) Å) suggesting some ionic character of bonds. For comparison, the Mg-N bond lengths in ^{Dipp}NacNacMg^{n}Bu(THF) (^{Dipp}NacNac = [(Dipp)NC(Me)]$_2$CH) are 2.071(1) Å and 2.063(1) Å.[33] It is noted that bond lengths Mg1-P1 and Mg1-P2 are very similar, 2.5937(8) Å and 2.6186(8) Å respectively.

Moving to the next novel phosphaamidine ligand in the sequence, treatment of slightly larger Tipp containing ligand **21** with one equivalent of ^{n}Bu$_2$Mg at low temperature (-78 °C) results in the formation of alkyl-magnesium complex **30**, directly analogous to Mes derivative **29**. This can be isolated as a bright yellow crystalline solid from toluene at -20 °C.

Given the similarity between complexes **29** and **30**, it is reasonable that their spectroscopic properties are similar. The ^{31}P NMR spectrum of **30** displays a sharp singlet signal at δ = -55.3. A downfield doublet signal can be found in the ^{13}C NMR spectrum at δ = 211.2 ($J_{C\text{-}P}$ = 15 Hz) corresponding to the central carbon of the P-C=N phosphaamidine unit.

The introduction of three ^{i}Pr substituents makes the ^{1}H NMR spectrum of **30** more complex that of smaller derivative **29**. The isopropyl methyl groups appear as four separate signals. The *para*-isopropyl group is identified as a sharp doublet at δ = 1.14 ($J_{H\text{-}H}$ = 6.9 Hz), with the corresponding C-H signal appearing as a septet signal at δ = 2.70 ($J_{H\text{-}H}$ = 7.0 Hz). The remaining methyl signals consist of four doublets at δ = 1.66 ($J_{H\text{-}H}$ = 6.6 Hz), 1.56 ($J_{H\text{-}H}$ = 6.8 Hz), δ = 1.52 ($J_{H\text{-}H}$ = 6.7 Hz) and 0.66 ($J_{H\text{-}H}$ = 6.8 Hz). These *ortho*-isopropyl groups share a common broad C-H signal at δ = 4.55. The methyl groups associated with the mesityl group are all inequivalent, with three singlet signals seen at δ = 2.41, 1.96 and 1.87.

Next the magnesium-butyl group was identified. The CH_2 adjacent to the magnesium centre displays a AA'XX' multiplet at δ = 0.41 (cf. δ = 0.49 in **29**) in the ^{1}H NMR spectrum of **30**. The

terminal CH_3 protons are identified as a triplet signal at δ = 1.30 ($J_{H\text{-}H}$ = 7.3 Hz). The signals associated with the internal CH_2 protons of the butyl group are not immediately apparent, however a ^1H-^1H COSY experiment revealed that they are broadened and lie under other signals (Figure 62).

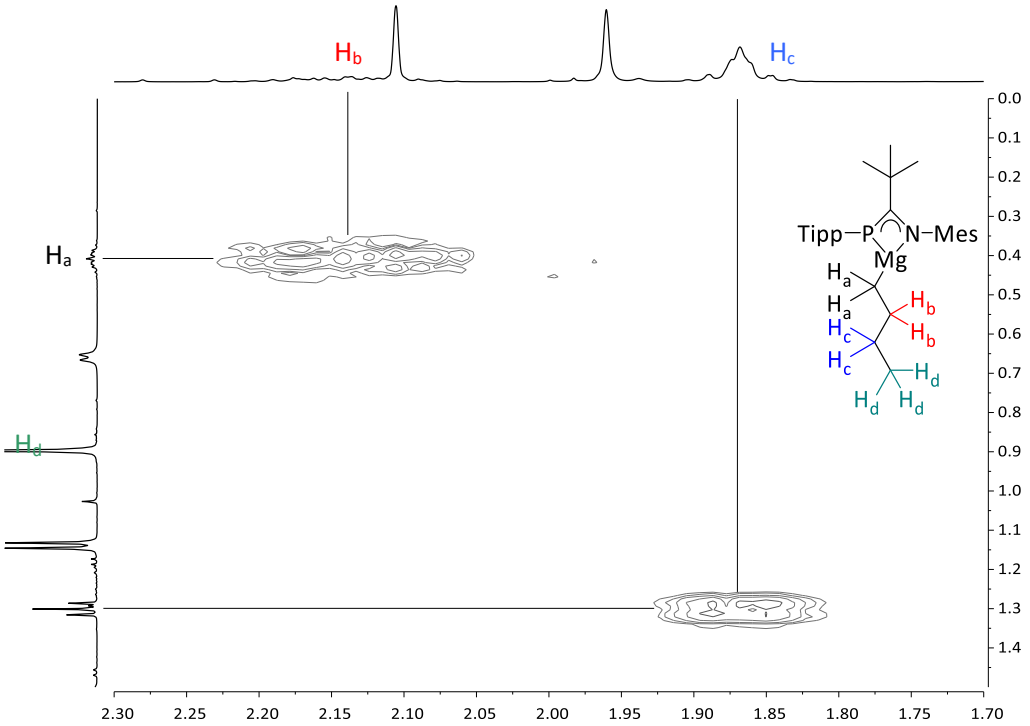

Figure 62 *^1H-^1H COSY spectrum of* ***30***

The preparation of **30** in hexane results in the precipitation of X-ray quality crystals, the resulting solid-state structure is shown in Figure 63. Like the previous example **29** it is dimeric in the unit cell, and the asymmetric unit is consistent with the Lewis structure in Scheme 75.

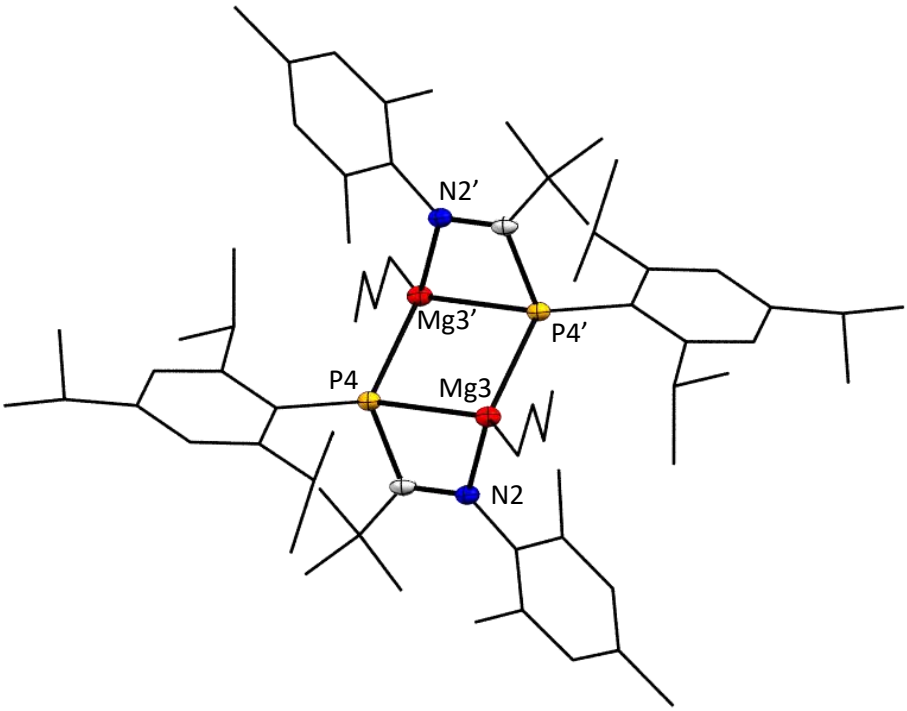

Figure 63 *X-Ray crystal structure of* ***30****. Two molecules are present in unit cell, only one is shown here. Hydrogen atoms are omitted for clarity. Selected bond lengths (Å): P4'-Mg3 2.6293(7). Selected bond angles (°): P4-Mg3-P4' 90.99(2).*

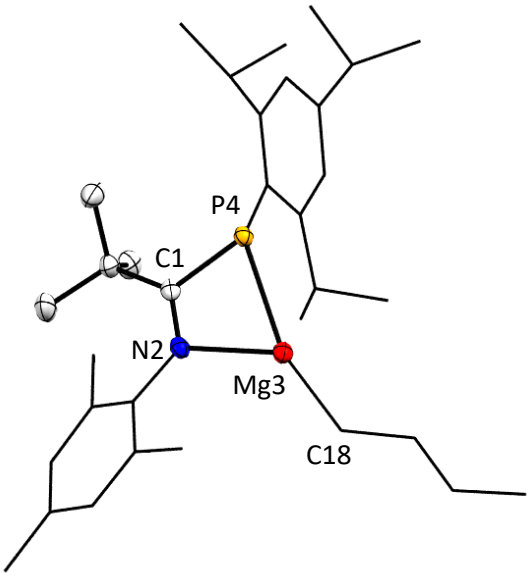

Figure 64 *Asymmetric unit of* ***30****. Hydrogen atoms are omitted for clarity. Selected bond lengths (Å): P4-Mg3 2.6071(7), N2-Mg3 2.1583(14), P4-C1 1.8545(16), N2-C1 1.301(2), Mg3-C18 2.1127. Selected bond angles (°): P4-C1-N2 107.89(11), P4-Mg3-N2 64.51(4).*

The bond lengths of **30** are consistent with a P4-C1=N2 central unit; P-C 1.8545(16) Å and C-N 1.301(2) Å (compared to 1.8527(19) Å and 1.303(3) Å in **29** respectively). The internal P4-C1=N2 angle in **30** is slightly smaller than the corresponding angle in **29** (107.89(11)° and 108.03(13)° respectively), indicating that the introduction of the Tipp group on the phosphorus has increased the effective steric bulk of the ligand framework (see section 4.2.3).

To further this series of compounds, a C_6D_6 solution of the super mesityl (Mes*) substituted phosphaamidine **22** was also treated with one equivalent of $^{n}Bu_2Mg$ in an attempt to synthesise a compound analogous to **29** and **30**. However, the only product formed was identified by ^{1}H and ^{31}P NMR experiments as the *bis*-ligated species **31** (see section 4.2.4).

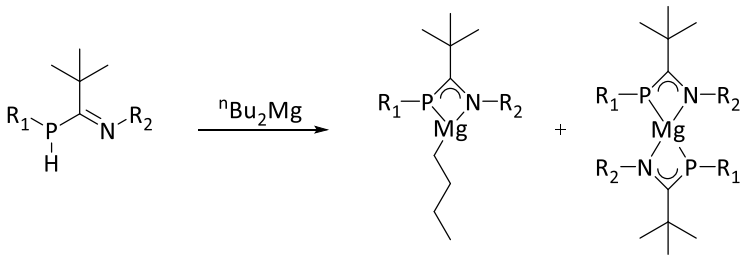

22	R_1=Mes* R_2=Mes	n/a	**31**
23	R_1=Mes, R_2=Dipp	**32**	**33**

Scheme 76 *Addition of one equivalent of $^{n}Bu_2Mg$ to **22** forms only L_2Mg type compound*

The reaction of Dipp phosphaamidine **23** with one equivalent of $^{n}Bu_2Mg$ also gave the *bis*-ligated species **33** as the major product (77% by integration of the ^{31}P NMR spectrum, see section 4.2.4). In this case a second product is observed by ^{31}P NMR spectroscopy at δ = -44.8, corresponding to 22% of the product mixture by integration of the ^{31}P NMR spectrum. This second, minor signal is attributed to the targeted $LMg^{n}Bu$ species, as the chemical shift is similar to that of both **29** and **30**. The crude mixture of **32** and **33** was difficult to separate, and only pure samples of **33** were isolated. In the reactions described in Scheme 76, changing the stoichiometry so that there was an excess of $^{n}Bu_2Mg$ did not change the distribution of products. Homoleptic phosphaamidinate magnesium complexes **31** and **33** will be discussed in further detail in section 4.2.4.

4.2.2 Preparation of a Monomeric, Three-Coordinate ^{n}Butyl Magnesium Complex

Unlike the other phosphaamidines investigated thus far, addition of one equivalent of $^{n}Bu_2Mg$ to a toluene solution of bulky phosphaamidine **28** does not result in a reaction at room temperature, however heating the solution to 90 °C overnight produced a colour change from colourless to dark orange. ^{31}P NMR spectroscopy of this solution revealed a new product at δ = -7.03, corresponding to alkyl-magnesium complex **34**. This is significantly downfield of the ^{31}P NMR signals for similar complexes supported by less bulky ligands **29** and **30** (δ = -42.0 and -55.3 respectively), suggesting a substantial structural difference.

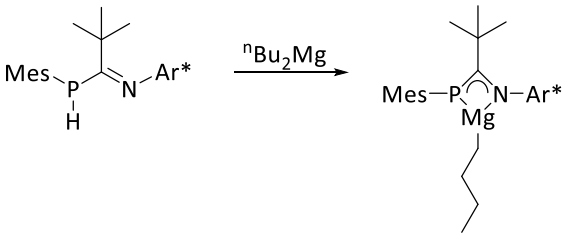

28 **34**

Scheme 77 *Reaction of bulky phosphaamidine **28** with $^{n}Bu_2Mg$ to form **34**. Ar* = 2,6-bis(diphenylmethyl)-4-methyl phenyl*

A preparative scale reaction allowed the isolation of **34** as an orange solid in 78% yield. In the ^{1}H NMR spectrum of **34** the aromatic region is understandably complex, as there are six inequivalent phenyl proton groups present. The resonance corresponding to the C(H)Ph_2 proton appears close to this aromatic region, at δ = 5.92. The *ortho*-methyl mesityl groups are observed as a singlet signal at δ = 2.74, where the corresponding *para*-methyl group is further upfield at δ = 2.11. The backbone ^{t}Bu appears at δ = 1.14, which is shifted from the corresponding resonance in the protonated ligand **28** (δ = 0.85).

The signals associated with the n-butyl group can also be identified. The terminal methyl group is observed as a triplet at δ = 1.02 ($J_{H\text{-}H}$ = 7.6 Hz), and the adjacent CH_2 group is observed as a sextet around δ = 1.43 ($J_{H\text{-}H}$ = 7.6 Hz). Close to this is an undefined multiplet signal around δ = 1.60 – 1.50, assigned to the next CH_2 in the chain by a ^{1}H-^{1}H COSY experiment. Finally, the Mg-CH_2 signal is also observed as a broad multiplet at δ = − 0.56 to − 0.73, the only signal observed in this work below δ = 0.

At δ = 221.2 (J_{C-P} = 55 Hz) in the ^{13}C NMR spectrum, the signal associated with the central carbon of the P-C=N is shifted slightly downfield of similar carbon atoms in Mes derivative **29** (δ = 211.2 (J_{C-P} = 14 Hz)) and Tipp derivative **30** (δ = 211.3 (J_{C-P} = 15 Hz)). Additionally, **34** possesses a much higher ^{1}J C-P coupling constant than both dimeric complexes, these factors again suggest a very different structural environment of the phosphorus atom.

The solid-state structure of **34** was measured from single crystals grown from hexane at room temperature. Immediately apparent is that **34** is monomeric in the unit cell, with no interactions observed between molecules in the extended structure. A pyramidal phosphorus (ΣP = 309.7(4)°) confirms that its lone pair is localised.

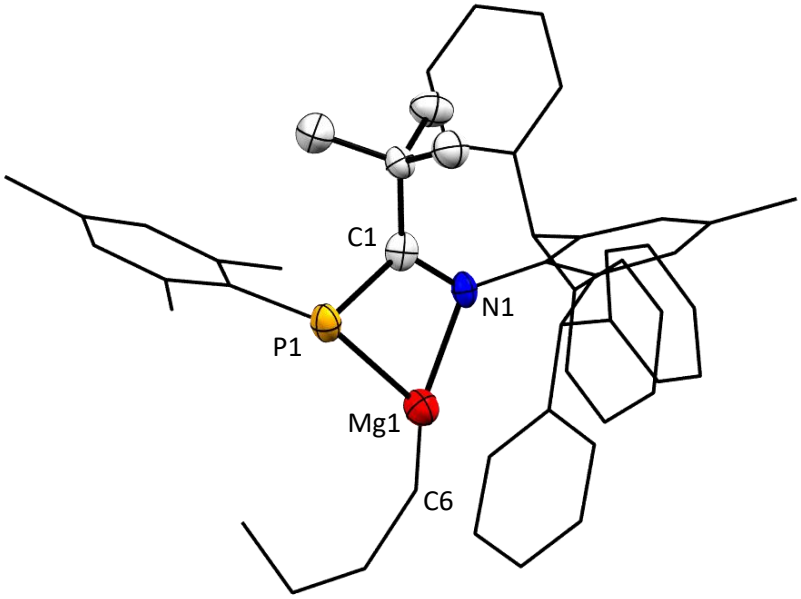

Figure 65 *X-Ray Crystal Structure of* ***34****. Hydrogen atoms omitted for clarity. Organic substituents are wireframe for clarity, full structure in the supporting information. Selected bond lengths (Å): Mg1-P1 2.522(2), P1-C1 1.813(5), C1-N1 1.335(6), N1-Mg1 2.124(5), Mg1-C6 2.09(2). Selected bond angles (°): P1-C1-N1 110.0(4), C1-N1-C19 126.8(4), C1-P1-C10 107.3(3), P1-Mg1-N1 67.25(16).*

Whilst three-coordinate solvent-free monomeric magnesium complexes can be readily prepared with more sterically demanding alkyl groups such as isopropyl[34] or *t*-butyl,[32] but examples bearing an *n*-butyl group are rare. One such complex is supported by a β-diketiminate ligand derived from the same bulky amine as phosphaamidine **28**.[23]

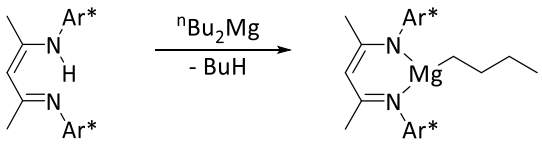

Monomeric

Scheme 78 *Preparation of a three-coordinate monomeric n-butyl magnesium centre. From solid-state structure: N-Mg 2.0463(13) Å and 2.0326(13) Å, Mg-C 2.089(4) Å. N-Mg-N 92.31(5)°*

When compared to protonated ligand **28**, the P-C bond in **34** is significantly shortened (1.813(5) Å vs 1.8801(18) Å) and the C-N bond is slightly elongated (1.335(6) Å vs 1.265(2) Å), indicating a small amount delocalisation across the central phosphaamidinate unit. The N-Mg bond is 2.124(5) Å, slightly shorter than the N-Mg bond in analogous complexes **29** and **30** (2.1717(17) Å and 2.1523(14) Å respectively). For comparison, the average N-Mg bond distance in the previously reported monomeric complex (Scheme 78) featuring the β-diketiminate ligand is 2.039(13) Å.[23] The "bite angle" (N-Mg-N) of the reported NacNac complex at 92.31(5)°, is much larger than the analogous P-Mg-N angle in **34**, which is 67.25(16)°.

The *n*-butyl group in **34** is not in its usual configuration, and is instead curved away from the nitrogen substituent. The space occupied by the Ar* group is forcing this distortion, something which can easily be observed in the spacefill diagram in Figure 66.

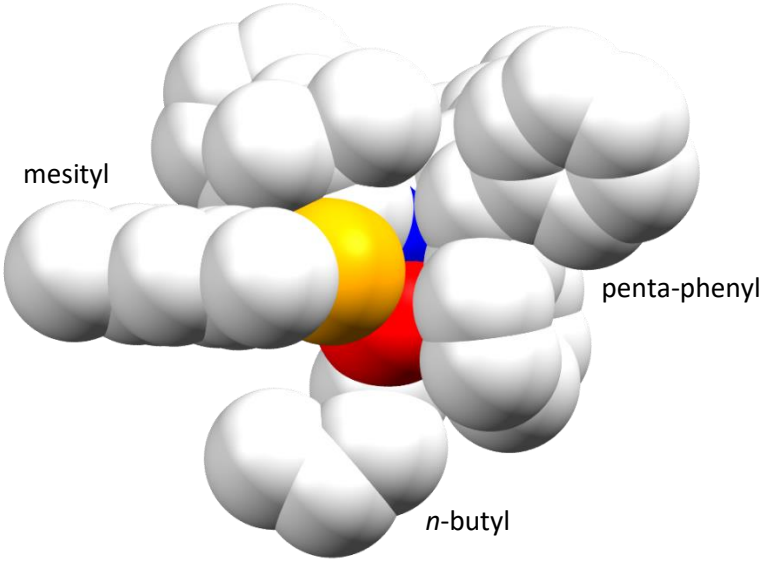

Figure 66 *Spacefill diagram of the X-ray crystal structure of* ***34***

4.2.3 Quantifying the Steric Factors between Butyl Magnesium Complexes

Kinetic stabilisation is often an important factor in the formation of reactive main-group species, and so typically bulky ligands are favoured. One method of quantifying the steric bulk of ligands in amidinate-metal complexes is by comparison of the internal angle N-C-N of the amidine.[35] A smaller internal angle typically indicates bulkier substituents, as the heteroatoms have been moved closer together in space to allow more space for the outer organic substituents. It is reasonable that this methodology can be applied to phosphaamidines.

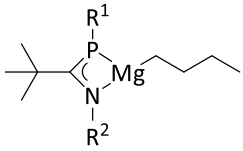	**P-Mg (Å)**	**N-Mg (Å)**	**P-C-N (°)**	**P-Mg-N (°)**	**%V_{bur}**
R_1=R_2=Mes (**29**)	2.5942(6)	2.1726(12)	108.09(9)	64.65(3)	38.8
R_1=Tipp; R_2=Mes (**30**)	2.6071(7)	2.1583(14)	107.89(11)	64.51(4)	40.7
R_1=Mes; R_2=Ar* (**34**)	2.522(2)	2.124(5)	110.0(4)	67.25(16)	58.9

Table 6 *Comparison of structural features between butyl magnesium phosphaamidinate complexes. For calculation of %V_{bur} values the n-butyl group was removed.*[36]

The P-C-N "internal" angles obtained from the solid-state structures of LMgBu complexes **29**, **30** and **34** are listed in Table 6. It becomes apparent in the structural comparison that complexes **29** and **30** are very similar. The difference between their internal angles is a negligible 0.2°, and so the addition of the isopropyl groups in Tipp-substituted **30** seems to have made little difference to the overall steric profile of the complex. Unexpectedly, the P-C-N of Ar* complex **34** is larger than in the complexes bearing the smaller ligands.

The "bite-angle" (N-Mg-N) has also been used to quantify the steric bulk in amidinate complexes.[35] The analogous angle in the phosphaamidinate complexes here is the P-Mg-N angle. It is again evident that dimeric species **29** and **30** are comparable, with only a 0.14° difference in these angles. The larger bite-angle of **34** enforces shortened P-Mg and N-Mg bonds. As the internal angle is also large, it suggests the metallacycle is compressed in comparison to the other complexes. This probably a consequence of the mononuclearity of

34; the metal centre receives all required electronic stabilisation from one ligand, so it is held closer to the P-C-N unit.

The effect of the steric bulk on the Mg-C bond is another factor to consider. In dimeric **29** and **30**, these bond lengths are comparable at 2.1195(17) Å and 2.1127(17) Å respectively, whilst in **34** this bond is slightly shorter at 2.09(2) Å. Although the lack of accuracy in the final does not all definitive conclusions to be drawn, the shorter Mg-C bond length may indicate a slightly stronger bond.

In 2009 Cavallo reported a method of calculating the percentage buried volume ($\%V_{bur}$) of a metal complex as a standardised method of comparing steric bulk around a metal centre[37] based on Tolman's reported relationship of cone angle to reactivity in phosphorus chemistry.[38] Using this method, the $\%V_{bur}$ has been calculated for a vast range of phosphine- and NHC-metal centres,[39] and the correlation of a ligand's steric bulk with complexes' activity in transition metal catalysis has been aided by $\%V_{bur}$ calculations.[40]

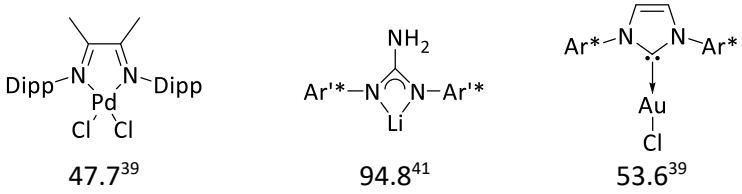

47.7[39] 94.8[41] 53.6[39]

Figure 67 *Examples of $\%V_{bur}$. Dipp = 2,6-dissopropylphenyl. Ar'*=2,6-bis-(diphenylmethyl)-4-tert-butyl phenyl*

Using Cavallo's method, the $\%V_{bur}$ of magnesium complexes **29**, **30** and **34** was calculated and the results are listed in Table 6. As expected, as the table is descended, the $\%V_{bur}$ increases. The values echo the bite-angle trend, with little difference seen between dimeric complexes **29** and **30**, then a larger change in monomeric complex **34**. A value for the largest complex of 58.9 confirms the substantial bulk of the ligand.

4.2.4 Preparation of Bis-Ligated Phosphaamidinate Magnesium Complexes

Bis-ligated amidinate complexes can be a major frustration in group 2 chemistry. Formed *via* the Schleck-rearrangement of heteroleptic species, they are commonly the thermodynamic minimum, representing deactivation pathways in catalysis.[42] This equilibrium can be observed experimentally. For example, Mandal demonstrated that heating the heteroleptic amidinate complex LMgCp results in the formation of a L_2Mg complex with elimination of Cp_2Mg.[43]

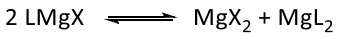

Scheme 79 *Schlenk equilibrium*

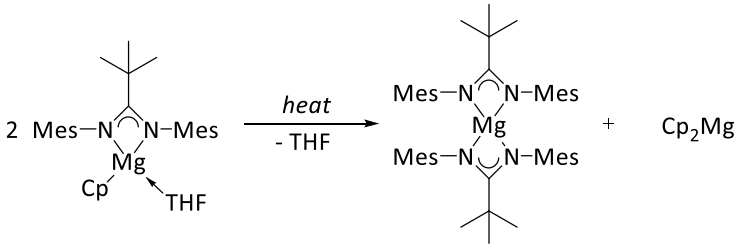

Scheme 80 *Formation of a four-coordinate magnesium centre with elimination of Cp_2Mg*

Typically, the solid-state structure of these *bis*-ligated complexes is tetrahedral around the magnesium centre. There are two exceptions to this, one of which features bidentate ligands bonded through carbon and a silylated nitrogen,[44] and the other an amidinate complex.[45] The odd geometry of the latter is attributed to the six aromatic groups around the periphery of the complex, as the orientation of these in space must be such that they all remain planar.

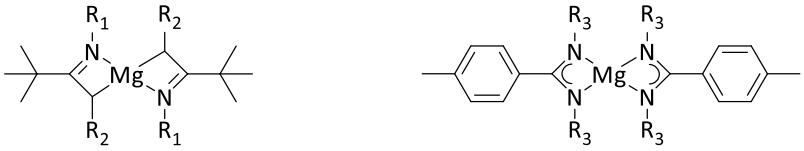

Figure 68 *Two reported examples of square planar bis-ligated magnesium complexes. R_1=R_2=$SiMe_3$, R_3 = 2,6-diisopropylphenyl.*

To target similar homoleptic L_2Mg complexes featuring phosphaamidinate ligands, a series of experiments were carried out where half an equivalent of $^nBu_2Mg$ was added to the protonated phosphaamidines **20**-**23**.

Addition of half an equivalent of $^{n}Bu_2Mg$ to a toluene solution of small phosphaamidine **20** initiates a colour change from colourless to bright yellow, much the same as in the formation of **29**. Looking to the ^{31}P NMR spectrum, the formation of a new signal at δ = -25.9 is observed. Recrystallisation from pentane allowed the product to be identified as **35**, with an isolated yield of 78%. As no signals for an n-butyl group were observed, there has been clean elimination of two equivalents of butane from the magnesium centre.

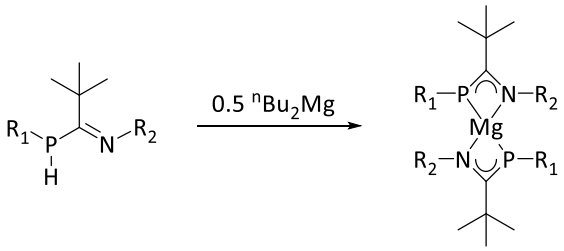

20	R_1=R_2=Mes	**35**
21	R_1=Tipp, R_2=Mes	**36**
22	R_1=Mes*, R_2=Mes	**31**
23	R_1=Mes, R_2=Dipp	**33**

Scheme 81 *Preparation of bis-ligated phosphaamidinate magnesium complexes*

The ^{t}Bu of the phosphaamidine backbone in **35** is found at δ = 0.97 in the ^{1}H NMR spectrum, which is a similar chemical shift to the corresponding alkyl-complex **29** (δ = 0.94). The signals associated with the mesityl group of the phosphorus substituent are seen at δ = 2.78 and 2.05 in a relative ratio of 2:1, and the corresponding nitrogen substituent is seen at δ = 2.01 and 2.14, again with a relative ratio of 2:1. This indicates the *ortho*-methyl groups of each mesityl group are equivalent, and a complex with high symmetry.

Analogous to both the protonated phosphaamidines and the alkyl-magnesium phosphaamidinate complexes, the central carbon of the P-C=N of **35** gives a very downfield doublet signal in the ^{13}C NMR spectrum at δ = 222.6 ($^{1}J_{C\text{-}P}$ = 60 Hz). The coupling constant is consistent with its corresponding protonated ligand **20** ($^{1}J_{C\text{-}P}$ = 59 Hz), yet very different to the LMgBu complex **29** ($^{1}J_{C\text{-}P}$ = 14 Hz).

To show that the elimination of two equivalents of butane occurs in a step-wise manner, an equivalent of protonated ligand **20** was added to alkyl-magnesium complex **29**, which resulted in the formation of *bis*-ligated complex **35** by ^{31}P NMR spectroscopy. The reverse

of this reaction is also possible; the addition of one equivalent of $^{n}Bu_2Mg$ to a solution of **35** results in the clean formation back to complex **29**.

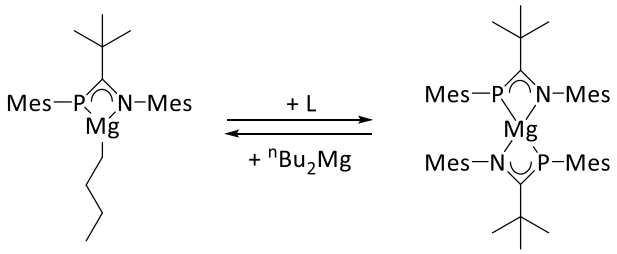

29 **35**

Scheme 82 *Synthetic route between the alkyl-magnesium complex **29** and the bis-ligated complex **35**. L = **20***

Following this trend of double butane elimination, and as alluded to in section 4.2.1, the analogous L_2Mg compound **31** can be prepared in an optimised procedure using Mes*-substituted **22** and half an equivalent of $^{n}Bu_2Mg$. The resulting L_2Mg complex is identified by a singlet signal in the ^{31}P NMR spectrum at δ = 12.5, with a series of signals in the ^{1}H NMR identifying that one ligand environment is present. The ^{31}P chemical shift of **31** is very different to smaller complexes **35** and **36** (δ = -25.9 and -34.2 respectively). In section 4.1.2, it was shown that the phosphaamidine **22** exists in solution as three discrete isomers, two of which are phosphaalkenes. It is possible that **31** is derived from only the P=C tautomers, and hence the P=C-N unit of **31** has significant phopshaalkene character, causing this dramatic downfield shift in the ^{31}P NMR spectrum of **31**.

It is noted that when the isomeric mixture of **22** is reacted, only one product isomer is formed. This implies that the isomers can interconvert in solution to the reactive configuration.

The central P-C-N carbon in **31** gives a ^{13}C NMR signal at δ = 220.0 ($^{1}J_{C\text{-}P}$ = 49 Hz), with a coupling constant slightly lower, but still comparable with, other L_2Mg compounds **35** (Mes, $^{1}J_{C\text{-}P}$ = 60 Hz) and **36** (Tipp, $^{1}J_{C\text{-}P}$ = 58 Hz). Whilst in other areas of phosphorus chemistry, the $^{1}J_{C\text{-}P}$ coupling constant can give substantial structural information,[5] however a structural study by Amrei concluded that in phosphaamidine chemistry the $^{1}J_{P\text{-}C}$ is not diagnostic.[9]

The X-ray crystal structure of **31** is shown in Figure 69. The expected four-coordinate magnesium centre displays a highly distorted tetrahedral geometry, for example, P1-Mg1-P2 140.38(3)° and P1-Mg1-N1 66.20(4)°. The bite-angle (P-Mg-N of a single ligand) is comparable with that of mononuclear phosphaamidinate n-butyl magnesium complex **34**, 66.20(4)° and 67.25(16)° respectively. This is most likely due to the large steric bulk associated with the super mesityl group.

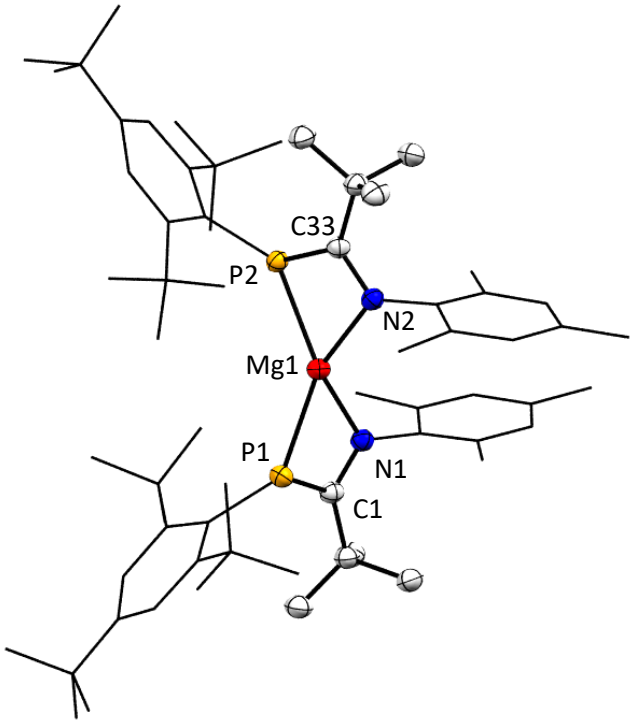

Figure 69 *X-Ray crystal structure of **31**. Two co-crystallised molecules of C_6D_6 omitted. Hydrogen atoms are omitted for clarity. Disorder in para-tertbutyl group of the Mes* is omitted. Selected bond lengths (Å): P1-C1 1.7883(17), P1-Mg1 2.5093(6), C1-N1 1.334(2), N1-Mg1 2.0930(15), P2-C33 1.7946(16), P2-Mg1 2.5064(7), N2-C33 1.334(2), N2-Mg1 2.0977(14). Selected bond angles (°): P1-C1-N1 107.81(12), P2-C33-N2 107.84(11), P1-Mg1-N1 66.20(4), P2-Mg1-N2 66.7(4), P1-Mg1-P2 140.38(3), N1-Mg-N2 119.94(6).*

Given that the corresponding protonated ligand of **31** is primarily an amino-phosphaalkene, it follows that at 1.7946(16) Å, the P-C bond of **31** is the shortest of the magnesium complexes in this work. However, it is still significantly longer than a standard P=C, suggesting its true bond-character is between single and double. With a distance of 1.334(2) Å, the C-N bond is also intermediary between single and double.

The next example in Scheme 81 is the case of the Dipp-substituted ligand **23**. As briefly discussed in section 4.2.1, this ligand is incapable of forming an isolable alkyl-magnesium complex. On addition of one equivalent of $^{n}Bu_2Mg$, the formation of two products is observed by ^{31}P NMR spectroscopy, the *mono*- and *bis*-ligated complex, **32** and **33** respectively. However, heteroleptic LMgBu **32** is consistently the minor product, with no pure sample obtained. Addition of 0.5 equivalents of the magnesium reagent to Dipp ligand **23** allows for sole formation of the *bis*-ligated complex **33**, however high solubility leads to a low isolated yield of 57%.

In the ^{31}P NMR spectrum of **33**, only one signal is seen at δ = -20.5. At 300 K, the ^{1}H NMR spectrum of **33** was found to be very broad, and signals for all protons in the complex could not be identified. Variable temperature ^{1}H NMR experiments allowed the signals to sharpen, and at 353 K all the signals of the molecule could be identified. A septet corresponding to the isopropyl groups is seen at δ = 3.29 (J_{H-H} = 6.7 Hz), and the adjacent methyl groups are seen as two doublet signals at δ = 1.24 (J_{H-H} = 6.8 Hz) and δ = 1.00 (J_{H-H} = 8.7 Hz). The *ortho*-methyl groups of the mesityl group share a singlet signal at δ = 2.60, and the *para*-methyl group is seen at δ = 2.14.

The final ligand in this series is the bulky Ar*-substituted phosphaamidine **28**. Addition of one equivalent of $^{n}Bu_2Mg$ to **28** produces the monomeric three-coordinate alkyl-magnesium complex **34** (section 4.2.2).

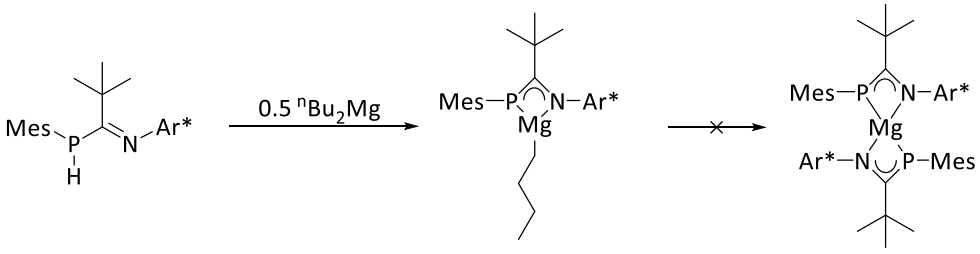

28 **34**

Scheme 83 *Attempted preparation of a bis-ligated magnesium complex featuring a super-bulky phosphaamidine*

The addition of half an equivalent of $^{n}Bu_2Mg$ to **28** does not result in a new L_2Mg product; only the n-butyl magnesium complex is formed. Even with prolonged heating, no formation

of the appropriate L_2Mg species is observed by ^{1}H or ^{31}P NMR spectroscopy. The observation that this phosphaamidine cannot form a *bis*-ligated magnesium complex is attributed to the great size of the ligand. This was the anticipated effect, given that a silyl-amide ligand derived from the same Ar* aniline has been shown to support a two-coordinate Mg(I) centre.[24] This suggests that this ligand has enough steric bulk to kinetically stabilise other main-group species, and perhaps even some low-valent species. Further, formation of heteroleptic L_2Mg species is reported to be a catalyst degradation pathway in amidinate chemistry.[42] Thus, as a catalyst in molecular transformation, **34** has a major advantage over Mesityl-substituted **29** and Tipp-substituted **30.** This is explored further in the ring-opening polymerisation of lactide in section 4.3.

4.2.5 Attempted Preparation of a Homoleptic Magnesium Hydride

Bridging magnesium hydrides supported by nitrogen based bidentate ligands, such as the example in Scheme 84, have many applications in molecular catalysis. These include many examples of hydroboration,[46–49] de-aromatisation of pyridines[50] and more recently C≡O homologation and reduction.[51–53]

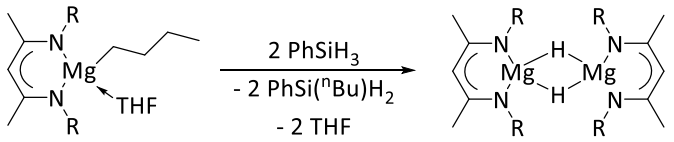

Scheme 84 *Synthesis of bridging magnesium hydride species using phenylsilane. R = 2,6-diisopropylphenyl*[56]

Magnesium hydrides have a tendency to be unstable in solution, and so a typical catalytic procedure includes the *in situ* formation of the hydride.[31] A common method of hydride synthesis is by reaction of the corresponding butyl magnesium complex with $PhSiH_3$, which forms $PhSi(^nBu)H_2$ as a by-product.[54] Using the same procedure magnesium hydride complexes were targeted in this work, using LMgBu complexes **29** and **34**.

Heating toluene or hexane solutions of dinuclear species **29** with one equivalent of $PhSiH_3$ does produce a reaction, however the sole product identified by ^{31}P NMR spectroscopy is the previously synthesised *bis*-ligated complex **35**.

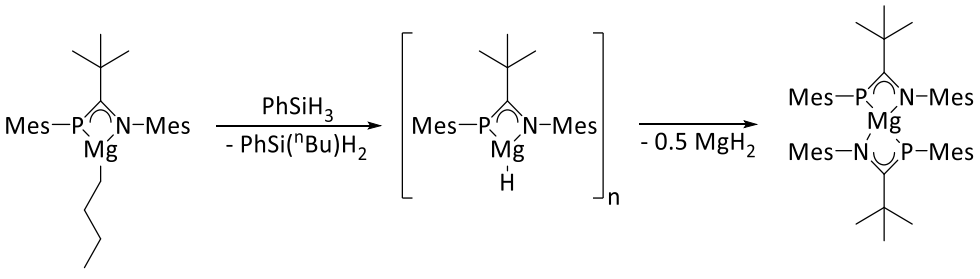

29 **37** **35**

Scheme 85 *Reaction of **29** with $PhSiH_3$ to form an unstable magnesium hydride species*

The expected byproduct ($PhSi(^nBu)H_2$) is observed by ^1H NMR experiments as a characteristic triplet signal from Si-H coupling to the α-protons of the butyl group at δ = 4.48 (t, $J_{H\text{-}H}$ = 3.7 Hz, $^1J_{H\text{-}Si}$ = 190 Hz). It is therefore suggested that the phosphaamidinate

magnesium hydride **37** was formed, however it has undergone Schlenk-type ligand redistribution with elimination of MgH_2, producing the more stable homoleptic complex **35**.

Mono-nuclear complex **34** was shown to be incapable of forming a *bis*-ligated complex in section 4.2.4, so preparation of a corresponding Mg-H should not undergo subsequent ligand redistribution.

Heating a C_6D_6 solution of **34** with $PhSiH_3$ for 48 hours reproducibly gave nine phosphorus containing products. One signal was attributed to phosphaamidine **28**. Of the other signals, the major product is a broad singlet signal ($\nu_{1/2} \approx 72$ Hz) at $\delta = -12.6$, accounting for 45% of the phosphorus containing material (by integration of the ^{31}P NMR spectrum). The anticipated $PhSi(^nBu)H_2$ was seen in the corresponding ^1H NMR spectrum, suggesting that this major product could be the desired magnesium hydride **38**. No signal attributed to the Mg-H was observed.

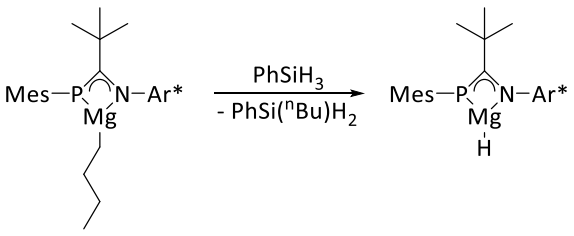

34 **38**

Scheme 86 *Reaction of **34** with $PhSiH_3$ to form a magnesium hydride*

Repeating this reaction on a preparative scale in toluene or hexane gives the same crude product distribution as the promising NMR scale reaction. Unfortunately, in both cases the only product isolated after work-up is protonated ligand **28**, suggesting the cautiously proposed magnesium hydride **38** is unstable.

4.2.6 Attempted Preparation of a Magnesium Halide Complex

Magnesium mono-halides offer a functionalised metal centre for further reactivity, for example the alkali-metal reduction of Mg-I complexes supported by bidentate nitrogen

ligand forms low-valent Mg(I) complexes, an example of which is shown in Scheme 87.[24,54–56]

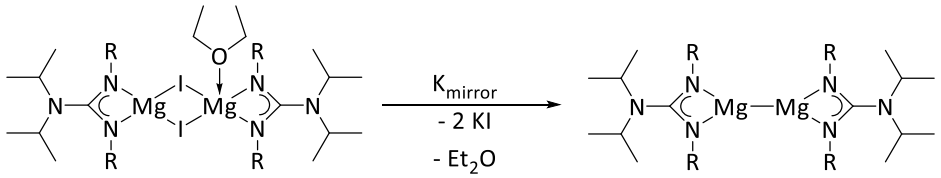

Scheme 87 *Reduction of a guanidate magnesium halide to a Mg-Mg bond. R=diisopropylphenyl*[55]

It was thought that the preparation of a phosphaamidinate magnesium iodide could therefore provide a path into low-valent magnesium chemistry. There are several different potential synthetic routes to magnesium halide complexes. The first pathway investigated was the reaction of the simple Grignard reagent MeMgI with phosphaamidines **20** or **28**, to eliminate methane. In both cases no reaction was observed by ^{1}H or ^{31}P NMR spectroscopy, even after heating in toluene to 80 °C for several days.

In aluminium chemistry, Al-I bonds can be formed by reaction of an alkyl-metal complex and elemental iodine,[57] something which, albeit rarer, can also be found in magnesium chemistry.[24] Following this, the n-butyl magnesium complexes **29** and **34** were each stirred with a stoichiometric amount of iodine. A reaction did occur, however in both cases a P-I bond has been formed. This was evidenced by a new signal in the ^{31}P NMR spectrum, shifted very downfield of the starting complexes at δ = 84.6 and 84.7 for **29** and **34** respectively. The multiplicity of these signals indicates coupling to iodine (*I* = 5/2). As these were not the intended products, they were not isolated or characterised further.

The final synthetic procedure attempted utilises lithium phosphaamidinate complex **43**, the formation and isolation of which will be further discussed in Section 5.1.3. $MgI_2(OEt_2)_2$ was added to a C_6D_6 solution of isolated lithium complex **43**, resulting in the clean formation of a new product by ^{31}P NMR spectroscopy at δ = -5.5. This signal is attributed to the formation of phosphaamidinate magnesium halide **39**. The ^{1}H NMR spectra of this NMR scale reaction is also consistent with a new phosphaamidinate environment.

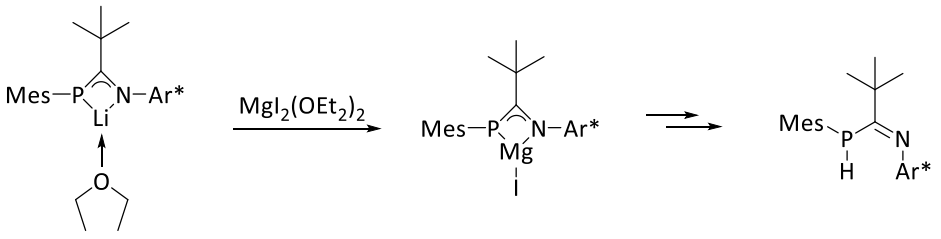

4 **39** **28**

Scheme 88 *Formation and degradation of a phosphaamidinate magnesium iodide complex*

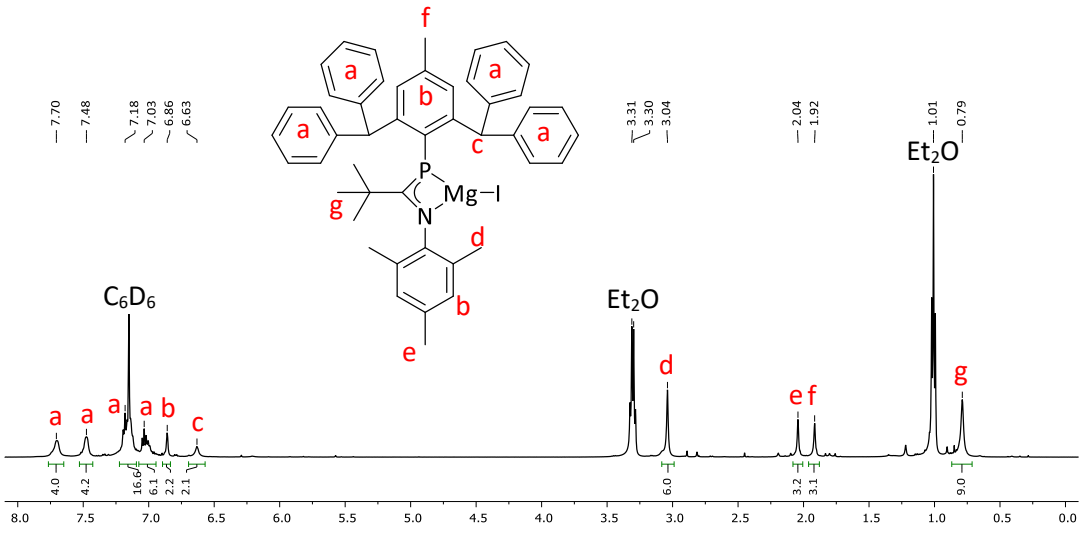

Figure 70 *^{1}H NMR (500 MHz, C_6D_6, 300K) of NMR scale reaction between lithiated phosphaamidine and $MgI_2(OEt_2)_2$, forming proposed magnesium iodide **39***

Repeating the reaction on a preparative scale appeared to hinder this reaction, with high amounts of protonated ligand **28** observed in crude material from reactions in toluene, presumably formed from degradation of **39**. Using C_6H_6 was slightly more successful, with which the product associated with the ^{31}P NMR signal at δ = -5.5 formed in 83% conversion by ^{31}P NMR spectroscopy. Purification of this product proved challenging, with no pure sample of **39** being isolated in this work.

4.3 Ring-Opening Polymerization Activity of Alkyl Magnesium Complexes

The work in this section was completed in collaboration with Dr Jennifer Garden at the University of Edinburgh.

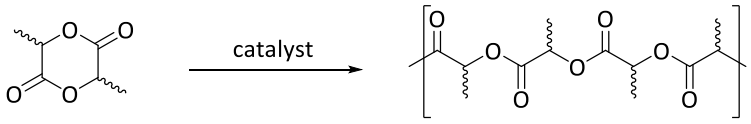

Rac-Lactide Polylactide

Figure 71 *Ring-opening polymerisation of rac-lactide to atactic polylactide*

Biodegradable plastics such as polylactide (PLA) are of huge industrial significance, as they retain most of the properties of conventional polymers whilst reducing the need for petrochemical-based starting materials. Along with the typical uses of plastics, PLA-based polymers have the advantage of being highly bio-compatible, and thus have unique applications such as in drug-delivery systems.[58] Hence, there is an ongoing effort to design catalysts based on the non-toxic metals of groups 2 and 12, with considerable focus on magnesium and zinc.[59]

Multidentate nitrogen ligand supported magnesium complexes typically have high activity for the ring-opening polymerisation (ROP) of lactide. Two commonly used ligand classes are scorpionate[60,61] and β-diketiminate ligands.[33,34,62] Modification of latter to include a phosphorus atom in the backbone resulted in the isolation of the solvated phosphinimino-amino magnesium complex in Scheme 89. This complex is capable of converting 92% of *rac*-lactide to PLA with 0.1 mol% catalyst in 60 minutes, and when cooled to 0°C gives heterotactic PLA (P_i = 0.02) with a catalyst loading of 1 mol%.[63]

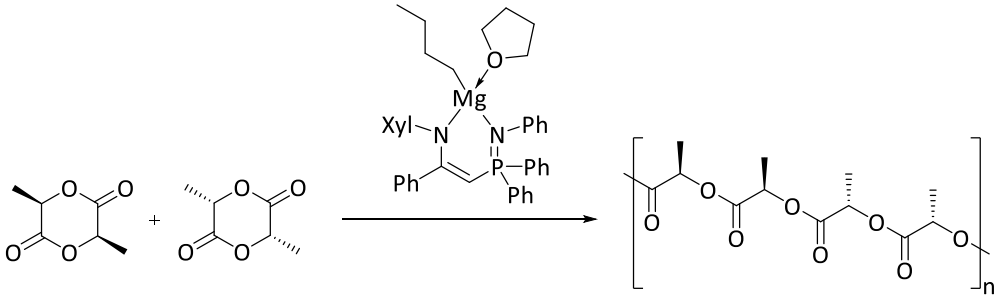

Scheme 89 *Preparation of heterotactic polylactide using an alkyl magnesium complex*[63]

4.3.1 Initial Activity Studies of LMgBu Complexes

Magnesium-based initiators can be used to initiate the ring-opening polymerisation (ROP) of lactide to form polylactide chains. A new polymer chain begins when an equivalent of lactide monomer coordinates to the metal centre and inserts into a reactive Mg-R bond,[64] where R is typically an alkoxide[34,61,62,65] or alkyl group.[33,63,66–69] $^{n}Bu_2Mg$ can initiate the formation of polylactide, but is not particularly active or controlled, taking 4 days to reach 87% conversion, with a relatively broad chain length dispersity (Đ) of 1.43.[66] A major advantage of using ligand supported systems is increased activity and narrower dispersity values, and some magnesium initiators featuring bidentate ligands are shown in Figure 72. To improve the molecular weight distribution, one catalytic equivalent of an alcohol can be added to the reaction as a co-initator.[62,69]

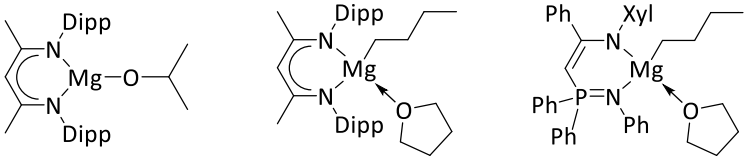

	Coates[62]	Chisholm[33]	Cui[63]
[Mg]	1 mol% + ^{i}PrOH	1 mol%	1 mol%
Conversion	97%/2 min	92%/1.5 min	92%/2 min
Đ	1.20-1.35	1.45	1.38-2.28

Figure 72 *Activity comparison of literature reported magnesium-based systems which can initiate ROP of lactide under analagous conditions to reactions carried out in this work (room temperature in dichloromethane). Dipp = 2,6-diisopropylphenyl. Xyl = 2,6-dimethylphenyl.*

It was hypothesised that n-butyl complexes **29**, **30** and **34** would be efficient single-site initiators for the ROP of lactide, as they possess reactive Mg-C bonds (sections 4.2.5 and 4.2.6). A common solvent for this type of reaction is tetrahydrofuran (THF),[63,66] however this solvent could interact with the magnesium complexes changing the dimeric structure of LMg^{n}Bu complexes **29** and **30**. Solvated THF adducts of butyl magnesium complexes are more common than their unsolvated congeners. The interaction of complexes **29**, **30** and **34** with of THF was investigated, with the expectation of forming four-coordinate magnesium centres of the type LMg(THF)^{n}Bu.

NMR scale reactions where a stoichiometric amount of THF was added to a C_6D_6 solution of complexes **29**, **30** and **34** revealed an unexpected mode of reactivity. With dimeric

complexes **29** and **30**, a downfield shift of the ^{31}P NMR signal was observed a few hours after addition of the THF, from δ = -42.0 to δ = -22.2 for mesityl derivative **29**, and from δ = -55.3 to δ = -34.1 for Tipp derivative **30**. In both cases the corresponding *bis*-ligated magnesium species has formed, presumably with $^{n}Bu_2Mg$ as a by-product.

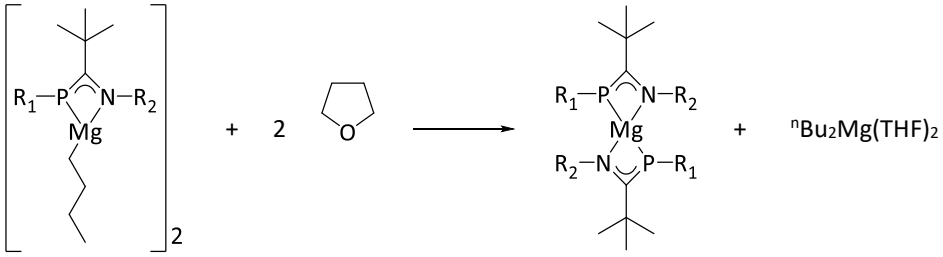

29 R$_1$=R$_2$=Mes **35**
30 R$_1$=Tipp, R$_2$= Mes **36**

Scheme 90 *Reaction of dimeric magnesium complexes with a stoichiometric amount of THF in C_6D_6*

This is a manifestation of the Schlenk equilibrium. Coordination of THF to the magnesium centre must occur, the product of which can undergo facile ligand redistribution resulting in the observed L_2Mg species. Presumably formation of $^{n}Bu_2Mg$ also occurs, to which the THF eventually coordinates.[70] Signals attributed to coordinated THF were observed at δ = 3.57 (t, $^{1}J_{H\text{-}H}$ = 6.5 Hz) and 1.40 (t, $^{1}J_{H\text{-}H}$ = 6.5 Hz, overlapped by another multiplet signal) for the reaction with **29**, slightly shifted from the residual values. As the signals in the ^{31}P NMR spectra are consistent with the signals observed in the base-free spectra of **35** and **36**, no THF coordination to these phosphaamidinate magnesium centres is suggested.

A similar Schlenk effect was seen in section 4.2.1, where targeted LMgBu type complexes were not formed when bulky Mes* ligand **22** or Dipp ligand **23** were reacted with $^{n}Bu_2Mg$. Instead, only the bis-ligated complexes **31** and **33** were isolated respectively.

Addition of THF to monomeric magnesium complex **34** produces an immediate colour change of the C_6D_6 solution from dark orange to pale yellow. The starting complex fully reacted as observed by ^{31}P NMR spectroscopy, and a new singlet signal is observed at δ = -69.8. The identity of this new signal is unknown, but given the high-field chemical shift, it is not the expected LMgBu.THF solvated adduct. A small amount of protonated ligand (approximately 16 % by ^{31}P NMR integration) is also present in this reaction mixture.

In amidinate chemistry, the formation of L_2Mg complexes is a catalyst deactivation pathway.[42] As even a stoichiometric amount of THF is enough to initiate the formation of L_2Mg complexes **35** and **36**, this is not the ideal solvent for the ring-opening polymerisation of lactide by **29**, **30** and **34**. Initially, toluene was chosen as an alternative solvent, however in test reactions it was found that the magnesium complexes were not sufficiently soluble to give an accurate representation of catalyst concentration. Dichloromethane has been used in ROP polymerisations mediated by magnesium complexes,[71] and does not interact with the magnesium complexes used here. Using this as the reaction solvent kept all material in solution during polymerisation.

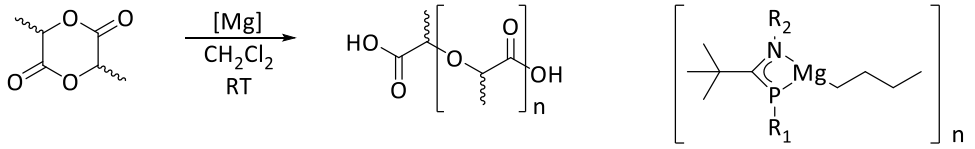

Rac-Lactide | Polylactide | R_1=R_2=Mes, n=2 **29**; R_1=Tipp, R_2=Mes, n=2 **30**; R_1=Mes, R_2=Ar*, n=1 **34**

Scheme 91 *Ring-opening polymerisation of racemic lactide to polylactic acid chains, initiated by phosphaamidinate magnesium complexes*

All three n-butyl magnesium complexes screened here showed high activity for the ring-opening polymerisation of *rac*-lactide in dichloromethane. Of note is the reaction initated by Tipp-substituted complex **30**, which at 1 mol% loading with the addition of MeOH gives 91.9% conversion in a controlled reaction with a dispersity (Đ) of 1.02. Table 7 summarises the results of these ROP reactions.

	Complex	Mol% [Mg]	Mol% MeOH	Time (min)	Conversion[a]	$M_n^{THEO\ b}$	M_n^{d}	$Đ^{d}$
1	R_1=R_2=Mes (**29**)	1.0	--	5	92.5	--	--	--
2		1.0	--	30	98.7	8250	5610	1.14
3		1.0	1.0	30	10.0	--	--	--
4		0.5	--	30	87.0	14550	5280	1.06
5		0.2	--	30	2.5	--	--	--
6	R_1=Tipp; R_2=Mes (**30**)	1.0	--	1	98.5	8236	11630	1.26
7		1.0	1.0	30	91.9	3800[c]	3840	1.02
8		0.5	--	5	98.8	16520	6800	1.21
9		0.2	--	30	3.5	--	--	--
10	R_1=Mes; R_2=Ar* (**34**)	1.0	--	2	99.1	8280	21570	1.37
11		1.0	1.0	2	98.4	4110[c]	9820	1.16
12		0.5	--	5	70.1	11720	24130	1.46
13		0.2	--	30	2.2	--	--	--

Table 7 *Conversions of DL-lactide to polylactic acid catalysed by butyl-magnesium complexes. General procedure: A stock solution of DL-Lactide (2 mL, 1.0 M in dichloromethane, 2.0 mmol) was added to the appropriate amount of complex in a J-Young tap ampoule using a syringe. After the time specified, the solution was exposed to air and poured over hexane (ca. 5 mL) and the volatiles removed.* [a]*Determined by* ^{1}*H NMR integration of methine region in* $CDCl_3$. [b]$M_n^{THEO} = 0.58 \times (\%conversion \times 144.13)/[Mg]$ *assumes 1 chain per metal centre. GPC referenced to styrene.* [c]$M_n^{THEO} = 0.58 \times (\%conversion \times 144.13)/([Mg] \times 2)$ *assumes two chains per metal centre due to chain transfer by MeOH. GPC referenced to styrene.* [d]*Determined by GPC as a solution in THF.*

At 1 mol% catalyst loading, the activity appears to be comparable across all three complexes, with near quantitative conversion after only a few minutes. This very high activity is highlighted in Figure 73, which monitors the progress of the reaction initiated by 1 mol% of Tipp-substituted complex **30**. This reaction had reached 97.2% completion in just 30 seconds, and plateaus at 98.5% conversion after 60 seconds.

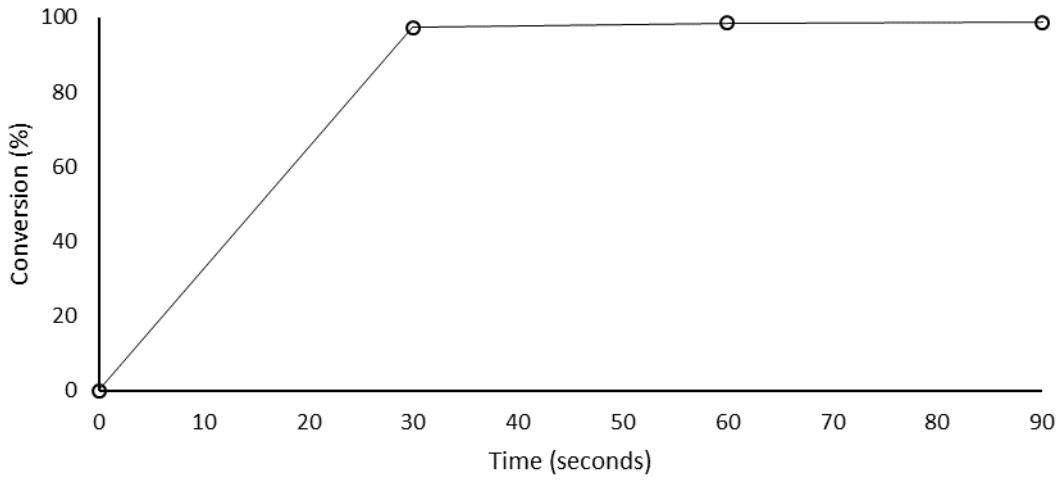

Figure 73 *Conversion to polylactide initiated by 1 mol% Tipp-substituted complex* ***30****. Percentage calculated by relative integration of product and starting material signals in the* ^{1}*H NMR spectrum, assuming 0% conversion at* t_0

Magnesium-based initiators typically display very high catalytic activities towards the ROP of lactide, and all three complexes used here are comparable with notable literature reported systems (Figure 72). For example, Coates' β-diketiminate supported complex at 1 mol% concentration in the presence of 2-propanol converts 97% of rac-lactide to polylactide in 2 minutes.[62]

The dispersity value (Đ) is an indicator of the uniformity of the polymer chain length, where the ideal value of 1.00 indicates that each polymer chain contains the same number of monomer units and hence indicates a very controlled reaction. There is a significant variance in Đ across the magnesium initiators in Table 7 at 1 mol%. Increasing the size of the supporting phosphaamidine system from mesityl-substituted **29** to Ar*-substituted **34** also increases Đ from 1.14 to 1.37 (Table 7, entries 2, 6 and 10). The lower end of this range represents very good values for a polymerisation initiated by a magnesium-based system, which are typically in the range of 1.20-2.00 (Figure 72).

Addition of one catalytic equivalent of anhydrous methanol to the ROP reactions slows the rate the reaction in all three cases (entries 2, 6 and 10). Initiation by the smallest dimeric complex **29** is most stunted by the addition of the alcohol, with conversion peaking at 10.0% after 30 minutes. High conversion was observed with bulkier complexes **30** and **34**. For the former complex, good agreement between the M_n^{THEO} and M_n values complement an excellent Đ value of 1.02, indicating a well-controlled polymerisation process.

At 1 mol% concentration, the activity of the three n-butyl complexes **29**, **30** and **34** is comparable. When lowering the concentration of the magnesium species to 0.5 mol% catalyst loading, slight differences between the complexes are observed. At this concentration, a slight decrease in activity is observed for the smallest mesityl complex **29** and the bulkiest, monomeric complex **34**. The latter complex seems to still react rapidly, but a lower final conversion perhaps indicates some other hindrance quenching the activity. Tipp complex **30** remains very active at 0.5 mol%, with 98.8 % conversion achieved within 5 minutes. The Đ values are comparable with the higher catalyst loading (1 mol%) value, which is expected as lowering the concentration of the initiator should not significantly affect the control of the polymerisation.

Monitoring the progress of the polymerisation initiated by 0.5 mol% of Tipp-substituted complex **30** over time gives some insights into the reaction kinetics. A plot of $Ln[M_0/M_t]$ against time results in a linear relationship (Figure 74, $R^2 = 0.996$), giving an observed rate constant (k_{obs}) of 1.4×10^{-3} s^{-1}. This is almost double the value of k_{obs} determined by Cui for the phosphinimino-amino complex (Figure 72) under similar reaction conditions ($k_{obs} = 7.06 \times 10^{-3}$ s^{-1} at 0.5 mol%). More experiments are required to completely evaluate the kinetics of the polymerisations in this work.

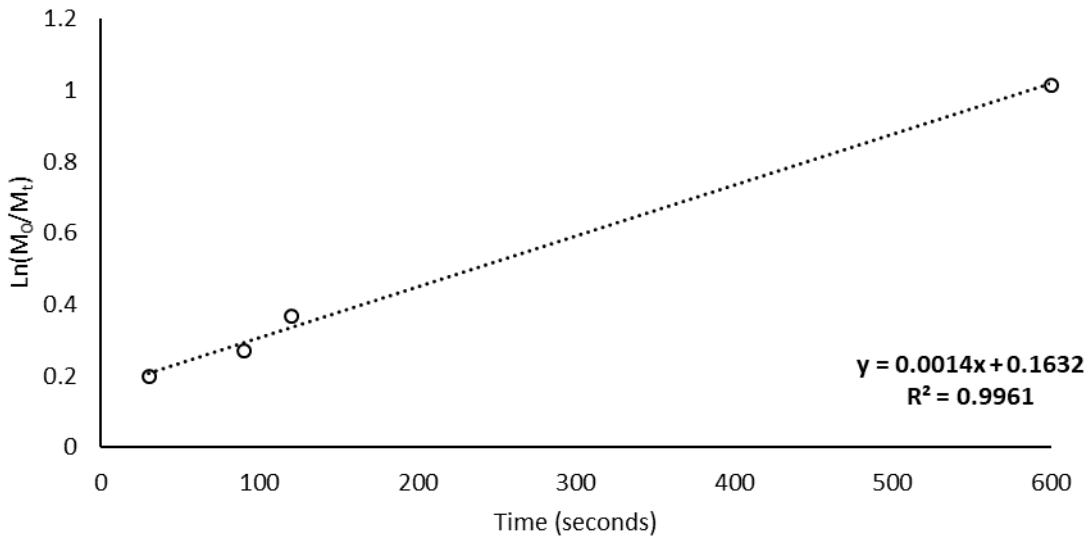

Figure 74 *Plot showing first order dependence of lactide polymerisation on initiation by 0.5 mol%* ***30****.* M_0 *= concentration of rac-lactide at* t_0*,* M_t *= concentration of rac-lactide at time t.*

A significant drop in activity is seen in with all three complexes when moving to a 0.2 mol% catalyst loading (entries 5, 9 and 13). This is attributed to the catalyst being extremely air and moisture sensitive, and thus at such a low catalyst concentration the magnesium complexes reaction with trace amounts of water in the solvent becomes significant, resulting in catalyst deactivation.

4.3.2 A Slight Isotactic Preference

As lactide has two stereocentres, it exists as three diastereomers (*R,R*, *S,S* and meso). The mechanism of polymerisation can affect the order of the stereocentres (tacticity) of the resulting chain.[72] The identified overall trend is that magnesium complexes tend to display higher activity than analogous zinc complexes, but that the latter tends to exhibit more stereocontrol.[59,72] The tacticity of a polylactide chain can be determined using $^{1}H\{^{1}H\}$ NMR spectroscopy.[73,74] The absolute chemical shift of the methine signals is determined by a the neighbouring stereocentres, for which there are multiple possibilities. For the purpose of this work, a series of four centres (tetrad) will be examined, giving rise to five different combinations (Figure 75: iii, iis, sis, isi, and ssi). Each tetrad has a literature defined ^{1}H NMR chemical shift in the $^{1}H\{^{1}H\}$ NMR spectrum.[73]

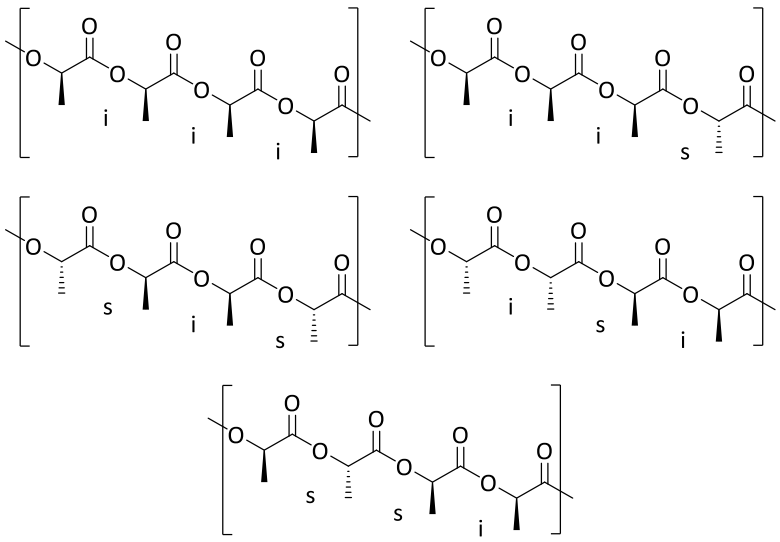

Figure 75 *Microstructures of PLA and tetrad nomenclature. i = iso (or meso), s = syndio (or racemic).*

The probability of a methyl group having two identical adjacent stereocentres (P_i) is calculated as the average occurrence of each tetrad.[75] A value of $P_i = 1.0$ would indicate an entirely isotactic polymer chain, where $P_i = 0.0$ would mean a heterotactic chain. An intermediate value $P_i = 0.5$ results from an atactic polymer, where the initiator is not selective for either lactide enantiomer.

Figure 76 shows a methine region comparison between a standard ^{1}H NMR spectrum of polylactide obtained using 1 mol% of Tipp complex **30** and a ^{1}H pureshift spectrum of the

same solution. The tetrad peaks in the latter spectrum were labelled according to literature reported chemical shifts.[74]

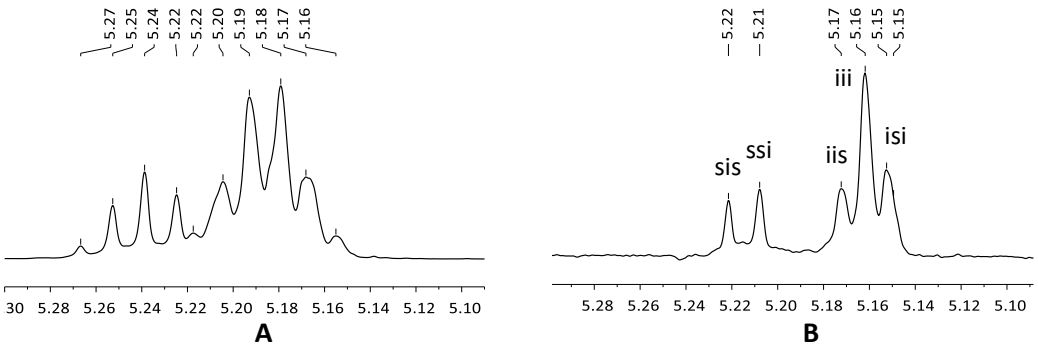

Figure 76 *^{1}H proton coupled (**A**, $CDCl_3$, 500 MHz, 300 K) and pureshift ^{1}H (**B,** $CDCl_3$, 500 MHz, 300 K) NMR spectra of PLA formed with 1 mol% Tipp complex **30**. Only the methine region is shown.*

The calculated P_i is compared across samples of polylactide prepared with 1 mol% of initiators **29**, **30** and **34** in Table 8. Bulkier complexes **30** and **34** show a small isotactic preference, with the P_i values hovering above 0.5. The most selective is Tipp complex **30** with a P_i value of 0.55, which is comparable to a magnesium initiator described as possessing a slight isotactic preference.[69] Addition of methanol as a co-initiator had little influence on the stereo-selectivity of the polymerisation.

	Complex	Mol% [Mg]	Mol% MeOH	P_i
1	R_1=R_2=Mes	1.0	--	0.48
2	R_1=Tipp; R_2=Mes	1.0	--	0.55
3		1.0	1.0	0.51
4	R_1=Mes; R_2=Ar*	1.0	--	0.52
5		1.0	1.0	0.53

Table 8 *Probability of isotactic PLA, calculated according to the method described by Coates et al.*[75]

Lowering the temperature of the polymerisation reaction has been shown to give some control of resulting polylactide tacticity initated magnesium complexes,[69] and this should be investigated with these initiators in the future. It has also been shown that carrying out the ROP reaction in dichloromethane produces more atatic polylactide in the case of LMgBu complexes, and more control is seen using THF as the reaction solvent.[33,76]

4.3.3 Initiation by an n-Butyl Group

Matrix-assisted laser desorption/ionization (MALDI) mass spectrometry was used to determine the end groups of the polylactide chain, and hence which groups initiated and terminated the polymerisation reaction. Spectra were collected of polylactide synthesised using dimeric complexes **29** and **30**, an example of which is shown in Figure 77.

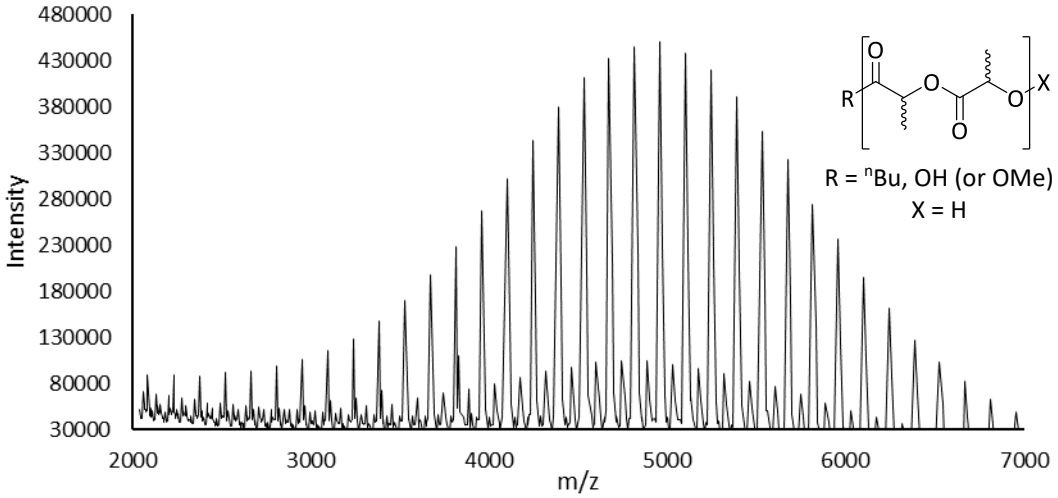

Figure 77 *The MALDI-TOF spectrum of polylactide formed using 0.5 mol% mesityl-substituted* ***29****. Matrix = dithranol, additive = KI, solvent = THF*

In all cases more than one series of signals were identified, indicating multiple initiation events may be occurring. This fits well with the previous observation (section 4.3.1) that the calculated molecular weights of the polymer chains are significantly greater than the experimentally observed values. The presence of chain transfer agents, such as methanol, can initiate a second polymer chain with the chain transfer agent as the terminus.

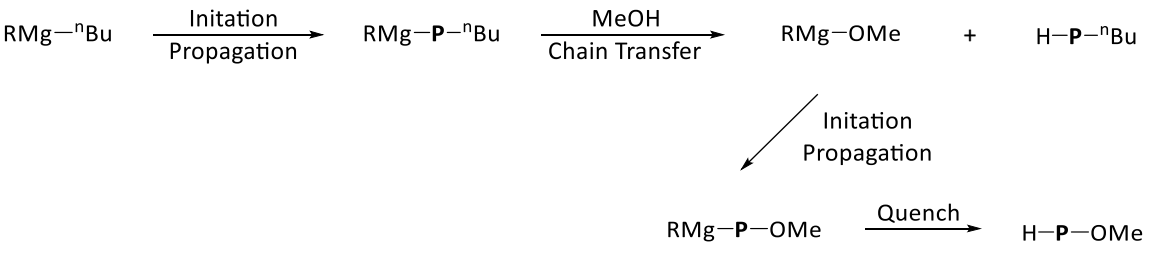

Scheme 92 *Chain transfer process mediated by MeOH. R = spectator ligand. P = polymer chain*[77]

One series consistent in the MALDI-TOF spectra of all the polylactide data collected here corresponded to chains initiated by an n-butyl group and terminated by a proton, indicating that complexes **29** and **30** had indeed initiated polymer formation in the expected fashion. Chains were also identified with similar end-groups, but possessing half a monomer unit. This is the product of transesterification processes and is commonly observed in the ring-opening polymerisation of lactide.

A second series seen in all spectra are chains initiated by an -OH functionality, with a proton at the terminating the chain which indicates possible interaction with trace amounts of residual water during the reaction, possibly acting as a chain transfer agent. This series also shows evidence of di-ester cleavage through transesterification. Evidence of chain transfer from the addition of one catalytic equivalent of MeOH was seen in the MALDI spectrum of polylactide formed by 1 mol% Tipp-substituted complex **30** and MeOH as chains initiated by MeO and terminated by H groups were observed.

4.3.5 Observation of the active species

To try to observe the active species, NMR scale reactions between mesityl-substituted complex **29** and lactide in C_6D_6 were carried out. Addition of two equivalents of *rac*-lactide to **29** forms a new phosphorus containing product by ^{31}P NMR spectroscopy with a new resonance observed at δ = 13.9. This signal is extremely broad, perhaps hinting at some sort of fluxional structure. This new signal may arise from the active species in the ROP, from the coordination and insertion of the di-ester into the Mg-C bond.

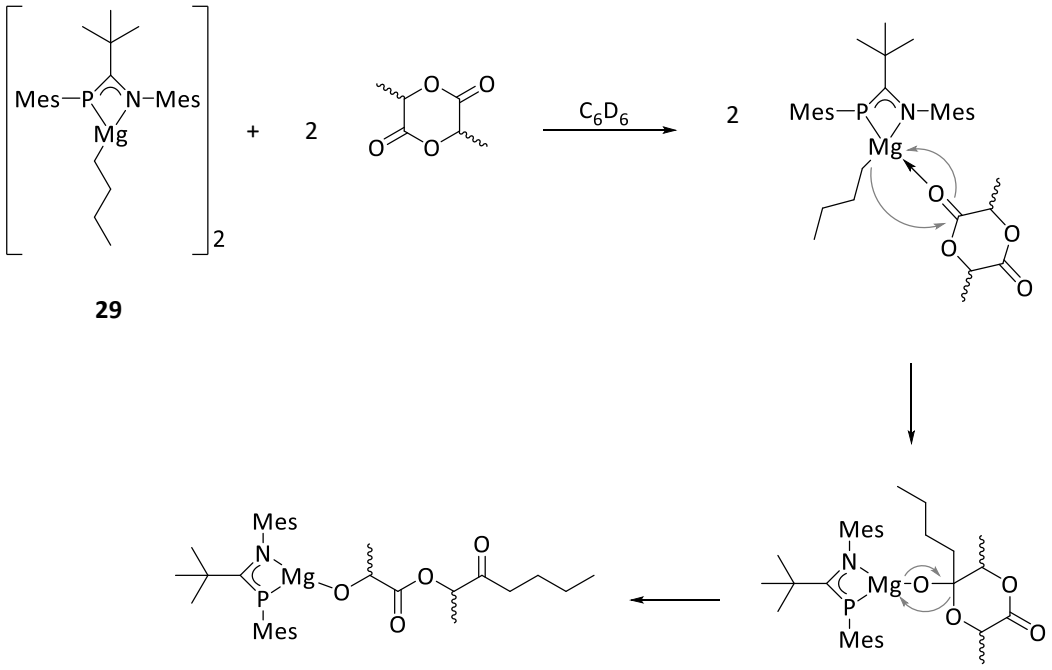

29

Scheme 93 *Reaction of dimeric mesityl complex **29** with 2 equivalents of racemic lactide*

Along with this new signal, a substantial amount of protonated ligand **20** is formed in this reaction (approximately 37% by ^{31}P NMR integration) indicating cleavage of the phosphaamidine from the metal centre. This is a possible catalyst deactivation pathway.

The ^{1}H NMR of this mixture is complex, however a signal was observed at δ = 0.85 with a characteristic AA'XX' shape for a CH_2 group on an ^{n}Bu chain (section 4.2.1, Figure 59), and is slightly downfield of the corresponding signal in the starting dimeric complex, at δ = 0.50. A new quartet signal at δ = 3.72 ($^{1}J_{H\text{-}H}$ = 6.7 Hz) is attributed to a new lactide environment,

significantly upfield of the starting lactide signal, δ = 5.06 ($^{1}J_{H\text{-}H}$ = 6.7 Hz), and that of polylactide δ = 5.26 - 5.15 (m).

Addition of 10 equivalents of lactide per magnesium centre in **29** results in substantial conversion to polylactide by ^{1}H NMR spectroscopy (an accurate conversion is not possible due to overlapping signals). ^{31}P NMR spectroscopy reveals the same broad signal at δ = 13.9 ($\nu_{1/2}$ ≈ 103 Hz), as well as some ligand protonation to cleave the phosphaamidine (25% by ^{31}P NMR integration). Addition of 10 further equivalents of racemic lactide per magnesium centre to the same solution produces further polylactide, but the phosphorus containing product ratio is not disturbed by ^{31}P NMR spectroscopy. Unexpectedly, the ^{31}P NMR signal at δ = 13.9 becomes sharper; its linewidth has decreased from $\nu_{1/2}$ ≈ 103 Hz to $\nu_{1/2}$ ≈ 75 Hz.

These observations are allude to lactide coordination, suggesting that the standard coordination and insertion mechanism associated with the ROP of lactide is likely occurring, which is depicted in Scheme 93.[64,77]

4.4 Summary

Five new phosphaamidine ligands **20**-**23** and **28** have been prepared, with substituents ranging in size from mesityl to a super bulky Ar* group. Even though each phosphaamidine has eight possible isomers, most are isolated with a single geometry which is substituent dependant. The exception to this is Mes*-substituted **22**, which shows three isomers by ^{31}P NMR spectroscopy. Density functional theory calculations aided the identification of these as E-syn P=C, Z-anti P=C and Z-syn N=C as depicted in Figure 78.

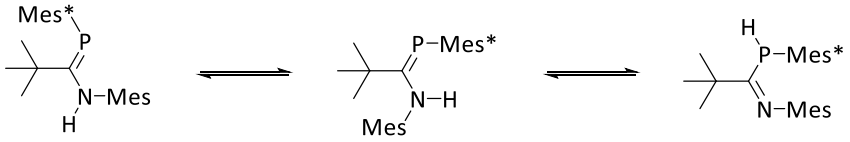

E-syn P=C	Z-anti P=C	Z-syn N=C
22a	**22b**	**22c**
^{31}P δ 98.3	^{31}P δ 80.2	^{31}P δ -53.6
$^{3}J_{P-H}$ = 18 Hz		$^{1}J_{P-H}$ = 253 Hz

Figure 78 *Isomers of phosphaamidine **22** correlated to ^{31}P NMR chemical shift*

Addition of one equivalent of $^{n}Bu_2Mg$ to these phosphaamidines furnishes dimeric heteroleptic complexes of the type LMgBu (L = phosphaamidine) **29**, **30** and **32**, the latter of which is not isolated.

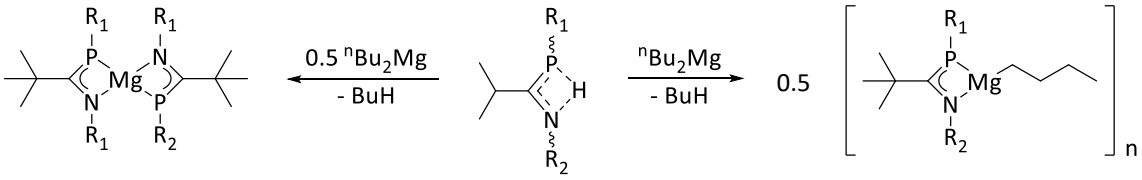

35	$R_1 = R_2$ = Mes	**20**	**29** (n=2)
36	R_1= Tipp; R_2= Mes	**21**	**30** (n=2)
31	R_1= Mes*; R_2= Mes	**22**	n/a
33	R_1= Mes; R_2= Dipp	**23**	[**32**] (n=2)
n/a	R_1= Mes, R_2= Ar*	**28**	**15** (n=1)

Scheme 94 *Reactivity of phosphaamidines **20**-**23** with $^{n}Bu_2Mg$*

The corresponding homoleptic complexes **31**, **33**, **35** and **36** were prepared by reaction of the phosphaamidine with half an equivalent of $^{n}Bu_2Mg$. X-Ray crystallography of Mes* substituted complex **31** shows a tetrahedral geometry around the magnesium centre. It is noted that only a single isomeric product is obtained from the reaction of the mixture of **22a, 22b** and **22c**.

Addition of $^{n}Bu_2Mg$ to the bulkiest ligand in this series **28** results in monomeric heteroleptic complex **34**. The molecularity of **34** was hinted at in the corresponding ^{31}P NMR spectrum, and the three-coordinate magnesium centre confirmed by X-Ray crystallography experiments. Double substitution of n-butyl groups from $^{n}Bu_2Mg$ to form an L_2Mg complex is not possible using this bulky ligand system; only the heteroleptic complex is observed.

Reaction of n-butyl complex **34** with phenylsilane produces $PhSi(Bu)H_2$, presumably by displacement of the ^{n}Bu group at the metal centre by a hydride ligand forming the tentatively proposed magnesium hydride **38**, which can be observed by ^{31}P NMR spectroscopy δ = -12.6. Lithiation of the phosphaamidine **28** and subsequent reaction with MgI_2 forms the proposed magnesium halide complex **39**. Unfortunately, both functional magnesium complexes **38** and **39** are unisolable.

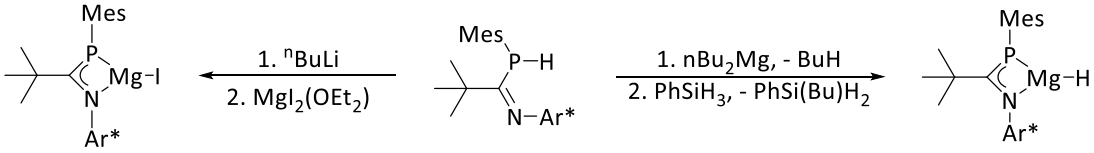

[**39**] **28** [**38**]

Scheme 95 *Reactivity of bulky phosphaamidine* ***28***

The n-butyl group of complexes **29**, **30** and **34** can rapidly initiate the ring-opening polymerisation of *rac*-lactide, with Tipp-substituted complex **30** showing a slight isotactic preference (P_i = 0.55) at room temperature. All three complexes show high catalytic activity and relatively good control, evidenced by low polydispersity values (Đ = 1.02-1.46).

4.5 References

1 K. Issleib, H. Schmidt and H. Meyer, *J. Organomet. Chem.*, 1978, **160**, 47–57.
2 T. van Dijk, S. Burck, M. K. Rong, A. J. Rosenthal, M. Nieger, J. C. Slootweg and K. Lammertsma, *Angew. Chem Int. Ed.*, 2014, **53**, 9068–9071.
3 R. T. Boeré, M. L. Cole, P. C. Junk, J. D. Masuda and G. Wolmershäuser, *Chem. Commun.*, 2004, 2564–2565.
4 X. Li, H. Song and C. Cui, *Dalton Trans.*, 2009, 9728–9730.
5 K. Paasch, M. Nieger and E. Niecke, *Angew. Chem. Int. Ed.*, 1995, **34**, 2369–2371.
6 J. D. Masuda and R. T. Boeré, *Dalton Trans.*, 2016, **45**, 2102–2115.
7 M. Westerhausen, M. H. Digeser and W. Schwarz, *Inorg. Chem.*, 1997, **36**, 521–527.
8 J. D. Masuda, Master Thesis, University of Lethbridge, 2000.
9 L. M. Amrei, PhD Thesis, University of Lethbridge, 2015.
10 Y. Takeda, T. Nishida and S. Minakata, *Chem. Eur. J.*, 2014, **20**, 10266–10270.
11 T. van Dijk, M. K. Rong, J. E. Borger, M. Nieger, J. C. Slootweg and K. Lammertsma, *Organometallics*, 2016, **35**, 827–835.
12 J. Moebus, Q. Bonnin, K. Ueda, R. Froehlich, K. Itami, G. Kehr and G. Erker, *Angew. Chem. Int. Ed.*, 2012, **62**, 1954–1957.
13 Y. van den Winkel, H. M. M. Bastiaans and F. Bickelhaupt, *J. Organomet. Chem.*, 1991, **405**, 183–194.
14 M. Karplus, *J. Am. Chem. Soc.*, 1962, **85**, 2870–2871.
15 M. J. Minch, *Concepts Magn. Reson.*, 1994, **6**, 41–56.
16 D. G. Gorenstein, *Phosphorus-31NMR: Principles and Applications*, Academic Press Inc., 1984.
17 W. H. Hersh, S. T. Lam, D. J. Moskovic and A. J. Panagiotakis, *J. Org. Chem.*, 2012, **77**, 4968–4979.
18 S. E. Wheeler, *Acc. Chem. Res.*, 2013, **46**, 1029–1038.
19 M. Alonso, T. Woller, F. J. Martín-Martínez, J. Contreras-García, P. Geerlings and F. de Proft, *Chem. Eur. J.*, 2014, 4931–4941.
20 M. Swart and T. Van Der Wijst, *J. Mol. Model.*, 2007, **13**, 1245–1257.
21 C. R. Martinez and B. L. Iverson, *Chem. Sci.*, 2012, **3**, 2191–2201.
22 A. Chartoire, C. Claver, M. Corpet, J. Krinsky, J. Mayen, D. Nelson, S. P. Nolan, I. Peñafiel, R. Woodward and R. E. Meadows, *Org. Process Res. Dev.*, 2016, **20**, 551–557.
23 M. Arrowsmith, B. Maitland, G. Kociok-Köhn, A. Stasch, C. Jones and M. S. Hill, *Inorg. Chem.*, 2014, **53**, 10543–10552.
24 A. J. Boutland, D. Dange, A. Stasch, L. Maron and C. Jones, *Angew. Chem. Int. Ed.*, 2016, **55**, 9239–43.
25 E. W. Y. Wong, A. D. Dange, A. L. Fohlmeister, T. J. Hadlington and C. Jones, *Aust. J. Chem*, 2013, 1144–1154.
26 W. Uhlig and A. Tzschach, *Z. anorg. allg. Chem.*, 1989, **576**, 281–283.
27 G. Becker, O. Mundt, M. Roessler and E. Schneider, *Z. anorg. allg. Chem.*, 1978, **53**, 42–52.
28 R. T. Boeré and J. D. Masuda, *Can. J. Chem*, 2002, **80**, 1607–1617.
29 H. Kawanami, K. Toyota and M. Yoshifuji, *J. Organometalic Chem.*, 1997, **535**, 1–5.
30 S. J. Bonyhady, C. Jones, S. Nembenna, A. Stasch, A. J. Edwards and G. J. McIntyre, *Chem. Eur. J.*, 2010, **16**, 938–955.
31 M. S. Hill, D. J. Liptrot, C. Weetman and M. S. Hill, *Chem. Soc. Rev.*, 2016, **45**, 972–988.

32 A. P. Dove, V. C. Gibson, P. Hormnirun, E. L. Marshall, J. A. Segal, A. J. P. White and D. J. Williams, *Dalton Trans.*, 2003, 3088–3097.
33 M. H. Chisholm, K. Choojun, J. C. Gallucci and P. M. Wambua, *Chem. Sci.*, 2012, 3445–3457.
34 A. P. Dove, V. C. Gibson, E. L. Marshall, A. J. P. White and D. J. Williams, *Chem. Commun.*, 2002, 1208–1209.
35 G. J. Moxey, F. Ortu, L. G. Sidley, H. N. Strandberg, A. J. Blake, W. Lewis and D. L. Kays, *Dalton Trans.*, 2014, **43**, 4838–4846.
36 L. Falivene, A. Poater, A. Petta, L. Serra, R. Oliva, V. Scarano and L. Cavallo, *Organometallics*, 2016, **35**, 2286–2293.
37 A. Poater, B. Cosenza, A. Correa, S. Giudice, F. Ragone, V. Scarano and L. Cavallo, *Eur. J. Inorg. Chem.*, 2009, 1759–1766.
38 C. A. Tolman, *Chem. Rev.*, 1977, **77**, 313–348.
39 H. Clavier and S. P. Nolan, *Chem Commun.*, 2010, 841–861.
40 A. Poater and L. Cavallo, *Dalton Trans.*, 2009, 8879–8883.
41 A. K. Maity, S. Fortier, L. Griego and A. J. Metta-Magana, *Inorg. Chem*, 2014, **53**, 8155–8164.
42 R. J. Schwamm, B. M. Day, E. Mansfield, Natalie, W. Knowelden, P. B. Hitchcock and M. P. Coles, *Dalton Trans.*, 2014, **43**, 14302–14314.
43 H. M. El-Kaderi, A. Xia, M. J. Heeg and C. H. Winter, *Organometallics*, 2004, 3488–3495.
44 C. F. Caro, P. B. Hitchcock and M. F. Lappert, *Chem. Commun.*, 1999, 1433–1434.
45 R. T. Boeré, M. L. Cole and P. C. Junk, *New. J. Chem.*, 2005, **29**, 128–134.
46 M. Arrowsmith, M. S. Hill, T. Hadlington, G. Kociok-Köhn and C. Weetman, *Organometallics*, 2011, **30**, 5556–5559.
47 M. Arrowsmith, T. J. Hadlington, M. S. Hill and G. Kociok-Köhn, *Chem. Commun.*, 2012, **48**, 4567–4569.
48 M. Arrowsmith, M. S. Hill and G. Kociok-Köhn, *Chem. Eur. J.*, 2013, **19**, 2776–2783.
49 C. Weetman, M. D. Anker, M. Arrowsmith, M. S. Hill, G. Kociok-Köhn, D. J. Liptrot and M. F. Mahon, *Chem. Sci.*, 2016, **7**, 628–641.
50 M. S. Hill, D. J. Macdougall and M. F. Mahon, *Dalton Trans.*, 2010, **39**, 11129–11131.
51 M. D. Anker, M. S. Hill, J. P. Lowe and M. F. Mahon, *Angew. Chem. Int Ed.*, 2015, **54**, 10009–10011.
52 M. D. Anker, C. E. Kefalidis, Y. Yang, J. Fang, M. S. Hill, M. F. Mahon and L. Maron, *J. Am. Chem. Soc.*, 2017, **139**, 10036–10054.
53 Y. Yang, M. D. Anker, J. Fang, M. F. Mahon, L. Maron, C. Weetman and M. S. Hill, *Chem. Sci.*, 2017, **8**, 3529–3537.
54 S. P. Green, C. Jones and A. Stasch, *Angew. Chem. Int. Ed.*, 2008, **47**, 9079–9083.
55 S. P. Green, C. Jones and A. Stasch, *Science*, 2007, **318**, 1754–1757.
56 A. Stasch, *Angew. Chem. Int. Ed.*, 2014, **53**, 10200–10203.
57 C. Cui, H. W. Roesky, H. Schmidt, M. Noltemeyer, H. Hao and F. Cimpoesu, *Angew. Chem. Int. Ed.*, 2000, **39**, 4274–4276.
58 Y. Ikada and H. Tsuji, *Macromol. Rapid Commun.*, 2000, **21**, 117–132.
59 C. A. Wheaton, P. G. Hayes and B. J. Ireland, *Dalt. Trans.*, 2009, 4832–4846.
60 A. Garcés, L. F. Sánchez-Barba, C. Alonso-Moreno, M. Fajardo, J. Fernández-Baeza, A. Otero, A. Lara-Sánchez, I. López-Solera and A. M. Rodríguez, *Inorg. Chem.*, 2010, **49**, 2859–2871.
61 M. Honrado, A. Otero, J. Ferna, L. F. Sa, U. Rey and J. Carlos, *Organometallics*, 2015,

34, 3196–3208.
62 B. M. Chamberlain, M. Cheng, D. R. Moore, T. M. Ovitt, E. B. Lobkovsky and G. W. Coates, *J. Am. Chem. Soc*, 2001, **123**, 3229–3238.
63 H. Xie, Z. Mou, B. Liu, P. Li, W. Rong, S. Li and D. Cui, *Organometallics*, 2014, **33**, 722–730.
64 F. E. Kohn, J. G. Van Ommen and J. Feijen, *Eur. Polym. J.*, 1983, **19**, 1081–1088.
65 M. H. Chisholm, N. W. Eilerts, J. C. Huffman, S. S. Iyer, M. Pacold and K. Phomphrai, *J. Am. Chem. Soc*, 2000, **122**, 11845–11854.
66 H. R. Kricheldorf and S.-R. Lee, *Polymer*, 1995, **36**, 2995–3003.
67 T. Chivers, C. Fedorchuk and M. Parvez, *Organometallics*, 2005, 580–586.
68 C. N. Ayala, M. H. Chisholm, J. C. Gallucci and C. Krempner, *Dalton Trans.*, 2009, 9237–9245.
69 F. Drouin, T. J. J. Whitehorne and F. Schaper, *Dalton Trans.*, 2011, **40**, 1396–1400.
70 S. C. Cole, M. P. Coles and P. B. Hitchcock, *Organometallics*, 2004, **23**, 5159–5168.
71 A. P. Dove, V. C. Gibson, E. L. Marshall, A. J. P. White and D. J. Williams, *Dalton Trans.*, 2004, 570–578.
72 M. J. Stanford and A. P. Dove, *Chem. Soc. Rev.*, 2010, 486–494.
73 M. H. Chisholm, S. S. Iyer, M. E. Matison, D. G. McCollum and M. Pagel, *Chem. Commun.*, 1997, **11**, 1999–2000.
74 M. T. Zell, B. E. Padden, A. J. Paterick, K. A. M. Thakur, R. T. Kean, M. A. Hillmyer and E. J. Munson, *Macromolecules*, 2002, 7700–7707.
75 M. Cheng, A. B. Attygalle, E. B. Lobkovsky and G. W. Coates, *J. Am. Chem. Soc.*, 1999, **121**, 11583–11584.
76 M. H. Chisholm, J. Gallucci and K. Phomphrai, *Inorg. Chem.*, 2002, **41**, 2785–2794.
77 O. Dechy-Cabaret, B. Martin-Vaca and D. Bourissou, *Chem. Rev.*, 2004, **104**, 6147–6176.

Chapter 5:

Phosphaamidine Complexes Featuring Reactive Lithium and Aluminium Centres

5. Phosphaamidine Complexes Featuring Reactive Lithium and Aluminium Centres

5.1 Preparation of Lithium Complexes

Heteroleptic magnesium complexes can be used to transfer ligands to another metal centre (the classical example is Grignard reagents), but it is more common to see lithium complexes used in these sorts of transformations across organometallic and main-group chemistry, through salt methasis reactions. Therefore, lithiated phosphaamidinates are potentially very useful reagents.

The deprotonation of various phosphaamidines has been reported using the common organolithium reagent ^{n}BuLi.[1,2] Whilst some retain their geometry from their protonated form,[1] Boeré found that the lithiation of a Dipp-substituted phosphaamidine results in a single product with a P-C-N core geometry different to the starting material.[2] The isomer from which the resulting lithium complex is formally derived is present as a minor component of the isolated phosphaamidine in solution (ca. 10% by ^{31}P NMR integration).

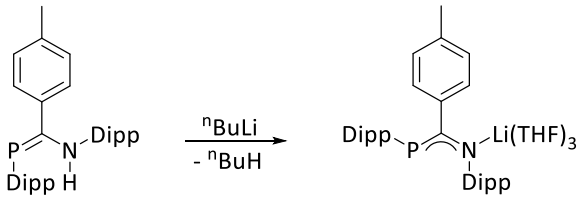

Z-anti P=C *E-syn*

Scheme 96 *Deprotonation of a phosphaamidine can change its geometry*

A lithiated phosphaamidinate complex has been used to transfer a phosphaamidinate to the transition metals rhodium and gold.[1] Along with demonstrating the ligand transfer capability of this class of compounds, these reactions highlight two contrasting bonding modes (chelating versus P-coordination) that are available to phosphaamidinates in response to different metal centres.

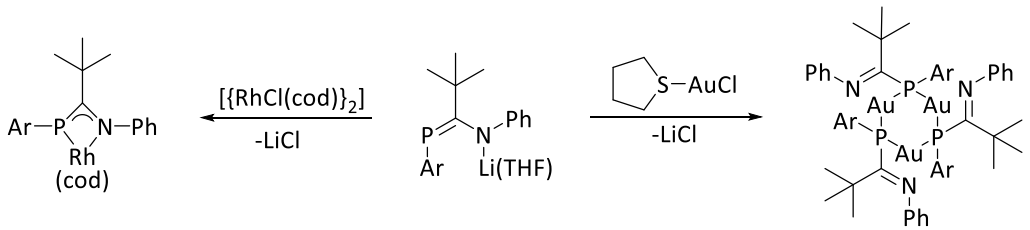

Scheme 97 *Preparation of phosphaamidinate transition metal complexes using a lithiated species. Ar = 2,4,6-tritertbutylphenyl*

5.1.1 Generation of Lithium Phosphaamidinate Complexes in Situ

In order to expand the scope of metallic complexes available to the phosphaamidines prepared in this work, the formation of possible ligand transfer reagents was investigated. The low temperature addition of one equivalent of n-butyl lithium to a THF solution of phosphaamidine **20** results in an immediate colour change from colourless to bright yellow, signifying formation of lithium complex **40**. *In situ* ^{31}P NMR spectroscopy of this solution shows a new broad signal at δ = -33.5 as the major component of the mixture. The value of this chemical shift is similar to that of Boere's lithium phosphaamidinate DippPC(Tol)N(Dipp)Li.THF (δ = -22.9, Dipp = 2,6-diisopropylphenyl, Tol = *p*-tolyl) which features delocalisation across the P-C-N unit.[2]

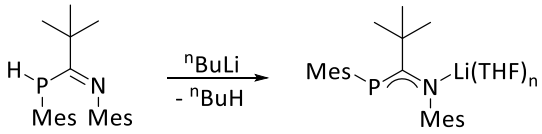

20 **40**

Scheme 98 *Deprotonation and lithiation of **20** to form lithium phosphaamidinate complex **40***

Under analogous conditions to the formation of **40**, deprotonation and lithiation of Dipp-substituted phosphaamidine **23** gives a similar colour change from colourless to bright yellow signifying formation of lithium complex **41**. Whilst the chemical shift of **41** is comparable to smaller lithium phosphaamidinate **40**, the observed multiplicity in the ^{31}P and ^{7}Li NMR spectra indicate a product with a different bonding situation to that of the delocalised anion in **40**.

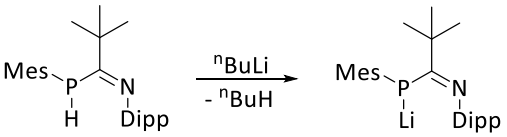

23 **41**

Scheme 99 *Deprotonation of phosphaamidine to a lithium phosphanide*

In situ ^{31}P NMR spectroscopy of **41** displays a 1:1:1:1 quartet signal at δ = -29.2 ($^{1}J_{P\text{-}Li}$ = 105 Hz). This is the result of the coupling of phosphorus to the ^{7}Li nucleus (*I* = 3/2). This is verified by the ^{7}Li NMR spectrum of **41**, which shows a doublet signal at δ = -2.64 ($^{1}J_{Li\text{-}P}$ = 105 Hz) indicating coupling to the phosphorus nucleus (*I* = 1/2). These observations suggest a

Lewis structure for **41** as depicted in Scheme 99, featuring a lithium phosphanide bond. It is the result of direct removal of the phosphine proton generating a negative charge is localised at phosphorus.

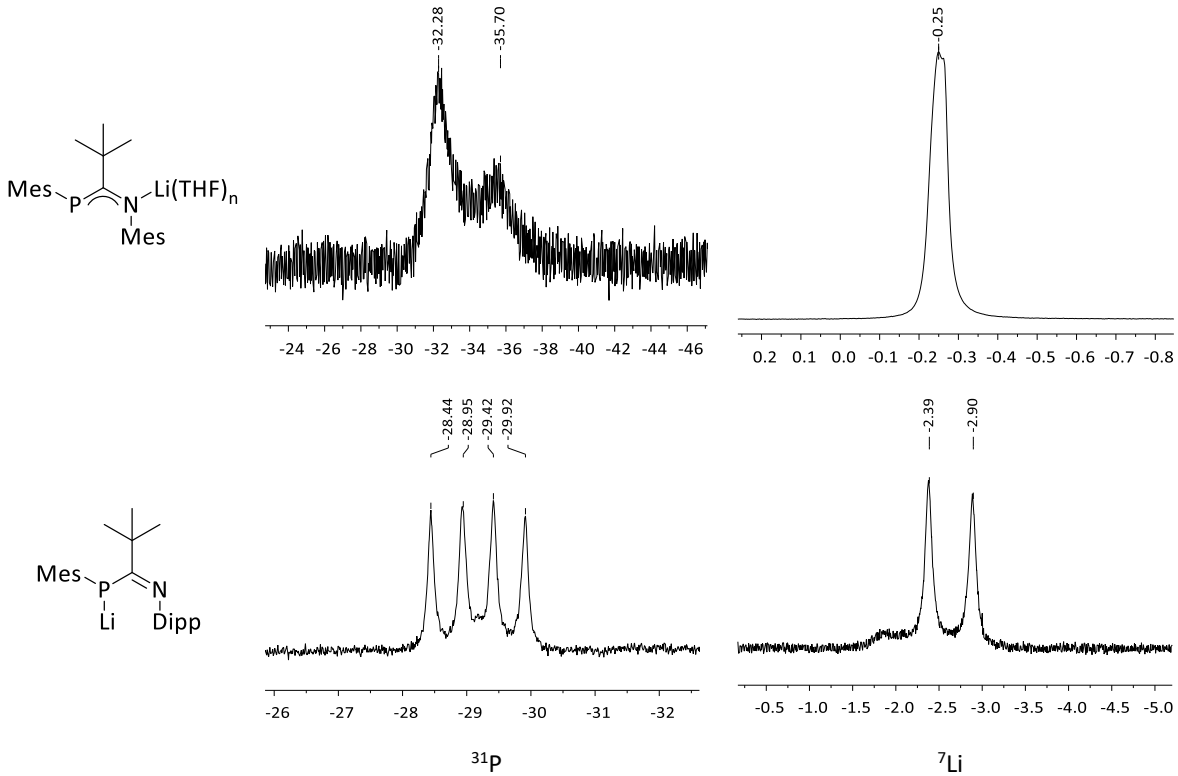

Figure 79 *Comparison of ^{31}P NMR (298 K, 202.5 MHz, THF) and ^{7}Li (298 K, 194 MHz, THF) of lithium complexes **40** and **41***

Whilst the formation of **40** and **41** was shown to be almost quantitative by *in situ* ^{31}P NMR spectroscopy, isolation of the lithium phosphaamidinate complexes proved challenging. Attempts at work-up under various conditions resulted in the isolation of protonated phosphaamidines **20** and **23** respectively.

5.1.2 Coordination of the Lithium Cation using 12-Crown-4

Lithium phosphaamidinate **40** is unstable to work-up, but sequestering the lithium cation using 12-crown-4 may aid in its isolation. Phosphaamidine **20** was lithiated at low temperature in the presence of 12-crown-4, resulting in lithium phosphaamidinate **42**. The solution had a similar bright yellow colour to the solutions of **40**, but the broad ($\nu_{1/2}$ ≈ 232 Hz) singlet signal in the ^{31}P NMR spectrum of **42** is shifted slightly downfield that that of **40**, at δ = -20.4 and δ = -33.5 respectively.

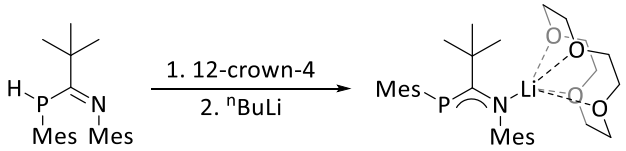

20 **42**

Scheme 100 *Lithiation of Mes-substituted **20** and encapsulation of cation*

The ^{1}H NMR spectrum of **42** is dominated by the sharp singlet signal of the crown ether CH_2 protons at δ = 3.51, which is only slightly shifted from its non-coordinated counterpart at δ = 3.48. In general, the signals of the phosphaamidinate fragment of **42** are very broad and featureless, and samples of **42** were always contaminated with small amounts of protonated ligand **20**. Monitoring a benzene solution of **42** by ^{1}H and ^{31}P NMR spectroscopy revealed more than half of the compound had transformed into protonated phosphaamidine **20** in a five-day time frame. It is suggested that **42** is extremely water sensitive, and that this it can react with trace water residues in the solution solvent.

Single crystals of **42** suitable for X-ray crystallography were grown from a saturated THF solution at room temperature, which confirms 12-crown-4 has successfully coordinated the lithium cation. It is also immediately apparent that the geometry of the phosphaamidinate ligand in **42** (E-syn) is different to that observed in the X-ray crystal structure of its protonated form **20** (Z-syn N=C, section 4.1.1). Unlike DippPC(Tol)N(Li)Dipp.THF_3 (section 5.1.0), the protonated ligand **20** exhibits only one signal in the ^{31}P NMR spectrum, corresponding to the Z-syn N=C isomer. Exact reasons for this geometry change upon deprotonation are unclear, however a Z-syn anionic phosphaamidinate would suffer from much steric strain, and an inversion at phosphorus would help alleviate this.

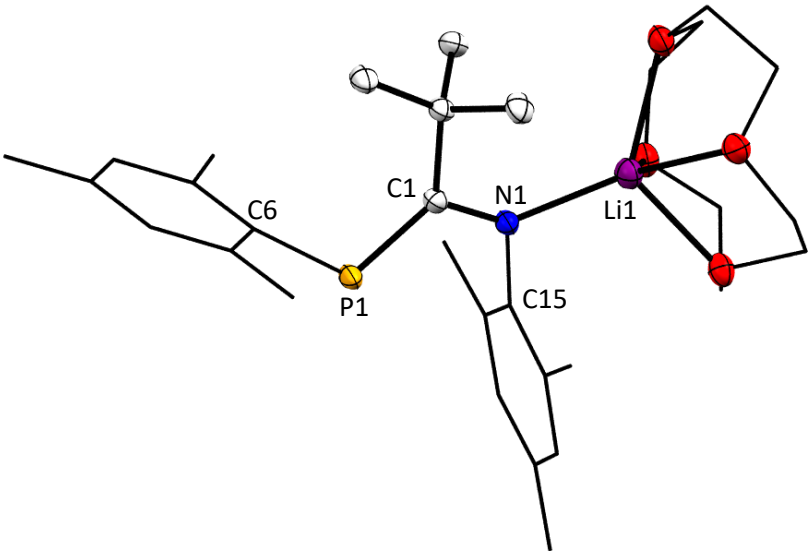

Figure 80 *X-Ray crystal structure of* ***42****. Co-crystallised with 2 molecules of THF, which are omitted for clarity. Hydrogen atoms omitted for clarity. Bond Lengths (Å): P1=C1 1.7690(13); P1-C6 1.8435(13); C1-N1 1.3347(17); N1-C15 1.4262(16); N1-Li1 2.075(3) Å. Bond angles(°): P1-C1-N1 118.68(10).*

The solid-state structure of **42** suggests the lithium amide bond is largely ionic in nature. At 2.075(3) Å, it is comparable with analogous bonds in reported lithiated phosphaamidinates (Boeré 2.060(5) Å; Slootweg 2.013(4) Å).

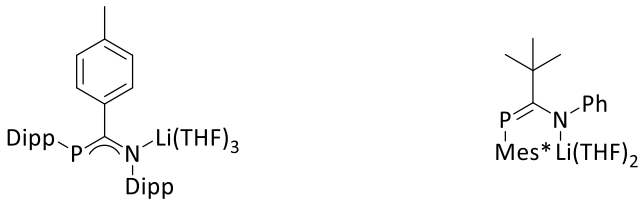

^{31}P δ = -22.9 — Boeré

^{31}P δ = 38.6 — Slootweg

Figure 81 *Previously reported crystalographically characterised lithium phosphaamidinate complexes*

The P1-C1 bond in the solid-state structure of **42** is slightly shorter than the analogous bond in its protonated form **20** (**20:** 1.872(3) Å; **42**: 1.7690(13) Å), and the N1-C1 bond is elongated (**20:** 1.279(4) Å; **42**: 1.3347(17) Å). This suggests delocalisation of the negative charge across the central P1-C1-N1 phosphaamidine unit. Three reasonance forms can be considered for this delocalisation, as shown in Scheme 101.

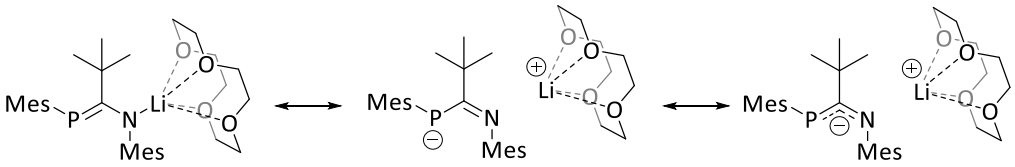

Scheme 101 *Possible resonance forms of lithium complex* ***42***

Density functional theory (DFT) was used to investigate this possible delocalisation. Using the solid-state structure of **42** as an initial geometry, the structure was optimised using M062X/def2svp and was found to converge easily. Table 9 lists the key bond lengths of solid-state structure **42** and the optimised structure **42**$^{\#}$, which are very similar. The most notable difference is in the N-Li bond length, with the optimised structure underestimating this value by 5.2%. The bond angles between **42** and **42**$^{\#}$ are also comparable, with the biggest discrepancy in the angle associated with the lithium.

Bond	42 – X-Ray	42$^{\#}$ - Optimised	Angle	42 – X-Ray	42$^{\#}$ - Optimised
P1-C1	1.7690(13)	1.769	**P1-C1-N1**	118.68(10)	117.3
C1-N1	1.3347(17)	1.341	**C1-N1-Li1**	139.36(11)	142.7
N-Li	2.075(3)	1.968	**C1-P1-C6**	111.11(6)	111.0
P1-C6	1.8435(13)	1.855			

Table 9 *Comparison of bond lengths and angles of* ***42*** *and its optimised structure* ***42***$^{\#}$ *(M062X/def2svp)*

The visualised molecular orbitals of **42**$^{\#}$ which are consistent with delocalisation are shown in Figure 82. The HOMO-7 orbital shows a bonding interaction across the entire P-C-N unit. Interestingly, the HOMO (+3.952 eV above HOMO-7) orbital indicates a phosphaalkene bond. This contrasts with the phosphaamidine bonding in starting material **20**, which contains imine and phosphine functionality, and perhaps gives a reason for the geometric rearrangement observed upon complexation. Higher in energy again (+10.31 eV from HOMO), the LUMO+5 shows antibonding interactions across the P-C-N unit.

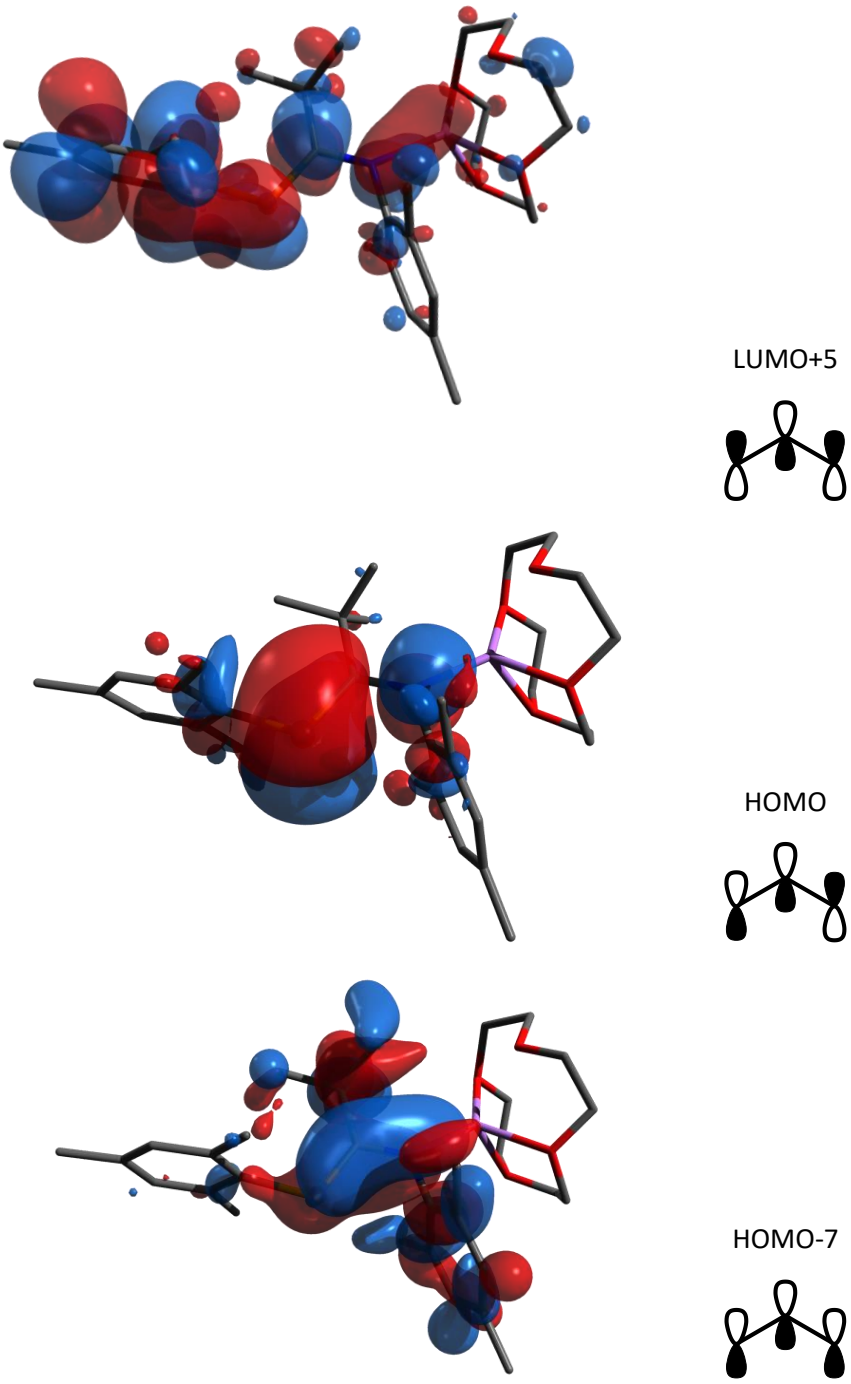

Figure 82 *Visualised molecular orbitals of* ***42***$^{\#}$ *calculated at the M02X/def2svp level*

The Wiberg bond indices (WBI) of **42**[#] were also calculated, and are listed in Table 10. Both the P-C and N-C index values indicate partial multiple bond character, which supports the delocalisation in the visualised molecular orbitals. The bond index between N and Li is very low (0.0546), indicating little covalent bonding between these atoms.

Bond	Crystal Structure Bond Length (Å)	WBI
P-C1	1.7690(13)	1.4192
C1-N	1.3347(17)	1.3661
N-Li	2.075(3)	0.0546

Table 10 *Comparison of bond length and the calculated Wiberg bond order using M062X/def2svpp*

It is concluded that the anionic component of lithium complex **42** has a negative charge delocalised across the P-C-N phosphaamidinate unit. This is suggested by the P1-C1 and C1-N1 bond lengths in the solid-state structure and supported by the calculated molecular orbitals and Wiberg bond indices.

5.1.3 Isolation of a Bulky Lithium Phosphaamidine with Two Isomers

In a similar fashion to **40** and **41**, the low temperature addition of ^{n}BuLi to an ethereal solution of Ar*-substituted phosphaamidine **28** gives a striking colour change, in this case from colourless to dark red. *In situ* ^{31}P NMR spectroscopy of this solution shows two products have formed, with resonances at δ = 25.3 and δ = -27.4 ($^{1}J_{P\text{-}Li}$ = 101 Hz), with the latter corresponding to the major component.

The more upfield ^{31}P NMR signal at δ = - 27.4 reproducibly accounts for approximately 80 % of the mixture by integration. Like in the ^{31}P NMR spectrum of lithium amide **41**, this signal is a 1:1:1:1 quartet, the result of phosphorus coupling to the NMR active ^{7}Li nucleus. This signal is assigned to structure **43a**. The other signal at δ = 25.3 is a sharp singlet signal, and is assigned to structure **43b**, as the value of the chemical shift suggests phosphaalkene character and the absence of any P-Li coupling suggests a lithium amide structure. These suggestions are supported by the ^{7}Li NMR, which displays two signals at δ = -2.28 (d, $^{1}J_{Li\text{-}P}$ = 101 Hz) and δ = -5.29.

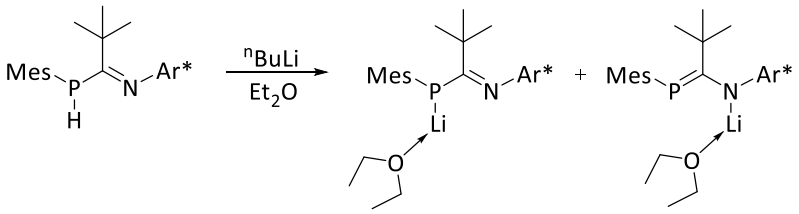

28 **43a** **43b**

Scheme 102 *Reaction of bulky phosphaamidine **28** with ^{n}BuLi to form inseparable isomers*

Products **43a** and **43b** were found to be inseparable under the work-up conditions used here. The ^{31}P NMR spectrum of the isolated material is shown in Figure 83. It shows a similar distribution of products to the reaction aliquots, with lithium phosphanide **43a** being the major component of the mixture (approximately 79%).

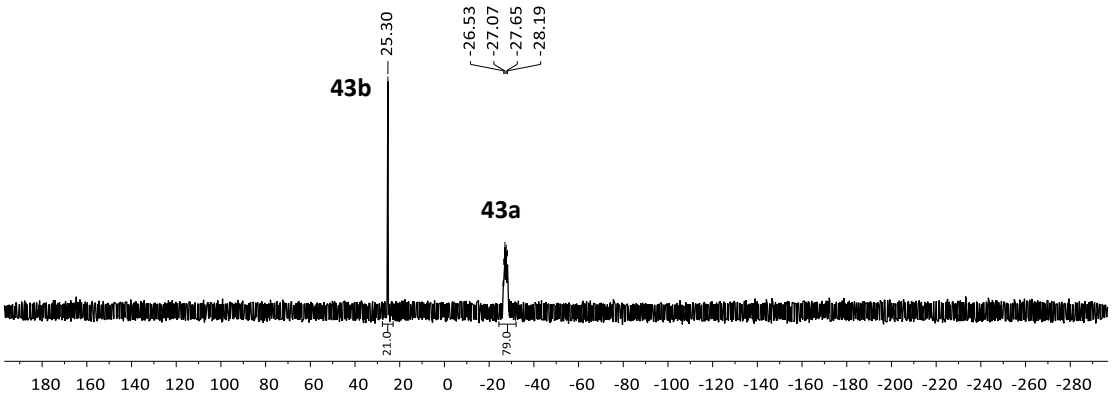

Figure 83 *^{31}P NMR spectrum (300 K, 202.5 Hz, C_6D_6) spectrum of isolated lithium phosphaamidinate* ***43a*** *and* ***43b***

To determine whether these isomers can interconvert, variable temperature ^{31}P NMR spectroscopy was carried out. Starting from an initial ratio as shown in Figure 83 (21:79), increasing the acquisition temperature to 333 K increases the amount of lithium phosphide (δ = -27.4) slightly (new ratio 16:84). Upon cooling to 300 K the initial ratio is restored.

Two independent sets of signals are identified in the ^{1}H NMR spectrum which can be assigned to **43a** and **43b**. In some cases these signals overlap, for example the ^{t}Bu methyl signal is seen at δ = 1.21 for **43a** and δ = 1.19 for **43b**. Other signals are well separated; the mesityl *p*-methyl group is seen at δ = 1.77 and δ = 1.96 respectively. A ^{1}H-^{31}P HMBC experiment revealed long-range heteronuclear coupling from the ^{31}P δ = 25.3 signal to the ^{1}H signals assigned to **43b**. No cross-peaks from the ^{31}P δ = -27.4, and this is attributed to the broader signals resulting from coupling both to the ^{31}P and ^{7}Li nuclei.

It is apparent from the ^{1}H NMR spectrum of the isomeric mixture that one equivalent of Et_2O is coordinated to the lithium centre in both isomers, with signals at δ = 2.77 (q, $^{1}J_{H\text{-}H}$ = 7.0 Hz) and δ = 0.63 (t, $^{1}J_{H\text{-}H}$ = 7.0 Hz) significantly shifted upfield from the solvent's residual signals.[3] Due to low solubility, little information could be ascertained from the ^{13}C NMR spectrum.

5.2 Preparation of Aluminium Hydride Complexes

One method of aluminium hydride preparation is dihydrogen elimination from a protonated ligand using $Me_3N.AlH_3$.[8] Where this atom-efficient process is not possible, initial lithiation of the protonated ligand and subsequent transfer to an aluminium centre allows the isolation of a range of complexes with functional Al-R bonds (i.e. alkyl, halide, hydride etc).[9–12] As with the magnesium chemistry discussed in chapter 4, the coordination-mode of amidine ligands to aluminium is dependent on the steric bulk of the ligand,[8,13] as well as the thermal conditions.[14]

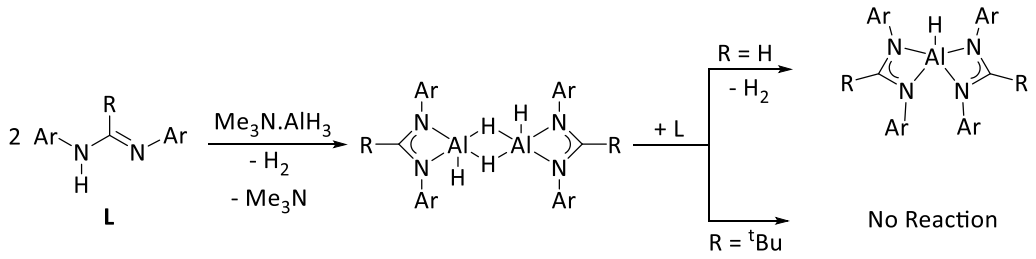

Scheme 103 *By increasing the steric bulky of the amidine ligand, access to the aluminium monohydride is restricted.[8] Ar = 2,6-diisopropylphenyl.*

Accessing aluminium(II) complexes is possible with support from amidinate ligands. Using a magnesium(I) reducing agent, examples of amidinato aluminium dihydrides have been reduced to dialanes.[15] Further reduction of the aluminium centres was not observed.

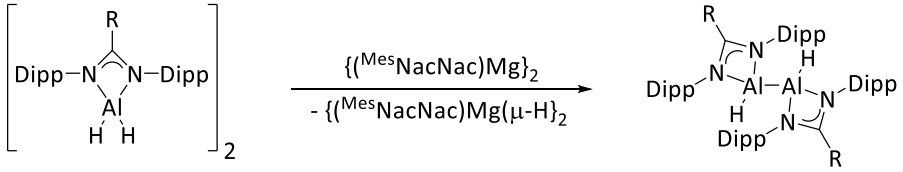

Scheme 104 *Reduction of an amidinate aluminium dihydride using a Mg(I) reducing agent. Dipp = 2,6-diisopropylphenyl, R=Me, p-tolyl, tBu or NiPr2*

As aluminium complexes featuring amidinate ligands have been used to catalyse the polymerisation of lactide[4] and ethylene,[5–7] targeting similar complexes featuring phosphaamidinate ligands could produce compounds with interesting reactivity. Currently, no phosphaamidinate aluminium compounds are reported, and synthesis of the "parent" hydride ($LAlH_2$) complexes was undertaken.

*5.2.1 Reaction of **40** with $Me_3N.AlH_3$*

Targeting an aluminium dihydride $LAlH_2$ (L = phosphaamidine), mesityl-subsituted ligand **20** was treated with $Me_3N.AlH_3$ in C_6D_6, however no reaction was observed after several days. Reaction of lithiated complex **40**, formed *in situ*, with $Me_3N.AlH_3$ was more successful. *In situ* ^{31}P NMR spectroscopy showed formation of a new species, with a singlet signal observed at δ = -23.6. This chemical shift is very similar that of the homoleptic L_2Mg compound with the same ligand **35**, δ = -25.9, and so this product was tentatively identified as aluminium hydride **44**. The same phosphorus containing product was identified whether one equivalent or half an equivalent of aluminium hydride was used.

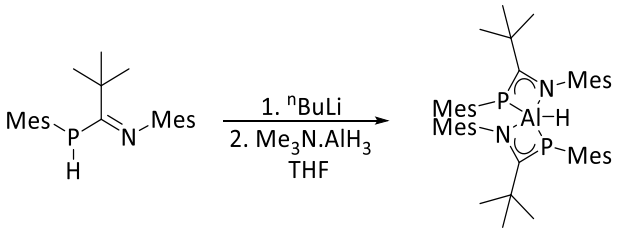

20 **44**

Scheme 105 *In situ lithiation and reaction of **20** with ^{n}BuLi and $Me_3N.AlH_3$*

The ^1H NMR spectrum of isolated bright yellow solid **44** displayed only signals associated with a new ligand environment. The ^{t}Bu resonance is observed at δ = 1.01, upfield of the same signal in protonated ligand **20** at δ = 1.33, and comparable with the analogous resonance in L_2Mg compound **35** (δ = 0.97). All the mesityl-methyl groups are inequivalent in **44**, with six singlet signals identified. Broad singlets at δ = 2.86, 2.54, 2.44 and 2.31 are attributed to the *ortho*-methyl groups, and sharp singlets at δ = 2.05 and 2.01 for the *para*-methyl groups.

A key signal conclusively identifying the product would that be associated with Al-H hydride, however no such signal was identified. This is not unusual, as aluminium is a quadrupolar nucleus and coupling broadens these signals into the baseline (compare with the activation of pinacol borane in section 3.1). This missing signal means that the structure of **44** cannot be confirmed by NMR studies alone. No signal for **44** was observed in the ^{27}Al NMR spectrum.

X-ray crystallography confirmed the structure of **44** as the *bis*-ligated aluminium monohydride shown. There is C_2 rotational symmetry with an axis along the Al-H bond, as both phosphaamidinate ligands have identical structural parameters.

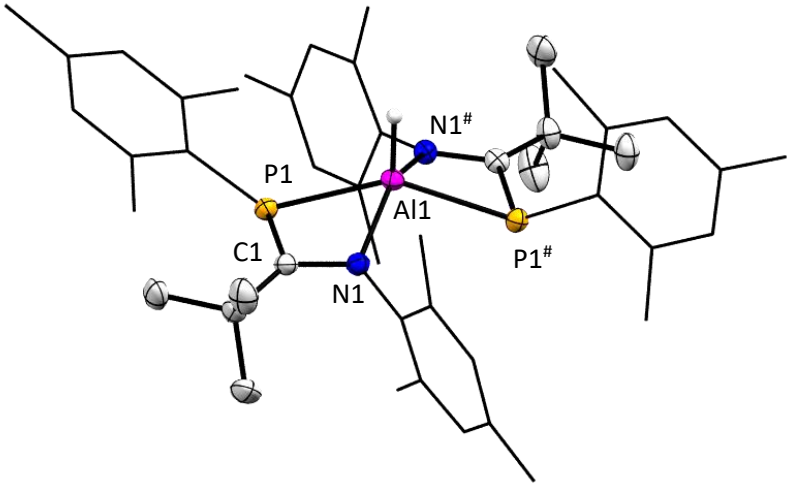

Figure 84 *X-Ray crystal structure of* ***44****. Mesityl groups are wireframe and C-H hydrogen atoms are omitted for clarity. Selected bond lengths (Å): P1-C1 1.7886(14), C1-N1 1.3389(18), P1-Al1 2.4698(4), N1-Al1 1.9960(11). Selected bond angles (°): P1-C1-N1 106.17(10), P1-Al1-N1 67.99(3), P1-Al1-N1# 98.65(4).*

Hydride **44** features a five-coordinate aluminium centre in a heavily distorted square pyramidal geometry. The sum of phosphaamidinate angles around the aluminium is 333.28(18)° indicating the aluminium centre is not co-planar with the P_2N_2 core. Within each phosphaamidinate ligand, the P1-C1-N1 fragment is planar, and the P1-C1 and C1-N1 bond lengths are similar those in lithium complex **42**, (**44**: P1-C1 1.7886(14) Å and C1-N1 1.3389(18) Å; **42**: P1-C1 1.7690(13) Å and C1-N1 1.3347(17) Å). The combination of these observations suggests delocalisation across the phosphaamidinate ligands.

The Al1-N1 bonds (1.9960(11) Å) in **44** are comparable with similar bonds found in amidinate complexes are of the type L_2AlH.[8,10] By comparison, the Al1-P1 bond, at 2.4698(4) Å, is substantially longer than the Al1-N1 bond, which is attributed to the larger van der Waals radius of phosphorus (1.8 Å) compared to nitrogen (1.55 Å).[16]

5.2.2 Isolation of Lithium Aluminate Intermediate

Carrying out the preparation of aluminium hydride **44** in diethyl ether instead of THF gave some insight into how the reaction proceeds. The addition of $Me_3N.AlH_3$ to lithiated complex **40** shows the formation of a second product **45** by ^{31}P NMR spectroscopy, evidenced by a broad multiplet signal around δ = -9.0. The shape of this signal is very similar to the corresponding mestyl-substituted lithium phosphaamidinate **40**, but the chemical shift is significantly downfield.

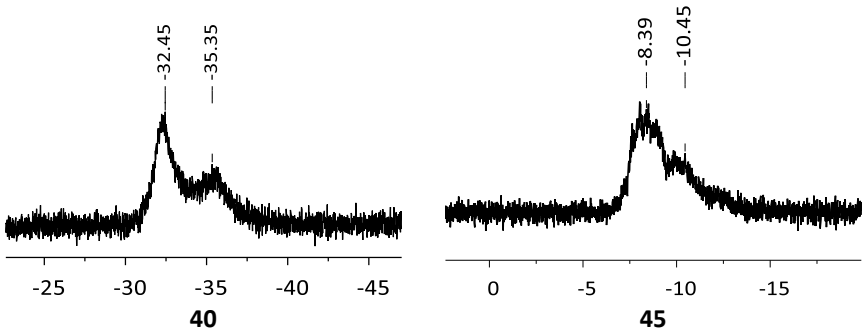

Figure 85 *Comparison of the ^{31}P NMR spectra (Et_2O, 202 MHz, 298 K) of **40** and **45***

Monitoring this solution shows that the amount of **45** present decreases over time, while the amount of **44** increases. It is hence suggested that **45** is a lithium aluminate intermediate, the proposed structure shown in Scheme 106. This intermediate can eliminate LiH to form aluminium hydride **44**.

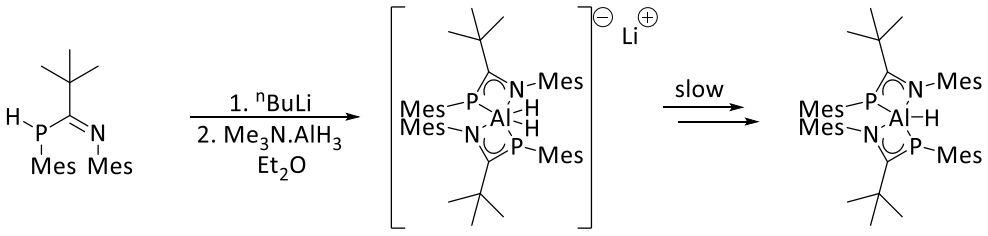

Scheme 106 *In situ lithiation and reaction of **20** with $Me_3N.AlH_3$ in Et_2O*

Using short reaction times at low temperature, **45** was isolated in approximately 90 % purity by ^{31}P NMR spectroscopy, which was confirmed by elemental analysis (section 7.3.30). The ^{1}H NMR spectrum of this bright yellow solid is extremely broad and essentially featureless.

Dissolving **45** in THF-d_8 demonstrated that **45** is fully transformed into **44** over approximately 30 minutes at room temperature, further indicating that **45** is an intermediate on the way to the formation of **44**.

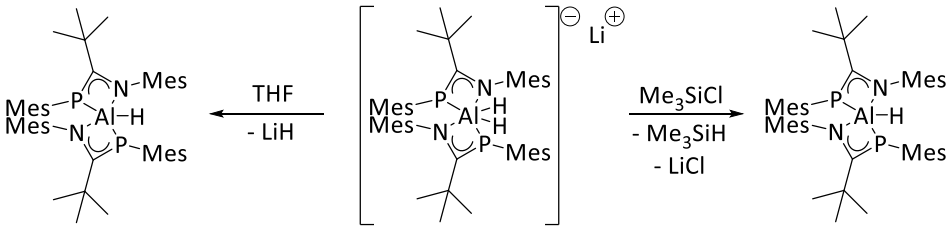

44 **45** **44**

Scheme 107 *Formation of **44** from the isolated intermediate material **45***

Lithium alkylborohydrides can react with trimethylsilyl chloride producing the corresponding neutral borane with elimination of lithium chloride and trimethylsilane, even with bulky alkyl groups (Scheme 108).[17] Similar reactivity with lithium aluminate **45** would support the suggested structure.

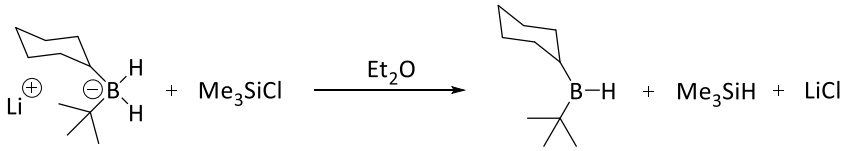

Scheme 108 *Reaction of lithium alkylborohydride to make a alkylborane[17]*

The crude isolated solid **45** was suspended in C_6D_6 and one equivalent of trimethylsilylchloride was added, which caused the precipitation of a white solid. Whilst the ^{1}H NMR spectrum of this solution was very broad due to precipitate formation, Me_3SiH could be identified by a singlet signal at δ = 4.17 ($^1J_{Si\text{-}H}$ = 179 Hz).[18] The corresponding ^{31}P NMR spectrum shows only the formation of aluminium hydride **44**. This reaction was repeated on a preparative scale in Et_2O, and a pure sample of **44** was isolated by recrystallisation from hexane.

A proposed mechanism for the formation of **44** in diethyl ether is shown in Scheme 109. It is suggested that the intended aluminium dihydride is formed initially, potentially with some solvent molecules coordinated. Addition of a further equivalent of lithium phosphaamidinate **40** forms observed intermediate **45**. Coordination of solvent molecules

to the lithium cation could be the cause of this complex's instability, with coordination by THF precipitating the dissociation of lithium hydride and forming the ultimately isolated phosphaamidinate aluminium hydride **44**.

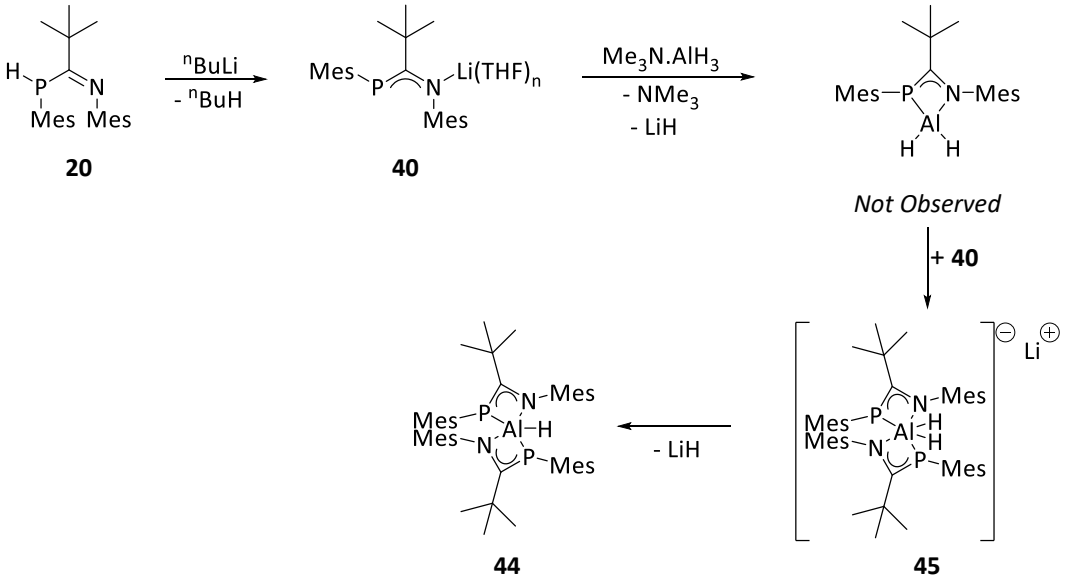

Scheme 109 *Proposed mechanism of formation of bis-phosphaamidinate aluminium hydride* ***44***

This facile addition of a second equivalent of **40** to the aluminium centre negates the possibility of isolating the targeted aluminium dihydride. In amidinate chemistry, the steric bulk of the ligand is one of the determining factors in the ability to isolate such reactive species.[8] With other sterically bulky ligands which could possibly give more kinetic stability on hand, the next avenue of investigation was clear.

5.2.3 Increasing the Steric Bulk to Isolate an Aluminium Dihydride

Following the isolation of the *bis*-phosphaamidinate aluminium hydride **44** with the smallest ligand in the phosphaamidine series described in this work, the reaction with $Me_3N.AlH_3$ with other lithium phosphaamidinate complexes (section 5.1) was investigated.

It was expected that reaction of the Dipp-substituted lithium complex **41** with $Me_3N.AlH_3$ would result in an L_2AlH aluminium hydride analogous with **44**. However, the formation of **41** followed by addition of the alane unexpectedly resulted in phosphine elimination by ^{31}P NMR spectroscopy, producing $MesPH_2$ as the only phosphorus-containing product. Many products were identified by ^{1}H NMR spectroscopy.

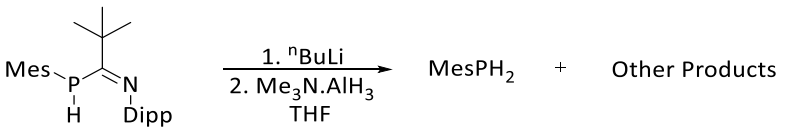

23

Scheme 110 *In situ lithiation and reaction of **23** with $Me_3N.AlH_3$*

Direct reaction of phosphaamidine **23** with $Me_3N.AlH_3$ in the absence of $^{n}BuLi$ also produces a substantial amount of $MesPH_2$. For comparison, a similar mixture of mesityl ligand **20** and $Me_3N.AlH_3$ undergoes no reaction, even when heated. The reasons for this difference in reactivity are unclear, perhaps the ligand itself is unstable to the presence of nucleophilic aluminium hydride.

Treating **28,** the bulkiest ligand in the phosphaamidinate series, with one equivalent of $Me_3N.AlH_3$ gives no reaction in C_6D_6 even with heating to 80 °C. However, the addition the alane to a C_6D_6 solution of isolated lithium phosphaamidinate isomers **43a** and **43b** causes a prominent colour change, from deep red to bright yellow. ^{31}P NMR spectroscopy of this solution shows the formation of new product as a sharp singlet at δ = -37.7, which accounts for 41.9 % of the phosphorus containing material by integration. The other components of the mixture are lithium complexes **43a** (49.6 %) and **43b** (6.5 %), and a small amount of protonated ligand **28** (2.0 %). The reaction did not proceed any further, despite heating the solution for extended periods. As a significant proportion of lithium phosphanide **43a** remains present, it is assumed that lithium amide **43b** is the sole reactive conformation.

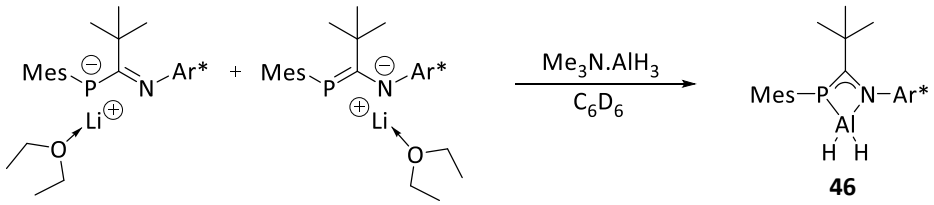

43a **43b** **46**

Scheme 111 *Reaction of lithium phosphaamidinate isomers* ***43a*** *and* ***43b*** *with* $Me_3N.AlH_3$ *to form unisolable aluminium dihydride* ***46***

The identity of this new signal is suggested as aluminium dihydride **46**. Even though no Al-H signal can be identified by ^{1}H NMR, bis-ligation is ruled out on the basis that this coordination mode was shown to be unavailable in the magnesium chemistry discussed in section 4.2.4. Further, the ^{31}P chemical shift of **46** is upfield of aluminium hydride complex **44** (δ = -37.7 and -23.6 respectively), suggesting a different geometric structure.

Repeating this reaction on a preparative scale, either with isolated lithium complex **43** or forming it *in situ*, did not produce a similar reaction, and all material recovered from these reactions was identified as either **43a**, **43b** or its constitute phosphaamidine **28**.

5.3 Summary

The reaction of phosphaamidines **20, 23** and **28** with ^{n}BuLi in ethereal solvents results in the clean deprotonation to form butane and lithium complexes **40**, **41**, ***43*a** and **43b**. The examples featuring smaller ligands are found to be difficult to isolate. Using a bulkier ligand enables isolation as a mixture of tautomers, with the major component being lithium phosphanide **43a**.

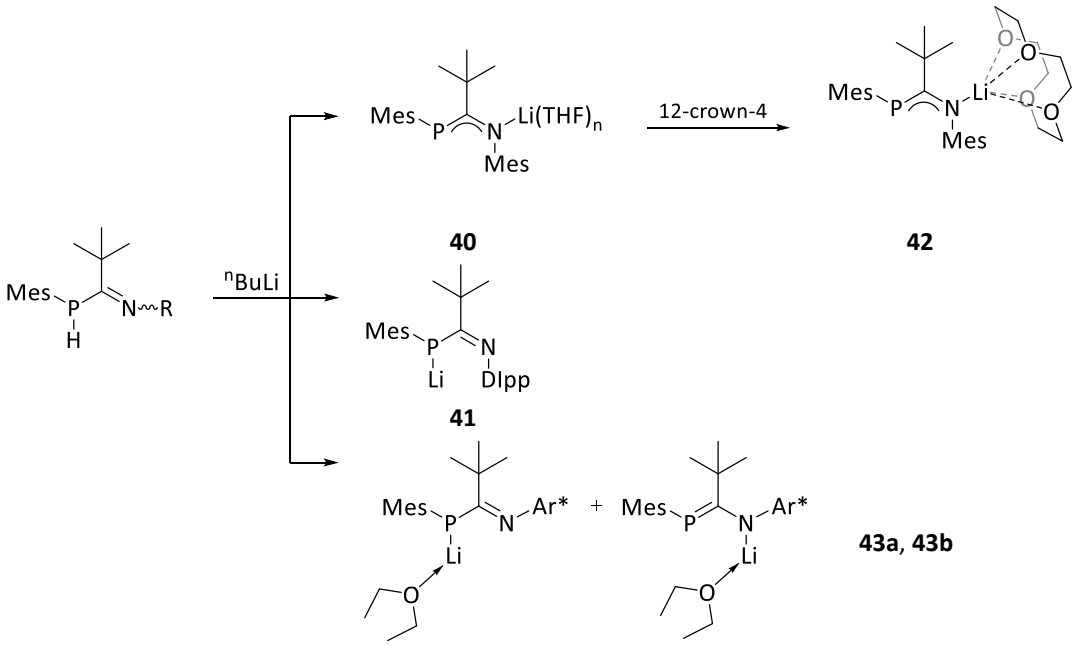

Scheme 112 *Reaction of phosphaamidines **20, 23** and **28** with ^{n}BuLi results in lithium complexes with different structures*

The location of the resulting negative charge is dependent on the steric bulk of the amine substituent. Coordination of the lithium cation in **40** using 12-crown-4 allows the isolation of lithium complex **42**, and using the resulting solid-state structure the properties of the phosphaamidinate anion were examined. The calculated molecular orbitals M062X/def2svp suggest allylic delocalisation across the P-C-N unit, which is supported by the calculated Wiberg bond indices showing partial multiple bond character in both bonds (P-C 1.42 and N-C 1.37).

Reaction of lithium phosphaamidinate **40** with $Me_3N.AlH_3$ forms the *bis*-ligated aluminium hydride **44**. Isolation of lithium aluminate **45** is made possible by carrying out the reaction

at low temperature in the more weakly coordinating solvent Et_2O. The identity of this intermediate is demonstrated through its onwards reactivity with trimethylsilyl chloride.

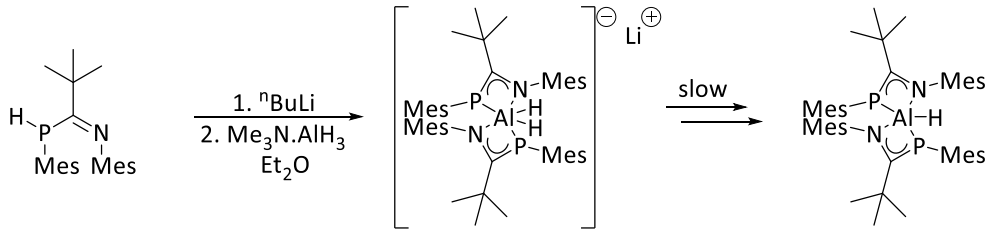

20 **45** **44**

Scheme 113 *Formation of aluminium hydride **44** via lithium aluminate **45***

The formation of **44** does not represent a general pathway to phosphaamidinate supported aluminium hydrides. Employing the same synthetic procedure using Dipp-substituted lithium phosphanide **41** results in cleavage of the P-C bond and formation of $MesPH_2$. Reaction of the isomeric mixture of super bulky **43** with $Me_3N.AlH_3$ forms a neutral, unisolable proposed aluminium dihydride complex **46**.

5.4 References

1 T. van Dijk, S. Burck, M. K. Rong, A. J. Rosenthal, M. Nieger, J. C. Slootweg and K. Lammertsma, *Angew. Chem.*, 2014, **126**, 9214–9217.

2 R. Boere, M. L. Cole, P. C. Junk, J. Masuda and G. Wolmersha, *Chem. Commun.*, 2004, 2564–2565.

3 G. R. Fulmer, A. J. M. Miller, N. H. Sherden, H. E. Gottlieb, A. Nudelman, B. M. Stoltz, J. E. Bercaw and K. I. Goldberg, *Organometallics*, 2010, **29**, 2176–2179.

4 F. Qian, K. Liu and H. Ma, *Dalton Trans.*, 2010, **39**, 8071–8083.

5 M. P. Coles and R. F. Jordan, *J. Am. Chem. Soc.*, 1997, **119**, 8125–8126.

6 P. H. M. Budzelaar, *Organometallics*, 2000, **19**, 5691–5695.

7 G. Talarico, V. Busico and P. H. M. Budzelaar, *Organometallics*, 2001, **20**, 4721–4726.

8 M. L. Cole, C. Jones, P. C. Junk, M. Kloth and A. Stasch, *Chem. Eur. J.*, 2005, **11**, 4482–4491.

9 M. P. Coles, D. C. Swenson, R. F. Jordan and V. G. Young, *Organometallics*, 1997, **16**, 5183–5194.

10 R. Duchateau, A. Meetsma and J. H. Teuben, *Chem. Commun.*, 1996, **86**, 223–224.

11 N. E. Mansfield, M. P. Coles and P. B. Hitchcock, *Dalton Trans.*, 2005, 2833–2841.

12 S. L. Aeilts, M. P. Coles, D. C. Swenson, R. F. Jordan and V. G. Young, *Organometallics*, 1998, **17**, 3265–3270.

13 J. A. R. Schmidt and J. Arnold, *Organometallics*, 2002, **21**, 2306–2313.

14 A. L. Brazeau, Z. Wang, C. N. Rowley and S. T. Barry, *Inorg. Chem.*, 2006, **45**, 2276–2281.

15 S. J. Bonyhady, D. Collis, G. Frenking, N. Holzmann, C. Jones and A. Stasch, *Nat. Chem.*, 2010, **2**, 865–869.

16 A. Bondi, *J. Phys. Chem.*, 1964, **68**, 441–451.

17 T. E. Cole, H. C. Brown, R. K. Bakshi, M. Srebnik and B. Singaram, *Organometallics*, 1986, **5**, 2303–2307.

18 C. C. Mokhtarzadeh, C. E. Moore, A. L. Rheingold and J. S. Figueroa, *Angew. Chem. Int. Ed.*, 2017, **56**, 10894–10899.

Chapter 6:

Overall Summary and Outlook

6. Overall Summary and Outlook

6.1 Low Oxidation State Aluminium Chemistry has been Expanded

The first half of this thesis examined the mechanism of formation of the prototypical Al(I) compound, $(Cp^*Al)_4$ by reductive elimination, and its reactivity with unsaturated bonds. Reductive elimination of Cp*H from Cp^*_2AlH was found to proceed *via* a unimolecular transition state, which was experimentally determined to be 95.53 ± 4.74 kJ mol^{-1} above the energy of the starting material, which is consistant with a calculated density functional theory value of 91.54 kJ mol^{-1}. Also using density functional theory, the transition state **$TS_{1\text{-}2}$** was located; one Cp* ring moves away from the aluminium centre whilst the other undergoes a haptotropic shift to η^5 coordination mode. The charge localised at the Al-H was calculated to have increased from -0.373 in **1** to -0.049 in **$TS_{1\text{-}2}$**, suggesting a reduction in hydride character and that deprotonation of the aluminium centre in **$TS_{1\text{-}2}$** allows the formation of the observed products. Coordination of an NHC to the metal centre in **1** quenches the reductive elimination reactivity, most likely as the access to **$TS_{1\text{-}2}$** from a tetrahedral aluminium centre is restricted.

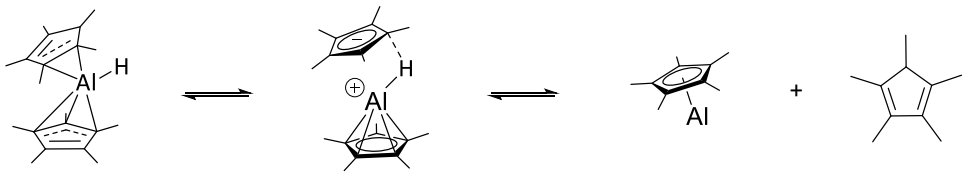

1 **$TS_{1\text{-}2}$** **2**

Scheme 114 *Mechanism of reductive elimination of Cp^*H from Cp^*_2AlH*

Using this mechanistic insight, a novel aluminium hydride was synthesised with attributes to allow the reductive elimination of a C-H bond. Heating neat samples of *bis*-fluorenyl aluminium hydride (**6**) under vacuum resulted in the expected sublimation of 9-methylfluorene, however the aluminium containing product could not be convincingly identified.

Given that the correct reductive elimination product was observed, this result is promising. Identification of this unknown aluminium species could be aided by employing trapping methods. For example, complexation of a possible low oxidation state aluminium compound with an electron deficient transition metal, such as Pt or Pd.[1–3] Addition of NHCs to this unknown species could also furnish an identifiable product.[4]

With the formation of $(Cp^*Al)_4$ understood, its reactivity with simple organic molecules was investigated. Whilst the N-H and B-H oxidative addition of 2,6-diisopropylaniline and pinacol borane was hinted at in NMR experiments, isolation of the products was not achieved. The high temperature reaction of **2** with diphenylacetylene quantitatively produces 1,4-dialuminacyclohexadiene derivative **11**. The aluminium centres in **11** retain their Lewis acidity, as demonstrated by coordination of ethereal solvents, and proposed coordination of DMAP and NHCs.

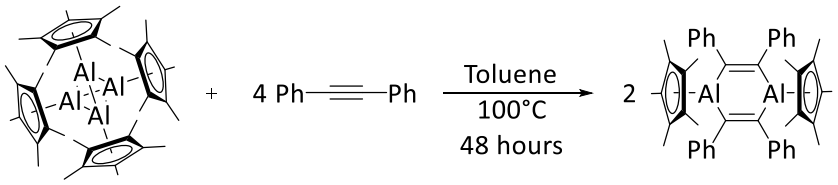

2 **11**

Scheme 115 *Reaction of Cp*Al with diphenylacetylene*

The Al-C_{Cp^*} bonds of **11** were found to be reactive, readily undergoing insertion reactions with unsaturated species, which are summarised in Scheme 116. Addition of an isonitrile to **11** resulted in aluminium-mediated C=C coupling, in a complex reaction which forms 6 new C-C bonds in a single step. The subsequent zwitterionic product **16** contains an aluminate anions countered by Cp* derived bridging carbocations, which is stabilised by homoconjugation.

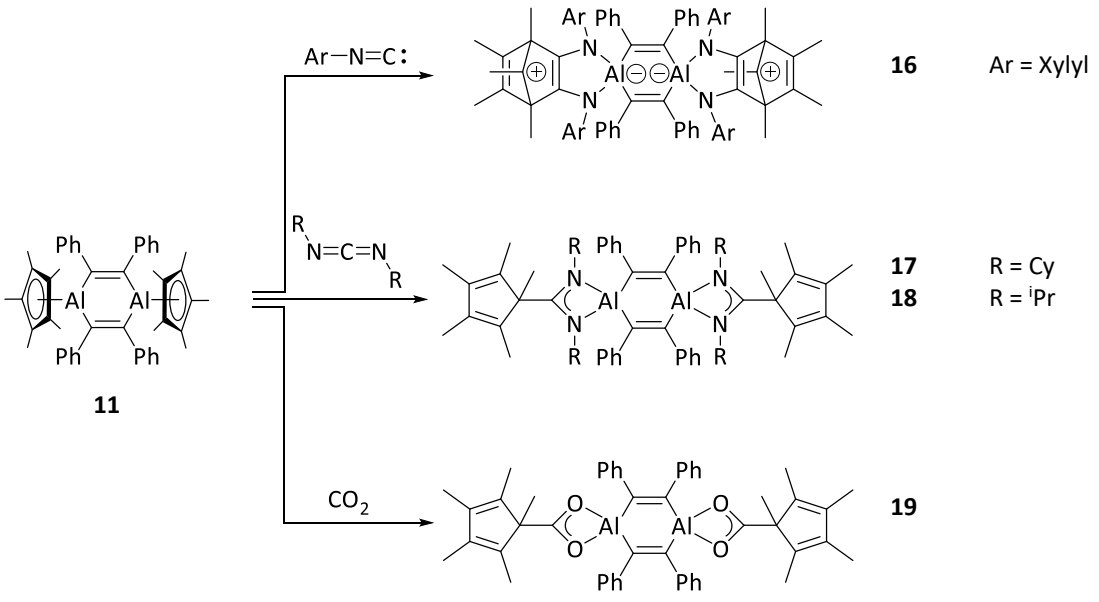

Scheme 116 *Summary of reactivity of 1,4-dialuminacyclohexadiene derivative **11***

Two examples of carbodiimide insertion have been demonstrated, **17** and **18**, which both form AlN_2C metallacycles. This method of aminidate formation is well documented, however such a ligand with a Cp* backbone is uncommon. A similar insertion reaction is observed between **11** and CO_2, forming proposed aluminium carboxylate **19**. Confident identification of this complex's novel bonding motif will only be achieved by X-ray crystal structure determination, which would be a priority if this work were to continue.

A future avenue of investigation could be the breakdown of compounds **16**-**19**. This could give insight into how to make this bond activation catalytic, and whether a low oxidation state species could be regenerated. Functionalisation of the alkene moiety instead of the $Al\text{-}C_{Cp^*}$ bond would be another expansion of this work, as it would allow for the Cp*Al starting material to be regenerated.

6.2 Application of Phosphaamidine Ligands in Main-Group Chemistry

A small library of five novel phosphaamidines was synthesised (**20**-**23** and **28**), where the steric bulk of the substituents was increased systematically, culminating in the isolation of a "super bulky" example **28.** The choice of substituent determines which of the eight possible phosphaamidine geometries is isolated, with the three examples crystallographically analysed here (**20**, **22** and **28**) displaying different P-C-N configurations (Figure 86). Mes*-substituted **22** was observed by ^{31}P NMR spectroscopy to exist as three isomers in solution, the identification of which was aided by DFT calculations (Figure 78).

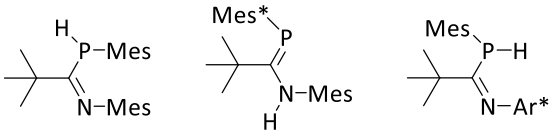

20 Z-syn N=C | **22** E-syn P=C | **28** Z-anti N=C

Figure 86 *Configuration of novel phosphaamidines crystallographically analysed in this work. Ar* = 2,6-bis(diphenylmethyl)-4-methylphenyl*

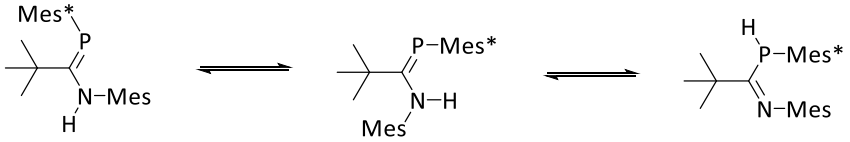

E-syn P=C **22a** ^{31}P δ 98.3 $^{3}J_{P\text{-}H}$ = 18 Hz | Z-anti P=C **22b** ^{31}P δ 80.2 | Z-syn N=C **22c** ^{31}P δ -53.6 $^{1}J_{P\text{-}H}$ = 253 Hz

Figure 87 *Isomers of phosphaamidine **22** correlated to ^{31}P NMR chemical shift*

Addition of $^{n}Bu_2Mg$ to these phosphaamidines results in deprotonation and formation of either a heteroleptic LMgBu complex (**29**, **30** and **34**) or a homoleptic L_2Mg complex (**35**, **36**, **31** and **33**) depending on the reaction stoichiometry.

When using less sterically hindered phosphaamidines, the resulting heteroleptic complexes (**29** and **30**) are dimeric in the solid-state, formed by the coordination of the phosphorus lone pair to adjacent magnesium centre. Reaction of **28** with $^{n}Bu_2Mg$ produces a monomeric three-coordinate magnesium centre (**34**). This change in nuclearity is reflected in the ^{31}P NMR chemical shift of the complexes, with dimeric **29** and **30** displaying resonances at δ = -42.0 and -55.3 respectively, where the resonance for **34** is downfield shifted at δ = -7.0.

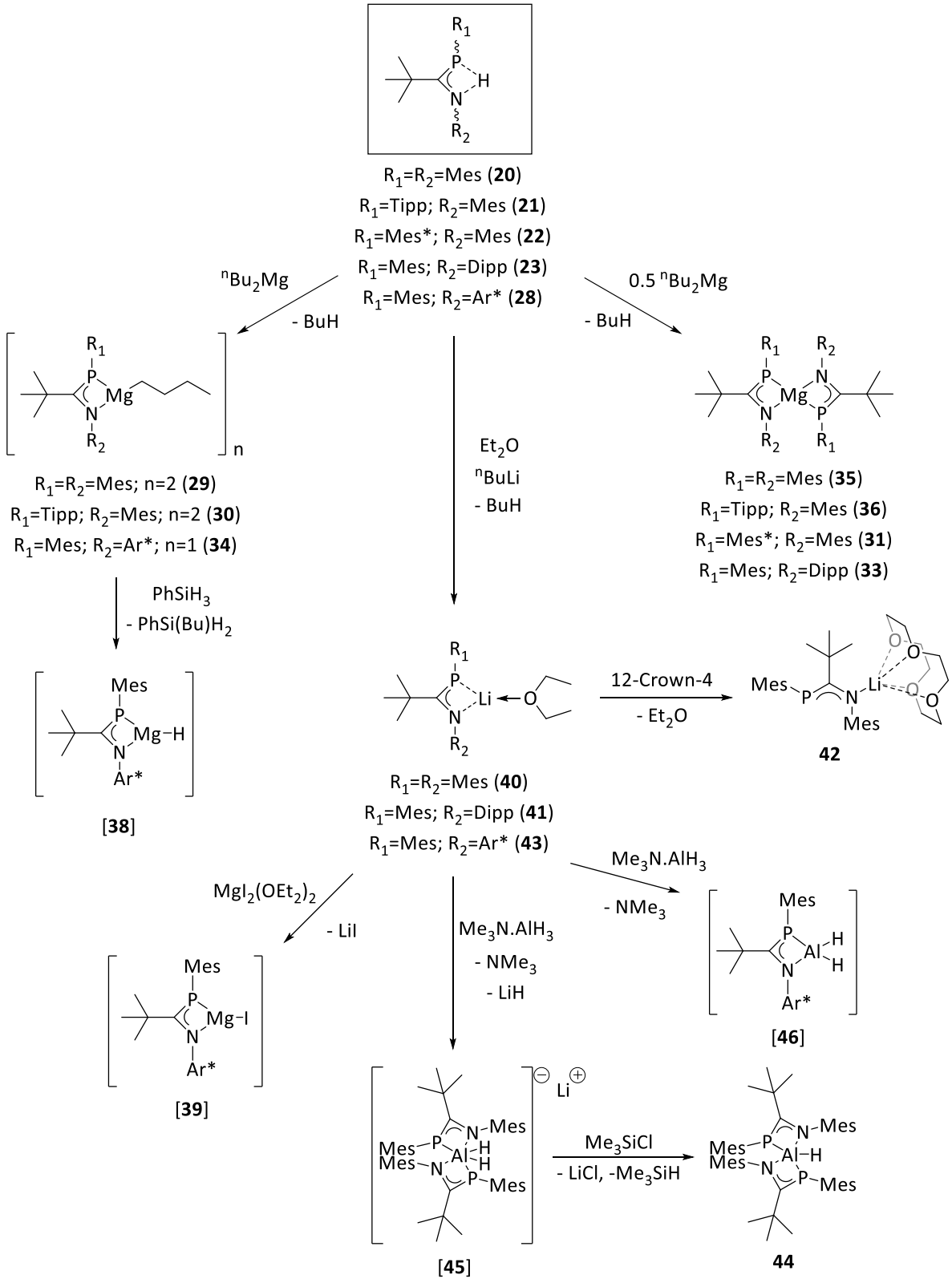

Scheme 117 *Summary of reactivity of phosphaamidines developed in this work*

Reaction of monomeric **34** with phenylsilane gives proposed phosphaamidinate-supported magnesium hydride **47**, which was not isolated. Bulky ligand **28** was found to not form a homoleptic complex, presumably due its significant size. This is promising for potential applications of this LMgBu complex in cataylsis, as the formation of L_2Mg species is reported to be a catalyst deactivation pathway in similar amidinate chemistry.[5]

Heteroleptic n-butyl complexes **29**, **30** and **34** were found to be highly active catalysts for the ring-opening polymerisation of *rac*-lactide. Initiation by Tipp-substituted **30** produces polymer chains of uniform chain lengths in the presence of MeOH as a co-initiator (Đ = 1.02), with a slight isotactic preference (P_i = 0.55).

Deprotonation of phosphaamidines using ^{n}BuLi was shown to form lithiated complexes **40**, **41** and **43**, and the bonding mode of the ligand (lithium amide versus lithium phosphanide) was found to depend on the phosphaamidine. In the case of **43**, a mixture of isomers was isolated, with the lithium phosphanide being the major species.

Complexation of the lithium cation with 12-crown-4 allowed **42** to be crystallised and the delocalisation of the central P-C-N unit was established by close inspection of the solid-state structure bond lengths, which was further supported by DFT calculations. Confirmation of the delocalisation in the anionic phosphaamidinate shows that these ligands could have potential in coordination chemistry, and could be applied more generally across the metallic periodic table, as β-diketiminate and amidinate ligands have been.

Generation of mesityl-substituted lithiated complex **40** and subsequent reaction with $MgI_2(OEt_2)_2$ allowed for a salt metathesis reaction where the phosphaamidinate ligand was transferred to the magnesium centre to form unstable magnesium halide **38**. Using the same lithiated complex **40**, two phosphaamidinate units were transferred to an aluminium centre, forming monohydride **44**, *via* lithium aluminate **45** as an intermediate. Observation of this intermediate shows that ligand **20** does not provide enough kinetic stabilisation to support an isolable aluminium dihydride. Reaction of the isomeric mixture of **44** with $Me_3N.AlH_3$ produces a new product by ^{31}P NMR spectroscopy, which is thought to be aluminium dihydride **43**, however this product was not isolated on a preparative scale.

Amidinato aluminium hydrides can be deprotonated to give cationic aluminium centres which are effective polymerisation catalysts,[6] and aluminium hydrides of the type R_2AlH are capable of catalytic hydroboration,[7] so exploration of **44** and **43** into these fields would be of interest.

Whist these complexes were challenging to isolate, this general principle of ligand transfer mediated by a lithium cation further demonstrates that phosphaamidinate ligands could be applied to a vast number of organometallic and main-group topics.

6.3 Final Perspective

The idea that low valent aluminium is a chemical curiosity is slowly being cast aside, as more knowledge about this reactive oxidation state is being discovered. This thesis was driven by a need to understand the unique characteristics of low oxidation state aluminium and its derived compounds, and in what ways they differ from the more ubiquitous Al(III).

This work has provided mechanistic insight which can be used in the future to design novel aluminium systems capable of reductive elimination, a significant step towards the development of transition metal redox-type catalysis with aluminium. Combining this with the aluminium-mediated C=C coupling described in chapter 3, it is clear that aluminium is capable of being more than a simple Lewis acid. Using the foundations laid here, perhaps the full potential of low valent aluminium can be developed both in molecular transformation, and perhaps more ambitiously, in bond forming catalysis.

The chemistry of phosphaamidines has been greatly expanded, and it has been shown that these ligands can be complexed to lithium, magnesium and aluminium. The demonstration of a useful application of the novel phosphaamidinate magnesium complexes in the polymerisation of *rac*-lactide shows this fledging ligand class worthy of further exploration. Use of these ligands as supports for main group systems could uncover new, and perhaps catalytic, activity. Lithiated phosphaamidines were shown here to be effective ligand transfer reagents to aluminium hydride centres, a process which could be widely applied across the periodic table.

Given that the bulky phosphaamidine was found here to support a monomeric, three-coordinate magnesium centre, a possible future direction could explore this ligand as a support for low valent species, be it magnesium, aluminium or some other main-group element.

6.4 References

1 D. Weiss, T. Steinke, M. Winter, R. A. Fischer, N. Frohlich, J. Uddin and G. Frenking, *Organometallics*, 2000, **19**, 4583–4588.

2 A. Kempter, C. Gemel and R. A. Fischer, *Chem. Eur. J.*, 2007, **13**, 2990–3000.

3 K. Nagata, T. Agou and N. Tokitoh, *Angew. Chem. Int. Ed.*, 2014, **53**, 3881–3884.

4 P. Bag, A. Porzelt, P. J. Altmann and S. Inoue, *J. Am. Chem. Soc.*, 2017, **139**, 14384–14387.

5 R. J. Schwamm, B. M. Day, E. Mansfield, Natalie, W. Knowelden, P. B. Hitchcock and M. P. Coles, *Dalton Trans.*, 2014, **43**, 14302–14314.

6 J. A. R. Schmidt and J. Arnold, *Organometallics*, 2002, **21**, 2306–2313.

7 A. Bismuto, S. P. Thomas and M. J. Cowley, *Angew. Chem. Int. Ed.*, 2016, **55**, 15356–15359.

Chapter 7:

Experimental

7. Experimental

7.1 General Considerations

All manipulations were carried out under an atmosphere of argon using standard Schlenk or dry-glovebox techniques, except compounds **25** and **26**. Benzene, toluene, hexane, pentane, dimethyoxyethane, diethylether and tetrahydrofuran were dried under argon over sodium dispersion and benzophenone and distilled before use. C_6D_6, Tol-d_8 and THF-d_8 were dried over a potassium mirror and distilled. CH_2Cl_2, CD_2Cl_2 and $CDCl_3$ were dried over CaH_2 and distilled. Methanol was dried over magnesium turnings and distilled. All solvents (protonated and deuterated) were stored over activated molecular sieves.

NMR spectra were recorded on a Bruker PRO 500 MHz, AVA 500 MHz or AVA 600 MHz spectrometer. ^{1}H and ^{13}C spectra were referenced to residual solvent signals, and ^{27}Al spectra were referenced externally to $Al(NO_3)_3$ in D_2O (1.1 M). Unless indicated, NMR spectra were acquired at 300 K.

Elemental analyses were determined externally by Stephen Boyer at London Metropolitan University. X-ray diffraction experiments were performed by Dr Gary Nichol at the University of Edinburgh.

The following starting materials were prepared using literature procedures: Cp^*_2AlH,[1] $(Cp^*Al)_4$,[1] 9-methylfluorene,[2] (*N*-mesityl)(tert-butyl)carbonitrilium triflate,[3] (*N*-(2,6-diisopropylphenyl))(tert-butyl)carbonitrilium triflate,[4] $MesPH_2$,[5] $TippPH_2$,[6] Mes^*PH_2,[7] 2,6-bis(diphenylmethyl)-4-methyl aniline,[8] $Me_3N.AlH_3$,[9] tetramethylimidazolylidene[10] and diisopropyldimethyl imidazolylidene.[10] Triethylamine and trimethylsilylchloride were stored over activated sieves under inert atmosphere. *Rac*-lactide was recrystallised from toluene and dried in high vacuum prior to use. Other reagents were purchased from commercial suppliers and used without further purification.

List of Numbered Compounds

1 Cp^*_2AlH

2

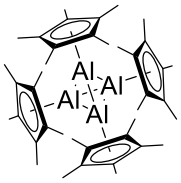

3

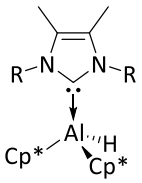

4

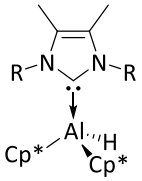

5

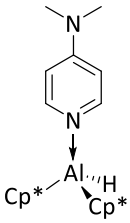

6

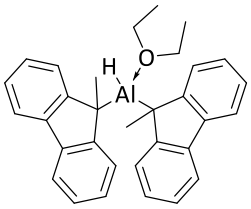

7 Structure Unknown

8

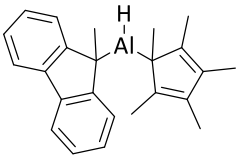

Not Formed

9

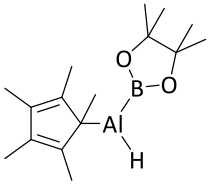

Not Isolated

10

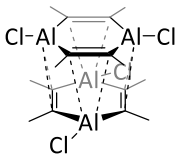

11

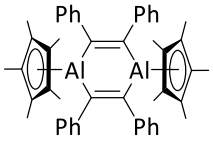

12

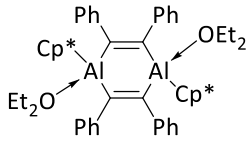

Not Isolated

13

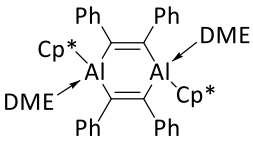

Not Isolated

14

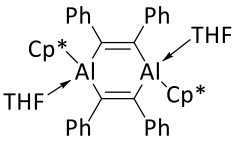

Not Isolated

15

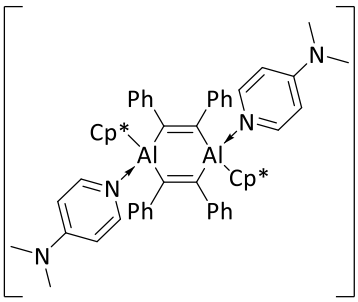

unstable

16

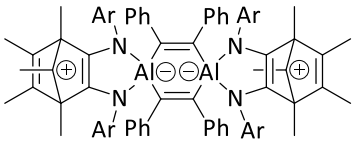

17

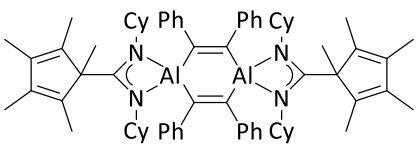

18

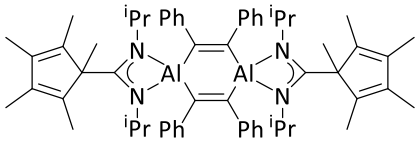

19

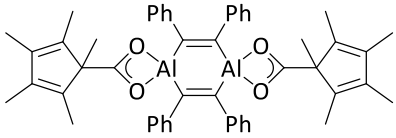

20

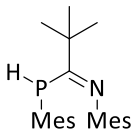

21

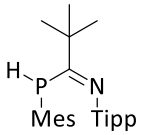

22

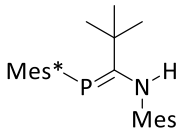

23

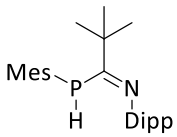

24

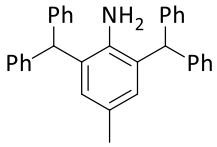

25

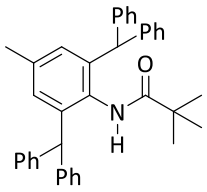

26

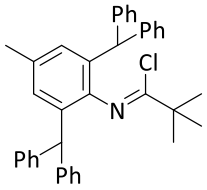

27

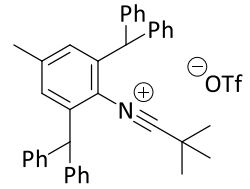

28

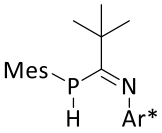

29

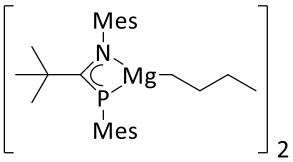

30

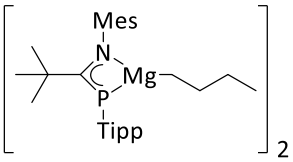

31

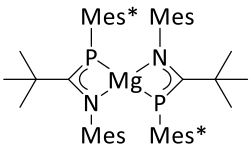

32

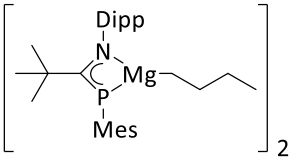

Not Isolated

33

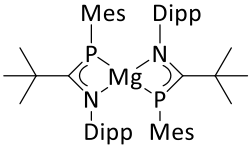

34

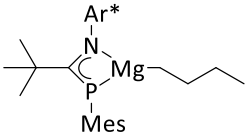

35

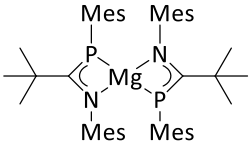

36

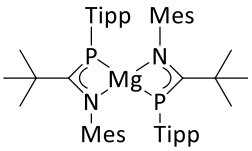

37

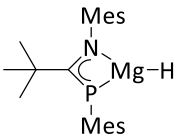

Not Observed

38

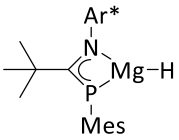

Not Isolated

39

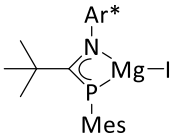

Not Isolated

40

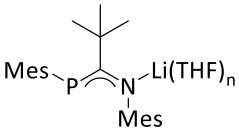

41

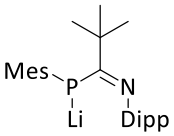

42

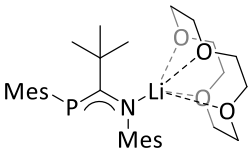

43b

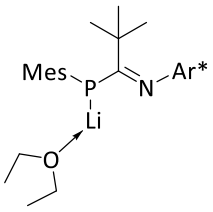

43b

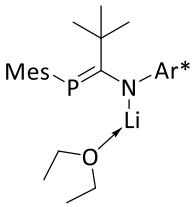

44

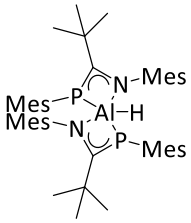

45

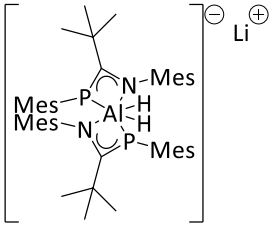

46

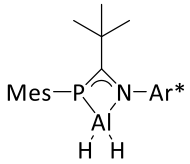

Not Isolated

7.2 Reductive Elimination Kinetic Data

The reductive elimination of Cp*H from Cp^*_2AlH was followed by ^1H NMR at a range of temperatures, using tritertbutylbenzene as an internal standard to calculate concentrations by integration. Rate constants were obtained by fitting the experimentally determined temporal concentration data to the model shown in Scheme 118 using the software package DynaFit4.[11]

Scheme 118 *Reductive elimination of Cp*H from Cp^*_2AlH to form Cp*Al*

General Procedure: solutions of tritertbutylbenzene (15.4 - 19.8 mM) and Cp^*_2AlH ($[\mathbf{1}]_0$; 16.6 – 41.2 mM) in toluene-d_8 were prepared and stored at –30 °C, and used with 48 hours. 0.5 mL of stock solution was used for each experiment. Concentrations were kept low to avoid precipitation of $Cp^*_4Al_4$ during data collection.

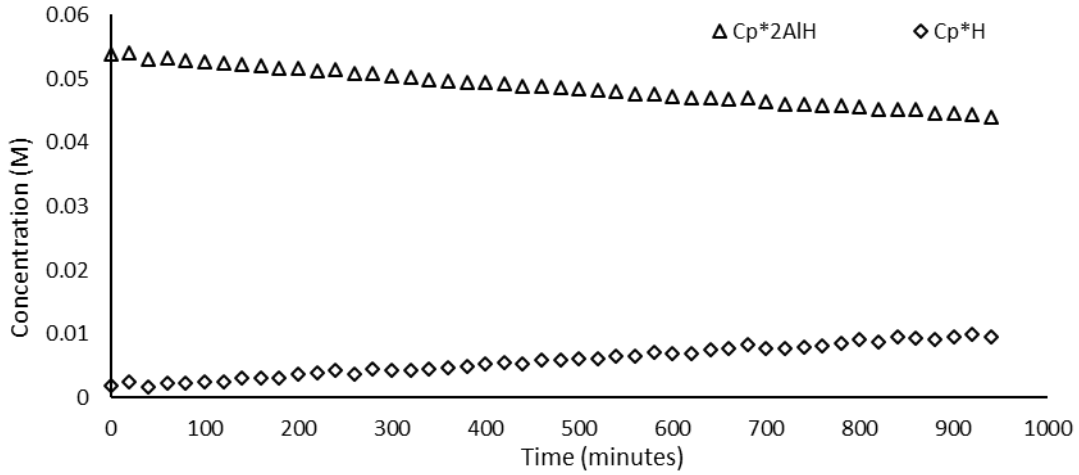

Figure 88 *Reaction progression at 313 K. $[\mathbf{1}]_0$ = 16.6 mM*

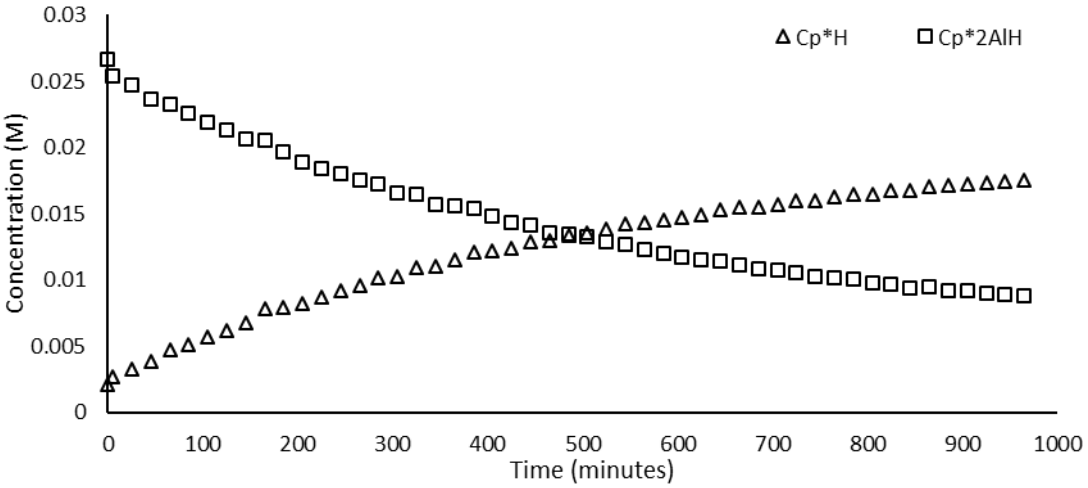

Figure 89 *Reaction progression at 333 K. [**1**]$_0$ = 36.8 mM.*

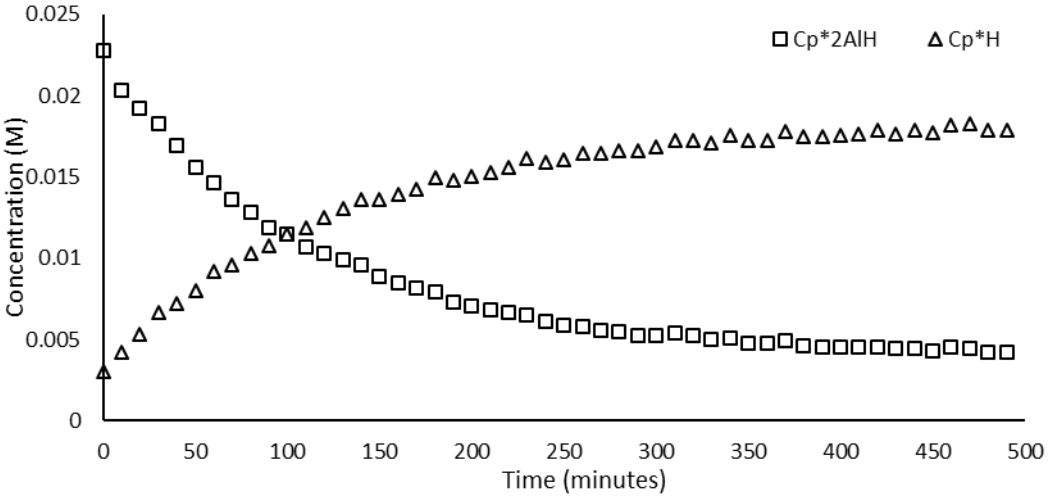

Figure 90 *Reaction progression at 343 K. [**1**]$_0$ = 26.8 mM.*

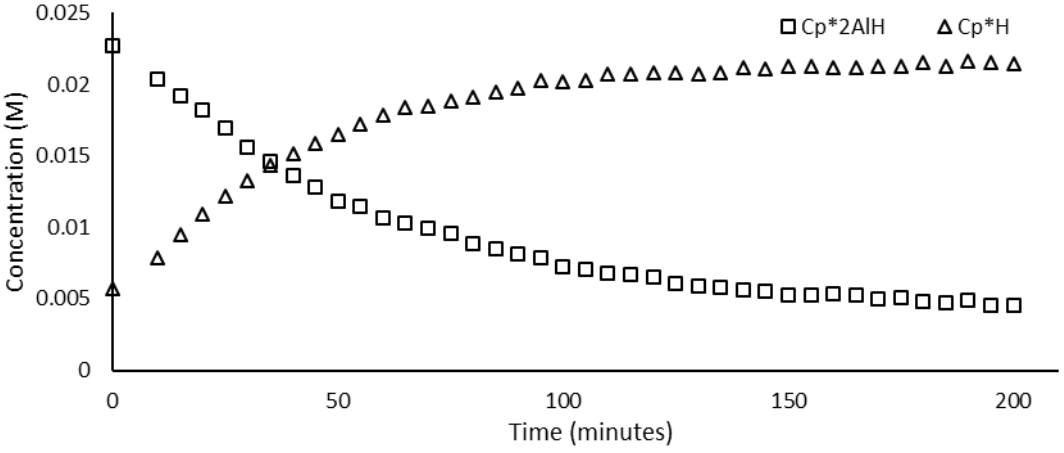

Figure 91 *Reaction progression at 353 K. [**1**]$_0$ = 36.8 mM.*

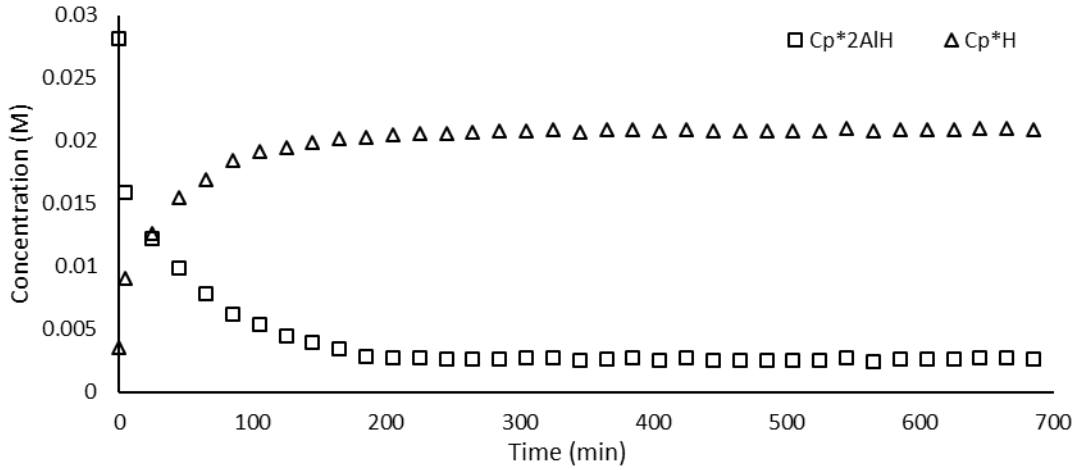

Figure 92 *Reaction progression at 363 K. [**1**]$_0$ = 41.2 mM*

7.3 Preparation of Novel Compounds

7.3.1 Preparation of ^{Me}IMe.Cp$_2$AlH **3***

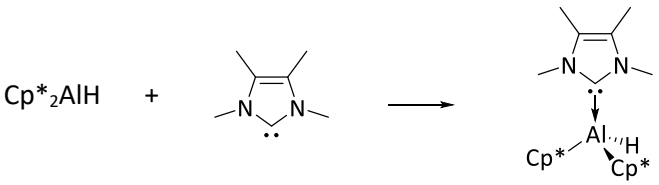

A mixture of tetramethylimidazolylidene (56.0 mg, 0.45 mmol) and Cp*$_2$AlH (133.8 mg, 0.45 mmol) was dissolved in C_6H_6 (10 mL) and stirred for 2 hours at room temperature. The volatiles were removed to give an orange powder (123.3 mg, 0.29 mmol, 65.2 %). Melting point: 165-168°C. ^{1}H NMR (500.2 MHz, 298 K, C_6D_6): δ = 3.27 (s, 3H, -(NHC)CC*H*$_3$), 2.64 (s, 3H, -(NHC)CC*H*$_3$), 1.98 (s, 30H, -CC*H*$_3$), 1.29 (s, 3H, -NC*H*$_3$), 1.15 (s, 3H, -NC*H*$_3$). ^{13}C{^{1}H} NMR (125.8 MHz, 298 K, C_6D_6): δ = 124.35 (-(NHC)*C*CH$_3$), 123.15 (-(NHC)*C*CH$_3$), 118.42 (-*C*CH$_3$), 34.88 (-NCH$_3$), 32.89 (-NCH$_3$), 12.73 (-CCH$_3$), 7.44 (-(NHC)CCH$_3$) 7.34 (-(NHC)CCH$_3$) *(carbene NCN carbon is not observed)*. ^{27}Al NMR (130.3 MHz, 298 K, C_6D_6): δ = 136.9. High Res Mass Spec (EI): m/z = 422.32606 (calculated 422.32362 for Cp*$_2$AlH[NHC]$^+$). Despite repeated attempts, satisfactory elemental analysis was not possible, most likely due to incomplete/poor combustion: Anal: Calcd. for $C_{27}H_{43}AlN_2$: C, 76.73; H, 10.26; N, 6.63. Found: C, 69.98; H, 8.90; N, 6.33%.

7.3.2 Preparation of ^{Me}I^{i}Pr.Cp$_2$AlH **4***

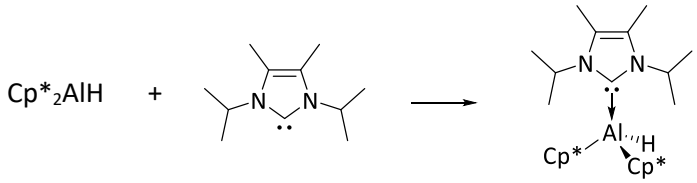

A mixture of diisopropyldimethyl imidazolylidene (78.2 mg, 0.43 mmol) and Cp*$_2$AlH (127.2 mg, 0.43 mmol) were dissolved in C_6H_6 (5 mL) and stirred for 1.5 hours at room temperature. The white precipitate that formed was isolated by filtration, dried in vacuo and then washed with hexane (3 mL). The microcrystalline white solid that so obtained was dried in vacuo (98.2 mg, 0.20 mmol, 47.1 %). Melting point: 154-156 °C. ^{1}H NMR (500.2

MHz, 298 K, C_6D_6): δ = 6.08 (broad s, 1H, -C*H*$(CH_3)_2$), 3.59 (broad s, 1H, -C*H*$(CH_3)_2$), 2.04 (s, 30H, -CC*H*$_3$), 1.45 (s, 6H, -(NHC)CC*H*$_3$). 1.12 (d, 12H, -CH(C*H*$_3)_2$). ^{27}Al NMR (130.3 MHz, 298 K, C_6D_6): 137.5 ppm. Due to poor solubility a ^{13}C NMR spectrum with satisfactory signal:noise ratio could not be obtained. High Res Mass Spec (EI): m/z = 298.22476 (calculated 298.22357 for Cp*$_2$AlH$^+$), 180.16219 (calculated 180.16210 for NHC$^+$). Anal: Calcd. for $C_{31}H_4AlN_2$: C, 77.77; H, 10.74; N, 5.64. Found: C, 77.55; H, 10.62; N, 5.85%.

7.3.3 Preparation of DMAP.Cp$_2$AlH* ***5***

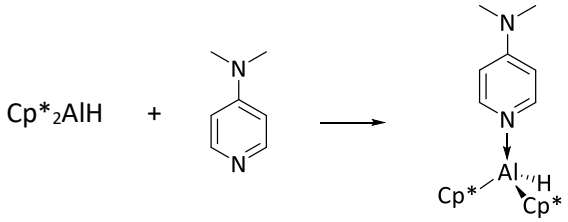

A solution of dimethylaminopyridine (50.6 mg, 0.41 mmol) in C_6H_6 was added dropwise to a solution of Cp*$_2$AlH (118.9 mg, 0.39 mmol) in C_6H_6. The resulting clear yellow solution was stirred for 2.5 hours. The volatiles were removed to give a white solid (115.1 mg, 0.27 mmol, 68.8 %). Melting point: 176-177°C. ^{1}H NMR (500.2 MHz, 298 K, C_6D_6): δ = 7.52 (d, ^3J = 6.0 Hz, 2H, -Ar*H*), 5.59 (d, ^3J = 7.0 Hz, 2H, -Ar*H*), 2.01 (s, 30H, -CC*H*$_3$), 1.92 (s, 6H, -N(C*H*$_3)_2$). ^{13}C NMR (125.8 MHz, 298 K, C_6D_6): δ = 154.87 (quaternary *C*), 146.07 (-Ar*C*), 118.53 (-*C*CH$_3$), 103.93 (-NAr*C*H), 37.79 (-NCH$_3$), 12.47 (-CCH$_3$). ^{27}Al NMR (130.3 MHz, a298 K, C_6D_6): δ = 146.7 (broad). High Res Mass Spec (EI): m/z = 298.22328 (calculated 298.22357 for Cp*$_2$AlH$^+$), 122.08470 (calculated 122.08385 for DMAP$^+$). Despite repeated attempts, satisfactory elemental analysis was not possible, most likely due to incomplete/poor combustion: Anal. Calcd. for $C_{27}H_{41}AlN_2$: C, 77.10; H, 9.83; N, 6.66. Found: C, 31.38; H, 3.86; N, 2.85%.

7.3.4 Preparation of bis-fluorenyl aluminium hydride etherate ***6***

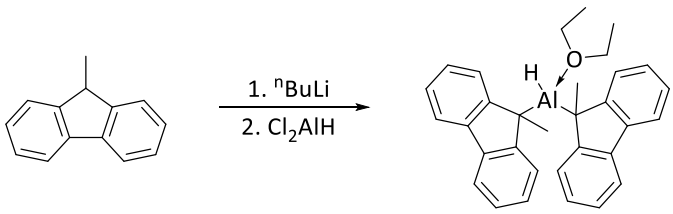

Aluminium chloride (639.3 mg, 4.79 mmol, 3.0 eq) was cooled to – 78 °C before being dissolved in Et_2O. A solution of $LiAlH_4$ (60.6 mg, 1.59 mmol, 1.0 eq) in Et_2O was added slowly at -78 °C, and the solution warmed to room temperature over 2 hours. The cloudy suspension was stirred for a further hour at room temperature before being cooled to -78 °C. Separately, 9-methylfluorene (2.30 g, 12.8 mmol, 8.0 eq) was dissolved in Et_2O and cooled to – 78 °C and ^{n}BuLi (5.25 mL, 2.5 M in hexanes, 13.1 mmol. 8.2 eq) was added. The solution was immediately warmed to room temperature and, once the solution had a bright red colour, was added dropwise to the cooled solution of Cl_2AlH. The reaction mixture was returned to room temperature and stirred for 4 hours. The volatiles were removed to an orange waxy solid, which was suspended in hexane and heated to the point of reflux, then filtered hot. The filtrate was concentrated and cooled to -20 °C to precipitate a peach coloured solid of the title product (910.0 mg, 2.10 mmol, 32.9 %). Melting Point: 134-136 °C. ^{1}H NMR (500 MHz, C_6D_6) δ = 7.83 – 7.80 (m, 2H, ArH), 7.77 (dt, *J* = 7.3, 1.1 Hz, 3H, ArH), 7.50 – 7.46 (m, 1H, ArH), 7.29 – 7.18 (m, 7H, ArH), 4.30 (broad s, 1H, Al-H), 2.27 (q, *J* = 7.1 Hz, 4H, O*C*H_2CH$_3$), 1.60 (s, 6H, CCH_3), -0.04 (t, *J* = 7.1 Hz, 6H, OCH$_2$*C*H_3). ^{13}C NMR (126 MHz, C_6D_6) δ = 153.45 (*C*CH$_3$) 152.69 (*C*CH$_3$), 138.15 (quaternary ArC), 138.00 (quaternary ArC), 125.57 (ArC), 125.44 (ArC), 123.18 (ArC), 123.08 (ArC), 123.01 (ArC), 119.61 (ArC), 119.45(ArC), 68.60 (O*C*H_2CH$_3$), 17.66 (C*C*H$_3$), 12.38 (OCH$_2$*C*H$_3$) ppm. ^{27}Al NMR = no signal observed. High Res Mass Spec (EI): m/z = 460.23413 $[C_{32}H_{33}OAl]^+$

*7.3.5 Reaction of (Cp*Al)$_4$ with HBpin*

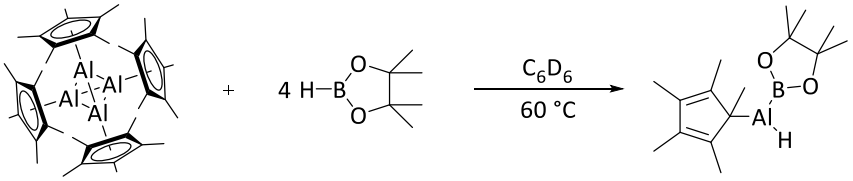

NMR Scale: (Cp*Al)$_4$ (14.7 mg, 90.6 µmol) was suspended in C_6D_6 (approx. 0.5 mL) and HBpin (13 µL, 89.5 µmol, 1 eq) was added. The mixture was heated to 60 °C for 3 days, after which time all solid material had dissolved to give a clear bright yellow solution. ^{11}B NMR spectroscopy showed full consumption of HBpin and the formation of a major new species at δ = 33.6. ^{27}Al NMR showed full compsumption of (Cp*Al)$_4$ with no new peaks noted.

Preparative Scale: (Cp*Al)$_4$ (48.9 mg, 0.3 mmol) was suspended in toluene (approx. 2 mL) and HBpin (90 µL, 0.6 µmol, 2 eq) was added. The yellow suspension was heated to 80 °C for 48 hours, after which time the solid had dissolved. The volatiles were removed to a yellow residue. Attempts to purify the residue through recrystalisation caused decomposition to many products by ^{11}B NMR spectroscopy.

*7.3.6 Preparation of 1,4-dialumininacyclohexadiene derivative **11***

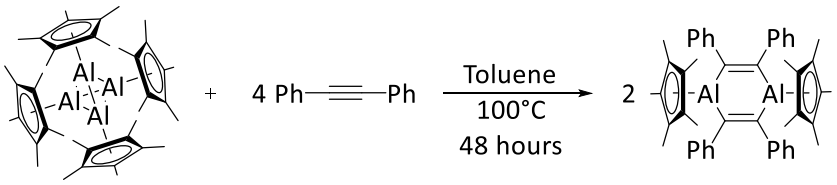

(Cp*Al)$_4$ (1.07 g, 1.65 mmol) and diphenylacetylene (1.16 g, 6.53 mmol, 4.0 eq) were weighed into a single flask and suspended in toluene (40 mL). The suspension was heated to 100 °C at which temperature all material dissolved to give a yellow solution. After two days heating the volatiles were removed from the dark orange solution. The residue was washed with hexane (5 mL) to give clean product as beige powder. (1.85 g, 2.72 mmol, 83.3 %). Melting Point: 258-260 °C (colour change to bright red upon melting). ^{1}H NMR (500.2 MHz, 298 K, C_6D_6): *δ* = 7.40 – 6.97 (m, 16H, -Ph), 6.84 – 6.75 (m, 4H, - *p*C*H*), 1.71 (s, 30H, -CC*H*$_3$) ppm. ^{13}C NMR (125.8 MHz, 298 K, C_6D_6): *δ* = 148.36 (-Al*C*=*C*Al), 128.06 (-Ph), 127.95 (-*i*Ph), 127.05 (-Ph), 123.67 (-*p*Ph), 115.88 (-*C*CH$_3$), 10.63 (-C*C*H$_3$) ppm. ^{27}Al NMR gave no

signal. Mass Spec (EI): m/z = 680.355469 $[C_{48}H_{50}Al_2]^+$. Anal: Calcd. for $C_{48}H_{50}Al_2$ Expected: C, 84.67; H, 7.40; Found: C, 80.91; H, 8.18.

*7.3.7 Reactions of **11** with ethers*

Compound **11** (ca. 20 µmol) was dissolved in C_6D_6 and two equivalents (ca. 40 µmol) of the appropriate ethereal solvent was added. The NMR of the resulting solutions is shown in main text (Figure 28, page 78), showing shifted signals indicating adduct formation.

Diethylether solvate ^{1}H NMR (500.2 MHz, 298 K, C_6D_6): δ = 7.02 – 6.97 (m, 16H, ArH), 6.85 – 6.75 (m, 4H, *p*ArH), 3.24 (q, J = 6.9 Hz, 8H, OCH_2CH_3), 1.74 (s, 30H, Cp*), 1.05 (t, J = 6.9 Hz, 12H, OCH_2CH_3).

Dimethoxyethane solvate ^{1}H NMR (500.2 MHz, 298 K, C_6D_6): δ = 7.03 – 6.98 (m, 8H, ArH), 6.98 – 6.93 (m, 8H, ArH), 6.83 (tt, J = 7.2, 1.4 Hz, 4H, *p*ArH), 3.14 (s, 12H, CH_2OCH_3), 2.97 (s, 18H, CH_2OCH_3), 1.90 (s, 30H, Cp*).

Tetrahydrofuran solvate ^{1}H NMR (500.2 MHz, 298 K, C_6D_6): δ = 7.04 – 6.98 (m, 16H, ArH), 6.87 – 6.80 (m, 4H, *p*ArH), 3.55 (s, 16H, OCH_2CH_2), 1.99 (s, 30H, Cp*), 1.12 (s, 16H, OCH_2CH_2).

*7.3.8 Reaction of **11** with 2,6-dimethylphenylisonitrile (**16**)*

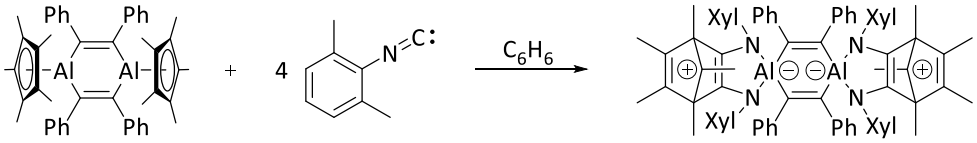

Compound **11** (216.7 mg, 0.32 mmol) was dissolved in C_6H_6 (0.5 mL) and a solution of 2,6, dimethyl isocyanide (167.6 mg, 1.27 mmol, 4 eq) in C_6H_6 (1.5 mL) was added dropwise. The dark red solution was left to stand without stirring for 48 hours. The precipitated dark red solid was filtered and dried (130.6 mg, 0.10 mmol, 32.0 %). Melting Point: Solid turned black at 160 °C, melting point >330 °C. ^{1}H NMR (601 MHz, 298 K, CD_2Cl_2): δ = 7.40 (s, C_6H_6), 7.19 (d, J = 7.3 Hz, 4H, Xylyl ArH), 7.03 (t, J = 7.3 Hz, 4H, Xylyl ArH), 6.95 – 6.91 (m, 4H, Xylyl

ArH), 6.75 (d, J = 8.2 Hz, 4H, PhH), 6.68 (d, J = 8.2 Hz, 4H, PhH), 6.55 – 6.50 (m, 4H, PhH), 6.46 (d, J = 7.3 Hz, 4H, PhH), 5.73 (d, J = 7.3 Hz, 4H, PhH), 2.71 (s, 12H, Xylyl-Me), 1.50 (s, 12H, Xylyl-Me), 1.41 (s, 12H, C=CCH_3), 0.58 (s, 12H, C^+CCH_3), 0.26 (s, 6H, C^+CH_3) ppm. ^{13}C NMR (125.8 MHz, 298 K, CD_2Cl_2): δ = 151.23 (d, J = 11.1 Hz, C^+), 146.63 (Al-*C*=*C*-Al), 136.55 (quaternary C), 133.97 (quaternary C), 133.57 (N-*C*=*C*-N), 133.13 (xylyl-*C*CH_3), 129.57 (xylyl-*m*PhH), 129.10 (xylyl-*m*PhH), 128.28 (xylyl-*m*PhH), 127.93 (phenyl-*m*PhH), 127.69 (phenyl-*m*PhH), 126.09 (phenyl-*o*PhH), 125.79 (phenyl-*o*PhH), 122.85 (xylyl-*p*PhH), 121.66 (phenyl-*p*PhH), 121.34 (phenyl-*p*PhH), 96.23 (C^+CCH_3), 61.83 (H_3CC=CCH_3), 23.28 (xylyl-*C*H_3), 20.55 (xylyl-*C*H_3), 11.12 (H_3CC=C*C*H_3), 8.90 (C^+CCH_3), 1.27 (C^+CH_3). ^{27}Al NMR gave no signal. High Res Mass Spec (EI): m/z = 1204.645859 $[C_{84}H_{86}N_4Al_2]^+$. Anal: Calcd. for $C_{48}H_{50}Al_2$ Expected: C, 84.21; H, 7.22; N 4.36; Found: C, 77.44; H, 7.00, N, 5.60.

*7.3.9 Reaction of **11** with dicyclohexylcarbodiimide (**17**)*

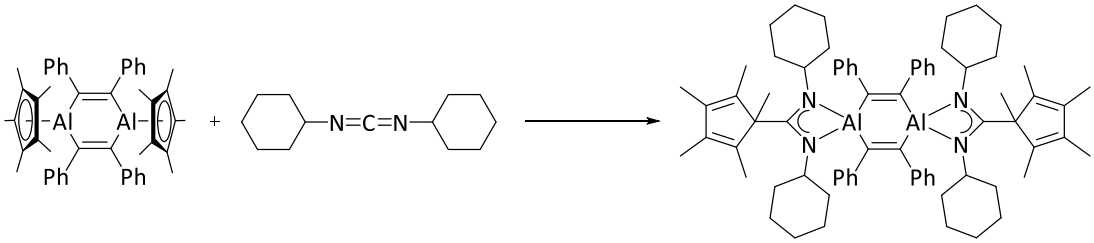

Compound **11** (203.4 mg, 0.29 mmol) was dissolved in toluene (15 mL) and cooled to -60° C. A solution of dicyclohexylcarbodiimide (123.3 mg, 0.60 mmol) in toluene (7 mL) was added dropwise, and the resulting solution stirred at -60°C for 1 hour. After warming to room temperature the volatiles were removed and the resulting oily residue was washed with hexane (5 mL) to a white powder. This was dried at high vacuum for 18 hours. ^{1}H NMR (500 MHz, C_6D_6) δ 7.37 – 7.30 (m, 4H, Ph), 7.10 (tt, J = 7.7, 2.1 Hz, 4H, Ph), 6.91 – 6.85 (m, 2H, Ph), 3.81 – 3.59 (m, 2H, NC*H*), 2.94 – 2.74 (m, 2H, Cy), 2.23 – 2.01 (m, 2H, Cy), 1.89 – 1.59 (m, 2H, Cy), 1.55 (s, 6H, Cp*), 1.51 (s, 3H, Cp*), 1.47 (s, 6H, Cp*), 1.43-1.27 (m, 4H, Cy), 1.18 – 0.90 (m, 6H, Cy) ppm. ^{13}C NMR (126 MHz, C_6D_6) δ 174.86 (N-C-N), 150.45 (Ph*C*=*C*Ph), 142.57 (ipso-PhC), 134.67 ($NCCH_3$), 129.20 (PhH), 126.87 (PhH), 122.96 (*p*PhH), 89.80 (H_3CC=CCH_3), 64.94 (H_3CC=CCH_3), 55.36 (NCH), 53.98 (NCH), 53.80 (NCH), 52.23 (NCH), 37.17 (Cy-CH_2), 36.62 (Cy-CH_2), 36.23(Cy-CH_2), 35.02 (Cy-CH_2), 26.54 (Cy-CH_2), 26.41 (Cy-CH_2), 25.93 (Cy-CH_2), 25.81 (Cy-CH_2), 25.65 (Cy-CH_2), 25.43 (Cy-CH_2), 25.10 (Cy-CH_2), 24.49 (Cy-CH_2), 10.67 (Cp*) ppm. ^{27}Al NMR gave no signal.

*7.3.10 Reaction of **11** with diisopropylcarbodiimide (**18**)*

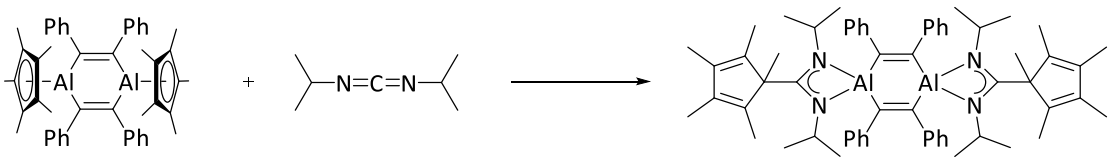

Compound **11** (189.1 mg, 0.277 mmol) was dissolved in hexane (25 mL) and cooled to -78°C. Diisopropylcarbodiimide (86 µL, 0.555 mmol, 2.0 eq) was added dropwise and the solution warmed to room temperature. After two hours the volume of the solution was reduced by half before filtration. The filtrate was stored at -20°C to give two crops of compound **17** (99.1 mg, 0.106 mmol, 38.2 %). Melting Point: 264-266 °C. ^{1}H NMR (500 MHz, C_6D_6) δ = 7.31 – 7.25 (m, 4H, PhH), 7.12 – 7.06 (m, 4H, PhH), 6.93 – 6.86 (m, 2H, *p*PhH), 4.14 – 3.94 (m, 1H, NC*H*$(CH_3)_3$), 3.33 – 3.16 (m, 1H, NC*H*$(CH_3)_3$), 1.51 – 1.46 (m, 12H, H_3CC=CCH_3), 1.26 (d, J = 6.1 Hz, 3H, NCH(CH_3)$_3$), 1.19 – 1.17 (m, 3H, CCH_3), 1.16 (d, J = 6.3 Hz, 3H, NCH(CH_3)$_3$) 1.07 (d, J = 6.1 Hz, 3H, NCH(CH_3)$_3$), 1.01 (d, J = 6.3 Hz, 3H, NCH(CH_3)$_3$). ^{13}C NMR (126 MHz, C_6D_6) δ = 174.81 (d, J = 3.6 Hz, N-C-N), 150.33 (d, J = 2.9 Hz, PhC=CPh), 141.97, (H_3C*C*=*C*CH_3), 141.70 (H_3C*C*=*C*CH_3), 134.73 (d, J = 1.6 Hz, ipso-PhC), 122.91 (d, J = 6.5 Hz, ArC), 126.99 (ArC), 122.91 (para-ArC), 64.68 (d, J = 12.8 Hz, NC*C*CH_3), 45.28 (N*C*H$(CH_3)_2$), 45.06 (N*C*H$(CH_3)_2$), 43.76 (N*C*H$(CH_3)_2$), 43.73 N*C*H$(CH_3)_2$), 26.95 (NCH(*C*$H_3)_2$), 26.41 (NCH(*C*$H_3)_2$), 26.17 (NCH(*C*$H_3)_2$), 25.85 (NCH(*C*$H_3)_2$), 23.00 (NC*C*CH_3) 22.34 (NC*C*CH_3), 10.61 (H_3*C*C=C*C*H_3). ^{27}Al NMR gave no signal. Elemental Analysis $C_{62}H_{78}Al_2N_4$ Expected C, 79.79; H, 8.42; N, 6.00; Found C, 79.63; H, 8.80; N, 5.94.

*7.3.11 Reaction of **11** with carbon dioxide (**19**)*

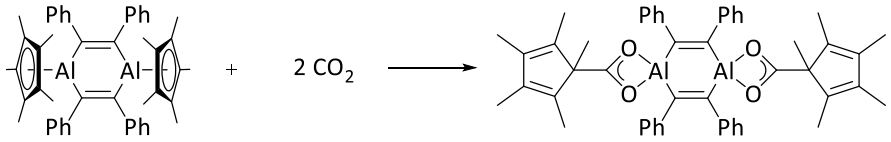

A solution of **11** (154.6 mg, 0.227 mmol) in C_6H_6 (15 mL) was degassed and backfilled with 0.5 bar CO_2. This was stored at room temperature for 18 hours without stirring. The resulting precipitate was filtered and washed with hexane (5 mL) and dried to a white

powder (71.6 mg, 0.093 mmol, 41.0 %). Melting Point: 252-254°C. ^{1}H NMR (500 MHz, THF-d_8) δ = 6.90 (t, J = 7.5 Hz, 2H, ArH), 6.80 – 6.73 (m, 3H, ArH), 1.80 (s, 3H, =CCH_3), 1.76 (s, 2H, CCH_3), 1.73 (s, 2H, =CCH_3). ^{13}C NMR (126 MHz, THF-d_8) δ = 180.51 (O-C-O), 149.24 (Ph*C*=*C*Ph), 137.95 (=*C*CH_3), 135.20 (=*C*CH_3), 131.29 (ipso-ArC), 127.63 (ArC), 126.67 (ArC), 122.40 (para-ArC), 63.85 (*C*CH_3), 18.15 (CCH_3), 10.31 (=CCH_3), 9.97 (=CCH_3). ^{27}Al NMR gave no signal. High Res Mass Spec (EI): m/z = 769.34127 ($[C_{50}H_{50}O_4Al_2]^+$). Elemental Analysis $C_{50}H_{50}O_4Al_2$ Expected C, 78.10; H, 6.55; Found C, 67.94; H, 7.14.

*7.3.12 Preparation of N-(2,2-dimethyl-1-(mesitylphosphino)propylidene)2,4,6-trimethylaniline **20***

Preparation and characterisation by Martin W. Stanford

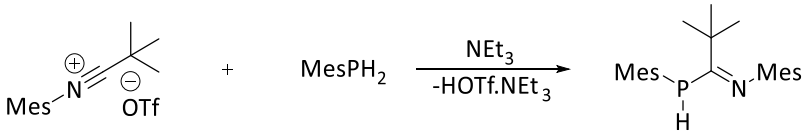

(N-mesityl)(tert-butyl)carbonitrilium triflate[3] (6.04 g, 17.1 mmol) was dissolved in dichloromethane (50 mL) and cooled to -78 °C. A solution of mesitylphosphine (2.59 g, 17.0 mmol, 1.0 eq) in dichloromethane (10 mL) was added, followed by triethylamine (2.40 mL, 17.2 mmol, 1.0 eq). The cold bath was removed after 5 minutes, and once the reaction reached room temperature it was stirred for a further 2 hours. The volatiles were removed and the residue extracted into pentane (75 mL) and filtered through neutral alumina pre-washed with pentane. The alumina was washed with pentane again and the combined pentane filtrates were combined and concentrated to ca. 5 mL and cooled to – 20 °C to yield off-white crystals of compound **20** over two crops (3.85 g, 10.8 mmol, 63.9 %). Melting Point: 76-78 °C. ^{1}H NMR (500.2 MHz, 298 K, C_6D_6): δ = 6.76 (s, 1H), 6.59 (s, 2H), 6.53 (d, *J* = 1.9 Hz, 1H), 4.96 (d, *J* = 245.2 Hz, 1H), 2.34 (s, 6H), 2.25 (s, 3H), 2.16 (s, 3H), 2.00 (d, *J* = 2.5 Hz, 6H), 1.33 (s, 9H) ppm. ^{13}C NMR (125.8 MHz, 300 K, C_6D_6): δ = 182.6 (d, *J* = 59 Hz, P-*C*=N), 146.9 (d, *J* = 7.5 Hz, N-*ipso*-*C*(Ar)), 143.9 (d, *J* = 14 Hz, P-*ipso*-*C*(Ar)), 139.1 (d, *J* = 1.3 Hz, P-*p*-*C*(Ar)-Me), 131.2 (s, N-*p*-*C*(Ar)-Me), 129.0 (s, NAr*C*-H), 128.7 (d, *J* = 4.6 Hz, PAr*C*-H), 128.5 (s, NAr-*m*-C-H), 126.4 (d, *J* = 14 Hz, P-*o*-*C*(Ar)-Me), 125.4 (s, N-*o*-*C*(Ar)-Me), 123.5 (d, *J* = 1.3 Hz, N-*o*-*C*(Ar)-Me), 44.7 (d, *J* = 14 Hz, *C*Me_3), 29.3 (d, *J* = 3.5 Hz, C(*C*H_3)$_3$), 24.0 (d, *J* = 13 Hz, PAr-*o*-*C*H_3), 20.7 (s, NAr-*o*-*C*H_3), 20.5 (s, NAr-*p*-*C*H_3), 18.0 (d, *J* = 4.2 Hz, NAr-*o*-*C*H_3), 17.7 (d, *J* = 8 Hz, PAr-*p*-*C*H_3) ppm. ^{31}P NMR (C_6D_6, 202.5 MHz, 300 K): δ = - 80.59 (d, J = 245.2 Hz) ppm.

High Res Mass Spec (EI): m/z = 353.226232 ($[C_{23}H_{22}NP]^+$). Elemental Analysis $C_{23}H_{32}NP$ Expected C, 78.15; H, 9.13; N, 3.96; Found C, 78.21; H, 9.23; N, 4.19.

*7.3.13 Preparation of N-(2,2-dimethyl-1-(triisopropylphenylphosphino)propylidene)2,4,6-trimethylaniline **21***

Preparation and characterisation by Martin W. Stanford

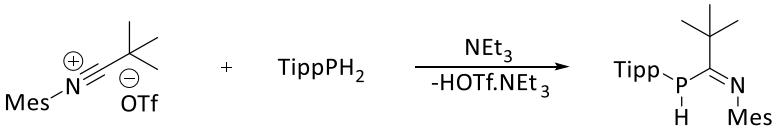

A solution of triisopropylphenylphosphine (2.93 g, 12.4 mmol) in dichloromethane (15 mL) was added dropwise via cannula over 5 minutes to a solution of (N-mesityl)(tert-butyl)carbonitrilium triflate (4.36 g, 12.4 mmol) in DCM (75 mL) at – 78 °C. After stirring at this temperature for 10 minutes, triethylamine (1.75 mL, 1.27 g, 12.5 mmol) was added dropwise over 2 minutes and the reaction was stirred for a further 10 minutes. Subsequently, the cold bath was removed and the reaction was stirred for an additional 2.5 hours giving a yellow/orange mixture. After removal of the volatiles, the solid was extracted with pentane (100 mL), filtered through neutral alumina and washed through with pentane (2 x 100 mL). The resultant solution was concentrated and crystallised at – 20 °C to afford yellow crystals of compound **21** (3.09 g, 7.06 mmol, 57 %). ^{1}H NMR (500.2 MHz, C_6D_6, 300 K): δ 7.06 (d, J = 2.4 Hz, 2H, PAr-H), 6.88 – 6.87 (m, 1H, NAr-H), 6.74 – 6.73 (m, 1H, NAr-H), 5.03 (d, J = 252 Hz, 1H, P-H), 3.48 (br s, 2H, o-CHMe2), 2.67 (sept, J = 6.9 Hz, 1H, p-$CHMe_2$), 2.28 (s, 3H, NAr-o-CH3), 2.23 (s, 3H, NAr-o-CH3), 2.17 (s, 3H, NAr-p-CH3), 1.29 (s, 9H, C(CH3)3), 1.26 (d, J = 6.8 Hz, 6H, o-CH(CH3)2), 1.15 (br d, J = 6.8 Hz, 6H, o-CH(CH3)2), 1.13 (dd, J = 6.9, 1.12 Hz, 6H, p-CH(CH3)2). ^{13}C NMR (125.8 MHz, C_6D_6, 300 K): δ 182.7 (d, *J* = 61 Hz, P-<u>C</u>=N), 154.5 (br s,P-*ipso*-<u>C</u>(Ar)), 151.5 (d, *J* = 1.2 Hz, PAr-*p*-<u>C</u>(Ar)-*i*Pr), 146.5 (d, *J* = 7.4 Hz, NAr-*ipso*-<u>C</u>(Ar)), 131.7 (s, NAr-*p*-<u>C</u>(Ar)-Me), 129.1 (s, NAr-*m*-<u>C</u>-H), 128.9 (s, NAr-*m*-<u>C</u>-H), 125.5 (d, *J* = 16 Hz, P-*o*-<u>C</u>(Ar)-*i*Pr), 124.9 (s, NAr-*o*-<u>C</u>(Ar)-Me), 124.7 (d, *J* = 2Hz, NAr-*o*-<u>C</u>(Ar)-Me), 121.5 (d, *J* = 4.6 Hz, PAr-*m*-<u>C</u>-H), 44.7 (d, *J* = 16 Hz, <u>C</u>Me_3), 34.3 (s, PAr-*p*-<u>C</u>Me_2), 33.0 (d, *J* = 15 Hz, PAr-*o*-<u>C</u>Me_2), 29.3 (d, *J* = 2.9 Hz, C(<u>C</u>H_3)$_3$), 24.3 (br s, PAr-*o*-C(<u>C</u>H_3)$_2$), 23.6 (br s, PAr-*o*-C(<u>C</u>H_3)$_2$), 23.6 (s, PAr-*p*-C(<u>C</u>H_3)$_2$), 20.5 (s, NAr-*p*-C(<u>C</u>H_3)$_2$), 18.1 (d, *J* = 13 Hz, NAr-*o*-C(<u>C</u>H_3)$_2$), 17.7 (d, *J* = 1.1 Hz, NAr-*o*-C(<u>C</u>H_3)$_2$). ^{31}P NMR (202.5 MHz, C_6D_6, 300 K): δ (ppm) –

88.9 (d, *J* = 252 Hz) High Res Mass Spec (EI) m/z: 437.320939 $[C_{29}H_{44}N_1P_1]^+$ Elemental Analysis Found: C, 79.42; H, 10.18; N, 3.22. Calc. for $C_{23}H_{32}NP$: C, 79.59; H, 10.13; N, 3.20.

7.3.14 Preparation of N-(2,2-dimethyl-1 tritertbutyllphenylphosphino)propylidene) 2,4,6-trimethylaniline ***22***

Characterisation by Martin W. Stanford

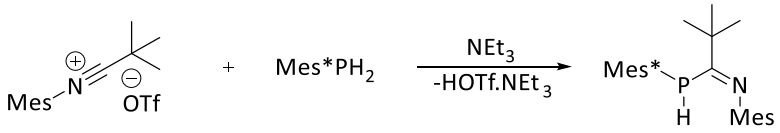

(N-mesityl)(tert-butyl)carbonitrilium triflate (2.21 g, 6.27 mmol, 1.1 eq) was dissolved in DCM (40 mL) and cooled to -78°C, and to this a solution of Mes^*PH_2 (1.51 g, 5.44 mmol, 1.0 eq) in DCM (25 mL) was added, followed by neat triethylamine (0.87 mL, 6.24 mmol, 1.1 eq). After 10 minutes the cold bath was removed and the solution warmed to room temperature and stirred for 2.5 hours. The volatiles were removed to give a sandy residue, which was extracted into toluene (80 mL) and passed through 5 cm of neutral alumina. The alumina was washed with more toluene (100 mL), and the combined filtrates were concentrated to 5 mL and cooled to -20°C to give beige crystals of compound **22** (1.92 g, 4.00 mmol, 73.5 %). Melting Point: 76-78 °C. A large number of signals were observed in the ^{1}H NMR and ^{13}C spectra, and so were unable to be confidently assigned. ^{31}P NMR (202.5 MHz, C_6D_6, 300 K): δ (ppm) 98.4 (d, J = 18 Hz, E-syn P=C, 41.3%), 80.2 (s, Z-anti P=C, 9.8%), –53.6 ppm (d, J = 253 Hz, Z-syn N=C 48.9%).

7.3.15 Preparation of N-(2,2-dimethyl-1-(mesitylphosphino)propylidene)2,6-diisopropylaniline ***23***

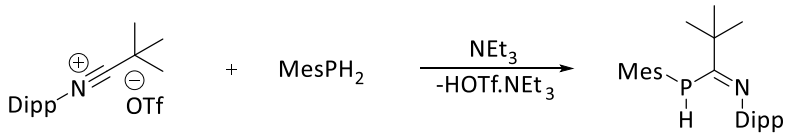

A solution of mesitylphosphine (1.59 g, 10.5 mmol) in DCM (5 mL) was added slowly to a solution of (*N*-(2,6-diisopropylphenyl))(tert-butyl)carbonitrilium triflate (4.53 g, 11.5 mmol, 1.1 eq) in DCM (80 mL) at -78 °C. This was followed by the slow addition of triethylamine (1.60 mL, 11.5 mmol, 1.1 eq). The solution was warmed to room temperature and stirred

for a further 2.5 hours. The volatiles were removed and the sticky residue extracted into hexane (100 mL) and filtered through 2 cm of neutral alumina. The alumina was then washed through with a further 20 mL hexane and the filtrates concentrated to around 30 mL and cooled to -20 °C to give white crystals of **23** in multiple crops (2.89 g, 7.31 mmol, 69.6 %). Melting Point: 83-85 °C. ^{1}H NMR (C_6D_6, 500.2 MHz, 300 K) δ = 7.19 – 7.15 (m, 1H, *covers solvent peak*), 7.06 – 6.97 (m, 1H), 6.65 – 6.60 (m, 2H), 4.89 (d, J_{H-P} = 249.3 Hz, 1H), 3.19 (sept, J_{H-H} = 6.9 Hz, 1H), 2.87 (sept, J_{H-H} = 6.9 Hz, 1H), 2.34 (s, 6H), 2.00 (s, 3H), 1.35 (d, *J* = 7.0 Hz, 3H), 1.31 (s, 9H), 1.26 (d, J_{H-H} = 6.6 Hz, 1H), 1.23 (d, J_{H-H} = 6.7 Hz, 3H), 1.18 (d, J_{H-H} = 6.8 Hz, 3H) ppm. ^{13}C NMR (C_6D_6, 125.8 MHz, 300 K) δ = 182.29 (d, J_{C-P} = 58.7 Hz), 146.78 (d, J_{C-P} = 7.8 Hz), 143.95 (d, J_{C-P} = 14.4 Hz), 139.22, 135.55, 134.00, 128.94 (d, J_{C-P} = 4.5 Hz), 126.63 (d, J_{C-P} = 15.5 Hz), 123.40 122.83 122.53 44.85 (d, J_{C-P} = 13.32 Hz), 28.96 (d, J_{C-P} = 2.8 Hz), 28.33 28.28 (d, J_{C-P} = 5.8 Hz), 23.99, 23.88, 23.79, 23.71, 21.11, 21.08 (d, J_{C-P} = 2.6 Hz), 20.63 ppm. ^{31}P NMR (C_6D_6, 202.5 MHz, 300 K) δ = – 78.59 (d, J_{P-H} = 249.3 Hz) ppm. Mass Spec (EI): m/z = 395.27364 ($[C_{26}H_{38}NP]^+$). Elemental Analysis: C, 78.95; H, 9.68; N, 3.54. Found: C, 78.28; H, 9.83; N, 3.74.

*7.3.16 Modified Preparation of Ar*N(H)C(=O)^{t}Bu (**25**)*

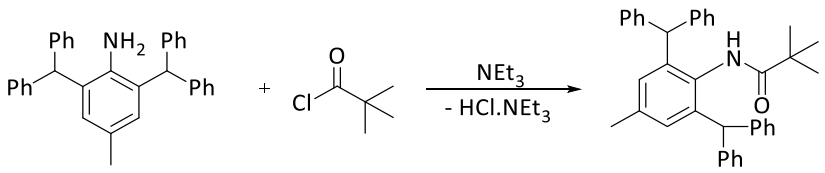

2,6-bis(diphenylmethyl)-4-methyl aniline (6.00 g, 13.6 mmol) was dissolved in dichloromethane (130 mL), and to this solution trimethylamine (1.90 mL, 13.6 mmol, 1.0 eq) and trimethylacetyl chloride (1.70 mL, 13.8 mmol, 1.0 eq) were added. The peach coloured solution was stirred for 4 hours, after which time there was a white precipitate. The volatiles were removed and the residue taken up into tetrahydrofuran (200 mL). The cloudy solution was washed with brine (300 mL) and the organic layers dried to give the product as a white solid (6.76 g, 12.9 mmol, 94.8 %). ^{1}H NMR (500 MHz, $CDCl_3$) δ 7.28 – 7.18 (m, 12H, ArH), 7.17 – 6.94 (m, 8H, ArH), 6.53 (s, 2H, *m*ArH), 6.00 (s, 1H, NH), 5.57 (s, 2H, C(*H*)Ph_2), 2.13 (s, 3H, *p*CH_3), 0.96 (s, 9H, C(C*H*$_3$)$_3$). NMR matches that of literature.[12]

*7.3.17 Modified Prepartation of Ar*N=C(Cl)^{t}Bu (**26**)*

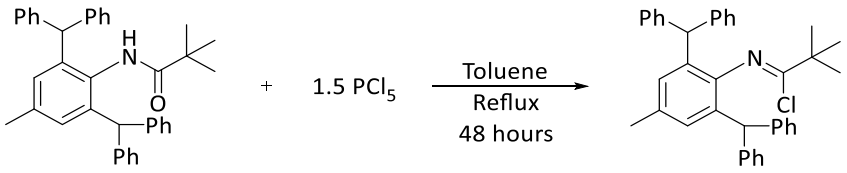

A mixture of **25** (4.00 g, 7.63 mmol) and PCl_5 (2.51 g, 12.0 mmol, 1.6 eq) was dissolved in toluene (125 mL), and the flask fitted with a condenser and two dreschel bottles, the second of which was filled with aqueous KOH. The setup was flushed with inert gas. The solution was heated to 110°C for 48 hours. After cooling under argon, the yellow suspension was filtered and the solid dried under vacuum to give a pale yellow powder (2.59 g, 4.77 mmol, 62.5 %). This was stored under an argon atmosphere to prevent hydrolysis. ^{1}H NMR (500 MHz, $CDCl_3$) δ 7.28 – 7.17 (m, 12H, ArH), 7.12 – 7.09 (m, 4H, ArH), 7.02 – 6.99 (m, 4H, ArH), 6.58 (s, 2H, *m*ArH), 5.38 (s, 2H, C(H)Ph_2), 2.14 (s, 3H, *p*CH_3), 1.08 (s, 9H, C(C*H*$_3$)$_3$). NMR matches that of literature.[12]

*7.3.18 Preparation of N-(2,2-dimethyl-1-(mesitylphosphino)propylidene)-2,6-bis(diphenylmethyl)-4-methyl aniline **28***

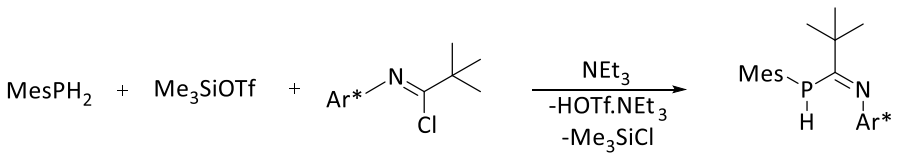

$MesPH_2$ (1.15 g, 7.55 mmol, 1.2 eq) in 10 mL toluene was added to a solution of **26** (3.40 g, 6.26 mmol, 1.0 eq) in 100 mL toluene, followed by triethylamine (1.05 mL, 7.53 mmol, 1.2 eq) and trimethylsilyl triflate (1.36 mL, 7.51 mmol, 1.2 eq). The suspension was then heated to 95°C for 18 hours, after which time all the solid had dissolved. The solution was cooled and passed through neutral alumina pre-eluted with toluene, and followed with a further 50 mL toluene. The combined filtrates were dried in vacuo, and the resulting white residue washed with hexane (15 mL) and dried thoroughly to give compound **28** (2.86 g, 4.35 mmol, 69 %). Melting Point: 214-215 °C. ^{1}H NMR (500 MHz, C_6D_6) δ = 7.44 (d, $J_{H\text{-}H}$ = 7.4 Hz, 2H, ArH), 7.39 (d, $J_{H\text{-}H}$ = 7.5 Hz, 2H, Ar*H*), 7.25 – 7.17 (m, 6H, ArH), 7.12 – 7.08 (m, 6H, ArH), 7.06 – 6.98 (m, 4H, ArH), 6.96 (s, 1H, N^{m}Ar*H*), 6.80 (s, 1H, N^{m}Ar*H*), 6.70 (s, 2H, PMesAr*H*), 5.93 (s,

1H, C*H*(Ph)$_2$), 5.82 (s, 1H, C*H*(Ph)$_2$), 5.19 (d, $J_{H\text{-}P}$ = 250.6 Hz, 1H, P*H*), 2.45 (s, 6H, PMes^{o}C*H*$_3$), 2.03 (s, 3H, NArC*H*$_3$), 1.90 (s, 3H, PMes^{p}C*H*$_3$), 0.85 (s, 9H, C(C*H*$_3$)$_3$) ppm. ^{13}C NMR (126 MHz, C_6D_6) δ = 180.95 (d, $J_{C\text{-}P}$ = 59.0 Hz, P-*C*=N), 145.60 (d, $J_{C\text{-}P}$ = 8.6 Hz, PMes^i*C*), 144.75 (NPh^{i}C), 144.22 (Ar), 144.09 (d, $J_{C\text{-}P}$ = 7.5 Hz, PMes^p*C*), 143.18 (Ar), 139.70 (NPh^{p}Ar), 137.50 (NPh^{o}Ar), 131.41 (Ar), 130.42 (Ar), 130.26 (d, $J_{C\text{-}P}$ = 3.0 Hz, PMes^{o}C), 130.19 (Ar), 129.68 (Ar), 129.44 (N^{m}Ar), 129.33 (N^{m}Ar) , 129.24 (PMes^{m}C), 128.95 (Ar), 128.27 (Ar), 128.18 (Ar), 126.20 (d, *J* = 8.6 Hz, Ar), 125.97 (d, $J_{C\text{-}P}$ = 3.6 Hz, Ar), 125.32 (Ar), 51.89 (d, $J_{C\text{-}P}$ = 2.0 Hz, *C*(Ph)$_2$), 45.07 (*C*(CH$_3$)$_3$), 27.89 (C(*C*H$_3$)$_3$), 24.21 (d, $J_{C\text{-}P}$ = 12.9 Hz, PMes^{m}CH$_3$), 21.07 (NPh^{p}CH$_3$), 20.79 (d, $J_{C\text{-}P}$ = 16.6 Hz, PMes^{p}CH$_3$). ^{31}P NMR (202 MHz, C_6D_6) δ = -74.94 (d, *J* = 249.8 Hz) ppm. Elemental Analysis: Expected C, 85.81; H, 7.35; N, 2.31. Found C, 82.74, H, 7.68, N, 2.13.

*7.3.19 Reaction of **20** with ^{n}Bu$_2$Mg (**29**)*

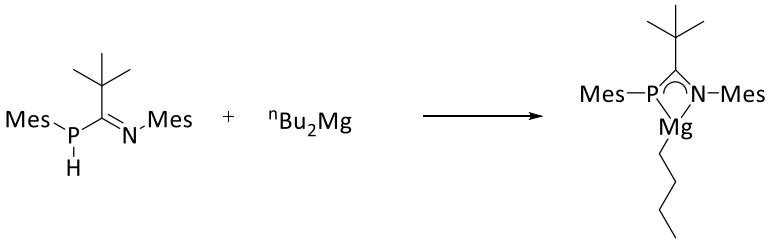

A solution of **20** (155.1 mg, 0.438 mmol) in toluene (25 mL) was cooled to -60 °C. ^{n}Bu$_2$Mg (1.25 mL, 0.438 mmol, 0.35 M in heptane) was added slowly and after 10 minutes the cold bath was removed. After 45 minutes the volatiles were removed to yield a bright yellow powder of compound **29** (141.6 mg, 0.326 mmol, 74.4 %). Melting Point: 237-238 °C. ^{1}H NMR (400 MHz, C_6D_6, 300 K): δ = 6.86 (s, 1H, ArH), 6.68 (s, 2H, ArH), 6.36 (s, 1H, ArH), 2.91 (s, 3H, N-*p*CH$_3$), 2.49 (s, 3H, N-*o*CH$_3$), 2.42 (s, 3H, P-*o*CH$_3$), 2.22 – 2.12 (m, 2H, C*H*$_2$CH$_2$CH$_3$), 2.03 (s, 3H, N-*o*CH$_3$), 1.99 (s, 3H, P-*o*CH$_3$), 1.85 (s, 3H, P-*p*CH$_3$), 1.83 – 1.75 (m, 2H, CH$_2$C*H*$_2$CH$_3$), 1.26 (t, *J* = 7.3 Hz, 3H, CH$_2$C*H*$_3$), 0.94 (s, 9H, C(CH$_3$)$_3$), 0.54 – 0.46 (m, 2H, Mg-C*H*$_2$). ^{13}C NMR (126 MHz, C_6D_6) δ 211.17 (d, *J* = 14.1 Hz, P-C-N), 145.03 – 144.72 (m, N-*i*ArC), 141.85 (t, *J* = 6.7 Hz, P-*o*ArC), 138.03 (P-*p*ArC), 133.58 (N-*p*ArC), 131.30 (N-*o*ArC), 129.07 (t, *J* = 18.8 Hz, P-*i*ArC), 128.72 (N-*m*ArC), 126.63 (P-*m*ArC), 46.69 (t, *J* = 3.5 Hz, *C*(CH$_3$)$_3$), 32.84 (Mg-CH$_2$*C*H$_2$), 31.87 (Mg-CH$_2$CH$_2$*C*H$_2$), 29.37 (C(*C*H$_3$)$_3$), 25.82 (d, *J* = 4.0 Hz, N-*o*Me), 25.50 (t, *J* = 6.1 Hz, P-*o*Me), 20.69 (P-*p*Me), 20.30 (N-*p*Me), 19.47 (N-*o*Me), 18.38 (t, *J* = 5.3 Hz, P-

*o*Me), 14.23 (CH_2CH_3) 10.63 (t, *J* = 9.6 Hz, $MgCH_2$). ^{31}P NMR (202.5 MHz, C_6D_6, 300 K): δ -42.0 ppm. High Res Mass Spec (EI) m/z: 433.331252. Elemental Analysis: Expected: C, 74.74; H, 9.29; N, 3.23. Found: C, 69.06; H, 9.65; N, 2.98.

*7.3.20 Reaction of **21** with $^{n}Bu_2Mg$ (**30**)*

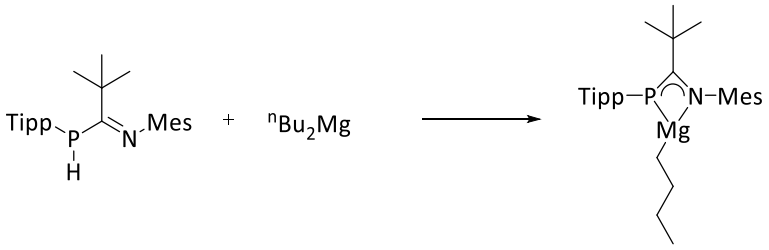

Compound **21** (366.3 mg, 0.84 mmol) was dissolved in toluene (20 mL) and cooled to -78°C, $^{n}Bu_2Mg$ (0.85 mL, 1.0 M in heptane, 0.85 mmol, 1.0 eq) was added slowly and after 5 minutes the cold bath was removed. After a further 1 hour stirring, the solution was concentrated to half the volume and cooled to -20°C overnight to give a crop of bright yellow crystals (234.8 mg, 0.038 mmol, 45.9 %). Melting Point: 236-238°C. Turned red just before melting and when cooled it returned to the original colour. ^{1}H NMR (500 MHz, C_6D_6) δ = 7.21 (s, 1H), 6.63 (s, 1H), 6.11 (s, 1H), 4.55 (br s, 2H, $^{ortho}CH(CH_3)_2$), 2.70 (sept, J = 7.0 Hz, 1H, $^{para}CH(CH_3)_2$), 2.41 (s, 3H), 2.21 – 2.04 (m, 2H, $MgCH_2CH_2CH_2$), 1.96 (s, 3H), 1.92-1.81 (m, 2H, $-CH_2CH_2CH_3$), 1.87 (s, 3H), 1.66 (d, J = 6.6 Hz, 3H, $^{ortho}CH(CH_3)_2$), 1.54 (dd, J = 17.5, 6.7 Hz, 6H, $^{ortho}CH(CH_3)_2$), 1.30 (t, J = 7.3 Hz, 3H, $-CH_2CH_3$), 1.14 (d, J = 6.9 Hz, 6H, $^{para}CH(CH_3)_2$), 0.90 (s, 9H, $C(CH_3)_3$), 0.66 (d, J = 6.8 Hz, 3H, $^{ortho}CH(CH_3)_2$), 0.47 – 0.35 (m, 2H, $MgCH_2CH_2$) ppm. ^{13}C NMR (126 MHz, C_6D_6) δ = 211.30 (t, J = 15.0, 12.9 Hz, P-*C*=N), 155.98 ($Tipp^{o}CCH(CH_3)_2$), 154.11 ($Tipp^{ipso}C$), 150.25 ($Tipp^{p}CCH(CH_3)_2$), 145.10 (t, J = 10.0 Hz, $Mes^{ipso}C$), 137.50 ($Mes^{o}CCH_3$), 133.52 ($Mes^{p}CCH_3$), 129.25 (toluene), 128.94 ($Mes^{m}CH$), 128.71 (toluene), 128.53 (toluene), 128.17 ($Mes^{m}CH$), 125.31 (toluene), 121.96 (d, J = 57.2 Hz, $Tipp^{m}CH$), 46.94 (t, J = 3.1 Hz, $C(CH_3)_3$), 34.73 – 34.25 (m, ($Tipp^{o}CH(CH_3)_2$), 34.02 ($Tipp^{p}CH(CH_3)_2$), 33.25 ($MgCH_2CH_2$), 32.26 (CH_2CH_3), 30.07 ($C(CH_3)_3$), 26.62 ($Tipp^{o}CH(CH_3)_2$), 23.55 (d, J = 5.2 Hz, $Tipp^{o}CH(CH_3)_2$), 23.43 ($Tipp^{p}CH(CH_3)_2$), 23.29 ($Tipp^{p}CH(CH_3)_2$), 21.05 (toluene), 20.26 ($Mes^{o}CH_3$), 19.27 ($Mes^{o}CH_3$), 18.96 ($Mes^{p}CH_3$), 14.04 (CH_2CH_3), 9.93 (t, J = 10.4 Hz, $MgCH_2$) ppm. ^{31}P NMR (202 MHz, C_6D_6) δ = - 55.34 (s) ppm. High Res Mass Spec (EI) m/z: 517.36838 $[C_{33}H_{52}NMgP]^{+}$ Elemental Analysis: $C_{40}H_{60}MgNP$ Expected: C, 76.73; H, 9.91; N, 2.30. Found: C, 70.82; H, 8.05; N, 2.59.

*7.3.21 Reaction of **22** with $^{n}Bu_2Mg$ (**31**)*

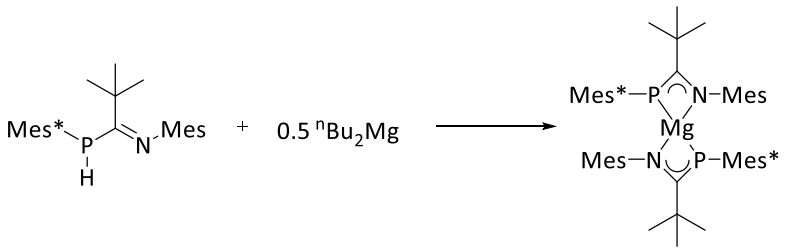

$^{n}Bu_2Mg$ (0.24 mL, 1.0 M in heptane, 0.24 mmol) was added to a toluene (5 mL) solution of **22** (202.2 mg, 0.42 mmol, 1.8 eq.) at -78°C. After 5 minutes the cold bath was removed and the solution changed from colourless to bright yellow as it warmed to room temperature. This was stirred for 1 hour and the volume reduced by half, and the solution cooled to -20°C for 24 hours, after which time a yellow crystalline solid had precipitated. (112.9 mg, 0.115 mmol, 54.6 %). Melting Point: 214-218 °C. ^{1}H NMR (500 MHz, C_6D_6) δ = 7.53 (s, 2H, Mes*C*H*), 6.61 (s, 2H, MesC*H*), 2.15 (s, 3H, Mes$^{p}CH_3$), 2.10 (s, 6H, Mes$^{o}CH_3$), 1.87 (s, 18H, Mes*$^{o}CH_3$), 1.32 (s, 9H, Mes*$^{p}CH_3$), 0.84 (s, 9H, $C(CH_3)_3$) ppm. ^{13}C NMR (126 MHz, C_6D_6) δ = 219.92 (d, $^{1}J_{C\text{-}P}$ = 49.0 Hz, P=C-N), 156.42 (Mes*^{o}*C*$CH(CH_3)_2$), 149.57 (Mes*^{p}*C*$CH(CH_3)_2$), 145.73 (t, $^{3}J_{C\text{-}P}$ = 6.6 Hz, Mes^{i}*C*), 132.88 (Mes^{m}*C*H), 132.28 (t, $^{4}J_{P\text{-}C}$ = 3.5 Hz, Mes^{o}*C*CH_3), 128.94 (Mes^{p}*C*CH_3), 121.86 (Mes*^{m}*C*H), 44.55 (t, $^{2}J_{P\text{-}C}$ = 3.1 Hz, *C*$(CH_3)_3$), 39.28 (Mes*^{o}C*C*$H(CH_3)_2$), 34.62 (Mes*^{p}*C*$CH(CH_3)_2$), 34.32 (t, $^{5}J_{P\text{-}C}$ = 3.4 Hz, Mes*^{o}CCH(*C*$H_3)_2$), 31.16 (Mes*^{p}CCH(*C*$H_3)_2$), 29.23 (C(*C*$H_3)_3$), 20.46 (Mes^{p}*C*H_3), 18.96 (Mes^{o}*C*H_3) ppm. (^{i}C-P not observed). ^{31}P NMR (202 MHz, C_6D_6) δ = 12.53 (s) ppm. High Res Mass Spec (EI): Expected = 980.70503 $[C_{64}H_{98}MgN_2P_2]^{+}$ Elemental Analysis: $C_{64}H_{98}MgN_2P_2$ Expected: C, 78.30; H, 10.06; N, 2.85. Found: C, 70.92; H, 9.80; N, 2.76.

*7.3.22 Reaction of **23** with 0.5 $^{n}Bu_2Mg$ (**33**)*

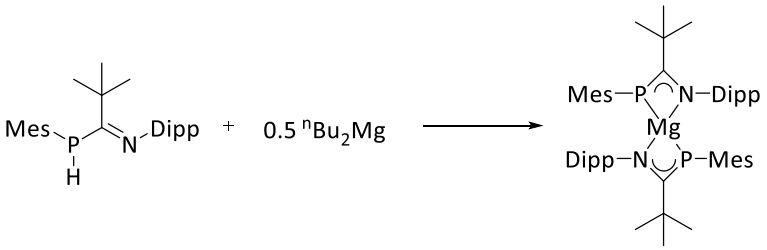

$^{n}Bu_2Mg$ (0.27 mL, 1.0 M in heptane, 0.27 mmol) was added to a solution of **23** (211.9 mg, 0.54 mmol, 2 eq) in toluene (10 mL) at room temperature. The colourless solution changed to a bright yellow colour after stirring for 18 hours. The volatiles were removed and the oily residue washed with hexane (5 mL) and dried in vacuo to give the product as a dark yellow powder (127.2 mg, 0.16 mmol, 57.0 %). Melting Point: 237-240 °C. ^{1}H NMR (Tol-d_8, 500 MHz, 353 K) δ = 6.97 – 6.90 (m, 3H, dipp-Ar*H*), 6.77 (s, 5H, Mes-Ar*H*), 3.29 (sept, *J* = 6.7 Hz, 2H, C*H*$(CH_3)_2$), 2.60 (s, 6H, Mes-$^{o}CH_3$), 2.14 (s, 3H, Mes-$^{p}CH_3$), 1.24 (d, *J* = 6.8 Hz, 6H, CH(C*H*$_3)_2$), 1.04 (s, 9H, C(C*H*$_3)_3$), 1.00 (d, *J* = 8.7 Hz, 6H, CH(C*H*$_3)_2$) ppm. ^{31}P NMR (Tol-d_8, 202.5 MHz, 353 K) δ = – 20.55 (s) ppm. Elemental Analysis: Expected: C, 76.78; H, 9.17; Mg, 2.99; N, 3.44; P, 7.62. Found: C, 67.18; H, 8.35; N, 3.04.

*7.3.23 Reaction of **28** with $^{n}Bu_2Mg$ (**34**)*

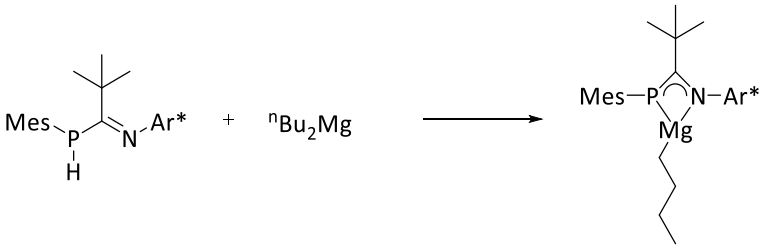

A toluene (25 mL) solution of **28** (398.6 mg, 0.61 mmol) and $^{n}Bu_2Mg$ (0.60 mL, 1.0 M in heptane, 0.60 mmol, 1 eq) was heated to 90 °C for 18 hours. The orange solution was dried to an oily solid which was washed with hexane (2 mL) and dried to a yellow powder (348.0 mg, 0.47 mmol, 78.5 %). Melting Point: 198-201 °C. ^{1}H NMR (500 MHz, C_6D_6) δ = δ 7.27 – 7.16 (m, 12H, ArH), 7.14 – 6.95 (m, 8H, ArH), 6.87 (s, 2H, Mes*H*), 6.82 (s, 2H, N-Ph*H*), 5.92 (s, 2H, C*H*$(Ph)_2$), 2.74 (s, 6H, Mes$^{o}CH_3$), 2.11 (s, 3H, Mes$^{p}CH_3$), 1.83 (s, 3H, NAr*C*H_3), 1.60 – 1.50 (m, 2H, LMg$CH_2CH_2CH_2CH_3$), 1.43 (sext, J = 7.6 Hz, 2H, LMg$CH_2CH_2CH_2CH_3$), 1.14 (s, 9H, C(C*H*$_3)_3$), 1.02 (d, J = 7.6 Hz, 3H, LMg$CH_2CH_2CH_2CH_3$), -0.56 – -0.73 (m, 2H, LMg$CH_2CH_2CH_2CH_3$). ^{13}C NMR (126 MHz, C_6D_6) δ = 221.18 (d, J = 55.4 Hz, P-*C*=N), 145.44 (d, J

= 9.6 Hz, ArC), 143.62 (d, J = 9.6 Hz, ArC), 143.35 (ArC), 142.76 (ArC), 137.23 (ArC), 136.70 (d, J = 6.1 Hz, ArC), 135.11 (d, J = 35.4 Hz, ArC), 133.05 (ArC), 129.85 (ArC), 129.41 (ArC), 129.33 (P-*m*ArC), 128.89 (ArC), 128.80 (d, J = 3.0 Hz, ArC), 128.50 (ArC), 126.62 (ArC), 52.40 ($CH(Ph)_2$), 47.10 (d, J = 6.1 Hz, -$CC(CH_3)_3$), 31.47 ($LMgCH_2CH_2$), 31.24 (d, J = 3.0 Hz, -$CC(CH_3)_3$), 31.08 (CH_2CH_3), 25.16 (P-*o*Me), 20.78 (N-*p*Me), 20.75 (P-*p*Me), 14.02 (CH_2CH_3), 7.89 (d, J = 14.7 Hz, $MgCH_2$). ^{31}P NMR (202 MHz, C_6D_6) δ = -7.03 ppm. Elemental Analysis: Expected C, 82.86; H, 7.77; N, 1.89; Found: C, 66.68; H, 6.25; N, 1.55.

*7.3.24 Preparation of bis-N-(2,2-dimethyl-1-(mesitylphosphino)propylidene)2,4,6-trimethylaniline magnesium **35***

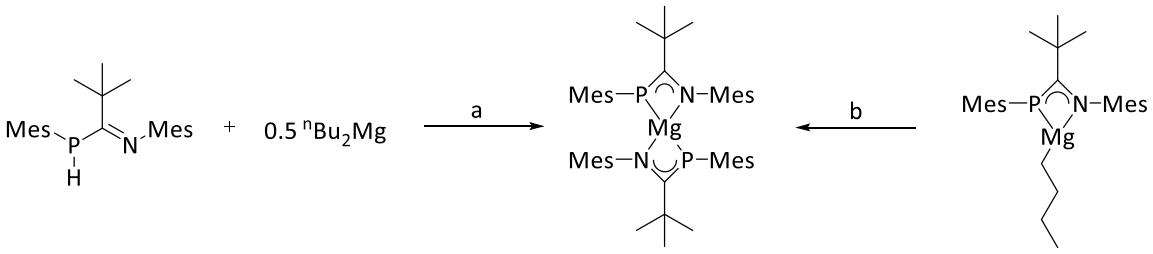

Method A: $^{n}Bu_2Mg$ (0.75 mL, 0.75 mmol, 1.0 M in heptane) was added to a solution of **20** (532.0 mg, 1.5 mmol, 2.0 eq) in toluene (20 mL) at room temperature. After 5 hours the volatiles were removed from the bright yellow solution. The residue was recrystallised from pentane (0.5 mL) at – 20 °C to give a bright yellow powder (310.5 mg, 0.58 mmol, 78.2 %). *Method B:* Toluene (25 mL) was added to a flask containing a mixture of solids **20** (250.2 mg, 0.71 mmol) and **29** (303.2 mg, 0.70 mmol) and stirred for 5 hours. The solution was dried *in vacuo* and extracted into hexane. The filtrate was concentrated to *ca* 3 mL and cooled to -20 °C to precipitate the product as a yellow solid (373.3 mg, 0.51 mmol, 73.1 %). Melting Point: 148-150 °C (Turned orange upon melting). ^{1}H NMR (500.2 MHz, C_6D_6, 300 K): δ = 6.78 (s, 4H, PMes-ArH), 6.62 (s, 4H, NMes-ArH), 2.78 (s, 12H, PMes-orthoCH_3), 2.14 (s, 6H, NMes-paraCH_3), 2.05 (s, 6H, PMes-paraCH_3), 2.01 (s, 12H, NMes-paraCH_3) 0.97 (s, 18H, ^{t}Bu-CH_3) ppm. ^{13}C NMR (125.7 MHz, C_6D_6, 300 K): δ = 222.40 (d, $^{3}J_{C\text{-}P}$ = 60.1 Hz, P-*C*=N), 145.40 (d, $^{3}J_{C\text{-}P}$ = 8.6 Hz, NMes-ipso*C*), 143.33 (d, $^{3}J_{C\text{-}P}$ = 10.4 Hz, PMes-ortho*C*CH_3), 136.95 (PMes-para*C*CH_3) , 135.38 (d, $^{3}J_{C\text{-}P}$ = 38.3 Hz, PMes-ipso*C*), 132.97 (NMes-para*C*CH_3), 129.79 (NMes-ortho*C*CH_3), 128.96 (Ar*C*H), 128.54 (Ar*C*H), 46.43 (^{t}Bu*C*CH_3), 29.58 (^{t}Bu*C*CH_3), 25.41 (d, $^{3}J_{C\text{-}P}$ = 13.8 Hz, PMes-ortho*C*CH_3), 20.72 (PMes-para*C*CH_3), 20.47 (NMes-paraCCH_3), 18.61 (NMes-ortho*C*CH_3) ppm. ^{31}P NMR (202.5 MHz, C_6D_6, 300 K): δ = -25.9 ppm. Mass Spec (EI):

m/z = 728.41956 ([$C_{46}H_{62}MgN_2P_2$]$^+$) Elemental Analysis: Expected: C, 75.76; H, 8.57; N, 3.84. Found: C, 69.62; H, 8.65; N, 3.69.

*7.3.25 Reaction of **21** with 0.5 ^{n}Bu$_2$Mg (**36**)*

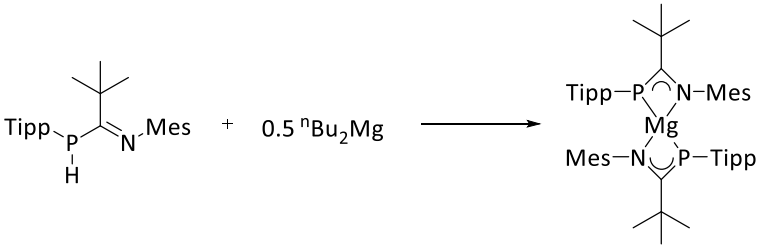

Compound **21** (313.9 mg, 0.717 mmol) was dissolved in toluene (25 mL) and at room temperature ^{n}Bu$_2$Mg (0.35 mL, 0.35 mmol, 1.0 M in heptane) was added. After stirring the solution overnight the volatiles were removed to an oily residue. This was dissolved in hexane (2mL) and cooled to -20 °C to precipitate 4.19 as a yellow solid (124.9 mg, 0.139 mmol, 38.8 %). ^{1}H NMR (500 MHz, C_6D_6): δ = 7.15 (s, 4H, P-ArH), 6.70 (s, 4H, N-ArH), 4.62 (broad s, 4H, ortho-C*H*$_2$(CH$_3$)$_2$), 2.82 (sept, *J* = 6.9 Hz, 2H, para-C*H*$_2$(CH$_3$)$_2$), 2.22 (s, 6H, para-CH$_3$), 2.02 (s, 12H, ortho-CH$_3$), 1.54 (d, *J* = 6.8 Hz, 12H, ortho-CH$_2$(C*H*$_3$)$_2$), 1.28 (d, *J* = 6.8 Hz, 12H, para-CH$_2$(C*H*$_3$)$_2$), 1.26 (d, *J* = 6.9 Hz, 12H, ortho-CH$_2$(C*H*$_3$)$_2$), 1.11 (s, 18H, CC*H*$_3$) ppm. ^{13}C NMR (126 MHz, C_6D_6): δ = 222.16 (d, *J* = 57.9 Hz, P-C-N), 153.23 – 152.32 (m, P-*i*ArC), 148.32 (P-*p*ArC), 134.94 (d, *J* = 38.0 Hz, P-*o*ArC), 130.50 (d, *J* = 2.8 Hz, N-oArC), 128.65 (N-*m*ArC), 121.25 (d, *J* = 41.3 Hz, P-*m*ArC), 46.54 – 45.39 (m, *C*(CH$_3$)$_3$), 34.28 (*pC*H(CH$_3$)$_2$), 34.12 – 33.87 (m), 29.85 (N-*o*Me), 25.20 (*p*CH(*C*H$_3$)$_2$), 23.89 (d, *J* = 7.4 Hz, C(*C*H$_3$)$_3$), 22.75 (N-*o*Me), 20.53, 18.32 ppm. ^{31}P NMR (202 MHz, C_6D_6): δ = -34.24 ppm.

7.3.26 General Procedure for Lactide Polymerisation Reactions

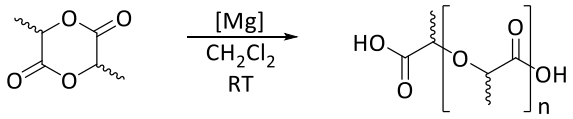

A solution of rac-lactide (2.0 mL, 1.0 M in dichloromethane) was transferred into a J-young's tap ampule charged with the appropriate amount of **29**, **30** or **34** stirred vigorously. When the reaction was complete the reaction solution was poured over 5 mL hexane. The volatiles were removed and the residue dissolved in $CDCl_3$ to record ^1H NMR spectra.

*7.3.27 Reaction of **20** with ^{n}BuLi and 12-crown-4 (**42**)*

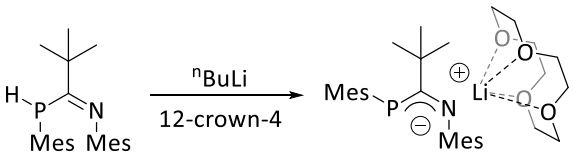

A solution of **20** (241.5 mg, 0.683 mmol) in THF (25 mL) was cooled to -78 °C. 12-crown-4 (110 µL, 0.679 mmol 1.0 eq) was added, followed by ^{n}BuLi (0.28 mL, 2.5 M in hexanes, 0.700 mmol, 1.0 eq). After 10 minutes stirring the bright yellow solution was warmed to room temperature and stirred for a further 1.5 hours. The volatiles were removed and the residue washed with hexane (2 mL) and dried to a yellow powder (245.0 mg, 0.457 mmol, 67.0 %). Melting point 264-275 °C. ^1H NMR (500 MHz, THF-d_8) δ: 6.58 (broad s, 2H, ArH) 6.43 (broad s, 2H, ArH) 3.51, (s, 16H, crown ether), 2.56 (s, 6H, Me), 2.16 (s, 6H, Me), 2.10 (s, 5H, Me) 1.24 (s, 8H, C(CH_3)$_3$) ppm. Due to low solubility ^{13}C NMR was not possible. ^{31}P NMR (202 MHz, THF-d_8) δ = -23.2 (s) ppm. No sample pure enough (by NMR) for elemental analysis was isolated.

*7.3.28 Reaction of **28** with ^{n}BuLi (**43**)*

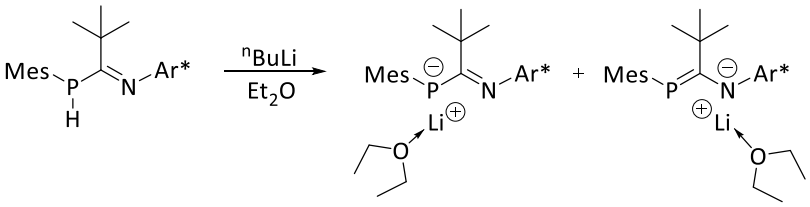

Compound **28** (251.7 mg, 0.38 mmol) was dissolved in diethyl ether (25 mL) and cooled to –78 °C, and ^{n}BuLi (0.20 mL, 2.5 M in hexanes, 0.50 mmol, 1.3 eq) was added slowly. The solution was immediately warmed to room temperature and stirred for a further 2 hours. The volatiles were removed from the deep red solution and the residue washed with hexane (15 mL) to give a mustard coloured solid, a mixture of **43a** and **43b** (158.4 mg, 0.21 mmol, 56.1 %). ^{1}H NMR **43a** (500 MHz, C_6D_6) δ = δ 7.72 (d, J = 7.1 Hz, 8H, ArH), 6.17 (s, 3H, C*H*$(Ph)_2$), 3.11 (s, 6H, P-*o*Me), 2.19 (s, 3H, P-*p*Me), 1.77 (s, 3H, N-*p*Me), 1.22 (s, 9H, $C(CH_3)_2$). ^{1}H NMR **43b** (500 MHz, C_6D_6) δ = 7.77 (d, *J* = 7.6 Hz, 7H, ArH), 7.36 (d, *J* = 7.2 Hz, 7H, ArH), 6.36 (s, 3H, C*H*$(Ph)_2$), 2.99 (s, 8H, P-*o*Me), 2.23 (s, 5H, P-*p*Me), 1.96 (s, 4H, N-*p*Me), 1.20 (s, 9H, $C(CH_3)_3$). ^{7}Li NMR (194 MHz, C_6D_6) δ = -2.28 (d, $J_{Li\text{-}P}$ = 105.1 Hz, Li-P-C=N, major), -5.29 (s, P=C-N-Li, minor) ppm. Due to low solubility ^{13}C NMR was not possible. ^{31}P NMR (202 MHz, C_6D_6) δ = -25.3 (s, P=C-N-Li), 27.3 (q, $J_{P\text{-}Li}$ = 105.6 Hz, Li-P-C=N) ppm.

*7.3.29 Reaction of **20** with ^{n}BuLi and $Me_3N.AlH_3$ (**44**)*

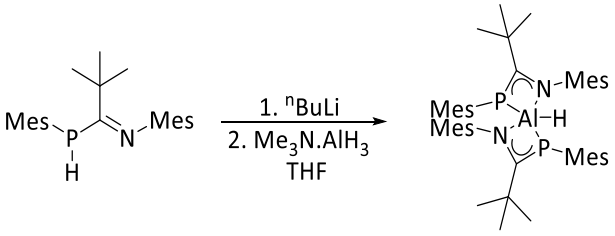

Compound **20** (309.3 mg, 0.875 mmol) was dissolved in Et_2O (20 mL) and cooled to -60 °C. nBuLi (0.35 mL, 2.5 M in hexanes, 0.875 mmol, 1.0 eq) was added and the solution warmed to room temperature. After 45 minutes, the solution was cooled to -78°C and a solution of $Me_3N.AlH_3$ (39.4 mg, 0.442 mmol, 0.5 eq) in Et_2O (5 mL) was added and the solution again warmed to room temperature. Me_3SiCl (54 µL, 0.425 mmoL) was added and the reaction

stirred for a further 5 hours. The volatiles were removed to a yellow residue which was extracted with hexane and dried (78.9 mg, 0.107 mmol, 13.3 %). ^{1}H NMR (500 MHz, C_6D_6) δ = 6.75 (s, 4H, N-ArH), 6.61 (s, 2H, P-ArH), 6.41 (s, 2H, P-ArH), 2.87 (s, 6H, N-*o*Me), 2.54 (s, 6H, N-*o*Me), 2.44 (s, 6H, P-*o*Me), 2.37 (s, 6H, P-*o*Me),2.05 (s, 3H P-*p*Me) 2.01 (s, 3H, N-*p*Me) 1.01 (s, 18H, C(C*H*$_3$)$_3$) ppm. ^{31}P NMR (202 MHz, C_6D_6) δ = -23.64 (s) ppm. Elemental Analysis: Expected: C, 75.17; H, 8.91; N, 3.81. Found: C, 52.67; H, 7.23; N, 2.66.

*7.3.30 Isolation of aluminium dihydride intermediate (**45**)*

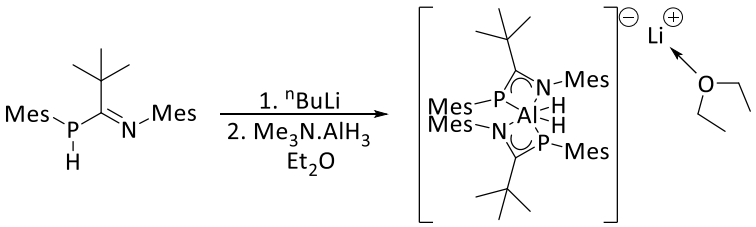

Compound **20** (827.5 mg, 2.34 mmol) was dissolved in Et_2O (25 mL) and ^{n}BuLi (1.05 mL) was added at -78 °C. The solution was warmed to room temperature and stirred for 30 minutes. The yellow solution was cooled back to -78 °C, where a solution of $Me_3N.AlH_3$ (105.6 mg, 1.18 mmol, 1 eq) in Et2O (15 mL) was added. After one hour the solution was layered with pentane (15 mL) and the precipitated solid was filtered to give the lithium aluminiate product **45** (326.0 mg, 0.40 mmol, 33.8 %). ^{1}H NMR was broad and featureless, but some key resonances were identified (500 MHz, C_6D_6): δ = 3.06 (q, JH-H = 7.1 Hz, OC*H*$_2$CH$_3$), 0.95 (s, C(C*H*$_3$)$_2$) ppm. Due to low solubility ^{13}C NMR was not possible. ^{31}P NMR (202 MHz, C_6D_6) δ = -2.8 - -19.2 (m) ppm. Elemental Analysis $C_{50}H_{74}AlLiN_2OP_2$: Expected: C, 73.68; H, 9.15; N, 3.44. Found: C, 67.09; H, 8.42; N, 3.26.

7.4 Crystallography data

	3	**4**	**5**	**6**
Formula	$C_{27}H_{43}AlN_2$	$C_{31}H_{51}AlN_2$	$C_{27}H_{41}AlN_2$	$C_{32}H_{33}AlO$
$D_{calc.}$/ g cm^{-3}	1.074	1.110	1.100	1.183
μ/mm^{-1}	0.093	0.092	0.095	0.839
Formula Weight	422.61	478.71	420.60	460.56
Colour	colourless	colourless	colourless	colourless
Shape	prism	block	block	block
Size/mm^3	0.42x0.20x0.11	0.21x0.10x0.05	0.37x0.33x0.17	0.24×0.16×0.07
T/K	120.0	120.0	120.0	120.0
Crystal System	monoclinic	monoclinic	monoclinic	monoclinic
Space Group	$P2_1/c$	$P2_1/c$	Ia	$P2_1/c$
a/Å	10.7729(3)	8.8699(7)	15.5778(7)	21.1293(5)
b/Å	15.6899(4)	16.0945(13)	11.6033(4)	14.7951(4)
c/Å	16.0285(5)	20.2907(17)	15.6858(7)	17.9035(5)
α/°	90	90	90	90
β/°	105.321(3)	98.473(7)	116.418(5)	112.445(3)
γ/°	90	90	90	90
V/Å^3	2612.93(13)	2865.0(4)	2539.2(2)	5172.8(3)
Z	4	4	4	8
Z'	1	1	1	2
Wavelength/Å	---	---	---	1.54184
Radiation type	---	---	---	CuK_α
Θ_{min}/°	3.122	3.119	3.140	3.748
Θ_{max}/°	29.719	25.681	29.651	76.298
Measured Refl.	46010	22402	22186	42682
Independent Refl.	6853	5441	6273	10751
Reflections Used	5373	4180	5769	8245
R_{int}	0.0544	0.0737	0.0377	0.0969
Parameters	289	327	287	629
Restraints	0	0	2	0
Largest Peak	0.296	0.288	0.210	0.487
Deepest Hole	-0.245	-0.305	-0.218	-0.421
GooF	1.046	1.072	1.084	1.028
wR_2 (all data)	0.1280	0.1262	0.1010	0.1658
wR_2	0.1176	0.1167	0.0980	0.1505
R_1 (all data)	0.0724	0.0846	0.0495	0.0794
R_1	0.0514	0.0602	0.0437	0.0603

	11	**16(C_6D_6)**	**17(C_6H_{14})$_2$**	**20**
Formula	$C_{48}H_{50}Al_2$	$C_{90}D_6Al_2H_{86}N_4$	$C_{83}H_{115}Al_2N_4$	$C_{23}H_{32}NP$
$D_{calc.}$/ g cm^{-3}	1.172	1.210	1.114	1.128
μ/mm^{-1}	0.911	0.751	0.086	1.180
Formula Weight	680.84	1289.67	1222.74	353.46
Colour	colourless	dark red	Colourless	colourless
Shape	Block	Prism	Block	block
Size/mm^3	0.12×0.11×0.09	0.13×0.08×0.08	0.30×0.22×0.09	0.33×0.16×0.05
T/K	120.0	120.0	120.0	120.0
Crystal System	triclinic	monoclinic	Triclinic	monoclinic
Space Group	P-1	Ia	*P*-1	Cc
a/Å	11.0642(4)	15.4666(6)	13.0024(5)	9.9879(3)
b/Å	11.5289(4)	15.1699(5)	14.3253(5)	22.8188(7)
c/Å	16.8850(4)	30.7695(10)	20.5627(9)	9.1930(3)
α/°	99.424(2)	90	74.703(4)	90
β/°	98.234(2)	101.336(4)	85.071(3)	96.441(3)
γ/°	111.443(3)	90	80.963(4)	90
V/Å^3	1928.70(11)	7078.5(4)	3644.5(3)	2081.96(12)
Z	2	4	2	4
Z'	1	1	1	1
Wavelength/Å	1.54184	1.54184	0.71073	1.54178
Radiation type	CuK_α	CuK_α	MoK_α	CuK_α
Θ_{min}/°	4.238	4.122	2.829	3.874
Θ_{max}/°	76.188	76.497	28.980	76.040
Measured Refl.	29640	34446	74410	25149
Independent Refl.	7908	13900	17052	3962
Reflections Used	6635	8661	11300	3904
R_{int}	0.0797	0.1336	0.0729	0.0639
Parameters	461	884	873	239
Restraints	0	2	84	2
Largest Peak	0.387	0.396	0.741	0.365
Deepest Hole	-0.378	-0.480	-0.540	-0.330
GooF	1.031	0.916	1.035	1.096
wR_2 (all data)	0.1442	0.1875	0.1520	0.1307
wR_2	0.1342	0.1719	0.1315	0.1301
R_1 (all data)	0.0616	0.1037	0.1083	0.0514
R_1	0.0516	0.0728	0.0644	0.0510

	22	**28**	**29(C_6D_6)**	**30**
Formula	$C_{69}H_{112}N_2P_2$	$C_{47}H_{48}NP$	$C_{60}D_6H_{80}Mg_2N_2P_2$	$C_{66}H_{104}Mg_2N_2P_2$
$D_{calc.}$/ g cm^{-3}	1.055	1.154	1.135	1.062
μ/mm^{-1}	0.886	0.106	0.139	0.124
Formula Weight	1031.54	657.83	951.90	1036.07
Colour	colourless	colourless	light yellow	colourless
Shape	block	plate	block	block
Size/mm^3	0.29×0.08×0.07	0.88×0.20×0.06	0.51×0.42×0.35	0.57×0.36×0.21
T/K	120.0	170.0	120.0	120.0
Crystal System	monoclinic	monoclinic	triclinic	triclinic
Space Group	$P2_1/c$	$P2_1/n$	P-1	*P*-1
a/Å	10.26764(11)	9.7307(3)	11.4632(2)	12.2616(3)
b/Å	9.95168(15)	20.1041(6)	11.6067(2)	14.4715(3)
c/Å	31.7681(4)	19.6654(6)	11.7719(2)	18.5159(4)
α/°	90	90	71.5570(10)	87.4135(18)
β/°	90.6629(9)	100.170(3)	78.6600(10)	80.7322(18)
γ/°	90	90	70.3520(10)	89.7074(18)
V/Å^3	3245.86(7)	3786.61(19)	1392.14(4)	3239.32(13)
Z	2	4	1	2
Z'	0.5	1	0.5	1
Wavelength/Å	1.54184	0.71073	0.71073	0.71073
Radiation type	CuK_a	MoK_a	MoK_a	MoK_a
Θ_{min}/°	4.306	2.938	2.768	2.692
Θ_{max}/°	76.225	25.350	28.356	29.676
Measured Refl.	27126	70599	47924	87659
Independent Refl.	6732	6928	6740	16891
Reflections Used	6152	5706	6035	13179
R_{int}	0.0632	0.0543	0.0258	0.0541
Parameters	356	546	308	675
Restraints	0	97	0	0
Largest Peak	0.657	0.281	0.669	1.143
Deepest Hole	-0.365	-0.180	-0.544	-0.545
GooF	1.056	1.079	1.030	1.039
wR_2 (all data)	0.1594	0.1107	0.1254	0.1361
wR_2	0.1546	0.1044	0.1210	0.1246
R_1 (all data)	0.0626	0.0681	0.0481	0.0747
R_1	0.0580	0.0516	0.0430	0.0540

	31(C_6D_6)$_2$	**34**	**42(THF)$_2$**	**44**
Formula	$C_{76}H_{98}D_{12}MgN_2P_2$	$C_{51}H_{56}MgNP$	$C_{39}H_{63}LiNO_6P$	$C_{46}H_{63}AlN_2P_2$
$D_{calc.}$/ g cm^{-3}	1.074	1.165	1.180	1.141
μ/mm^{-1}	0.935	0.116	0.986	1.360
Formula Weight	1149.98	738.24	679.81	732.90
Colour	yellow	yellow	translucent pale yellow	colourless
Shape	block	block	plate	plate
Size/mm^3	0.35×0.18×0.13	0.19×0.12×0.07	0.46×0.23×0.04	0.10×0.09×0.04
T/K	120.0	120.0	120.0	120.0
Crystal System	triclinic	monoclinic	orthorhombic	monoclinic
Space Group	P-1	$P2_1/c$	Pbca	P2/n
a/Å	11.59612(18)	10.7159(16)	18.98712(8)	13.1018(2)
b/Å	13.7848(3)	30.407(3)	15.63788(8)	8.10353(13)
c/Å	22.4931(4)	13.7933(17)	25.77481(11)	20.1040(3)
α/°	97.7496(14)	90	90	90
β/°	90.9709(13)	110.522(15)	90	92.4888(14)
γ/°	93.1255(14)	90	90	90
V/Å^3	3556.32(10)	4209.1(10)	7653.01(6)	2132.45(6)
Z	2	4	8	2
Z'	1	1	1	0.5
Wavelength/Å	1.54178	0.71073	1.54184	1.54184
Radiation type	CuK_α	MoK_α	CuK_α	CuK_α
Θ_{min}/°	3.562	2.679	4.044	3.950
Θ_{max}/°	76.229	17.525	75.985	76.049
Measured Refl.	100870	44911	120308	31922
Independent Refl.	14774	2667	7976	4430
Reflections Used	12956	2212	7533	3862
R_{int}	0.0687	0.1423	0.0813	0.0866
Parameters	822	531	498	242
Restraints	81	35	49	0
Largest Peak	0.752	0.297	0.307	0.449
Deepest Hole	-0.442	-0.165	-0.342	-0.386
GooF	1.086	1.079	1.042	1.048
wR_2 (all data)	0.1657	0.1126	0.1405	0.1449
wR_2	0.1605	0.1063	0.1384	0.1377
R_1 (all data)	0.0662	0.0585	0.0533	0.0603
R_1	0.0601	0.0459	0.0515	0.0526

7.5 Density Functional Theory Data

7.7.1 Optimisation of Cp$_2$AlH, Cp*Al and Cp*H*

The work in this section was carried out by Dr David Rogers in Edinburgh.

The BP86 exchange-correlation functional and def2-SVP/def2-TZVPP basis sets were employed to study the reductive elimination of Cp*H from Cp*$_2$AlH in the gas phase. Structures were optimised and confirmed as minima by performing frequency calculations. The transition states located have one imaginary frequency. Gaussian 09 Rev. A.02 was the software employed.[13]

Table 11 shows the relative energies for reactants, transition state, and products predicted for reductive elimination of Cp*H from Cp*$_2$AlH. The transition state structure TS1-2 has an imaginary frequency of 724i at the BP/def2-SVP level of theory. A reaction barrier of 93.61 kJ/mol is predicted at the BP86/def2-SVP level, which is lowered to 89.38 kJ/mol when the zero-point-energy correction is included. Table 12 shows the relative energetics predicted at the BP86/def2-TZVPP level of theory using the BP86/def2-SVP optimised geometries. The reaction barrier is predicted to be 91.54 kJ/mol. The basis set superposition error (BSSE) is 2.4E-11 and -8.0E-12 au, respectively, for the BP86/def2-SVP and BP86/def2-TZVPP calculations.

Species	Energy	Energy + ZPE correction
Cp*$_2$AlH (1)	0 kJ mol^{-1}	0 kJ mol^{-1}
TS$_{1-2}$	93.61 kJ mol^{-1}	89.38 kJ mol^{-1}
Cp*Al and Cp*H	28.12 kJ mol^{-1}	39.03 J mol^{-1}

Table 11 *Relative energies predicted at the BP86/def2-SVP level of theory.*

Species	Energy	Energy + ZPE correction
Cp*$_2$AlH	0 kJ mol^{-1}	n/a
TS$_{1-2}$	91.54 kJ mol^{-1}	n/a
Cp*Al and Cp*H	18.44 kJ mol^{-1}	n/a

Table 12 *Relative energies predicted at the BP86/def2-TZVPP level, with the BP86/def2-SVP optimised geometries.*

7.7.3 Calculation of Phosphaamidine Tautomers

Using the solid-state structure of **22** as initial geometry, the structure of each of the eight tautomers was optimised using MO62X-def2vp to a minimum without imaginary frequencies using Gaussian 09 Rev. A.02.[13] Table 14 lists the absolute Hartree-Fock and relative energies of each tautomer. Structures of final geometries can be found on an accompanying USB drive.

	X-Ray	**Z-anti (P=C)**	**E-anti (P=C)**	**E-syn (P=C)**	**Z-syn (P=C)**	**Z-anti (N=C)**	**E-syn (N=C)**	**Z-syn (N=C)**
P-C (Å)	**1.7385(17)**	1.727	1.780	**1.722**	1.716	1.903	1.905	1.884
C-N(Å)	**1.375(6)**	1.373	1.400	**1.387**	1.370	1.271	1.264	1.267
P-C_{aryl} (Å)	**1.8583(15)**	1.875	1.863	**1.869**	1.866	1.863	1.843	1.859
N-C_{aryl} (Å)	**1.428(2)**	1.434	1.431	**1.424**	1.421	1.407	1.397	1.401
P-C-N (°)	**114.32(12)**	123.2	109.7	**114.7**	135.3	115.0	116.1	125.9
C_{tBu}-C-P (°)	**134.83(11)**	117.0	133.8	**135.1**	114.8	129.2	116.6	117.4
C_{tBu}-C-N (°)	**110.84(14)**	119.8	116.4	**110.3**	109.9	115.6	127.0	115.6

Table 13 *Summary of key structural parameters of optimised structures of* ***22***

Isomer	**NImag**	**Relative (kJ mol^{-1})**	**Absolute (kJ mol^{-1})**
Z-anti (P=C)	0	-10.3	-4316101.631
E-anti (P=C)	0	26.7	-4316085.826
E-syn (P=C)	0	0.0	-4316112.523
Z-syn (P=C)	0	3.6	-4316108.928
Z-anti (N=C)	0	10.9	-4316101.631
E-syn (N=C)	0	23.2	-4316089.319
Z-syn (N=C)	0	4.3	-4316108.199

Table 14 *Relative energies of optimised isomers predicted at the MO62X-def2vp level of theory.*

7.6 References

1 C. Ganesamoorthy, S. Loerke, C. Gemel, P. Jerabek, G. Frenking and R. A. Fischer, *Chem. Commun.*, 2013, 49, 2858-2860.

2 C. A. Fleckenstein and H. Plenio, *Chem. Eur. J.*, 2007, **13**, 2701–2716.

3 T. van Dijk, S. Burck, M. K. Rong, A. J. Rosenthal, M. Nieger, J. C. Slootweg and K. Lammertsma, *Angew. Chem. Int. Ed.*, 2014, **53**, 9068–9071.

4 T. van Dijk, M. K. Rong, J. E. Borger, M. Nieger, J. C. Slootweg and K. Lammertsma, *Organometallics*, 2016, **35**, 827–835.

5 Y. Takeda, T. Nishida and S. Minakata, *Chem. Eur. J.*, 2014, **20**, 10266–10270.

6 Y. van den Winkel, H. M. M. Bastiaans and F. Bickelhaupt, *J. Organomet. Chem.*, 1991, **405**, 183–194.

7 A. H. Cowley, N. C. Norman, M. Pakulski, G. Becker, M. Layh, E. Kirchner and M. Schmidt, *Inorganic Synthesis*, John Wiley & Sons Ltd, 1990.

8 A. Chartoire, C. Claver, M. Corpet, J. Krinsky, J. Mayen, D. Nelson, S. P. Nolan, I. Peñafiel, R. Woodward and R. E. Meadows, *Org. Process Res. Dev.*, 2016, **20**, 551–557.

9 J. K. Ruff and M. F. Hawthorne, *J. Am. Chem. Soc.*, 1960, **82**, 2141–2144.

10 N. Kuhn and T. Kratz, *Synthesis*, 1993, **6**, 561-562.

11 P. Kuzmic, *Anal. Biochem.*, 1996, **237**, 260–273.

12 E. W. Y. Wong, A. D. Dange, A. L. Fohlmeister, T. J. Hadlington and C. Jones, *Aust. J. Chem*, 2013, 1144–1154.

13 M. A. M. J. Frisch, G. W. Trucks, H. B. Schlegel, G. E. Scuseria, M. Robb, J. R. Cheeseman, G. Scalmani, V. Barone, B. Mennucci, G. A. Petersson, H. Nakatsuji, G. Caricato, X. Li, H. P. Hratchian, A. F. Izmaylov, J. Bloino, M. H. . Zheng, J. L. Sonnenberg, H. M. Ehara, K. Toyota, R. Fukuda, J. Hasegawa, M. Ishida, T. Nakajima, Y. Honda, O. Kitao, E. Nakai, T. Vreven, J. A. Montgomery, Jr., J. E. Peralta, F. Ogliaro, M. Bearpark, J. J. Heyd, V. N. S. Brothers, K. N. Kudin, A. R. roverov, R. Kobayashi, J. Normand, K. Raghavachari, J. B. J. C. Burant, S. S. Iyengar, J. Tomasi, M. Cossi, N. Rega, J. M. Millam, M. Klene, J. E. Knox, A. J. A. Cross, V. Bakken, C. Adamo, J. Jaramillo, R. Gomperts, R. E. Stratmann, O. Yazyev, Stin, G. A. V. R. Cammi, C. Pomelli, J. W. Ochterski, R. L. Martin, K. Morokuma, V. G. Zakrzewski, J. V. O. P. Salvador, J. J. Dannenberg, S. Dapprich, A. D. Daniels, Ö. Farkas, J. B. Foresman and 2009 J. Cioslowski, and D. J. Fox, Gaussian, Inc., Wallingford CT, *Gaussian 09, Revision E.01*, .